WEAR AND MICROSTRUCTURE RELATIONSHIPS IN CARBIDE-FREE BAINITIC RAIL STEELS

by
Catherine Erica Pitt
Clare College
Cambridge

A dissertation submitted for the degree of
Doctor of Philosophy,
at the University of Cambridge,
October 1999

To my husband, Mike

Preface

This dissertation is submitted for the degree of Doctor of Philosophy at the University of Cambridge. The research described in this dissertation was conducted under the supervision of Dr. H.K.D.H. Bhadeshia in the Department of Materials Science and Metallurgy at the University of Cambridge between October 1996 and October 1999. To the best of my knowledge this work is original, except where acknowledgement and reference is made to previous work. Neither this, nor any substantially similar dissertation, has been or is being submitted for any degree, diploma, or other qualification at this or any other university. This dissertation contains less than 60,000 words.

Catherine Pitt
October 1999

Acknowledgements

I would like to thank Professor A.H. Windle for the provision of laboratory facilities in the Department of Materials Science and Metallurgy at the University of Cambridge and British Steel Track Products for providing the financial support for this project.

I am very grateful to my academic supervisor, Dr. Harry Bhadeshia, for his guidance and unfailing enthusiasm for this work. I would like to thank my industrial supervisor, Dr. Vijay Jerath of British Steel Technology, for his help and the provision of many samples and data. I am indebted to Dr. Gavin Thompson and Dr. Howard Smith for the provision of data, wear testing, and the chance to study rails in track.

I would like to thank all the members of the Phase Transformations Group in Cambridge for their help; especially Mike Lord, John Street, Dave Cole, Naomi Chester and Sally Parker. Special thanks are due to Dr. Ian Hutchings for interesting discussions about this project and Dr. Mark Manning for his patient help with computer problems.

Finally, I am very grateful to my tutor at Clare College, Dr. Roger Tapp, for all his support and advice.

Abstract

Rail wear in track necessitates expensive and inconvenient maintenance. Efforts to produce wear resistant rail steels have concentrated on the production of high carbon fully pearlitic steels. Recently carbide-free bainites have shown great potential for wear resistance, greatly improved toughness, and enhanced fatigue resistance. The aim of this work was to study these steels in laboratory rolling-sliding wear tests and in real track to discover the reason for their improved wear resistance. The bainitic steels have been compared with conventional rail steels under identical conditions. The evolution of the surfaces of rails in track was studied over a period of two years and these results were compared with those from standard laboratory tests.

The bainitic steel is tough because of its fine microstructure and the presence of thin films of high-carbon retained austenite between the laths of bainitic ferrite. These can transform under strain to martensite, absorbing energy. The retained austenite was found not to be sensitive to the strains involved in the straightening process applied to all rails during manufacturing, although it would transform under higher strains.

The track test results were different from the laboratory tests. A greater variety of wear patterns was found on the real rails; including signs of what appeared to be abrasive wear. Wear in rails has been shown generally to take place by a process of material transfer between the contacting surfaces, followed by breaking off of wear particles from the weak transfer layer. The hardness of both rail and tyre is very important but this does not explain all of the wear behaviour. The properties of the transfer layer are very significant; it is found to be much softer in the more wear resistant bainitic steels than in pearlite, while the bulk is harder. Since the surface layers have been shown to be a mixture of both steels, the properties of the tyre steel are as important as those of the rail; improvements in rail wear could therefore be made by using bainitic tyres. The toughness of the steels is found to be a significant property for wear resistance; tougher steels will be more resistant to fracture and hence the production of wear particles. Surprisingly, the work-hardening properties of the bainitic steel were found to be the same as those of conventional rail steels, so the improved wear resistance cannot be due to these.

Table of Contents

1

Introduction

The use of railways is increasing and creating a demand for faster, more frequent and heavier trains. This creates a requirement to improve the current infrastructure. Suitable track must fulfill several requirements. The track must be strong enough to support and guide the train. It must be smooth to give a comfortable ride and avoid placing unnecessary restrictions on the vehicles travelling along it. It must not cause excessive noise or vibration during the progress of trains. The cost of buying and maintaining track components must be kept as low as possible [Srinivasan 1977, Stone 1982, Sperring 1986, Esveld 1989, Steele 1990].

Replacing worn rails is a very significant expenditure in maintaining railway track. In the 1950s, the main cause of height loss in rails was corrosion, but as trains have become longer, heavier, and faster, vertical head wear by deformation and fracture has become the most significant life-limiting process. Side wear in curves is also a problem, requiring the rails to be ground to keep the correct profile necessary to avoid derailments [Srinivasan 1977, Sperring 1986, Clayton 1996].

Consequently, much effort has been devoted to finding methods of reducing wear; however this has led to a rise in incidents of failure due to rolling contact fatigue on many railway lines [Steele 1990, ORE 1990]. New wear resistant grades of rail steel must therefore also have good fatigue resistance. Another important criterion is weldability. Modern track uses continuous welded rail rather than bolted rail. This does not have any gap between adjacent rails, thus providing a smooth ride and reducing stresses from

the trains on the rail. It is also easier to maintain [Esveld 1989].

Until recently the majority of rail steels were pearlitic. The wear resistance of these rails increased with the carbon content and reduction of free ferrite path, which is the average distance travelled by a dislocation in ferrite before encountering cementite. In a completely pearlitic microstructure this would be the interlammellar spacing; in a steel containing allotriomorphic ferrite it is a function of the size of these regions and the interlamellar spacing. This trend culminated in fully pearlitic steels which are heat-treated to have a fine interlamellar spacing [Steele 1990, Jerath 1992, Clayton 1996]. However, the interlamellar spacing of pearlite cannot be reduced indefinitely, and the high carbon contents needed to produce a totally pearlitic steel are associated with poor weldability. Consequently researchers started to investigate other microstructures such as martensite and bainite for the next generation of rail steels.

Some early work involved testing conventional rail steel compositions which were heat-treated to produce bainitic microstructures, and these steels generally proved to have inferior wear resistance to pearlitic steels, as did some alloys designed specifically to produce bainitic rails. However, the microstructures were often not well-characterised so it is hard to say what was actually tested [Ichinose *et al.* 1978, Ghonem *et al.* 1982, Matsumoto *et al.* 1978, 1982, Heller and Schweitzer 1982].

More recently it has been found that some bainitic microstructures can have wear resistance equal to or better than that of pearlitic steels, especially at high contact pressures. These steels are carbide-free upper bainite or lower bainite (in which the carbides are fine and hence do not initiate cracks). These bainites are much tougher than pearlitic rail steels and more weldable and so are promising candidates for the next generation of premium rail steels [Chang 1995, Clayton and Jin 1996, Jin and Clayton 1997].

Carbide-free bainitic rail steels are now being developed for commercial use by British Steel but the reasons for their excellent wear resistance were still not well understood when this project was inititated. Wear is a very complex problem and satisfactory models relating the absolute wear rate to material properties have yet to be developed.

1.1 Aim of this work

The main aim of this work is to study experimentally the wear behaviour of carbide-free bainitic rails and to compare them with conventional pearlitic rails. This is not only necessary to understand the wear behaviour of this novel microstructure but also to gain

confidence in the marketing of the steel in a safety-critical application.

A secondary aim was to compare the wear behaviour of rails in track with that of the same steels in laboratory wear tests, as it is not clear how well the latter simulate track conditions. For this it was necessary to develop a replica technique to enable rails in track to be studied without destruction.

The toughness of bainitic rail steels is an important property. Some problems have been experienced with chemical segregation in British Steel's experimental bainitic rail steels which have greatly affected the toughness. It was therefore intended to model the degree of segregation to assist in designing alloys which lead to the most uniform microstructures.

2

Review of the literature

Wear and rolling contact fatigue failure in rails are important economic issues [Clayton 1996]. It is necessary that better steels are developed to reduce the cost of replacing rails and also to offset the increased wear and rolling contact fatigue problems which arise with longer, heavier, and faster trains. Much effort in developing premium rail steels has focussed on wear resistant pearlite, which has been the microstructure of choice for rails for almost as long as railways have existed. Recently however, researchers have started to consider other microstructures and to examine the problem of rolling contact fatigue resistance which has become prominent with more wear resistant rails where the initial fatigue cracks are not removed by wear.

This review will be in five main sections: rail terminology, the characteristics of wear and rolling contact fatigue in real rails, a brief look at simple rail-wheel contact theory, attempts to model the processes occurring in wear and rolling contact fatigue, and the effects of microstructure on wear and rolling contact fatigue behaviour, including an examination of the reliability of laboratory simulations.

2.1 Rail Terminology

Before examining wear and rolling contact fatigue in rails it is necessary to define the terms used to describe the rail-wheel system, and to consider how the rails actually guide the train.

The rail is divided into three main parts: the head, the web, and the foot. These are illustrated in Figure 2.1. Many different rail profiles are available [British Steel Track

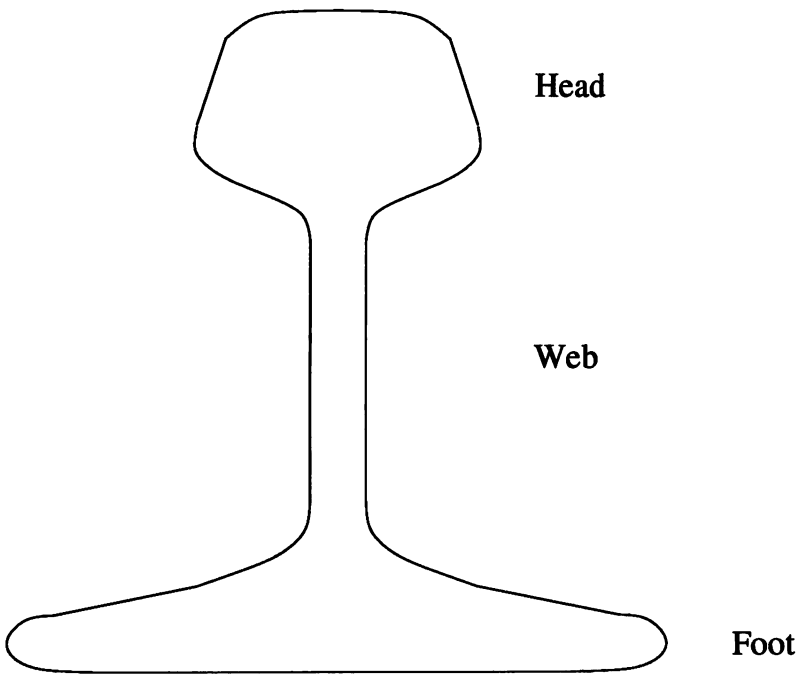

Figure 2.1: The parts of a rail

Products 1992] but the majority are of a shape similar to that illustrated in Figure 2.1. Rails are usually classified by weight per unit length: pounds per yard in Britain and the USA, and kilograms per metre elsewhere. In Britain, the most common rail has a weight of $113\,\mathrm{lb\,yd^{-1}}$. In the USA the most common weight is $136\,\mathrm{lb\,yd^{-1}}$. This is 56 and $67\,\mathrm{kg\,m^{-1}}$ in SI units. The heaviest rails, made to support cranes, go up to $167\,\mathrm{kg\,m^{-1}}$ and the lightest are as little as $10\,\mathrm{kg\,m^{-1}}$.

When rail is put into track it is inclined at a slight angle (Figure 2.2). This is in order to keep the contact point of the conical wheel in the centre of the rail head. The wheels are made conical so that, if the wheelset is displaced laterally, a centering force is exerted upon it. Therefore, in straight track the flanges should not touch the rail at all. Their purpose is to prevent derailment in tight curves when the lateral displacement is much greater. Contact between the rail and the flange causes very high wear rates on both wheel and rail. The side of the rail which comes into contact with the flange is called the gauge side, and the other side is called the field side.

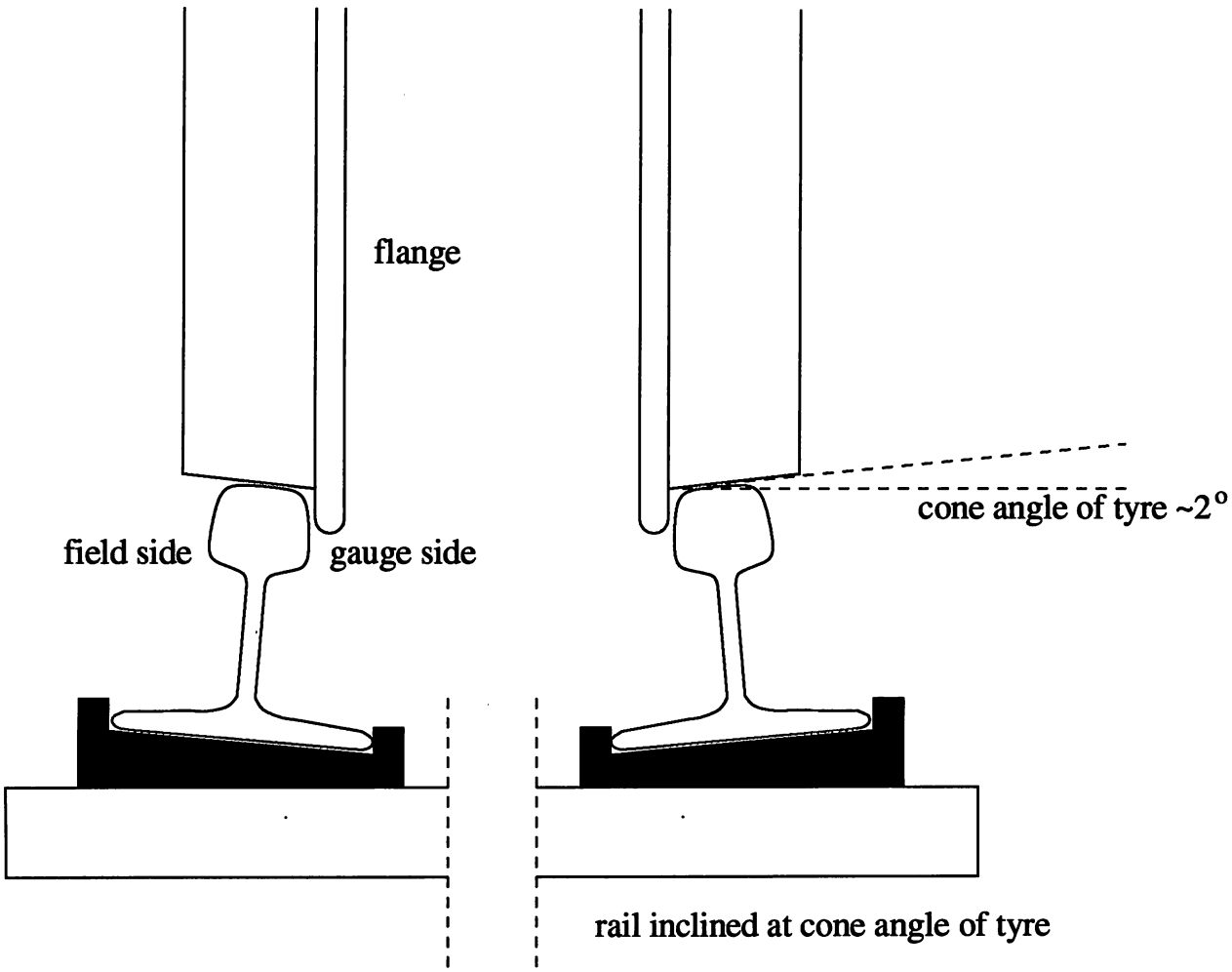

Figure 2.2: Wheels on rail

In tight curves the track is tilted by an amount called the cant (Figure 2.3) to compensate for the centrifugal acceleration which could cause the train to overturn, or the wheels to mount the rail, leading to derailment. This arrangement also reduces track distortion and noise nuisance. The ideal cant, where the lateral acceleration is completely compensated, is a function of speed, and all trains cannot be made to go round the curve at exactly the same speed. In particular, passenger and freight trains often share the same track but run at very different speeds. If the ideal cant for the fastest trains was used, the slower trains would cause excessive wear on the low rail. In practice, the cant is set so that there is a cant deficiency for fast trains. This leads to

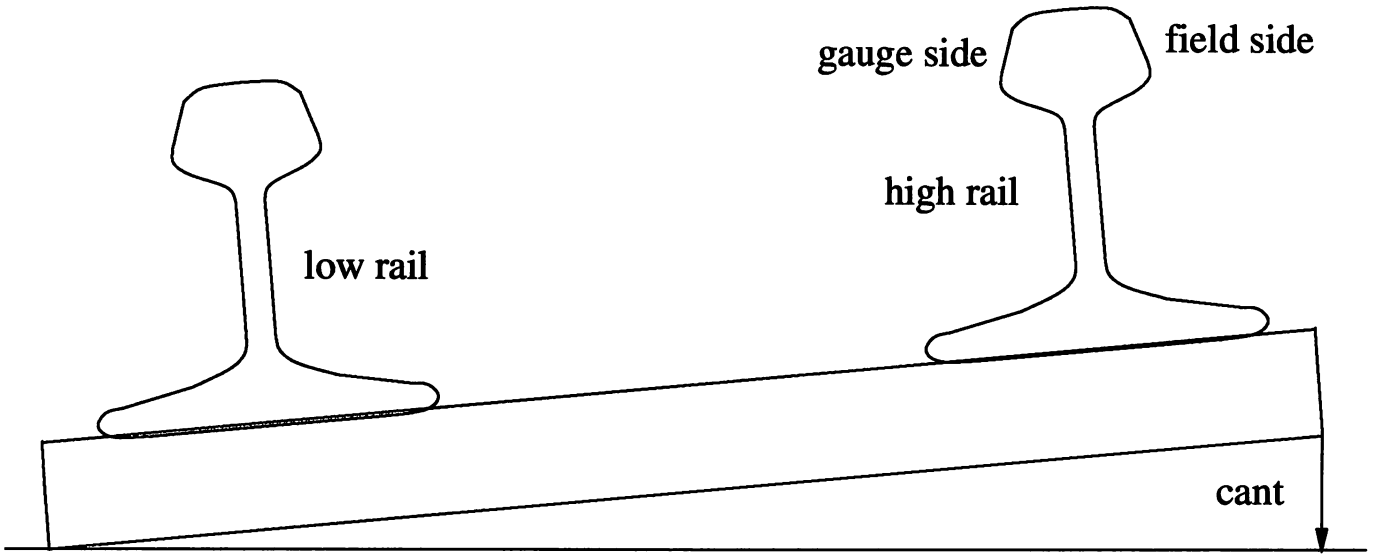

Figure 2.3: Rail in curves

flange contact and wear of the high rail but is cheaper in the long term than introducing speed restrictions on curves.

2.2 Wear and Rails

Wear is a major problem on all railways [Stone 1982, Sperring 1986, Muster *et al.* 1996]. The strength of a rail in bending depends on its depth and therefore on the amount of wear; every year many rails have to be replaced which have worn down to the maximum permissible extent. The cost of replacing worn rails is much greater than that of replacing any other damaged component of track. The vertical head wear is not the only important form of wear; another important type is side or flange wear. As a train goes round a curve the wheels exert lateral forces on the rails causing the side of the rail head to wear away. Eventually the rail profile can become sufficiently worn to allow the flange of the wheel to climb the rail, causing derailment [Sperring 1986, Esveld 1989]. This is a much greater problem on railways with a high proportion of curved track.

Attempts to reduce the wear rate have been made either by lubricating the track

or producing more wear resistant rails. Lubrication has been shown to increase the incidence of rolling contact fatigue defects [Muster *et al.* 1996, Clayton and Hill 1987, Johnson 1989] though it also reduces fuel costs. Wear resistant grades of rail steel, or head hardened rails, are often used on stretches of track which are particularly prone to wear.

2.3 Rolling contact fatigue and rails

Rolling contact fatigue is related closely to wear, and attempts to reduce wear often lead to an increase in rolling contact fatigue failures [Muster *et al.* 1996, Dikshit *et al.* 1991]. In ordinary, unlubricated, track the rail head wears down fast enough to remove initiating fatigue cracks from the surface whereas, if the track is lubricated, the wear rate is reduced but fatigue cracks get an opportunity to grow. This is not just due to the reduced wear rate; laboratory tests have shown that some form of lubrication is necessary to make the initiated fatigue cracks grow [Clayton and Hill 1987]. There are several possible reasons for this which will be explained in the section on models of rolling contact fatigue.

There are a number of important types of rolling contact fatigue defect [Chipperfield *et al.* 1981, Marich *et al.* 1978, Esveld 1989, Sperring 1986, Muster *et al.* 1996, Jerath 1996]. Table 2.1 provides a summary.

Name	Description
Head Check	Small cracks, appearing on the gauge corner. Rarely causes failure.
Squat	Small black circles appear on the centre of the rail head. Cracks grow into the rail and may become transverse defects. Squats are also known as "black spot" or "head shelling".
Shell	Internal cracks in the gauge corner region of the rail which break out to cause spalling of metal on corner. May cause a transverse defect to appear.
Transverse Defect	Transverse break in the rail head caused by either a squat or a shell. T.D.s caused by shells are sometimes called "shell detail fractures".
Tache ovale	Kidney shaped internal crack in rail head. Caused by hydrogen shatter cracks and now very rare.

Table 2.1: Summary of rolling contact fatigue defects

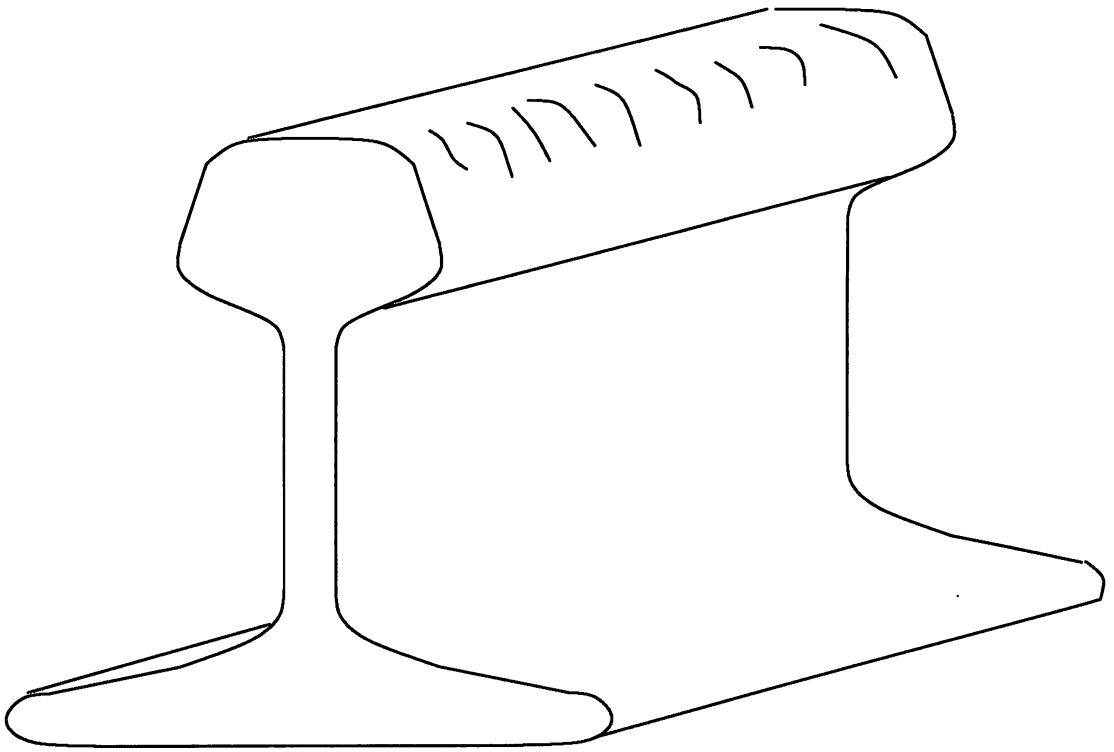

Figure 2.4: Head checks

2.3.1 Surface initiated defects

These are seen mostly in high speed passenger lines where axle loads are relatively light. They are not associated with specific microstructural features in the steel.

Head checks are small cracks which appear along the gauge corner of the rail, illustrated in Figure 2.4. They appear in groups, parallel to one another, with a spacing of a few millimetres. This spacing can vary between different types of rail steel laid in the same place in track. They may join up and cause spalling of the gauge corner, but head checks are not usually a major cause of rail failure [Cannon and Pradier 1996].

Squats, illustrated in Figure 2.5, are the major cause of rolling contact fatigue failure in Europe and Japan. This is probably because these countries have a high proportion of high speed passenger lines. They are also known as "black spot" or "head shelling". The

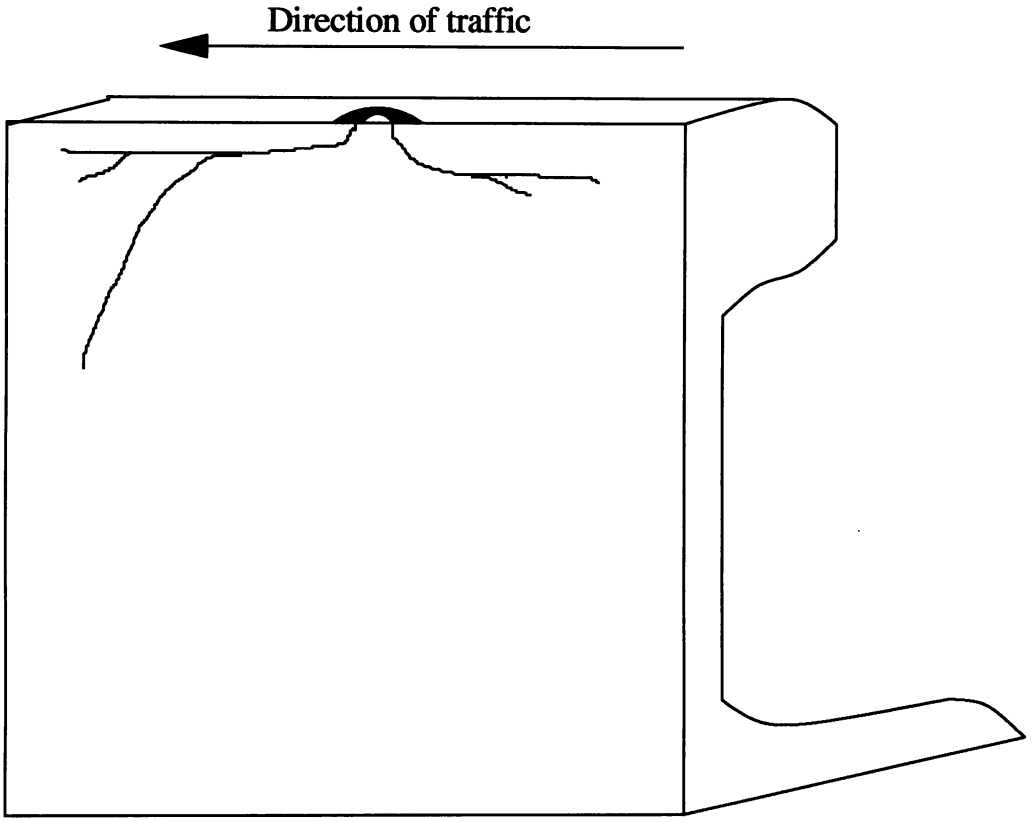

Figure 2.5: A squat. Cracks have grown in both directions but the one in the direction of travel is longer and has turned down.

surface appearance is one of black spots (hence the alternative name) along the centre of the rail. A crack initiates from the surface of the rail and starts to grow downwards at a shallow angle to the rail surface. When a rail is sectioned down the axis of symmetry it is seen that cracks grow both forwards and backwards from the same initiation site along the rail. If the rail only carries trains in one direction the crack in the direction of travel is usually the longer. The metal above the crack is free to flow under the stress caused by the passing of wheels, and this area sinks beneath the level of the uncracked rail. The sunken section is no longer worn by the wheels passing over the rail and so it corrodes, forming the characteristic black spot. Eventually the internal crack may form a branch which turns downwards to form a transverse defect. This is particularly

dangerous as the original horizontal crack may continue to grow and shield the vertical crack from ultrasonic detection until fracture and derailment actually occurs.

Squats are sometimes found to be initiated from small surface indentations in the rail which appear with a very regular spacing. It is thought that these defects are caused by small pieces of hard material becoming embedded in a carriage wheel and producing a dent at each revolution. Squats are also sometimes seen to initiate from cracks in the brittle layer of white phase which forms on the surface of the rail [Dikshit *et al.* 1991].

2.3.2 Subsurface initiated defects

These are most prevalent in heavy haul lines, where axle loads are very high and traffic speeds are lower. They are seen far more frequently in Australia and North America, where this sort of railway is common, than in Europe. They are generally found to initiate from inclusions or other defects in the steel.

Shells are the most important type of subsurface defect. Shelling usually inititates in the gauge corner of the high rail of curves, where the steel has been heavily cold worked. The cracks tend to initiate on alumina-type inclusions just beneath the plastically worked layer. The crack at first grows in an oval shape, parallel to the surface of the rail, but the end which is last loaded by the traffic may branch down at 70-80° to the surface of the rail and grow transversely. This is called a shell detail fracture, or sometimes just a transverse defect, and can cause a derailment. The original shell may also break out and cause shelling of the gauge corner, Figure 2.6. It is thought that the reason shells appear at the boundary between the plastic and elastic regions in the rail is because the stress field around the inclusions helps initiation to occur. When the steel is cooled from the melt the differential contraction between the inclusion and the matrix leaves high residual stresses in the steel. These stresses will have been relieved in the plastic region, so cracks will not initiate from inclusions there [Hellier *et al.* 1985].

Tache ovales or kidney defects are another sort of subsurface defect which initiate from hydrogen shatter cracks. These have virtually been eliminated from modern rails due to improved steel making practice.

2.4 Rail-Wheel Contact Mechanics

The rail-wheel system is extremely complex and it is thus difficult to calculate the stresses in the rail. Finite element analysis or semi-analytical calculations have had to be used to predict the position of the maximum shear stress in the rail head to analyse problems such as shelling. Nevertheless, simple models are also useful. In laboratory

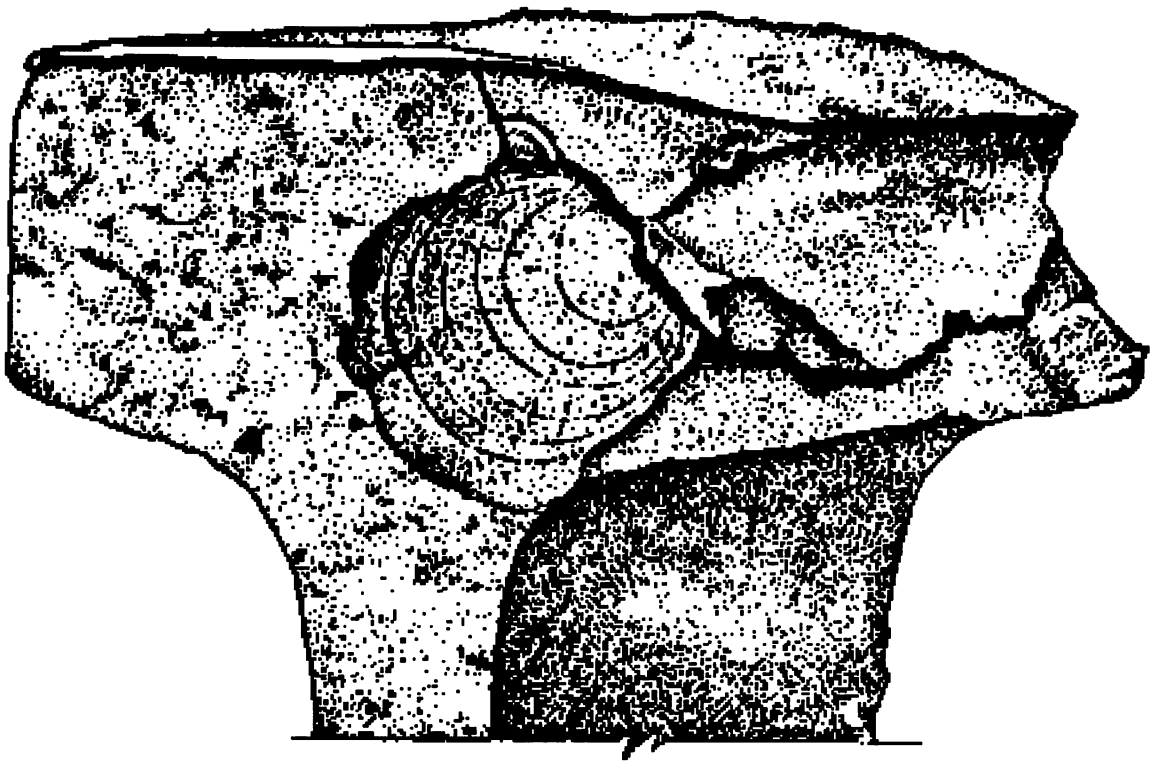

Figure 2.6: Shell with transverse defect; after Laufer *et al.* (1982)

wear testing it is necessary to calculate the maximum contact stress between the rollers which can be done using an equation derived from Hertzian contact theory, given below. This cannot be used in the case of real rail-wheel contact because of the extremely non-Hertzian nature of the contact conditions. The principal assumptions made in the model are these:

1. Each body can be considered to be an elastic half-space, *i.e.*a semi-infinite linear elastic solid.
2. The contact area is small compared to the dimensions of the bodies in contact and the radii of curvature of the surfaces.
3. The contact is frictionless.
4. The strains are small.

The elasticity and friction assumptions are incorrect for laboratory wear testing but this method gives an idea of the stresses involved. Consider the case of two cylinders, each of length l, and radii R_1 and R_2 respectively, in contact with their axes parallel to

one another. The y-axis of the coordinate system is taken to be parallel to the cylinder axes and the x-axis perpendicular to it in the plane of contact. The z-axis goes down into the lower cylinder. The arrangement is illustrated in Figure 2.7. A load W is applied to the cylinders so that the load per unit length $P = W/l$. The elastic moduli of the cylinders are taken to be E_1 and E_2 and the Poisson's ratios ν_1 and ν_2. The contact area will be a rectangle of length l and width $2a$. For the case of rails the equations can be simplified because both rollers are made of the same material so $E_1 = E_2 = E$, and $\nu_1 = \nu_2 = \nu$

The derivation will not be written out here, but can be found in Johnson (1985) and Timoshenko and Goodier (1984). The Hertz theory gives the following results:

$$a^2 = \frac{4PR}{\pi E^*} \tag{2.1}$$

where

$$\frac{1}{E^*} = \frac{1-\nu_1^2}{E_1} + \frac{1-\nu_2^2}{E_2} = \frac{2(1-\nu^2)}{E} \tag{2.2}$$

and

$$\frac{1}{R} = \frac{1}{R_1} + \frac{1}{R_2} \tag{2.3}$$

The pressure distribution over the surface is

$$p(x) = \frac{2P}{\pi a^2}\sqrt{a^2 - x^2} \tag{2.4}$$

The symmetry of the problem means that there is no term in y in this equation.

The maximum pressure is given by

$$p_0 = \sqrt{\frac{PE^*}{\pi R}}$$

and the mean pressure

$$p_m = \frac{\pi}{4}p_0 \tag{2.5}$$

The pressure distribution under the surface along the z-axis is given in Johnson (1985):

$$\sigma_x = -\frac{p_0}{a}\Big((a^2 + 2z^2)(a^2 + z^2)^{-1/2} - 2z\Big) \tag{2.6}$$

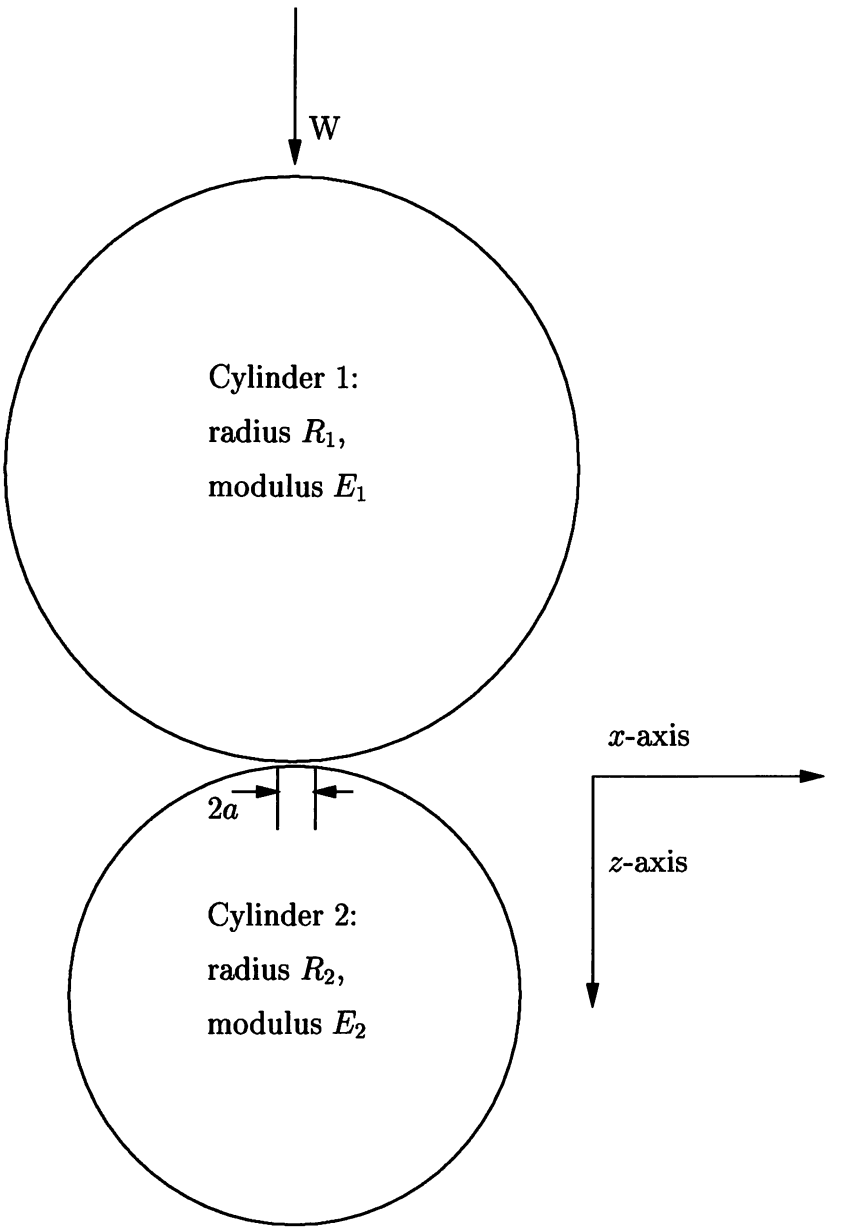

Figure 2.7: Coordinate system for Hertzian cylinders

$$\sigma_z = -p_0 a(a^2 + z^2)^{-1/2} \tag{2.7}$$

These are principal stresses so the principal shear stress can simply be found:

$$\tau_1 = \frac{p_0}{a}(z - z^2(a^2 + z^2)^{-1/2}) \tag{2.8}$$

from which it can be found that the maximum shear stress occurs at $z = 0.78a$ with a value of $0.30p_0$.

This is only valid for stationary rollers; when the wear test is actually in progress the frictional forces alter the situation. For an elastic-perfectly plastic cylinder rolling on a flat surface the location of the highest shear stress depends on the coefficient of friction; if it is greater than 0.25 then the highest shear stress occurs at the surface of the bodies [Bower and Johnson (1991)].

2.5 Models of Wear and Rolling Contact Fatigue

2.5.1 Wear

The wear of metals is a difficult process to model. Wear rates vary greatly depending on the active mechanism. These are not well understood. It can be very difficult to compare wear data under different experimental conditions because the mechanisms differ so much. Some models have been developed to predict general trends in wear behaviour but actual wear rates cannot yet be predicted from first principles.

2.5.1.1 Metals in contact

When two surfaces are touching, the apparent area of contact is usually much greater than the true area of contact, because the surfaces are not perfectly smooth. They therefore touch at the tips of the higher asperities on each surface. If it is assumed the asperities spherical tips with radius r the results of Hertz for a sphere pressed into a flat surface can be used to model the deformation of one asperity, which will support a load of w where

$$w = \frac{4}{3}E^* r^{1/2}(z - d)^{3/2} \tag{2.9}$$

E^* is the effective Young's modulus of the surfaces as defined above, z the height of the asperity above some reference plane, and d the distance between the reference plane and the surface the asperity is pressed into.

In a real surface the asperities are not all of the same height. It is assumed that they are all of the same radius, r, and that the height distribution is Gaussian. If the distribution of the heights of individual asperities s represented by $\varphi(z)$ then if there are J asperities on the surface, the number j actually in contact is

$$j = J\int_d^\infty \varphi(z)\,dz \tag{2.10}$$

and the total load supported is hence

$$W = \frac{4}{3} J E^* r^{1/2} \int_d^\infty (z-d)^{3/2} \varphi(z)\, dz \tag{2.11}$$

This may be integrated numerically, and shows that, for a typical surface, the actual contact area is proportional to the load [Moore 1975, Hutchings 1992].

This theory deals with elastic contact, but it can be used to find the proportion of asperity contacts at which yield occurs. This depends on the value of the plasticity index, ψ which is

$$\psi = \frac{E^*}{H}\left(\frac{\sigma^*}{r}\right)^{1/2} \tag{2.12}$$

where H is the indentation hardness of the material and σ^* is the standard deviation of $\varphi(z)$, the distribution of asperity heights. For most metals E^*/H is large so the contact will be plastic for all but the smoothest surfaces.

When one surface is slid over another, the movement is resisted by a frictional force. Several different theories have been proposed to explain how the force is generated (Moore 1975), but the widely accepted one is that of Bowden and Tabor: the frictional force arises from two terms, one for the adhesion force at the junctions which form between the surfaces, and one for the deformation force to plough the asperities on one surface through those of the other. The two terms are usually treated as independent, although strictly they are not. [Moore 1975, Hutchings 1992].

If the total true area of contact (*i.e.* the contact area of the asperities on the surfaces, not the apparent area of contact) is A, and the shear strength of the average junction is s, then the adhesion contribution to the frictional force is

$$F_{ad} = As \tag{2.13}$$

Since the true area of contact is proportional to the load and each asperity can support a stress approximately equal to the indentation hardness, then it can be said:

$$W \approx HA \tag{2.14}$$

and hence the coefficient of friction attributed to the adhesive force, μ_{ad} is

$$\mu_{ad} = F_{ad}/W \approx s/H \tag{2.15}$$

The shear yield stress s can be taken to be approximately twice the normal yield stress (the exact value depends on the yield criterion used) and the indentation hardness, H to be approximately three times the yield stress. Hence it is found

$$\mu_{ad} \approx 0.2 \tag{2.16}$$

The friction coefficient due to deformation alone is usually insignificant [Moore 1975] and so it can be said that μ for metals should be around 0.2. This is clearly wrong.

The model has not taken into account two effects: junction growth and work-hardening. Consider two surfaces in contact; the pressure at the asperity contacts rapidly becomes some critical yield pressure, approximately the indentation hardness, H. We will call it σ_H. Now add a small tangential force F attempting to slide the surfaces over one another. For the material to remain at just at the yield point, the normal stress must decrease. Using the von Mises yield criterion, rearranged:

$$\sigma^2 + 3\tau^2 = \sigma_H^2 \tag{2.17}$$

The tangential stress is given by:

$$\tau = F/A \tag{2.18}$$

and the normal stress

$$\sigma = W/A \tag{2.19}$$

Substituting these in equation 2.17 gives

$$W^2 + 4F^2 = A^2\sigma_H^2 \tag{2.20}$$

The normal load remains constant so as F increases, equation 2.20 can only be satisfied by increasing the area of contact A and so the value of μ also increases. In theory this process could go on until the true area of contact becomes as large as the apparent area of contact, but in practice this does not happen because the surfaces are not infinitely ductile and are contaminated by thin surface films [Hutchings 1992].

Work-hardening also tends to increase μ because the asperities harden as they deform, and hence develop a higher shear yield stress s. However, this effect is less important than the previously described junction growth.

2.5.1.2 Simple adhesion wear— the Archard model

Consider two surfaces sliding over each other. Assuming that a single asperity contact is circular with a radius a, the normal load supported by this one contact is

$$w = H\pi a^2 \tag{2.21}$$

where H is the indentation hardness. As the two asperities slide over each other, the load carried by them gradually decreases and is borne by other contacts elsewhere on the surfaces. If the junction between the asperities is stronger than the base materials

(as it may well be due to work-hardening) then the contact may break inside one of the materials instead of at the original plane of contact. Suppose a proportion κ of contacts produce a wear particle in this way and that the average wear particle produced is hemispherical in shape. Logically its size would be proportional to that of the original asperity contact, radius a, so the volume of one wear particle is

$$\delta V = \frac{2}{3}\pi a^3 \tag{2.22}$$

The asperities have to slide a distance $2a$ to completely cross over each other and generate the wear particle. The average wear volume produced per unit sliding distance is hence

$$\delta Q = \kappa \delta V / 2a \tag{2.23}$$

which gives

$$\delta Q = \kappa \pi a^2 / 3 \tag{2.24}$$

Summing this over the whole area of contact gives the total wear "rate" Q

$$Q = \kappa A / 3 \tag{2.25}$$

and since $W = HA$ (equation 2.14) it follows that

$$Q = \frac{\kappa W}{3H} = \frac{KW}{H} \tag{2.26}$$

where K is the wear coefficient.

This wear equation holds in many circumstances and K can be interpreted differently depending on the wear mechanism; for example, when wear occurs by a fatigue-type process, K may be a function of the number of cycles to rupture. An equation of the same form can also be derived by considering abrasive wear [Zum Ghar 1987].

This simple model predicts that wear resistance ζ (usually defined as the reciprocal wear rate) should be proportional to hardness. This has been shown to hold for pure metals but not for work-hardened metals or most steels. Mutton and Watson's graph of ζ *vs.* hardness for a wide variety of metals is reproduced in Figure 2.8. The surface layer of materials undergoing sliding wear suffers so much plastic deformation and hence work-hardening, that the initial dislocation density does not affect the wear rate. It is the properties of the highly strained layer at the surface that are significant.

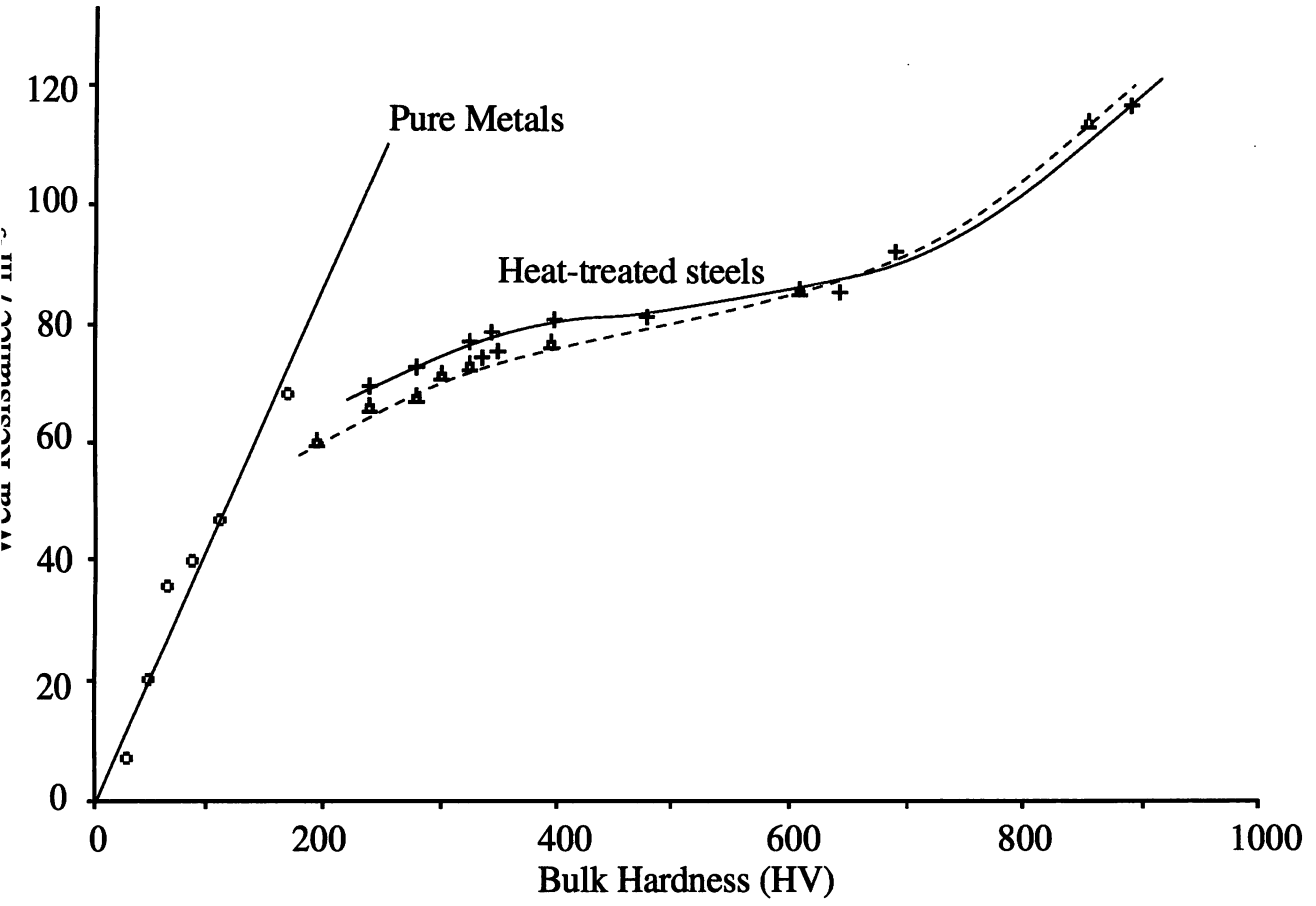

Figure 2.8: Graph of wear resistance against hardness for some common metals; after Mutton and Watson (1978). Wear resistance is measured as an inverse volume loss over a fixed sliding distance.

2.5.1.3 The Suh Delamination Theory

The delamination theory [Suh 1973, 1977] was put forward to try to explain particle formation by adhesive wear. It aimed to improve on the Archard wear model by explaining the observed shapes of wear particles and providing a plausible mechanism for their formation.

When two surfaces are slid over one another, normal and tangential loads are transmitted through the asperity contact points. Surface traction exerted by hard asperities on the opposing surface leads to the accumulation of plastic shear deformation. As this process continues, cracks are nucleated below the surface. Suh states that cracks will not nucleate at the surface because of the high compressive stresses there. The cracks then grow beneath the surface, and finally shear out at weak points, producing sheet-shaped wear particles.

The theory correctly predicts the types of wear particles observed but cannot be used

to estimate wear rates. The rate of wear should depend on three things: the resistance to plastic deformation (*i.e.* the hardness), the ease of crack nucleation and the ease of crack propagation, which brings toughness into consideration.

It is, however, hard to explain how the cracks can grow beneath the surface at all. Zum Ghar (1987) states that delamination of transfer layers, as opposed to the bulk material, may be what is occurring, especially in systems where there is high adhesion and a great deal of material transfer, such as rails. Material may be transferred back and forth between the surfaces until the interface between the transferred material and the substrate becomes weak enough for a wear particle, possibly consisting of many layers of transferred material, to break off.

2.5.1.4 The energy approach

Some researchers have looked at an energy approach to predicting wear resistance [Moore 1979, Wang *et al.* 1991, Wang and Lei 1996]. In this theory, the microstructures which absorb most energy would have the greatest wear resistance. Work may be expended on temperature rises, the creation of new surfaces, plastic deformation and elastic deformation. This may lead to phase transformations, recovery, and recrystallisation. Large temperature rises leading to recrystallisation are unlikely in rails but plastic deformation is very important. It is suggested that the reason pearlitic microstructures are wear resistant is due to the resistance to plastic deformation caused by the small mean free path for dislocations in the ferrite component of pearlite. This will be considered in more detail later. Wang also suggested that materials with a high work-hardening coefficient should be very resistant to sliding wear.

McEwen and Harvey (1985) used the simple hypothesis that every unit of energy expended through creepage between the rail and tyre removes a fixed amount of material. Creepage is the ratio of distance slid to distance rolled for the rail (see Johnson 1985 for a detailed explanation). This leads to a wear equation

$$Q = \frac{KF\xi}{A_{app}} \tag{2.27}$$

where Q is the wear rate, defined as the weight lost per unit area of contact per unit sliding distance, K is a wear coefficient as before, ξ is the creepage, F is the friction force, *i.e.* μW, and A_{app} is the apparent contact area. Their results, for a complex laboratory wear test rig which involved a full-sized tyre rolling against a 1.2 m length of real rail, showed that this equation worked well for the case of straight rails, though the constant of proportionality depended on the steels involved.

2.5.2 Rolling contact fatigue

2.5.2.1 The role of lubrication

It has always been found in laboratory tests that rolling contact fatigue type defects will not form in the absence of lubrication. [Kalousek *et al.* 1985b, Clayton and Hill 1987, Cannon and Pradier 1996, Clayton 1996, Ishida and Abe 1996, Muster *et al.* 1996, Tyfour *et al.* 1996]. The need for lubrication to make fatigue cracks grow explains why cracks are seen only on the rail disc in laboratory twin-disc tests. On the rail disc the mouth of the crack enters the roller gap first and is squeezed shut, trapping the fluid inside. On the tyre disc the root of the crack is compressed first, forcing the fluid out. Cracks can *initiate* without lubricant, as demonstrated in the work of Tyfour *et al.* (1996), but the presence of fluid is needed to make them propagate. Several reasons were put forwards to explain the need for the lubricant [Johnson 1989]:

1. The lubricant reduces crack face friction enabling the crack to grow in Mode II.
2. The lubricant transmits pressure from the mouth of the crack to the tip.
3. The lubricant becomes trapped inside the crack and generates a Mode I stress intensity at the crack tip when the crack mouth is forced shut.

These mechanisms have been investigated using fracture mechanics by calculating stress intensity factors for each case to see in what direction the crack should grow. It has been shown that the third mechanism is the only possibility which would produce the type of defects seen in practice. This produces a staggered cycle of Mode I and Mode II stress intensities as the wheel moves over the crack. When this loading cycle has been reproduced in the laboratory [Bold *et al.* 1991, Wong *et al.* 1996] cracks have been grown successfully on the plane of maximum shear stress and have exhibited large growth rates.

2.5.2.2 Modelling of shelling

Shells are usually considered to initiate from complex oxide inclusions in a small region near to the gauge corner of the rail [Chipperfield *et al.* 1981, Steele *et al.* 1987] although some work has shown that shells can form without the presence of oxides [Sugino *et al.* 1996]. Hellier *et al.* (1985) performed finite element modelling of the stresses in a rail head to attempt to show why shelling appears in such a narrow area of the rail. When a crack face friction term was added into their calculations, the shear stress range was found to be much greater in the gauge corner than in the rail head. The maximum shear stress range did not appear at the expected depth for shelling but higher up in

the plastically worked layer. This was explained by the fact that shells initiate due to the interaction of the shear stress with the stress field round an inclusion. This stress field is relieved in the plastically worked layer, so reducing the chance of crack initiation. This explains why cracks tend to start at the interface between the elastic and plastic regions of the rail where the shear stresses are still high and the inclusion stress fields are unaffected.

2.6 Laboratory testing of wear resistance

Large scale track trials of rail steels are expensive and time consuming. In order to investigate the properties of rail steels and to develop new alloys cheaply, a small-scale laboratory testing method is necessary. Pin-on-disc and pin-on-ring tests have been used which produce only sliding wear. Sliding-rolling wear tests have also been carried out using machines which run two discs against each other at a fixed velocity ratio. Rolling contact fatigue can be investigated by performing tests of this type with added lubrication. The creepage, ξ, which is the sliding distance to rolling distance ratio, can be varied in some of these machines to simulate different conditions in track or to provide accelerated testing. Kalousek *et al.* (1985a) used a complex method of simulating wheel-rail contact in curves using a scaled-down wheelset and rail, and varying the yaw angle between them (Figure 2.9) in a fixed pattern to produce contact conditions typical of curving.

Bolton and Clayton (1984) carried out a study to characterise the wear regimes found in laboratory testing of rail steels on an Amsler rolling-sliding wear machine, which is a twin disc machine with a fixed angular velocity ratio. The creepage is varied by using wheels of different diameter. These results were compared with the wear observed in actual rails. They found three regimes of wear which they labelled types I, II, and III. Type I was a mild wear regime where both oxide and metallic debris were formed, considered to be roughly equivalent to 'mild wear'. Types II and III produced entirely metallic debris, but in type III the surface became much rougher, with prominent score marks and gouges. Type II produced a rippled surface, though still much rougher than type I, and this was considered to correspond to 'severe wear' as it is usually defined. This was concluded to be the closest to the gauge face wear observed on rails removed from track in Britain. However, another study [Clayton and Danks 1987], concluded that type III wear was similar to wear observed on the gauge face of a rail which had been removed from a test track.

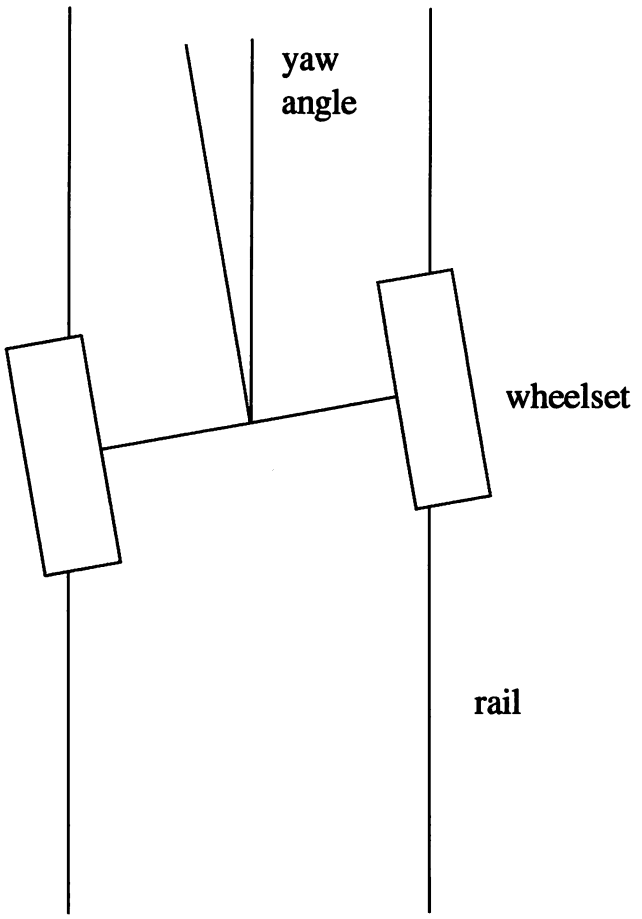

Figure 2.9: Yaw angle in curves

In that study Clayton and Danks carried out laboratory tests very similar to the previous work on plain eutectoid rail steels in an Amsler machine and compared these with pin-on-disc tests for the same steels, and worn Cr-Mo alloy rails removed from the FAST (Facility for Accelerated Service Testing) track in Colorado. They concluded that the Amsler tests provided the better simulation of rail wear, though the pin-on-disc test was also useful. They were unable to reproduce the findings of Bolton and Clayton on wear regimes; there was no large increase in wear rate between type I and type II regimes, and type II wear did not appear consistently in any case. They also raised the point that, on an Amsler machine, the smaller wheel has always been observed to wear faster. This can be either the tyre or the rail depending on which value of creepage is being used. The machine has a fixed angular velocity ratio so the diameter of the

wheels has to be varied to change the creepage. Clayton and Danks (1990) carried out more Amsler tests on eutectoid rail steels in an attempt to find a relationship between true interlamellar spacing of pearlite and wear rate. They identified the same three wear regimes but showed that there was a large amount of scatter in the wear data when tests were repeated. This made it difficult to develop quantitative relationships between wear behaviour and microstructure.

Zakarov *et al.* (1998) carried out tests on wheel steels using a twin disk rig that allowed the axes of the disks to be placed at an angle to each other, rather than parallel. This enables lateral creep, such as that seen in wheel flange-gauge face contact in curves, to be simulated. They identified no less than four wear regimes: mild, severe, heavy, and catastrophic wear, corresponding to Type I, Type II, a new wear mode, and Type III wear respectively. The new mode, 'heavy wear', was characterised by an increase in the wear rate of up to an order of magnitude over 'severe wear', an increase in the size of wear debris and a general darkening of the colour, and an increase in the roughness of the worn surfaces. The laboratory rollers were compared with surfaces of rails and tyres from Russian railways. Mild (Type I) wear was generally found on the rail and tyre running bands, and sometimes on the tyre flanges and rail gauge face. The other three types of wear were also found on the tyre flanges and rail gauge faces on some specimens.

Despite their limitations, the studies summarised above show that twin-disk rolling-sliding wear tests provide the best current simulation of track conditions in the laboratory. There is some variation in the type of wear seen in real rails which will of course vary with the track conditions. Typical gauge face wear appears to involve the formation of completely metallic particles, with the worn surface appearing very rough with gouges and other prominent scars.

2.7 Effect of Microstructure on Wear and Rolling Contact Fatigue

2.7.1 The relationship between microstructure and wear behaviour

Archard's wear law predicts that wear resistance should be proportional simply to hardness. This holds fairly true for pure metals but not necessarily so for steels [Mutton and Watson 1978, Hutchings 1992]. A review by Saka (1978) considered the relationship between friction and wear of metals and a broad range of microstructures. Grain size and shape should have little effect for all but very fine microstructures, since the size of most asperities is much smaller than the grain size. The most interesting results

presented were those for two-phase materials. Second phase particles raise the hardness of a material, but may lower the wear rate because they increase the crack nucleation rate, depending on their size and coherency; less coherent particles cause greater crack nucleation. Solid solution hardening should raise the hardness without greatly increasing the tendency to nucleate cracks, and so should be better for the wear rate.

In experiments on rail steels, bainite and martensite have often been shown to be less wear resistant than pearlite of the same hardness [Ichinose *et al.* 1978, Ghonem *et al.* 1982, Masumoto *et al.* 1978, 1982, Heller and Schweitzer 1982, Kalousek *et al.* 1985a, Garnham and Beynon 1992, Wang and Lei 1996], although some studies have suggested that bainites may have some potential for wear resistance: [Mutton and Watson 1978, Clayton *et al.* 1987, Devanathan and Clayton 1991, Xu and Kennon 1991, Clayton and Devanathan 1992, Chang 1995, Jin and Clayton 1997]. In particular the results of the latter two with novel carbide-free bainitic steels are very interesting. The wear resistance of pearlite, however, has been shown to depend on the interlamellar spacing (or mean free ferrite path, which is related to this) and hardness. As the hardness is controlled by the interlamellar spacing the two are equivalent [Bhattacharyya 1980, Clayton 1980, Heller and Schweitzer 1982, Clayton and Danks 1990, Fegredo *et al.* 1993, Singh and Singh 1993]. It is clear from this that predicting the wear of steel is not simple and that changes in the microstructure have a important effect on wear rates even at the same hardness level.

2.7.1.1 Pearlite

Pearlitic microstructures have always been used for rails because of their excellent wear resistance. The wear resistance increases with hardness, and so with decreasing interlamellar spacing. Consequently efforts have been made to produce rails with finer and finer interlamellar spacings by heat treatment of the rails after rolling. This is done by controlled cooling through the transformation by means of water sprays or compressed air to induce lower transformation temperature. Alternatively, rails are heat treated off-line by induction hardening of the rail head to produce a fine pearlitic microstructure. [Esveld 1989, British Steel Track Products 1992].

The good wear resistance of pearlite is due to its microstructure of fine lamellar carbides and ferrite. Under sliding wear the microstructure evolves by the deformation and fracture of the cementite lamellae which become orientated parallel to the sliding direction at the surface. The softer ferrite is squeezed out during this process, so the volume fraction of cementite close to the surface increases, presenting a much harder

and more wear resistant surface layer to the slider [Kalousek *et al.* 1985a, Perez-Unzueta 1992, Garnham and Beynon 1992].

Many attempts have been made to find a quantitative relationship between wear resistance and interlamellar spacing or other material properties/parameters for pearlitic structures.

In recent years it has seemed that pearlitic rails were approaching the limit of development for wear resistance and research has begun on bainitic and martensitic rails as alternatives for highly wear resistant rails [Steele 1990, Jerath 1992].

2.7.1.2 Bainite

As mentioned above, some recent studies have suggested that some types of bainite may offer as good or greater rolling-sliding wear resistance than pearlite. In particular relatively low carbon bainites, especially with carbide-free microstructures, have shown good wear resistance [Chang 1995, Clayton 1996, Clayton and Jin 1996, Jin and Clayton 1997, Shipway *et al.* 1997] and bainitic steels are being developed for use in railway crossings [Sperring 1986, Callender 1983]. Bainite also has the advantage of greater toughness over pearlitic rails, and bainites which are low in carbon have greater weldability than pearlitic rail steels which typically contain 0.7 weight percent carbon.

Some of the studies on the comparative wear resistance of bainite and pearlite may have been misleading for several reasons. The term 'bainitic' can cover a variety of microstructures which may have quite different wear properties. In some studies the steels used were not characterised well enough to be useful. Table 2.2 contains the compositions of all the bainites used in the studies reviewed here.

The bainitic Cr-Mo steel studied by Ghonem *et al.* (1982) had a mixed microstructure of upper bainite with bands of lower bainite and martensite. It has been shown in another study that cracking between the areas of bainite and martensite is detrimental to the wear resistance in a mixed microstructure, although the steel in that study had much larger regions of martensite [Devanathan and Clayton 1991].

The studies by Masumoto *et al.* (1978, 1982) into wear resistant rail steels concluded that their bainitic steel had much lower wear resistance than pearlitic steels. However the tests were carried out at a relatively low maximum contact pressure and the microstructure was not characterised. It has been shown in other studies [Devanathan and Clayton 1991] that the wear rate of some bainitic steels increases less with contact pressure than that of pearlitic steels. Thus at high contact pressures of over 1000 MPa their bainitic steels were equivalent to pearlitic steels in terms of wear resistance, and

Study	Steel	Composition in weight percent						
		C	Si	Mn	Cr	Mo	Ni	B
Ichinose *et al.* (1978)	11	0.33	0.31	1.20	1.25	0.20	-	0.0029
	12	0.33	0.31	1.20	1.25	0.20	-	0.0029
	13	0.27	0.34	1.24	0.61	0.22	-	-
Mutton and Watson (1978)	Cr-Mo	0.78	0.20	0.85	0.75	0.17	-	-
Masumoto *et al.* (1978)	LC	0.33	0.33	1.20	1.17	0.20	-	-
Ghonem *et al.* (1982)	Cr-Mo; no data							
Heller and Schweitzer (1982)		0.07	-	4.5	-	0.5	-	-
		0.3	-	-	2.7	0.2	-	-
Matsumoto *et al.* (1982)	LC	C less than 0.4%; no other data						
Kalousek *et al.* (1985a)		0.72	0.28	0.81	0.79	0.21	-	-
Clayton *et al.* (1987)	1	0.09	0.21	1.01	-	0.50	-	0.0029
	2	0.21	0.22	1.99	-	0.50	-	0.0026
	3	0.30	0.21	1.49	-	0.50	-	0.0027
	4	0.09	0.21	0.53	0.95	0.49	-	0.0028
	5	0.19	0.20	0.98	0.95	0.49	-	0.0028
	6	0.29	0.21	1.98	1.02	0.50	-	0.0030
	7	0.09	0.24	2.01	1.96	0.50	-	0.0029
	8	0.19	0.22	1.52	2.00	0.50	-	0.0025
	9	0.29	0.23	1.20	1.98	0.50	-	0.0030
Devanathan and Clayton (1991)	0.52C	0.52	0.23	0.35	1.71	0.26	1.43	-
	0.10C	0.10	0.27	0.59	1.71	0.58	4.09	-
	0.04C	0.04	0.21	0.73	2.76	0.26	1.91	-
Xu and Kennon (1991)	0.75%C; no other data							

Table 2.2: Compositions of bainitic steels used in wear studies Continued on next page

also had higher toughness and improved weldability compared with pearlite. It would be interesting to see how the bainite in the work of Masumoto *et al.* compared with pearlite at a range of contact pressures. However, the lack of information on the microstructure of this bainite means that the study is not very helpful in designing wear resistant bainitic steels.

Work by Heller and Schweitzer (1982) which showed that bainitic rail steels wore faster than pearlitic steels did not involve an investigation into the worn microstructure. Again, this makes it hard to compare this work with other studies on bainite of different

Clayton and Devanathan (1992)		0.71	0.4	0.88	0.57	0.2	0.1	-	
Garnham and Beynon (1992)	B04	0.04	0.19	0.80	2.76	0.25	1.93	0.0023	
	B20	0.20	0.16	0.67	2.29	0.27	1.68	0.0023	
	B52	0.52	0.22	0.37	1.70	0.27	1.44	0.0022	
Chang (1995)	A	0.27	1.98	2.18	1.9	-	-	-	
	K	0.49	1.53	2.03	-	-	-	-	
	L	0.22	1.39	1.97	-	-	-	-	
	P	0.49	1.44	0.51	-	-	3.5	-	
Su and Clayton (1996)	J1	0.18	1.13	2.01	1.94	0.48	-	0.003	
	J2	0.12	0.27	3.97	0.02	0.47	-	0.003	
	J4	0.02	0.27	2.02	1.96	0.48	-	0.003	
Wang and Lei (1996)	A10	0.79	0.23	0.32	0.02	-	-	-	
Clayton and Jin (1996)	J1	0.18	1.13	2.01	1.94	0.48	0.01	0.0027	
Jin and Clayton (1997)	J2	0.12	0.27	3.97	0.02	0.47	0.02	0.0027	
	J3	0.08	0.27	2.03	1.97	0.48	1.93	0.0082	
	J4	0.02	0.27	2.02	1.96	0.48	1.93	0.0071	
	J5	0.03	0.27	4.04	0.02	0.47	0.02	0.0030	
	J6	0.26	1.81	2.00	1.93	0.49	-	0.0030	
	J7	0.27	1.87	1.87	2.02	0.51	0.21	0.0050	
	J8	0.24	1.76	2.03	0.01	0.50	-	0.0030	
	J9	0.26	1.73	1.81	0.14	0.47	3.02	0.0020	
Shipway *et al.* (1997)	-	0.45	2.08	2.69	-	-	-	-	

Table 2.2: Compositions of bainitic steels used in wear studies

compositions which may have quite different microstructures and hence different wear behaviour. The work of Ichinose *et al.* (1978) concluded that the reason their bainite wore more than pearlite was that it contained a distribution of large carbides in the worn layer of the microstructure which can break out easily, forming wear particles. Their bainite was a typical rail steel composition, heat treated to produce a bainitic microstructure and then tempered. It was much higher in carbon than the bainites which have proved to have good wear resistance.

The work of Kalousek *et al.* (1985a) used contact pressures of 1800 MPa on a Cr-Mo rail steel heat treated to produce bainite, tempered martensite and pearlite at three

hardness levels in an extensive testing programme which attempted to simulate high and low rail wear, as well as the effects of various lubricants. The tempered martensite wore the most and the pearlite the least under dry wear conditions. The bainite in this study contained cementite but little more was said about it as most of the electron microscopy referred to the martensite and pearlite. Interestingly the bainite work-hardened the least of the three steels, as measured by microhardness tests in the worn layer. Microstructures which work-harden to a large extent under sliding wear, producing a harder surface layer, have been shown to have better wear resistance in other work [Devanathan and Clayton 1991, Garnham and Beynon 1992.]

The problems mentioned above mean that it is impossible to generalise these studies to all bainitic microstructures, especially under varying contact conditions. Other studies (mentioned previously) have shown that under some conditions bainite can be superior to pearlite. It is now necessary to look at the reasons why in order to find out how to design consistently good bainitic rail steels.

Several explanations have been given when bainite has proved superior to conventional rails. Devanathan and Clayton (1991) and Clayton and Jin (1996) suggested that the high work-hardening rate of bainite had enabled it to produce a harder surface layer than the pearlite. Alternatively, the greater ductility of their bainite (a low carbon carbide-free composition) might have had some effect. This was the only mechanical property to differ significantly between the pearlite and the bainite. Clayton *et al.* (1987) found an unexpected correlation between wear rate and strain at the fatigue limit. This could not be explained.

Mutton and Watson (1978) looked at the wear resistance of variety of steels and attempted to improve upon Archard's wear law, which was shown only to hold for pure metals. The theory that the wear resistance of a two-phase material is proportional to the weighted wear resistances of the phases was shown not to hold for pearlite or spheroidised steels. An equation which took into account work-hardening was also investigated:

$$\zeta = CHe^n \tag{2.28}$$

where ζ is the wear resistance, C is a constant, H is the hardness, e is the base of natural logarithms (2.71828...) and n is the strain-hardening exponent from the stress-strain relationship $\sigma = B\epsilon^n$ in which σ is stress, ϵ is strain, and B is a constant. This equation did not work either so the situation is more complicated than it appears if work-hardening is really the reason for improved wear resistance. Unfortuantely the

microstructure of the bainite in this study was not characterised so the study is of little use in designing improved rail steels.

Clayton *et al.* (1987) carried out a careful investigation of the wear resistances of nine different bainites with a variety of microstructures. Four sorts of bainitic structure were defined: granular bainite, a carbide-free bainite with interlath martensite and retained austenite, classical upper bainite with interlath carbides, and classical lower bainite with intralath carbides. The nine compositions contained various mixtures of the four types. In general, however, the 0.1 and 0.2 wt% carbon steels had carbide-free microstructures and the 0.3 wt% carbon steels contained a mixture of upper and lower bainites. Pin-on ring wear tests were carried out and it was found that the best bainitic steels had wear resistances which compared favourably with pearlitic rail steels. The relationship between contact pressure and wear resistance was non-linear, implying that at high contact pressures the bainitic steels may outperform the conventional pearlitic rail steels in which the relationship is always found to be linear. The most wear resistant bainite in this study was steel 8, which had a predominantly carbide-free structure, but in general there did not seem to be much correspondence between wear resistance and type of microstructure.

Tensile and fatigue tests were carried out to see what correlation there was between wear behaviour and such properties as ductility, strength, and fatigue limit. There was an unexpected agreement between wear rate and strain level at the fatigue limit but on the whole there was only a weak relationship between strength/hardness and wear resistance. The most significant variable was found to be chromium content but the authors could not explain this in terms of the effect chromium would have on the microstructure. It was suggested that a 4 wt% chromium steel would have excellent wear resistance, fatigue, and impact properties. This would be too expensive for a commercial rail steel.

Devanathan and Clayton (1991) carried out a study on the rolling-sliding wear resistance of bainitic steels. They used three bainites with carbon contents of 0.04, 0.10, and 0.52 wt%. The two low carbon steels had a microstructure which was characterised as carbide-free granular bainite. The 0.52 wt% C steel had a banded microstructure of lower bainite and martensite caused by segregation of chromium, managanese and silicon. This steel had the lowest wear resistance due to the formation of cracks between the bands. The 0.04 and 0.10 wt% C steels showed better wear resistance, with the 0.04 wt% C steel comparing favourably with pearlitic rail steels. Again, the relationship

between contact pressure and wear resistance was non-linear for the bainitic steels. The good wear resistance of the carbide-free bainites was attributed either to their superior work-hardening abililty, or their excellent ductility. The authors suggested that the initial high dislocation density of bainitic steels should play a part, but it is genrally found [Hutchings 1992] that the initial dislocation density plays little part in determining the wear rate. This is because very high strains are introduced into the material during wear testing which negates any effect of previous strain-hardening. This should hold true for the dislocations in bainite as well.

Xu and Kennon (1991) looked at steels of various carbon contents in a pin-on-drum abrasive wear test. Bainite containing 0.75 wt% C was found to have the greatest wear resistance. The microstructure was not characterised so it is hard to say why this bainite performed well. The authors mentioned the theory of Zum Ghar (1987) which states that the greater toughness caused by the retained austenite in the bainitic structure had made it more resistant to abrasion. In this case the abrasive was silicon carbide paper, wheras it is thought that the wear which takes place on rails is a mutual abrasion by soft abrasive particles [Clayton 1996]. Clayton and Devananthan (1992) conducted rolling-sliding wear tests on a Cr-Mo rail steel heat treated to produce different pearlitic and bainitic microstructures. Their bainites were an upper bainite, a lower bainite, and a mixed microstructure containing both types of structure. The lower bainite and the mixed microstructure were superior to pearlite in wear resistance. It was suggested that the better ductility of the bainite had had an effect and also the reduction in volume fraction of carbide in bainite.

Chang (1995) tested four experimental carbide-free bainitic steels under rolling-sliding conditions. Two of the steels had purely bainitic microstructures, one contained some allotriomorphic ferrite, and one had a martensitic matrix with large amounts of allotriomorphic ferrite. One of the carbide-free steels performed extremely well. The good wear resistance of the carbide-free bainites was attributed to their high retained austenite content, high strength, and high toughness.

Wang and Lei (1996) tested a high carbon steel (steel 1080) in pure sliding wear after various heat treatments to produce spheroidised, pearlitic, bainitc, and martensitic microstructures. The lamellar pearlitic microstructure showed the best wear resistance under all comditions from mild to very severe wear. The bainitic steel showed the second-best wear resistance, but its microstructure was not characterized in detail. They related their results to the energy consumed during sliding and found that the microstructures

which absorbed the most energy per unit volume of wear debris had the lowest wear rates. They suggested that for good wear resistance, a material should have a high work-hardening coefficient.

Clayton and Jin (1996), and Jin and Clayton (1997) carried out rolling-sliding wear tests on various low-carbon bainitic steels in as-rolled, air-cooled, and water-quenched conditions. Their microstructures were carbide-free bainite, granular bainite, and lower bainite. They found that carbide-free bainites had superior wear resistance to the carbide-containing lower bainite. Wear resistance was seen to increase with carbon content and cooling rate, which also increased the proportion of carbide-free bainite. The effect of the inter-lath retained austenite was unclear. They observed that bainitic steels usually showed superior wear resistance to pearlitic ones when tested under high strain conditions, and suggested that better work-hardening ability in the bainites might be the reason.

Shipway *et al.* (1997) carried out sliding wear tests on a medium carbon steel heat-treated to produce different bainitic, martensitic, and normalised microstructures. These were wear tested in a pin-on-disc machine. The most wear resistant bainitic steel had a very fine, carbide-free, upper bainitic microstructure with very little martensite present. This sample also showed a higher toughness than the microstructures containing more martensite. Its wear resistance was comparable with that of the normalised, pearlitic microstructure. They suggested that the toughening effect of the retained austenite and the extreme fineness of the bainitic microstructure conferred its good wear resistance by preventing the formation of wear particles by micro-fracture.

The role of retained austenite in influencing the wear resistance of bainite is rarely mentioned in the literature but two studies on the wear resistance of cast iron [Zhou and Zhou 1993 and Luo *et al.* 1995*] indicate that wear resistance goes up with increasing retained austenite content. It is suggested that this is because of the effect of the austenite on work-hardening. However, another study [Boutorabi *et al.* 1993], indicated that work-hardening of retained austenite, *i.e.* the degree to which austenite transformed during wear, had little effect on the wear resistance. Increasing the volume fraction of retained austenite, and thus increasing the work-hardening, did not compensate for the overall initial softening of the microstructure caused by increasing the austenite content.

* These are not included in the table of experimental compositions because they are bainitic cast irons rather than rail steels

From this it can be concluded that the wear resistance of bainite seems to be related to its ability to work-harden, but not in a simple way. The size and distribution of carbides is also important. Wear resistant bainites often have lower carbon contents than typical, pearlitic, rail steels, and carbide-free bainites have shown excellent wear resistance. It would be interesting to look at the wear resistance of bainites with different carbide distributions. The effect of the distribution of retained austenite in low-carbon bainites would also be worth investigating. The surprising correlation of wear resistance with fatigue properties should be examined further as this type of wear seems to proceed by an abrasive rather than a fatigue mechanism. Bainite does not seem to have been investigated as a possible tyre material as all the studies mentioned here used a pearlitic tyre as the other material in the wear couple.

2.7.1.3 Martensite

Relatively little work has been done on the wear resistance of martensite in the context of rails as opposed to bainite. In general martensite has been found to have a lower wear resistance than pearlite and sometimes lower than bainite.

Masumoto *et al.* (1982) looked at head-hardened martensitic rails for wear resistance. These turned out to be less good than as-rolled pearlitic rails and head-hardened pearlitic rails, but no attempt was made to examine the worn microstructure to find out why. Ichinose *et al.* (1978) included tempered martensite in their study of wear resistance. These samples had a typical rail steel composition and were heat treated to produce a martensitic structure, then tempered to hardnesses in the range of 260-360 HV. These samples were found to have a wear resistance intermediate between that of pearlite (best) and bainite (worst). There was a linear relationship between hardness and weight loss for all structures in this study. The worn microstructure was examined by transmission electron microscopy and it was seen that the distribution of carbides in the worn layer was much coarser in the martensite and bainite than the pearlite. It was suggested that these coarse carbides detach more easily, leading to higher wear rates. It was not explained why bainite behaved differently from martensite.

Kalousek *et al.* (1985a) included tempered martensite in their extensive study of the wear behaviour of rail steels. They heat-treated a Cr-Mo rail steel to produce varying microstructures. The martensitic structure wore the most, although wear rate decreased with increasing hardness. The worn layer in the martensite was softer than those in the pearlite and more cracks were observed in this layer. The cementite in the martensitic

struture was observed not to deform, so preventing the surface layer from adapting in the way that pearlite does under wear.

Xu and Kennon (1991) studied the abrasive wear of steels, including tempered martensite, in a pin-on-drum machine. Their martensites had between 0.38 and 1.2 wt% carbon and were tempered to a variety of hardnesses. The usual relationship between wear resistance and hardness in steels, *i.e.* a linear but not proportional relationship between the two, was found. They explained the higher wear resistance of bainite as compared to martensite by the fact that there is more retained austenite in the bainitic structure [Zum Ghar 1987]. They also suggested that the mean carbide spacing should affect the wear resistance in a similar way to that of pearlite; *i.e.* wear resistance should be proportional to $\lambda^{-1/2}$ where λ is the mean carbide spacing or mean free path in ferrite. Microcracks in the martensite were also blamed for its poor wear resistance compared to bainite. This was especially true for the high carbon structures.

2.7.2 Microstructure and rolling contact fatigue resistance

Little work has been done on the effects of microstructure on rolling contact fatigue as opposed to wear. Almost all of this work has concentrated on pearlitic rails. This is possibly because it has been less important to investigate rolling contact fatigue, as it is known that the shell defect is initiated by oxide inclusions and can be supressed by using making cleaner steel, and the head check and squat defects have been a comparatively recent cause for concern compared to the problem of rail wear.

2.7.2.1 Pearlite

Studies on the rolling contact fatigue resistance of pearlite have been carried out by Masumoto *et al.* (1978, 1982), Kalousek *et al.* (1985b), Clayton and Hill (1987), Garnham (1989), Dikshit and Clayton (1992), and Beynon *et al.* (1996).

Masumoto *et al.* (1978, 1982) carried out wear and rolling contact fatigue tests on several microstructures to determine which was the best for premium rails. A fine, head-hardened, pearlitic structure was shown to have the longest rolling contact fatigue life when tested in track and in the laboratory. No investigation into the changes taking place in the microstructure was undertaken.

Kalousek *et al.* (1985b) carried out rolling contact fatigue tests on a sophisticated testing machine designed to simulate the behaviour of wheels in curves. Samples were run for a fixed number of revolutions and the number and length of cracks which had formed were measured. Several different lubricants were used during the testing period.

A range of microstructures was tested, including a bainitic sample. The results for the pearlitic samples were inconclusive.

Clayton and Hill (1987) carried out a systematic testing program on a twin-disc wear machine using a variety of creepages, contact stresses, surface roughnesses, and lubricants, in order to develop a standard method of laboratory rolling contact fatigue testing. Reproducibility tests were also carried out. Their test material was a standard rail steel, run against standard tyre steel. The tests were stopped when pitting or collapse of the running track occurred. The rolling contact fatigue life was measured in cycles to failure of the rail. Metallographic examination of rails stopped at various fractions of the rolling contact fatigue life showed that cracks started to appear between 25 and 50% of the life, so the test involved both initiation and propagation of cracks.

They showed that surface roughness only had an effect below an R_a (average surface roughness) value of $0.5\mu m$ with water lubrication and 2% creepage. The effects of different lubricants produced interesting results: glycerol prolonged the rolling contact fatigue life compared to water. Graphite and molybdenum disulphide produced no failures even after 1,500,000 cycles. This confirms that rolling contact fatigue can only take place in the presence of a lubricant which can penetrate the crack and cause Mode I growth by pressurizing the tip. Experiments at different contact stresses at four different creepages produced power law relationships between pressure and life, but the exponent varied with the creepage from -1.8 at 0.3% to -4.2 at 5 and 10%. There was an interesting effect of creepage on rolling contact fatigue life at constant stress; the life was highest at zero creepage (no sliding), dropped to a local minimum at 0.3% then rose again to another peak at 1%. After this, life dropped steadily to a minimum at 5% creepage and remained constant thereafter. These results were not reproduced by Garnham (1989), who carried out studies into rolling contact fatigue initiation using an eddy-current method to detect the appearance of cracks too small for the eye to see. The tests were carried out with water lubrication on the same rail and tyre steels as Clayton and Hill. The relationship between cycles to initiation and contact pressure was found to be a similar power law, but with an exponent of -3.7. The results would not necessarily be expected to be the same as the previous tests involved propagation as well as initiation.

Dikshit and Clayton (1992) investigated pearlitic rails with a variety of interlamellar spacings run against a standard rail steel. They looked at different contact pressures at

a creepage of 10% and stopped the tests when visible pitting or spalling occurred. They found a linear relationship between rolling contact fatigue life N and contact pressure:

$$N = mp_0 + D \tag{2.29}$$

where m and D are constants which depend on the material hardness, and so on the interlamellar spacing. Harder steels increased rolling contact fatigue life. However this relationship did not explain all the variation seen in the results. It also has the fault that it predicts negative life for large contact pressures. It was suggested that a power relationship would be more appropriate over a wider range of contact pressures.

Beynon *et al.* (1996) investigated three different pearlitic rail steels using the same eddy-current method as Garnham; two naturally hardened rails and and a head-hardened rail, run against a standard wheel steel. The tests were at contact pressures of 1200-1800 MPa and creepages of up to about 6%. Tests were carried out to determine the effect of creepage, microstructure, and pressure on rolling contact fatigue life. It was found that the contact pressure had a large effect on crack morphology. At 1800 MPa, single, unbranched cracks were seen. These grew at a shallow angle to the surface while in the plastically deformed zone and then turned down towards the centre of the disc. At the lower contact pressures the cracks tended to form branched networks.

The effect of creepage on rolling contact fatigue life was not clear due to the scatter in the data, but life seemed to increase with creepage up to about 2.5% and then decrease. At low creepages there was an approximately linear relationship between rolling contact fatigue life and contact pressure similar to that found by Dikshit *et al.* (1991). The hardest steel was found to have the best rolling contact fatigue resistance. Interestingly, it was suggested in this paper that there is a perception at British Rail that head-hardened rails have inferior rolling contact fatigue resistance compared with ordinary rails. However, in Clayton's very useful review of rail-wheel contact (1996) it is stated that no convincing evidence for this belief has been found.

It seems that there is general agreement that head-hardened rails have the best rolling contact fatigue resistance. There appears to be a power-law relationship between contact pressure and life, although the value of the exponent is not certain. The effects of creepage on rolling contact fatigue life are not clear. This is an important point to investigate further as creepage on real railways only reaches a maximum of 3% in curves, but a lot of the work reviewed here involved much higher creepages and so may not be applicable to real situations. No real explanation has been given as to the reasons for

the improved rolling contact fatigue life of finer pearlites except the increase in strength. It would probably be beneficial to examine the literature on pearlite in ordinary fatigue testing to see what effect different microstructures have under those conditions.

2.7.2.2 Bainite

Even less work has been done on bainite than on pearlite in the context of rolling contact fatigue. The work of Masumoto *et al.* (1978, 1982) concluded that a fine pearlitic microstructure was better than either bainite or tempered martensite in laboratory and track tests, but did not give any reasons why. Kalousek *et al.* (1985b) included a nodular graphite cast iron with a bainitic matrix in their investigations. This had a hardness in the middle of the range of pearlitic steels it was compared with. Surprisingly, it showed the least fatigue cracking and the smallest plastically deformed layer in tests which were run for a fixed number of cycles. Again, no microstructural explanation was given for this effect.

The recent work of Su and Clayton (1996) on low carbon bainitic steels and pearlitic rail steels involved rolling contact fatigue tests at pressures from 850-2300 MPa and a creepage of 10%. They tested a carbide-free bainite, a lower bainite, and a granular bainite. The tests were stopped when the running surface collapsed or spalled, so the total life involved both initiation and propagation stages. For each steel, a power law relationship was found between contact pressure and life. The carbide-free bainitic steel had the best rolling contact fatigue resistance and the standard pearlitic steel the worst. The rolling contact fatigue resistance was observed to scale with yield strength. When rolling contact fatigue life was plotted against normalised contact pressure (p_0/k_e where k_e is the shear yield stress*), the data seemed to lie on a single curve, or possibly a bilinear relationship with a 'knee' at $p_0/k_e = 4$ which is the theoretical shakedown limit. A change in crack morphology was noticed above $p_0/k_e = 4$. Cracks rarely branched above this value, whereas below it networks of branched cracks were observed.

It seems that much more work needs to be done on the rolling contact fatigue resistance of bainitic steels before any clear picture emerges. So far it seems that the higher strengths of bainitic steels may improve the fatigue resistance irrespective of microstructure but this is not yet certain.

* In the literature k is the standard symbol for both wear constant and shear yield stress. To avoid confusion k is here kept for wear constant and k_e used for yield stress

2.8 Concluding remarks

Wear is still a problem in rails but rolling contact fatigue is also now a cause for concern. Improved rail steels must have good rolling contact fatigue resistance as well as wear resistance. Surface initiated defects such as the head check and the squat are the main fatigue problems which must be overcome. More work needs to be done on the microstructural characteristics which impart good rolling contact fatigue resistance, particularly in the bainitic steels which are under consideration as wear resistant grades of rail. Little work has been done in this area, and no really systematic evaluation of bainite or martensite has been made. An investigation of the literature which exists on conventional fatigue in these microstructures could also be useful here.

Wear is still a very difficult process to model although the characteristics of a good wear resistant rail steel appear to be a reasonably high hardness, and a high work-hardening rate which enables the near-surface microstructure to adapt under rolling-sliding contact conditions into a very hard, wear resistant layer. This is probably not the full explanation and more work should be done where bainite and, particularly, tempered martensite are concerned. The carbides in upper bainite seem to have a deleterious effect on the wear resistance which overcomes the advantages of increased hardness and work-hardening rate.

Bainitic rail steels offer interesting possibilities as the next generation of premium rail steels but more work needs to be done to find out why some bainites are better than pearlite and some are not. Track trials are needed as most of the work so far has only taken place in the laboratory. These, in combination with more laboratory work, should enable the development of new premium rails with non-pearlitic microstructures.

3

Worn surfaces and wear debris in bainitic rail steels

In the present work, rolling-sliding wear tests have been carried out on a promising carbide-free bainitic steel to investigate the mechanism of wear and so to discover the mechanical properties important for good wear resistance in this new microstructure for rails.

3.1 Experimental Methods

3.1.1 Wear Tests

Rolling-sliding wear tests were carried out at Swinden Technology Centre under a contact stress of 750 MPa and a creepage (ratio of sliding distance to rolling distance) of 25%. The contact stress was calculated from Hertz's equations for two elastic cylinders in contact (see Chapter 2 equations 2.1 to 2.9). The wear rate was measured as mg of mass lost per metre of sliding distance after a total of 135 m sliding distance. Before measurements began the samples were broken in by running them against each other until the surfaces looked evenly worn. Wear tests were carried out on conventional mill heat-treated (MHT) pearlitic steel, a martensitic steel, and carbide-free bainite (called Bainite 1) against a standard pearlitic tyre steel. Similar tests were carried out with tyres made out of bainite with different hardness values. These other bainites (Bainites 2 and 3) are not being investigated as rail steels in this work; they were used because they had convenient hardness values. The compositions and hardness data for the steels are shown in Table 3.1, and the results of the wear tests in Table 3.2.

Some special wear tests were also carried out: a MHT and another experimental

bainitic rail steel (Bainite 4) were tested against standard tyres at a creepage of 3% in an attempt to better simulate conditions on real track. It proved impossible to get an even wear pattern in these tests. A sample of the original bainitic steel that had been tempered at 500 °C for one hour in order to induce carbide precipitation was also tested against the standard pearlitic tyre steel.

Wear debris was collected from the tests numbered 900 and up; see Table 3.2 for details.

	Composition wt%										
Steel	C	Si	Mn	P	S	Cr	Mo	B	Al	Ti	N
MHT	0.76	0.25	0.85	0.015	0.014	-	-	-	-	-	-
Martensite	0.18	0.39	1.33	0.010	0.013	0.33	0.33	0.0023	0.018	0.028	0.0079
Pearlite	0.57	0.19	0.64	0.021	0.011	0.26	0.06	-	-	-	-
Bainite 1	0.21	1.97	1.98	0.013	0.015	0.48	0.47	0.0026	0.030	0.036	0.0082
Bainite 2	0.22	2.06	2.12	0.023	0.016	2.01	0.50	-	-	-	-
Bainite 3	0.22	1.97	2.00	0.014	0.013	0.49	0.24	0.0013	0.025	0.023	-
Bainite 4	0.27	1.86	1.98	0.014	0.015	0.50	0.59	-	0.007	-	-

Table 3.1: Compositions of wear samples

3.1.2 Wear Surfaces of Laboratory Samples

The wear debris collected from tests in the 900 series was mounted on aluminium stubs and examined in a JEOL 820 scanning electron microscope at 20 kV. The surfaces of the samples in the 800 series were examined and photographed using a CamScan S2 scanning electron microscope at 20 kV.

3.1.3 X-Ray Diffraction

The wear debris collected from each test in the 900 series was ground up in a pestle and mortar and examined on a vertical powder diffractometer. Samples 943, 942, and 938 were mounted in a standard sample holder but packed carefully from the back to reduce potential problems with orientation. The remaining samples were too small to fill the holder, and contained relatively few particles even after grinding. These were mounted on a silicon substrate on a rotating sample holder. Sample 943 was re-examined in the rotating sample holder to investigate some differences observed between the two types of holder. The samples were all scanned between 30° and 100° 2θ with a step size of 0.04° and a dwell time of 2 s at each point. The values of 2θ were chosen to include the peaks expected from α-iron, γ-iron, Fe_2O_3, and Fe_3C.

	Rail			Tyre		
Test Number	Type	Hardness HV	Wear rate $mg\,m^{-1}$	Type	Hardness HV	Wear rate $mg\,m^{-1}$
815	MHT	359	36.29	Pearlite	229	89.40
858	Martensite	412	40.37	Pearlite	236	76.66
865	Bainite 1	422	5.33	Pearlite	237	10.37
870	Bainite 1	407	1.70	Bainite 1	421	1.40
871	MHT	362	0.15	Bainite 1	428	0.66
932	MHT	420	0.22	Bainite 3	397	1.18
933	MHT	391	0.22	Bainite 1	420	0.59
934	MHT	401	0.07	Bainite 2	461	0.22
938	MHT	391	1.26	Pearlite	255	8.00
941	Bainite 1	418	1.11	Bainite 1	418	0.96
942	Bainite 1	398	6.37	Pearlite	253	1.18
943	Martensite	401	31.25	Pearlite	247	66.14
927*	Bainite 4	408	0.37	Pearlite	241	0.96
961†	Bainite 1	412	6.15	Pearlite	244	10.37
962*	MHT	357	0.07	Pearlite	248	0.89
-	Bainite 1	411	2.89	Pearlite	232	6.30

Table 3.2: Wear Tests Tests marked * were carried out at 3% creepage. The test marked † was done with bainite that had been tempered for one hour at 500 °C to induce carbide precipitation.

An undeformed piece of a bainitic rail was also examined in the diffractometer. The sample was prepared by polishing to a 1 μm finish and then etching with 2% nital to remove any remaining deformed layer. this sample was scanned between 45 and 125° 2θ in order to get several non-overlapping retained austenite peaks for analysis; these results are reported in Chapter 7.

Wear couples consisting of two different steels from the 800 series of tests were mounted on aluminium stubs and examined in a JEOL JSM 5800LV scanning electron microscope at 20 kV. EDX (energy dispersive X-ray) analysis was carried out to discover if the surface composition was different from that of the bulk. Five randomly chosen areas on each sample were analysed for silicon, manganese, chromium, and molybdenum, and the results averaged.

3.1.4 Surface hardnesses of laboratory wear specimens

Microhardness gradients were measured on the laboratory wear specimens from the worn surface into the bulk. In order to get a sufficient number of accurate readings, taper

sections of the samples were prepared. This was done by mounting the specimen in "Transoptic" mounting material, with a small cylindrical object parallel to it, placing the mount into a special holder which angled the surface at 20° and surface grinding through the sample, Figure 3.1. The precise angle cut was measured by photographing the elliptical shape made by the cylinder and taking the ratio of its semi-major and minor axes. The cylinders were made out of the ends of 1 mm twist drills.

The samples were then knocked out of the Transoptic and the drill discarded. The samples were nickel-plated for edge retention using the Watts Bath [Lowenheim 1974] with a current density of 70 $\mathrm{mA\,cm^{-2}}$ for 30 minutes, and then remounted in Bakelite. They were polished using the trailing edge method [Samuels 1967]. Errors in the taper angle introduced by polishing are estimated to be $\pm 1°$. The samples were polished and etched with 2% nital for metallographic examination before the microhardness gradients were measured. This was done on a Mitutoyo microhardness machine with a load of 50 g. Five readings were taken at each depth and averaged. The samples were also etched and photographed to show the microstructure.

3.1.5 Identification of carbides

In order to prove that there was carbide precipitation in the tempered bainite, carbon extraction replicas were made from the steel and examined in a JEOL 200CX transmission electron microscope (TEM). The replicas were made by polishing the steel down to a 1 μm finish and then etching it lightly with 2% nital. A carbon film was then evaporated onto the surface. The film and the carbides attached to it were separated from the steel by electrolytically dissolving the steel surface in a solution of 20% hydrochloric acid in methanol at a D.C. voltage of 3 V. Less concentrated solutions were also tried but were ineffective.

The diffraction patterns obtained from the carbides were analysed to identify the carbides present. Lattice parameters and structures of the possible carbides were taken from Bhadeshia (1992) for comparison with the diffraction patterns. The camera constant for the diffraction patterns was obtained by analysing a diffraction pattern from a gold film which consisted of very fine crystals, producing a diffraction pattern of rings. Knowing the lattice parameter of gold it is possible to calculate the camera constant for each ring. The average of the values from all the rings was used to get good accuracy. The camera constant was calculated to be 34.2 mm Å.

Some experiments were also carried out to discover whether the samples of experi-

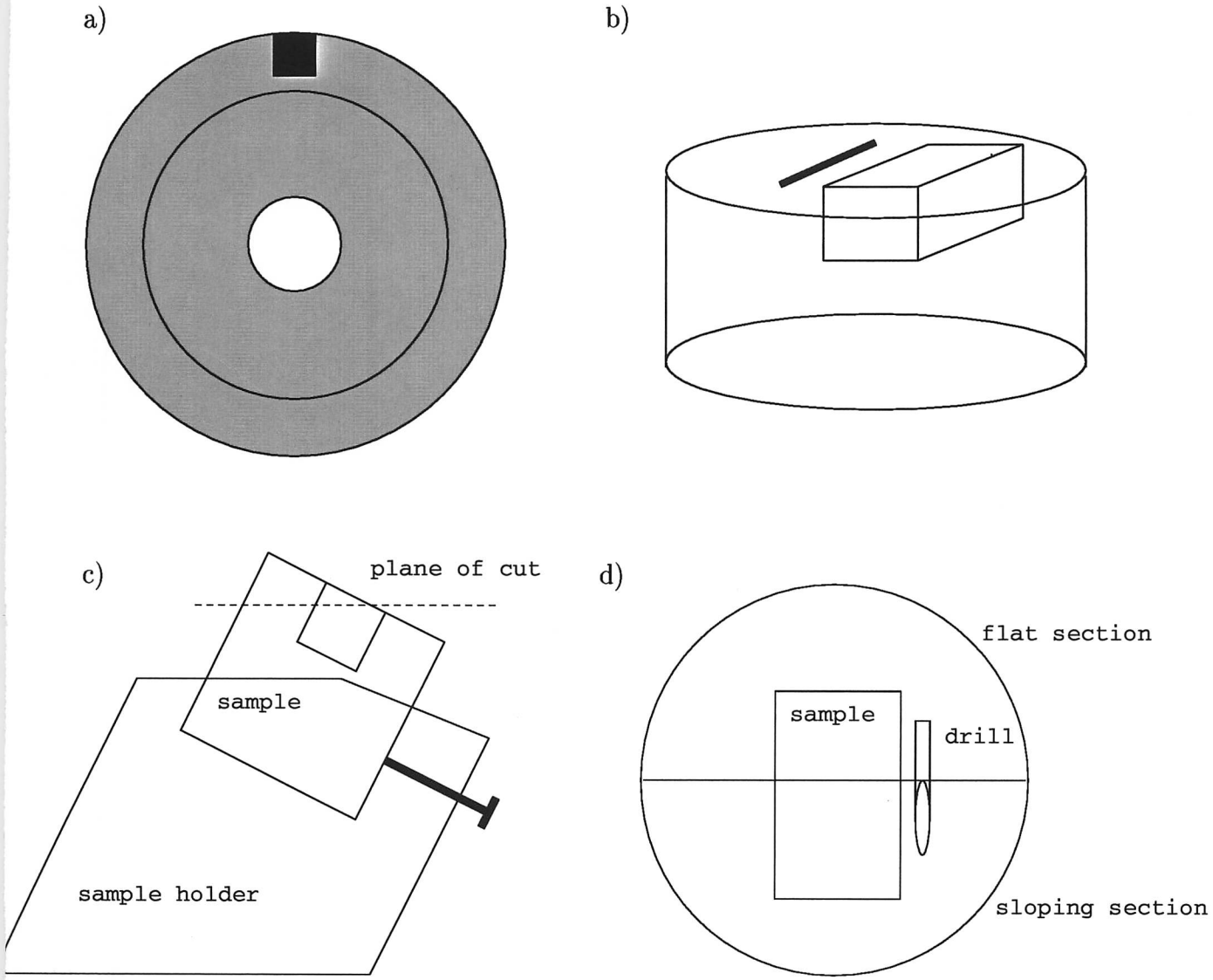

Figure 3.1: Making taper sections
a) Location of sample within wear wheel
b) Sample mounted in Transoptic with drill
c) Sample placed in special holder to be ground at an angle of 20°
d) Ground sample showing elliptical wire section used to measure precise angle

mental martensitic rail contained carbides. The hardness of the martensite was measured and then a sample was reaustenised at 1000 °C for one hour and quenched into water. The hardness was measured again. The original sample had cooled at approximately $0.1\,^{\circ}\mathrm{C\,s^{-1}}$. If there was an increase in hardness then the original sample had probably auto-tempered and hence would contain carbides.

3.2 Results

3.2.1 Wear Tests

The wear rates measured in each test are shown in Table 3.2 for completeness; interesting results are plotted in Figure 3.2(a)-(c).

When three different rails are run against ordinary pearlitic tyre steel, the bainitic rail has a much lower wear rate than the MHT or martensitic rail, although the hardnesses of the martensite and bainite are comparable. The bainitic rail also leads to a lower wear rate on the pearlitic tyre. The plot of MHT rails run against bainitic tyres of different hardnesses (Figure 3.2 (b)) shows that a harder bainitic tyre also dramatically reduces the wear rate on the rail and tyre. It seems as though rail wear is very dependent on the hardness and microstructure of the counterface as well as of the rail itself. The results of test 938 are also interesting when compared with 815; both tests involve an MHT rail run against a pearlitic tyre, but the MHT rail in 938 has been heat-treated differently to produce a harder microstructure than typical MHT, though it is not as hard as some of the bainites tested. The pearlitic tyre which froms the other half of the wear couple is also harder than in test 815. The wear rate for this rail drops below that for a bainitic rail run against a pearlitic tyre although the tyre wear rate is higher than than for a bainitic rail run against a pearlitic tyre of the same hardness (test 942).

British Steel Swinden Laboratory indicated that the error in the wear rates was about $3\,\mathrm{mg\,m^{-1}}$ from previous experience with repeated tests.

From the above results it seems that the properties of the tyre roller may have more effect on the wear rate than those of the rail roller; however it is clear that the hardness of both does matter.

The tempered bainite (test 961) compared with one of similar hardness (no test number provided) in Figure 3.2 (c), shows a higher wear rate. The TEM observations of this steel showed that it did contain carbides and that they were η-carbide. A picture and diffraction pattern are shown in Figure 3.3(a) and (b). Carbide precipitation would be expected to lower the toughness of the rail [Bhadeshia 1992]. Since the wear rate of the tempered rail is higher than that of a rail of the same hardness, but presumably higher toughness, it would seem that toughness is important for wear resistance in rails. This makes sense because the wear rate is measured as mass loss per unit sliding distance; particles would break off the wear surface from a brittle material more easily. A tougher material would be more resistant to particle fracture.

The martensitic rail had an original hardness of 412 HV but after reaustenising and quenching its hardness was 455 HV. This implies that auto-tempering had occured during the original slow cooling and hence that the steel that was wear tested contained carbides.

The preceding observations lead to the conclusion that the hardness of the rail and tyre is very important, although not the only variable of interest. Since tyres are usually made of much less sophisticated steels than rails, it would seem logical to try to improve tyre steels, which would be relatively easy, than to improve the rail steels which are almost at the limit of their wear resistance in the pearlitic grades, hence the need to study alternative microstructures such as bainite and martensite. However there are certain problems with tyres that mitigate against using more sophisticated steels: the need to avoid the formation of localised areas of martensite through the intense frictional heating and subsequent rapid cooling that can occur if the wheels lock and slide. Higher carbon pearlitic steels are more hardenable and so more likely to form martensite.

3.2.2 Wear surfaces of laboratory samples

Macrographs of the surfaces of laboratory samples are shown in Figure 3.4 and SEM micrographs of the features in Figure 3.5.

It can be seen from the macrographs that the rails run against bainitic tyres (870R and 871R) have much smoother surfaces and that the difference when run against pearlitic tyres (815 and 865) is more marked than that between bainitic and MHT rails (compare MHT rail 815 with bainitic rail 865 for example). Similar observations were made for the tyres.

When looking at the SEM micrographs it should be noted that the more interesting features of the smoother samples were photographed and are not typical of the surface as a whole which contained large featureless regions. In general the laboratory samples show shallow craters which may have produced plate-shaped wear particles, and evidence of plastic flow. Some of them (sample 815T in particular) show evidence of material transfer. This particular test involved particularly soft pearlite against ordinary MHT steel and so would be expected to show high adhesion. The wear surfaces appear to correspond to what Boulton and Clayton defined as "Type III wear" which Clayton and Danks (1987) and Zakharov *et al.* (1998) considered to be the type of wear usually seen on the gauge face of rails in curves.

The laboratory samples from the 800 series which were analysed by EDX gave vary-

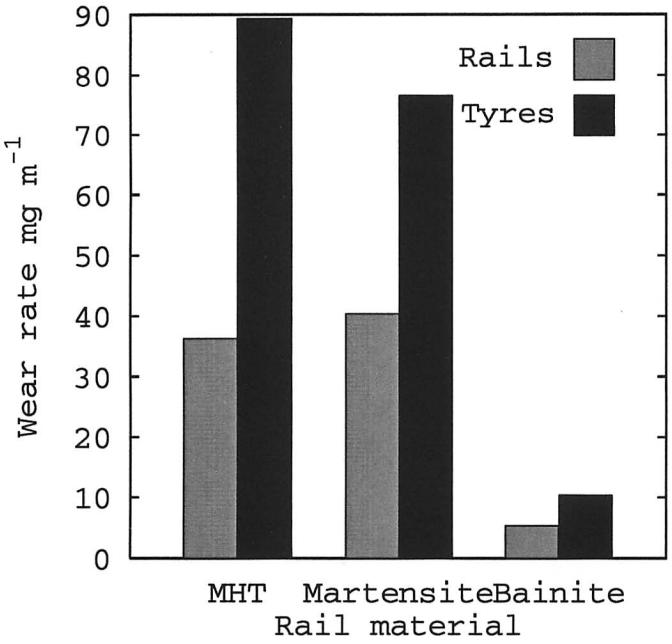

Figure 3.2(a): Wear rates for three different steels All of these samples were run against pearlitic tyres

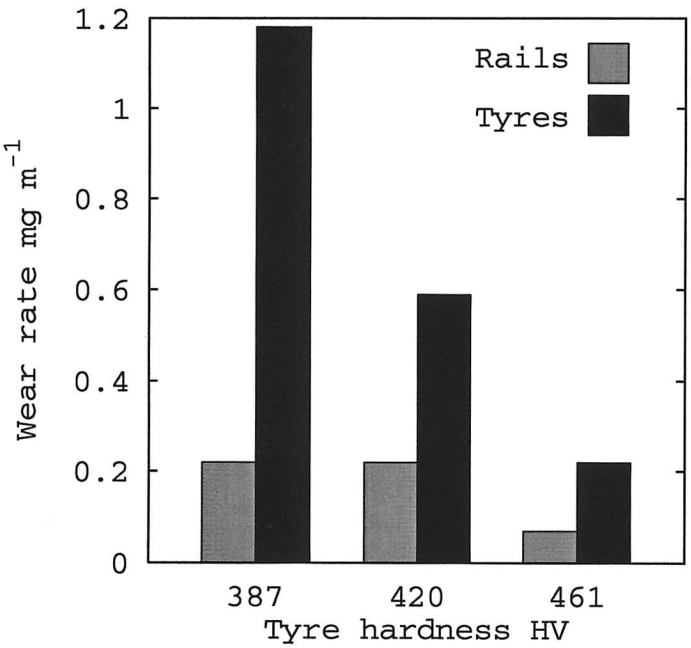

Figure 3.2(b): Wear rates for three different tyres All tyres were run against MHT rails. Note the difference in scale on the y-axis between this and the previous graph.

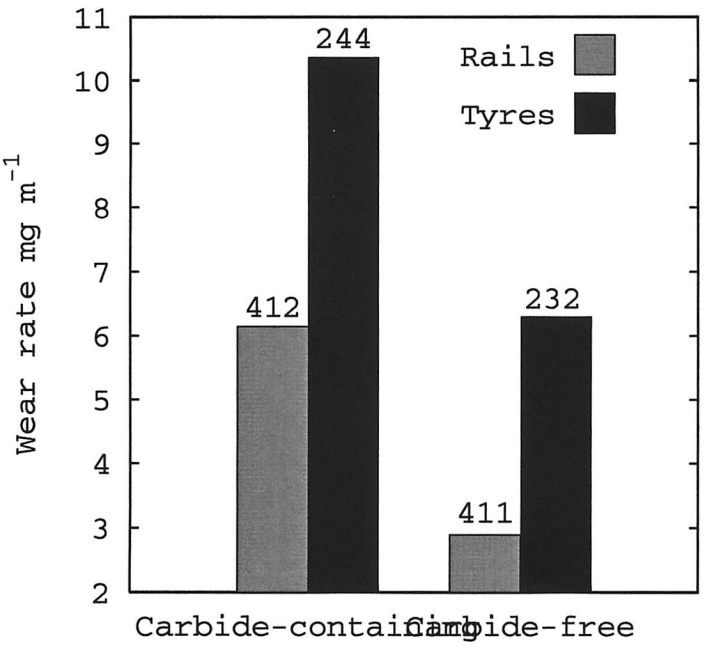

Figure 3.2(c): Effect of carbides on wear rate The carbide containing sample is Bainite 1 tempered at 500 °C for one hour; the carbide-free sample is an untempered bainite of a similar hardness

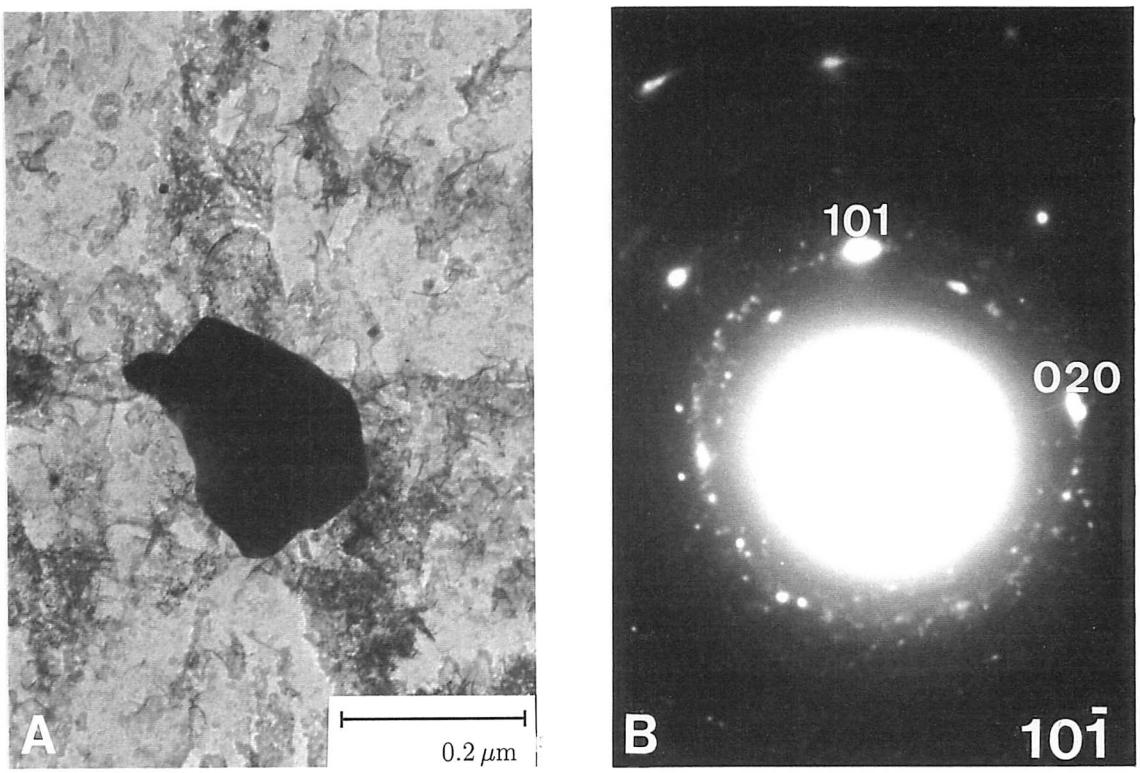

Figure 3.3: Carbides found in tempered bainite (a) Bright field image of carbide
(b) Diffraction pattern from carbide, identified as η-carbide. This has an orthorhombic lattice; $a = 4.704$ Å, $b = 4.318$ Å, and $c = 2.830$ Å

ing results which are plotted in Figure 3.6. Nevertheless, a few conclusions can be drawn. In the case of test 858, the tyre appears to have gained material from the rail but not *vice versa.*

This is in contrast to test 865 where the rail appears to have possibly gained a little material, though this is not certain as only the silicon result suggests it. The tyre has gained a lot of material from the rail. In test 871 the rail has definitely gained material from the tyre and the tyre appears to have gained a little from the rail, although again only the silicon result suggests this.

In all of these results, the softer partner in the wear couple is seen to gain material at the expense of the harder. This is puzzling because simple adhesion theory states that the hard material should gain bits of the softer material; junctions are formed between the two and broken in the softer material, bits of which then end up attached to the harder one. A possible explanation is that if wear particles are being formed by other means, they may be more likely to reattatch to the softer wheel due to the greater likelihood of adhesion with a softer material. Simple adhesion between the rollers will lead to material transfer rather than the immediate formation of wear particles. A transfer layer of mixed material will be built up on both surfaces and bits of this will eventually become detached and form wear particles.

3.2.3 Wear debris

Photographs of typical wear debris from the 900 series of tests are shown in Figure 3.7.

Only one picture is shown because all wear tests were found to produce identical particles; plate-shaped with the long diameters in the range 20–200 μm. The short diameters often appear to be $< 5\,\mu$m. Many of the particles appear to consist of several layers; this may be due to the presence of many cracks within them, or several particles having become attached to each other and consolidated into one. When the mechanism of wear changes the effects are often seen in the shape of the wear particles; these results therefore strongly suggest that the same wear mechanism is occurring in bainitic and pearlitic samples. Hence it should be possible to use the same interpretation for both cases.

The X-ray diffraction carried out on the wear samples showed them to consist wholly of α-iron. No iron oxide or carbides were found, nor any retained austenite. This does not mean that there was never any retained austenite in the microstructure; it is likely to have transformed during the enormous deformation the particles will have undergone.

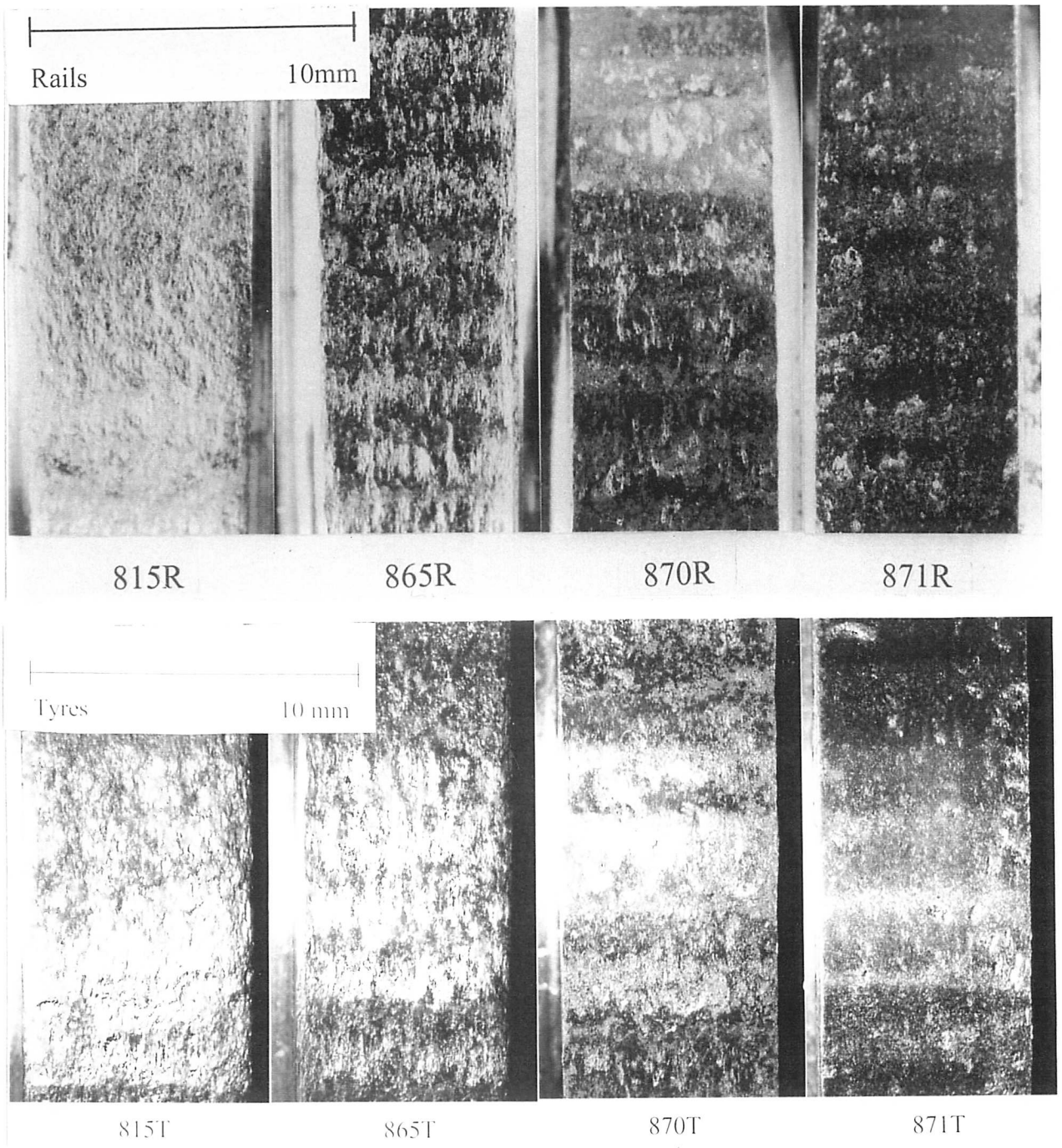

Figure 3.4: Surfaces of laboratory wear samples.

Test 815: MHT rail; pearlitic tyre. Both surfaces are very rough.

Test 865: Bainitic rail; pearlitic tyre. The tyre is similar to the previous test but the rail surface is much smoother.

Test 870: Bainitic rail; pearlitic tyre. Both rail and tyre are noticeably smoother than the previous test, especially the rail on which only isolated craters can be seen.

Test 871: MHT rail; bainitic tyre. The rail and tyre are even smoother than the previous test.

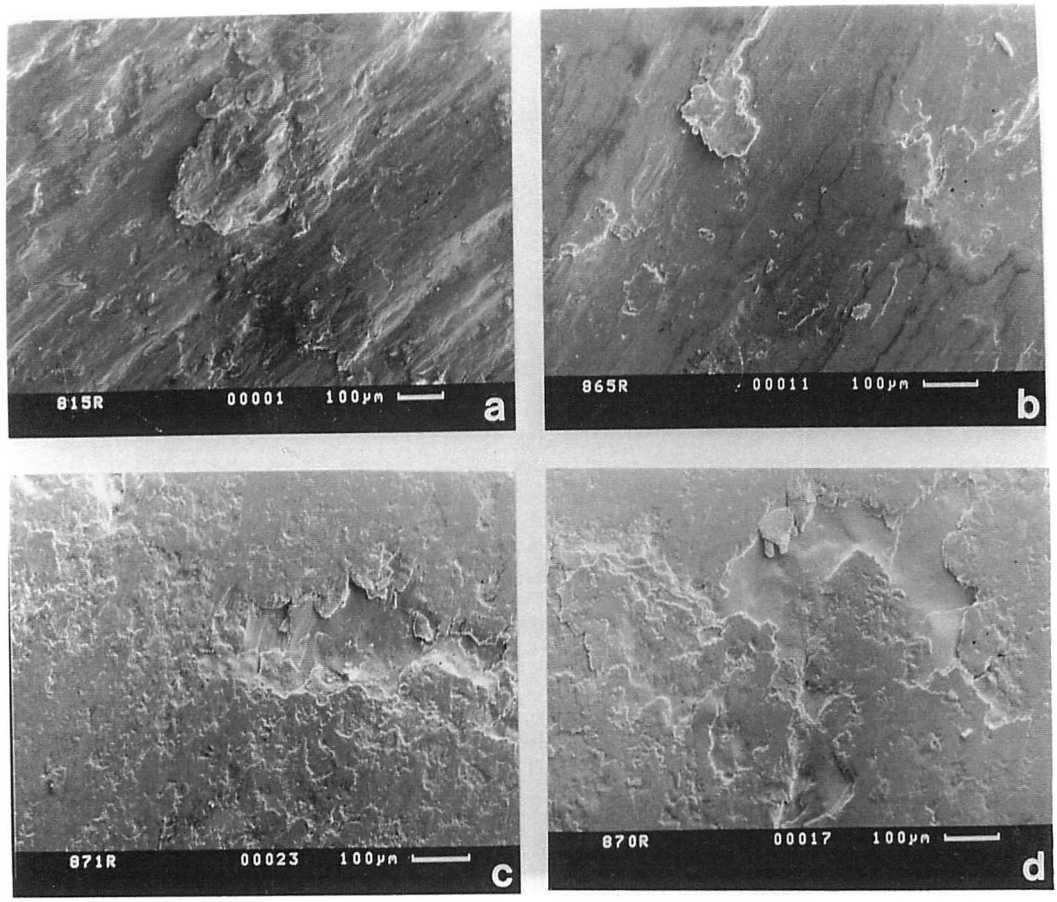

Figure 3.5(a): Surfaces of laboratory rail wear samples

a) MHT rail run against pearlitic tyre. The surface shows evidence of plastic flow. The layered appearance with high and low spots suggests that material transfer between rail and tyre is taking place

b) Bainitic rail run against pearlitic tyre. The surface is smoother than the previous specimen but the same type of features are present.

c) MHT rail run against bainitic tyre. This micrograph is of an interesting region on a mainly smooth surface. Some plastic flow and material transfer can be seen.

d) Bainitic rail run against bainitic tyre. Again this is an interesting region from a mostly smooth surface. Some plastic flow and material transfer can be seen.

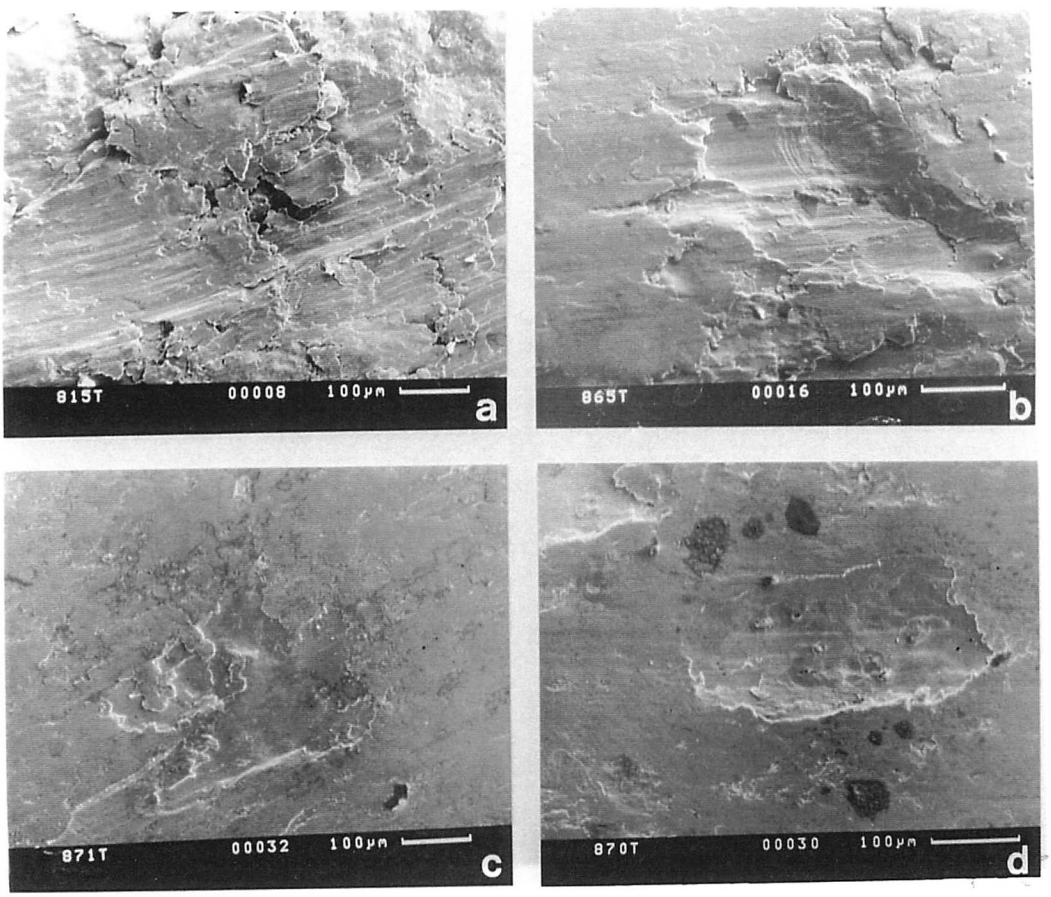

Figure 3.5(b): Surfaces of laboratory tyre wear samples

a) Pearlitic tyre run against MHT rail. A large amount of plastic flow and material transfer can be seen on this sample.

b) Pearlitic tyre run against bainitic rail. This is an interesting region on a mostly smooth surface. There is some evidence of material transfer and plastic flow.

c) Bainitic tyre run against MHT rail. An interesting region on a mostly very smooth surface. There has been a little material transfer.

d) Bainitic tyre run against bainitic rail. Again an interesting region on a very smooth surface. There has been a very small amount of material transfer.

a) 858R

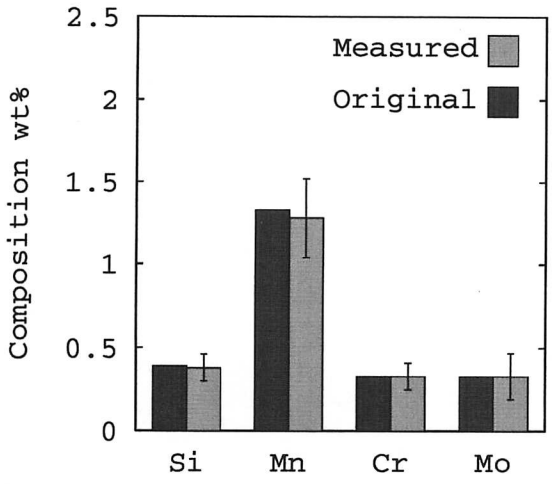

b) 858T

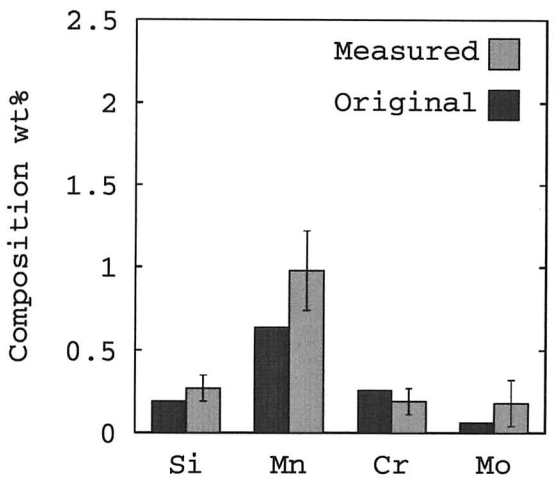

c) 865R

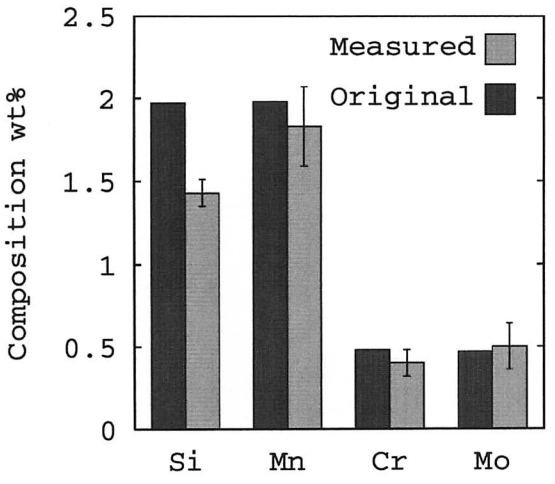

d) 865T

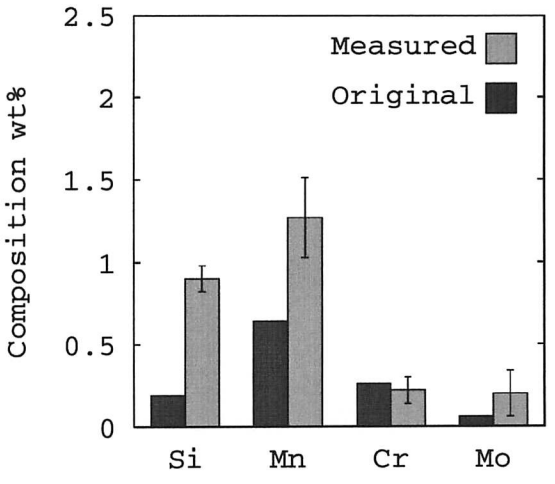

Figure 3.6 a)–d): EDX analysis results for surfaces

a) 858R Martensitic rail run against pearlitic tyre. There is no measurable change in the composition of the worn surface

b) 858T Pearlitic tyre run against martensitic rail. The manganese content has risen towards that of the counterface, 858R.

c) 865R Bainitic rail run against pearlitic tyre. The silicon content has dropped towards that of the counterface, 865T.

d) 865T Pearlitic tyre run against bainitic rail. The silicon and manganese contents have risen towards those of the counterface, 865R.

e) 871R

f) 871T

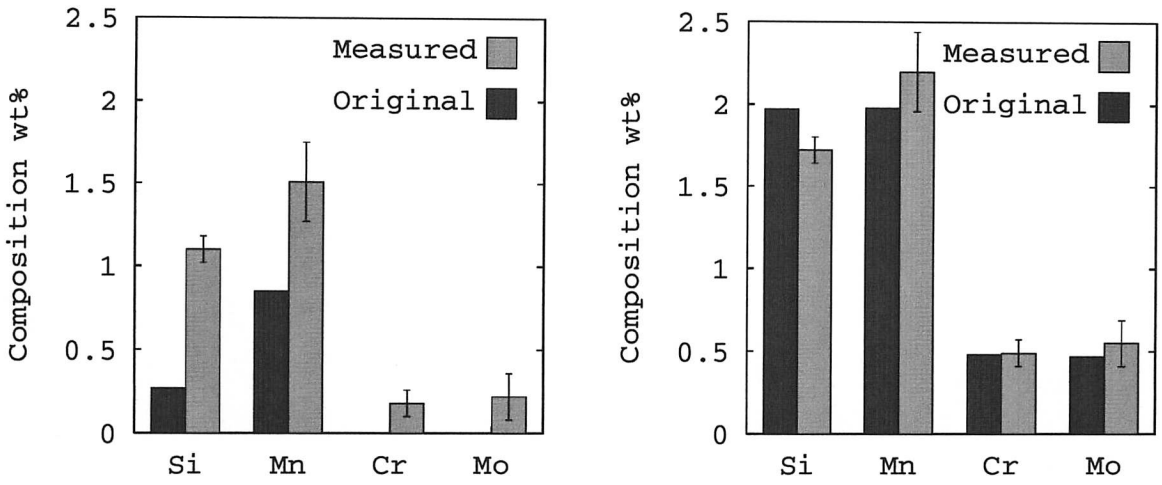

Figure 3.6 e)–f): EDX analysis results for surfaces
a) 871R MHT rail run against bainitic tyre. The alloy content of the worn surface has risen towards that of the counterface.
b 871T Bainitic tyre run against MHT rail. The Si content has dropped towards that of the counterface.

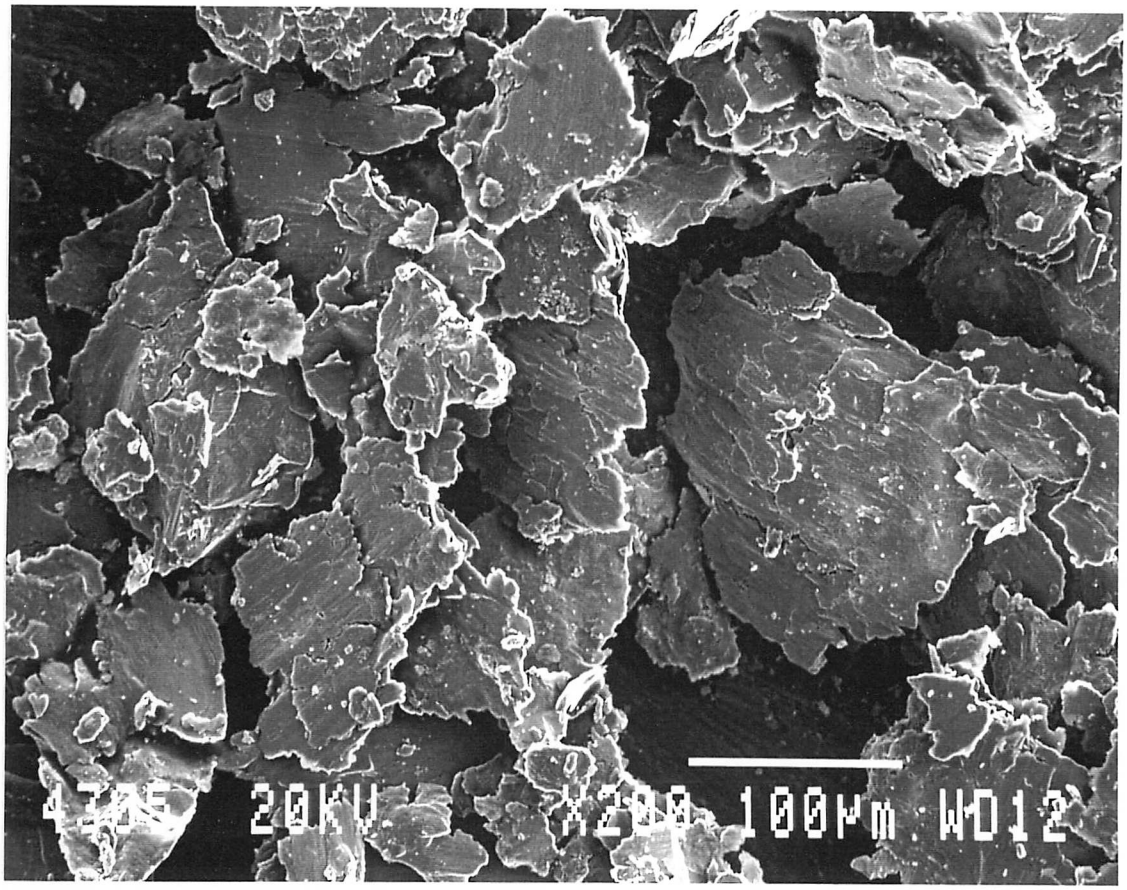

Figure 3.7: Typical wear debris from laboratory wear tests

A typical trace is shown in Figure 3.8.

The peaks are broadened due to the large strains the particles in the samples have undergone. A scan (Figure 3.9) taken of an undeformed sample showed sharper peaks and the presence of retained austenite.

Some of the deformed samples showed extra peaks present at about 38 ° and 78 ° 2θ which could not be identified. A typical example is shown in Figure 3.10. These could possibly be due to contamination, as paintbrush hairs and flakes of paint were present in the samples, or an effect of the strong orientation the samples are likely to have developed. Sample 943 was examined in both the conventional, and a rotating, sample holder and did not display the extra peaks in the rotating sample holder. From this it can be inferred that it is more likely that the extra peaks were caused by the orientation of the sample. As the samples were in the form of thin flakes which are very likely to

show a strong texture it was difficult to pack them into a conventional holder without them lining up; the rotating sample holder does not require the sample to be packed down.

EDX was carried out on particles from the wear debris. Only wear debris from tests where the steels in the wear couple were sufficiently different to be differentiated by EDX was measured. The majority of particles investigated turned out to be mixtures of the two steels in the wear couple. The exception was test 943, a martensitic rail run against a pearlitic tyre, where the majority of the particles were from the rail material. The results are shown in Table 3.3.

Test	Rail Material	Tyre Material	Number of particles			
			Rail	Tyre	Mixed	Total
932	MHT	Bainite 3	0	2	3	5
933	MHT	Bainite 1	0	0	7	7
934	MHT	Bainite 2	1	0	7	8
942	Bainite 1	Pearlite	0	1	7	8
943	Martensite	Pearlite	5	2	1	8

Table 3.3: EDX analysis results for wear debris

These results show that there is some form of adhesion going on in the wear process for the two different compositions to have become mixed, as found in the EDX results for the surfaces themselves.

3.2.4 Taper Sections

Photographs of the taper sections are shown in Figure 3.11(a)-(e). It can clearly be seen in Figure 3.11(b) that material transfer has taken place between the rail and the tyre. The samples which have high wear rates show extensive deformed and cracked surface layers. The cracks may be due to material transfer between the surfaces. The white coating seen on the surface of the samples in all the photographs is the protective nickel plating and is not actually part of the worn layer. It should be noted that the taper section causes an effective magnification in the vertical direction of about 3×.

The graphs of hardness against depth are shown in Figure 3.12(a)-(j). The depth of the work-hardened layer appears to be slightly less in the bainitic rails compared with the MHT rails when both are run against pearlitic tyres. The work-hardened depth is clearly less in bainitic tyres compared with pearlitic tyres. The bainitic tyres are much harder than the pearlitic tyres so the stress is supported by yielding/hardening of a

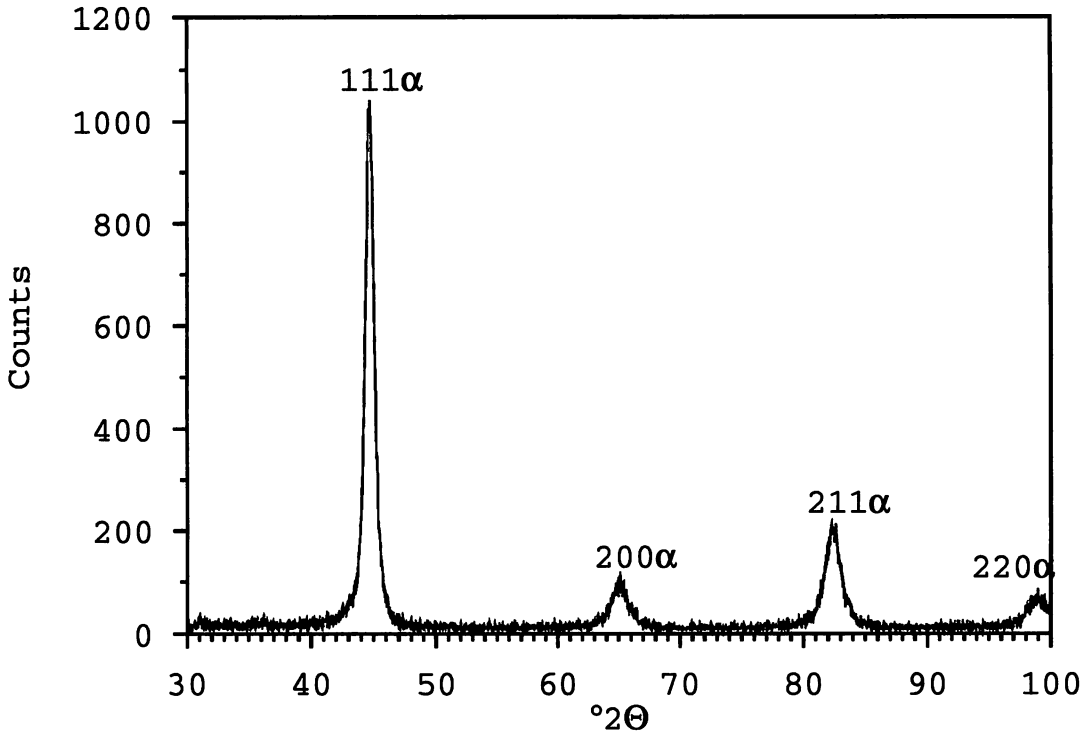

Figure 3.8: X-ray diffraction trace of sample 941

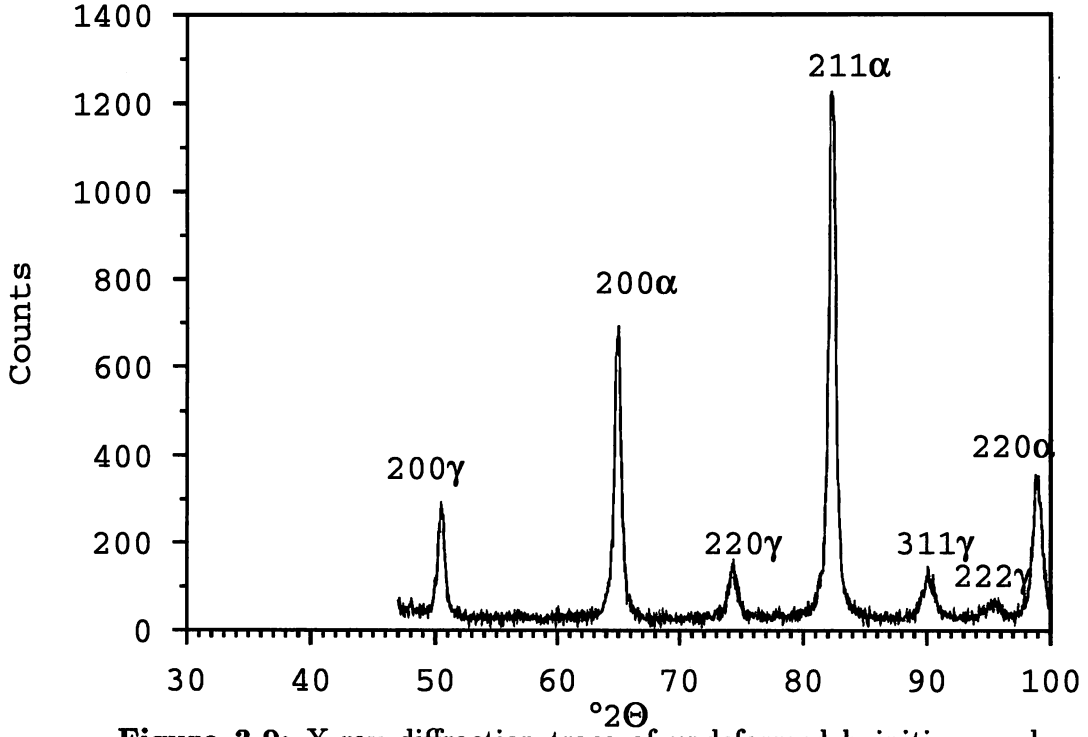

Figure 3.9: X-ray diffraction trace of undeformed bainitic sample This experiment was carried out over a different range of 2θ in order to get enough non-overlapping ferrite and austenite peaks to analyze the retained austenite content. These results will be discussed further in Chapter 7.

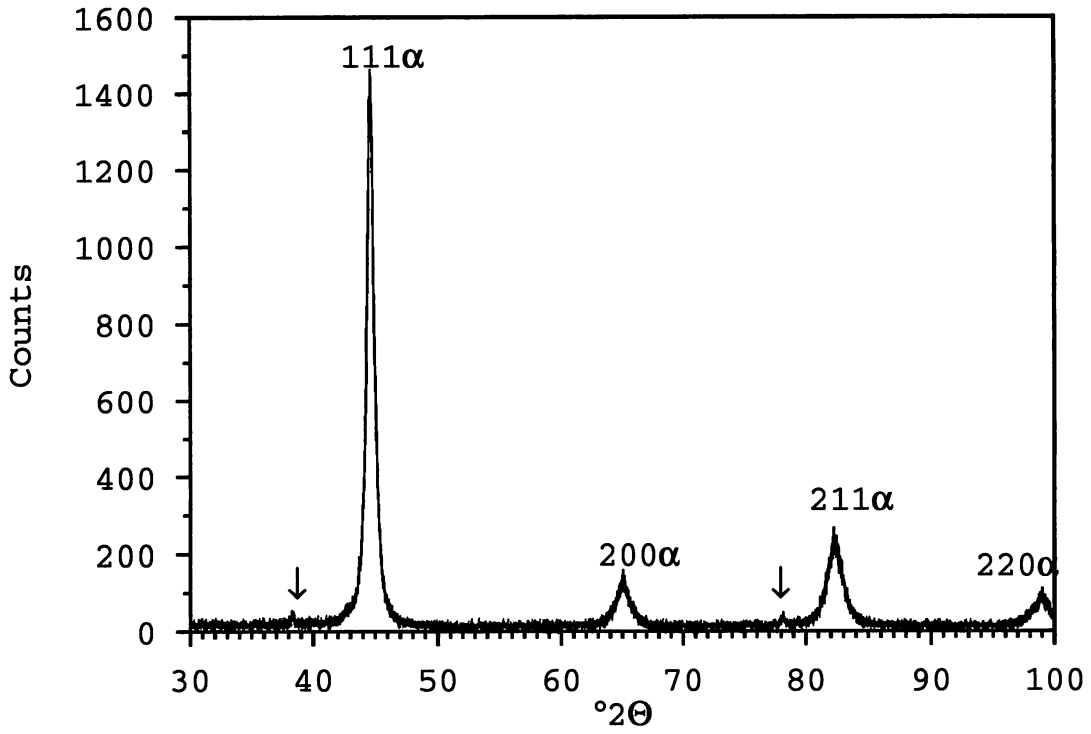

Figure 3.10: X-ray diffraction trace of sample 943 The unidentifiable peaks are marked with an arrow

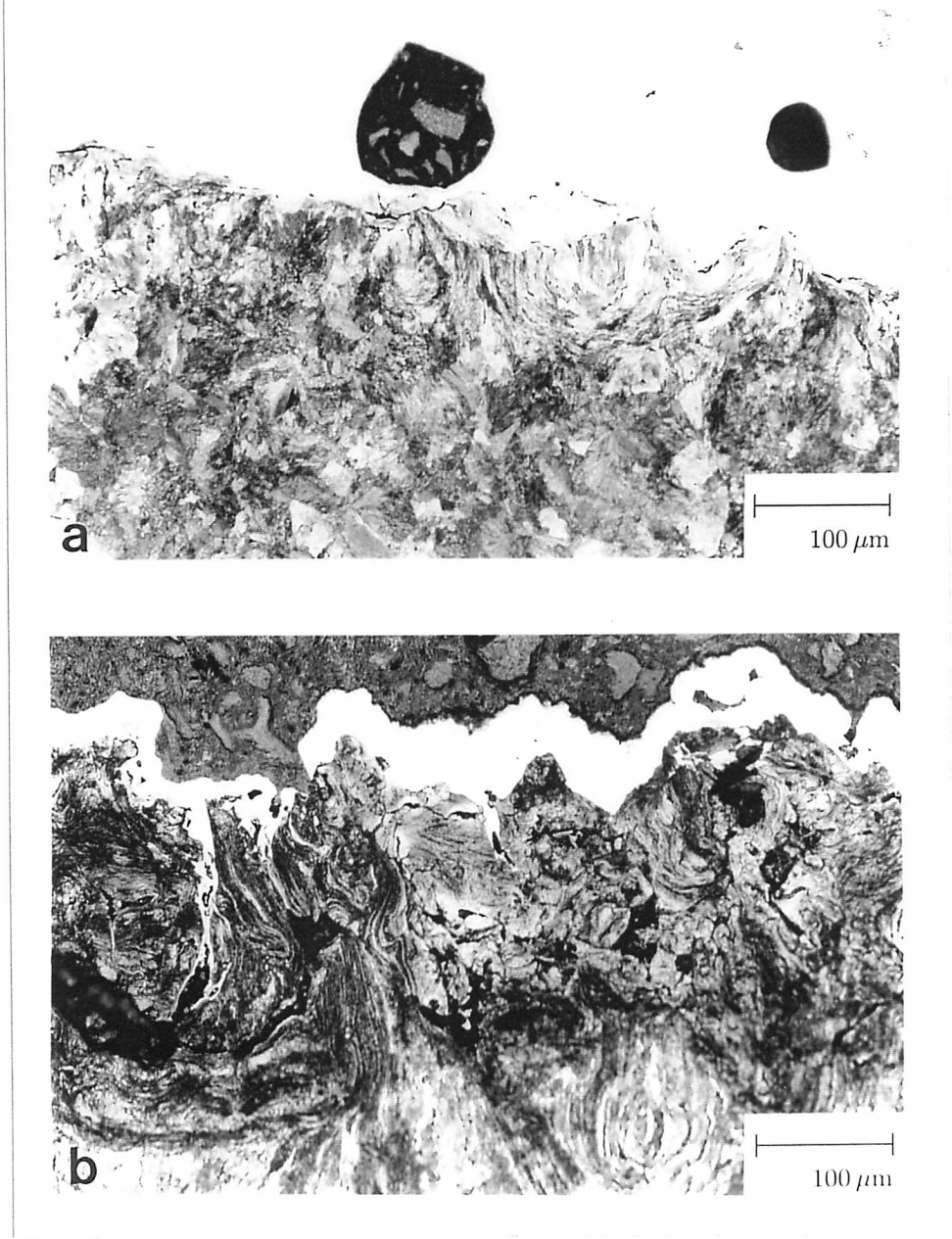

Figure 3.11(a): Taper sections from test 815
(a) MHT rail run against pearlitic tyre. There is a wide layer of deformed and transfer material.
(b) Pearlitic tyre run against MHT rail. There is a very deep deformed and transferred layer reflecting the high wear rate of this roller.

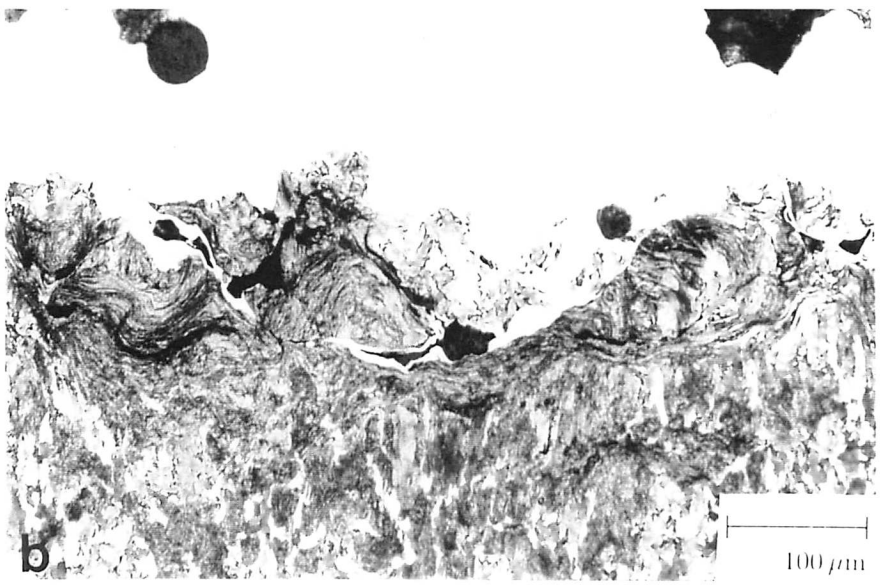

Figure 3.11(b): Taper sections from test 858
(a) Martensitic rail run against pearlitic tyre. Areas of pearlite can clearly be seen in the surface layers of the martensitic rail, providing clear evidence of material transfer.
(b) Pearlitic tyre run against martensitic rail. Again there is a deep deformed/transferred layer correlating with the high wear rate of this roller.

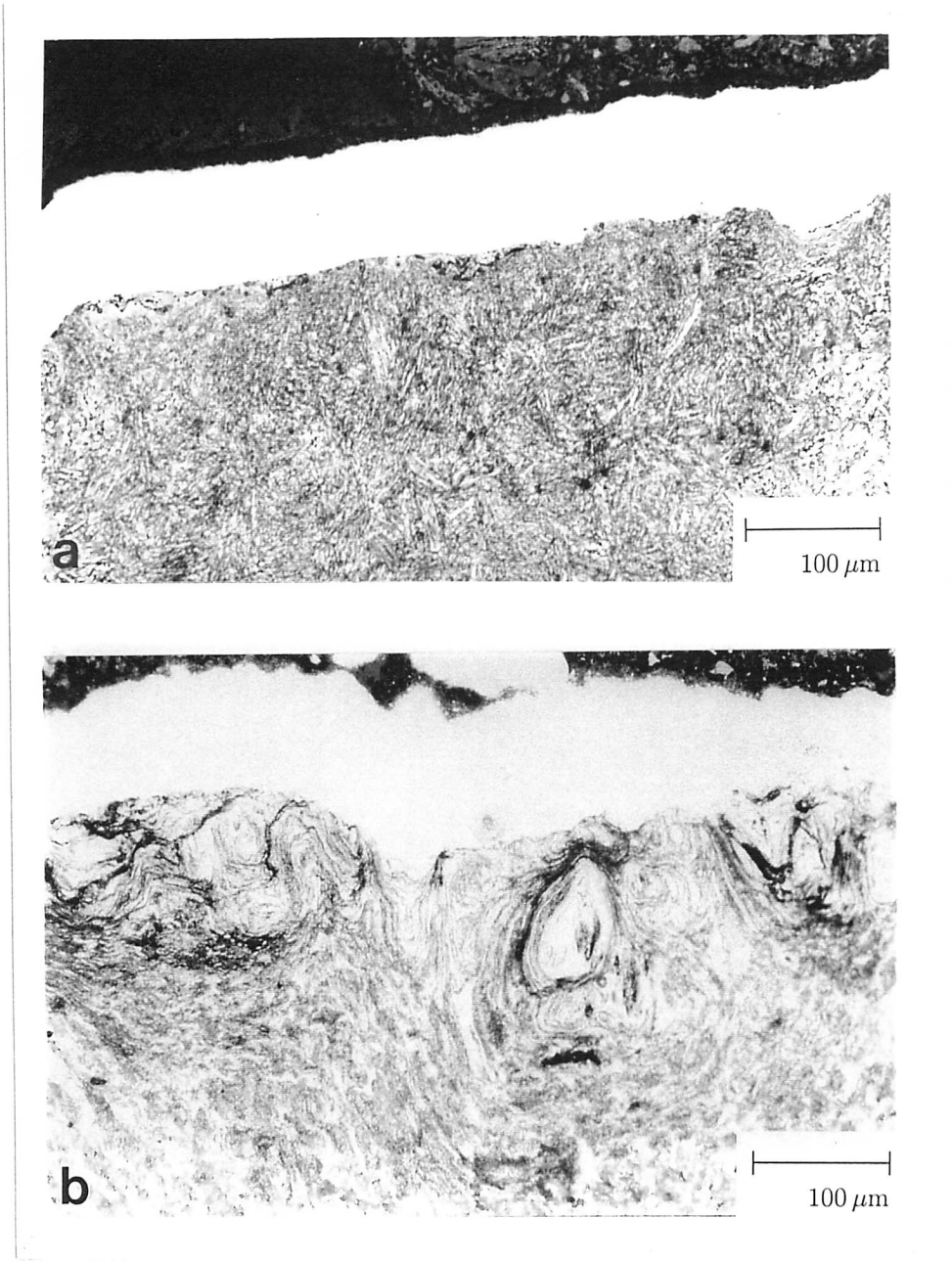

Figure 3.11(c): Taper sections from test 865
(a) Bainitic rail run against pearlitic tyre. There is little deformed layer in this sample, reflecting the low wear rate of the bainitic rail.
(b) Pearlitic tyre run against bainitic rail. The surface layer is cracked and deformed, but not as badly as the other two pearlitic tyres pictured.

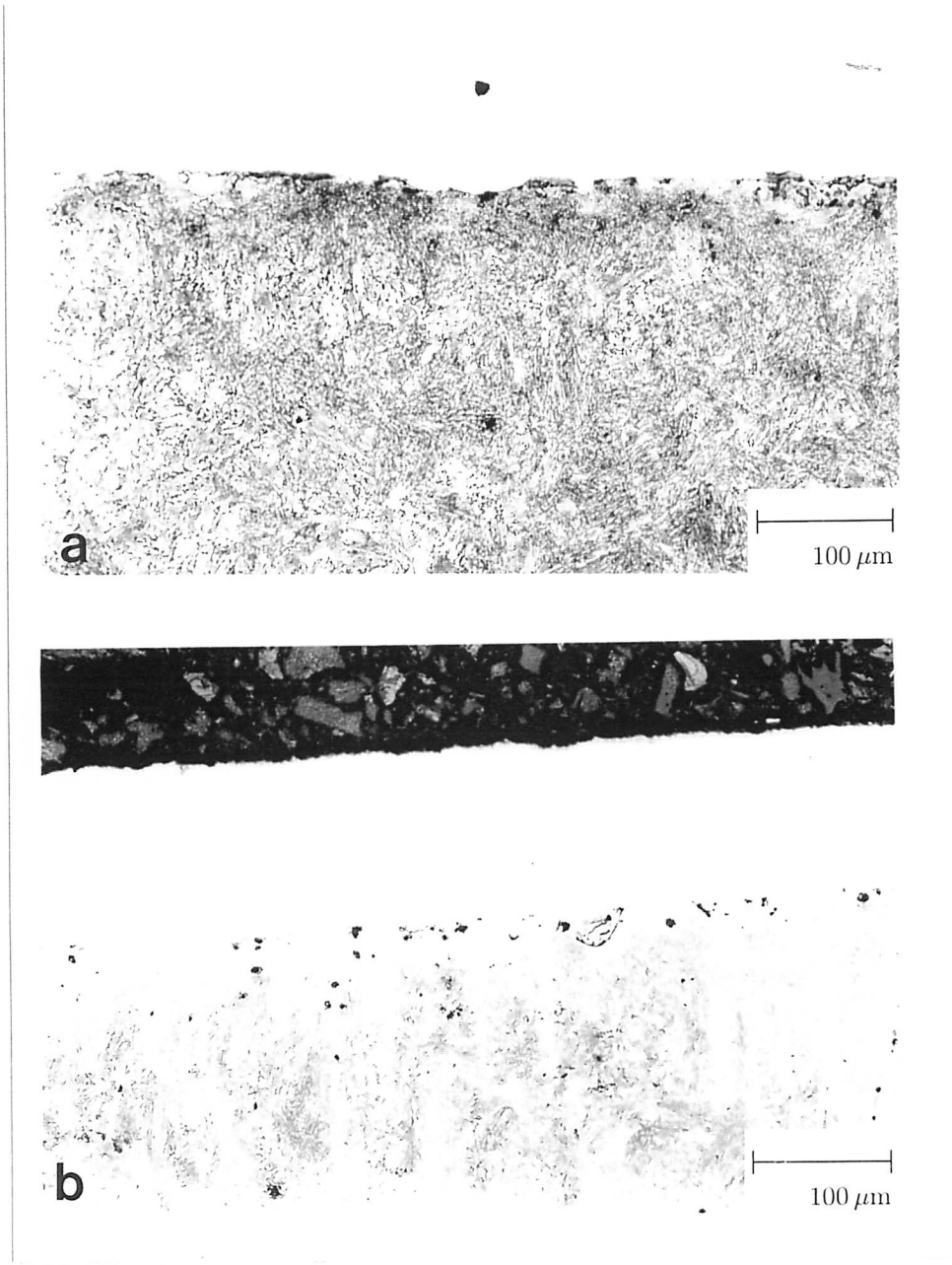

Figure 3.11(d): Taper sections from test 870
(a) Bainitic rail run against bainitic tyre. This sample is smooth and shows hardly any deformed layer. It had an extremely low wear rate.
(b) Bainitic tyre run against bainitic rail. The sample is smooth and hardly deformed.

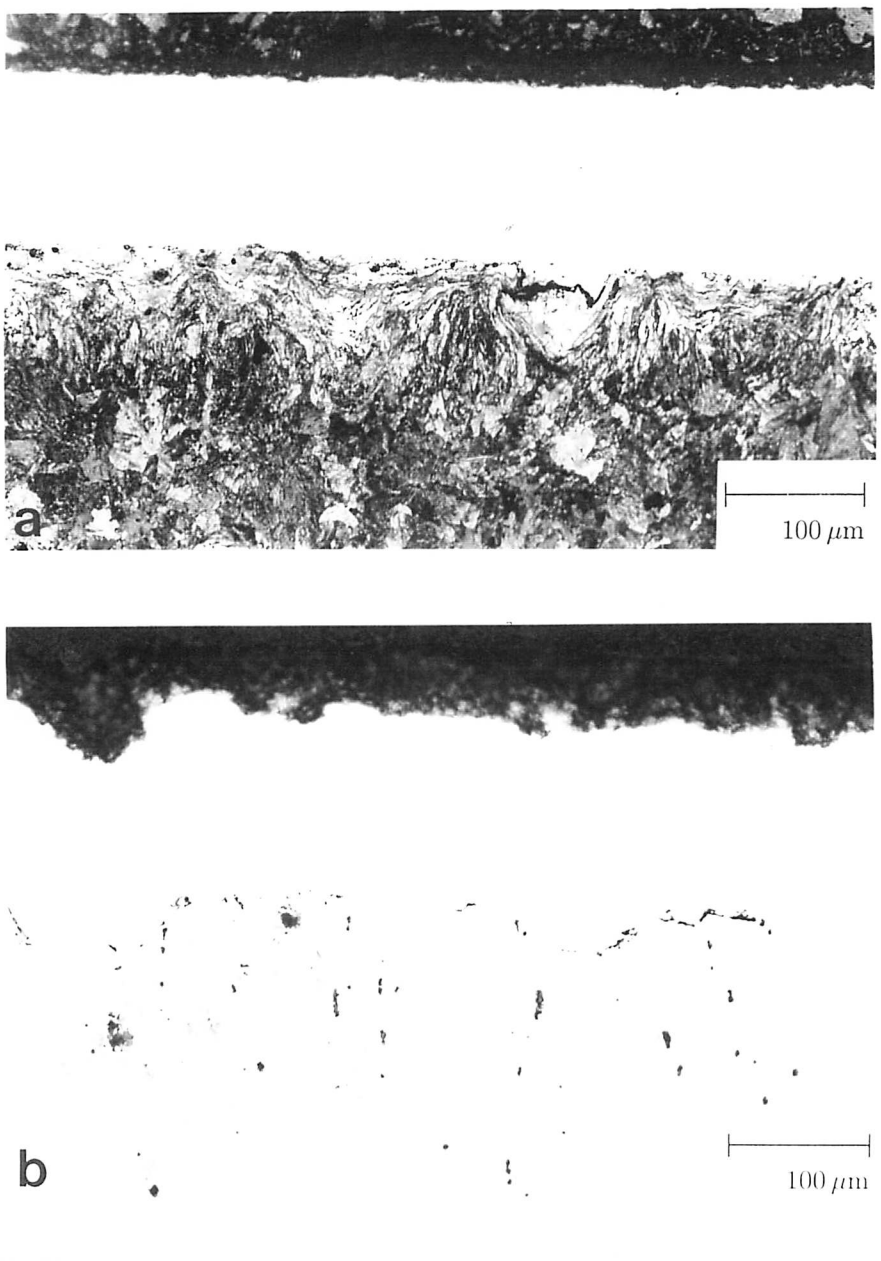

Figure 3.11(e): Taper sections from test 871
(a) MHT rail run against bainitic tyre. There is some surface deformation but much less than in the MHT rail run against conventional tyre (Figure 3.11 (a)). The wear rate of this sample was extremely low.
(b) Bainitic tyre run against MHT rail. The surface is not very smooth but there is very little deformed layer and again the wear rate is very low.

(a) 815R

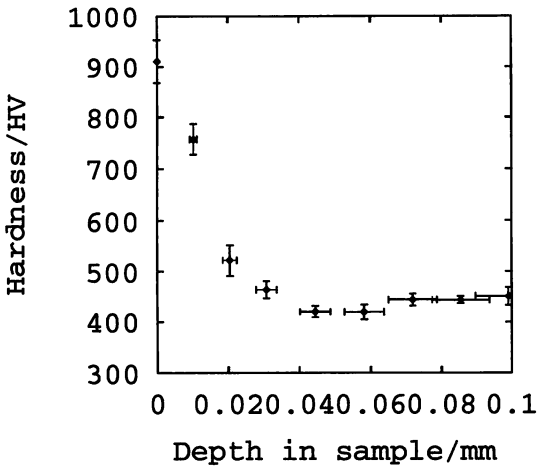

(b) 815T

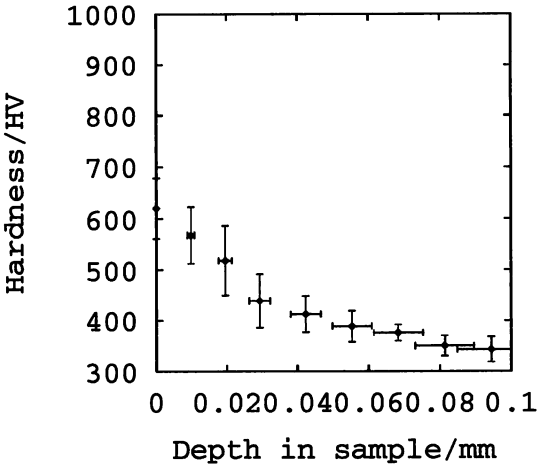

(c) 858R

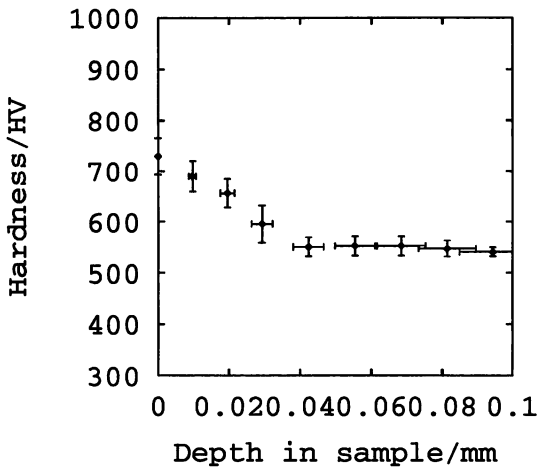

(d) 858T

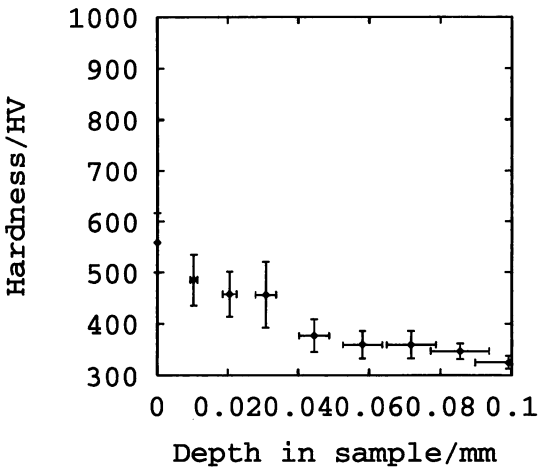

Figure 3.11(a)–(d): Microhardness gradients of worn samples a) MHT rail run against pearlitic tyre
b) Pearlitic tyre run against MHT rail
c) Martensitic rail run against pearlitic tyre
d) Pearlitic tyre run against martensitic rail

smaller part of the steel in these samples.

The MHT rails develop an extremely hard surface layer (hardness > 900 HV) compared with the bainitic and martensitic rails. This hard layer, sometimes called white

(e) 865R

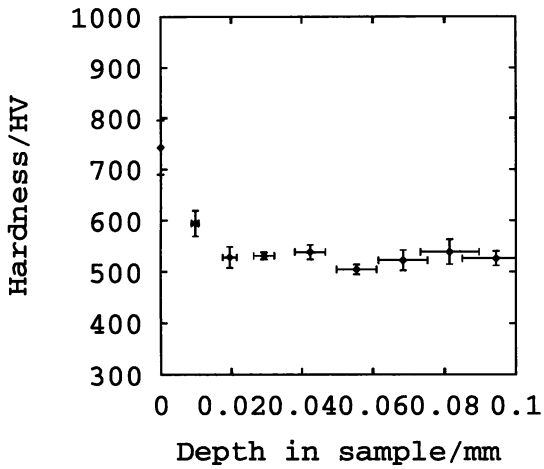

(f) 865T

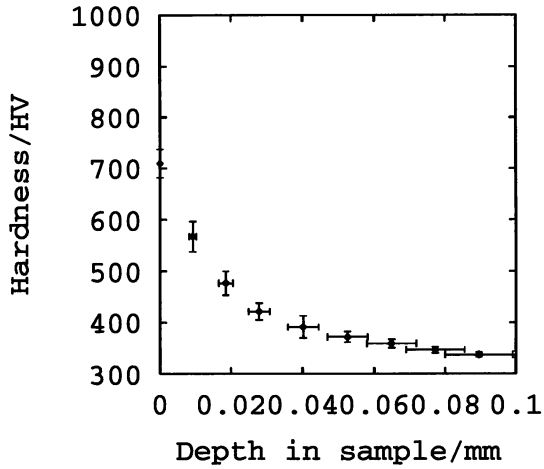

(g) 870R

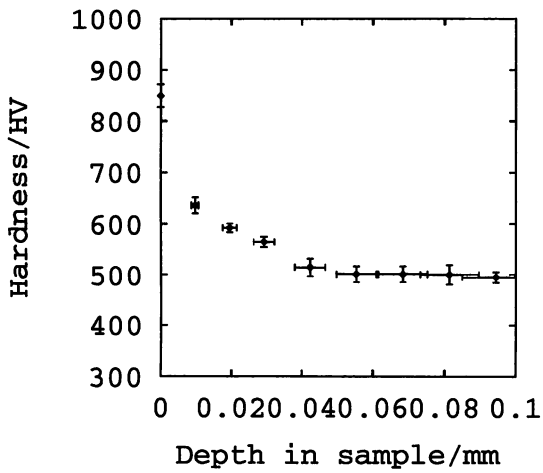

(h) 870T

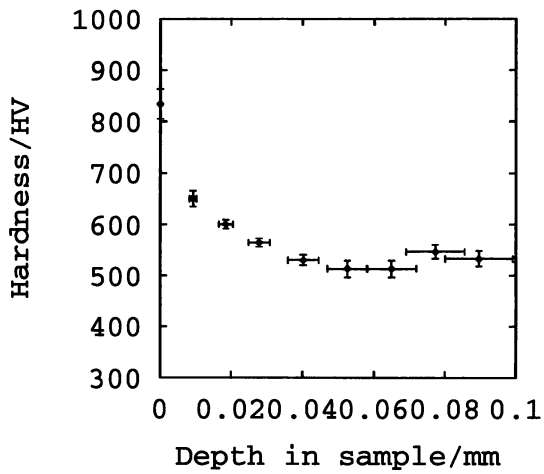

Figure 3.11(e)–(h): Microhardness gradients of worn samples e) Bainitic rail run against pearlitic tyre
f) Pearlitic tyre run against bainitic rail
g) Bainitic rail run against bainitic tyre
h) Bainitic tyre run against bainitic rail

phase or white-etching layer because etching does not reveal any structure within it, is thought to be the reason for the good wear resistance of pearlitic steels. However the bainitic steel shows good wear resistance without such an exceptionally hard surface.

(i) 871R

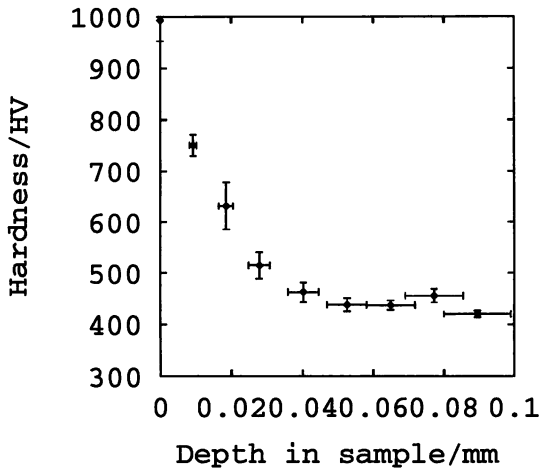

(j) 871T

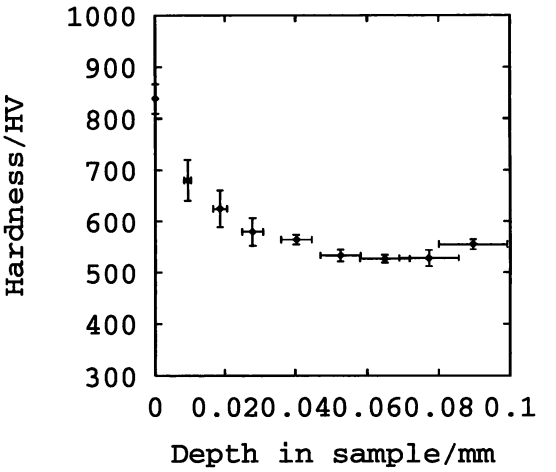

Figure 3.11(i)–(j): Microhardness gradients of worn samples i) MHT rail run against bainitic tyre
j) Bainitic tyre run against MHT rail

It has been observed [Zum Ghar 1987] that steels sometimes fail through cracking of extremely hard and brittle surface layers that develop during wear. A thin, hard surface layer is good for wear resistance but if it becomes too thick it is apt to crack as the soft material beneath it plastically deforms and moves, causing a strain mismatch which cannot be accommodated.

The bainitic rails with relatively soft surfaces presumably suffer this problem to a lesser extent. They have a hard but perhaps comparatively tough surface layer, so adhesion is small, as in hard, wear resistant pearlitic steels, but they also suffer less cracking in the tougher surface layers, so less wear debris is formed. It seems that a careful study of the properties of the deformed layer might then explain the differences in wear rate. The martensitic rail has similar surface hardness to the bainitic rail but a much greater wear rate. Attempts to measure the toughness of the surface layers by micro-indentation failed as it was found impossible to produce cracks.

Another interesting observation is that the pearlitic tyre develops a harder surface when run against a bainitic rail than a pearlitic rail. There must be some sort of interaction such as material transfer between the two for this to happen, so the properties of each surface may well not be the properties of the original material even after high

strains, but a mixture of the two.

It can also be seen from the graphs that the tyres in the more wear resistant couples (865, 870, and 871) develop a harder surface layer than in the less wear resistant couples (815 and 858). The hardness difference between the surfaces is thus reduced. This should be an advantage as a soft surface in contact with a very much harder one will suffer a large amount of damage as adhesive junctions will break mostly in the soft material. The higher hardness of the tyre rollers in tests 870 and 871 is due to their being bainitic rather than pearlitic; in test 865 there is evidence from EDX that the tyre surface has gained a great deal of material from the harder rail and so would be expected to become hard.

3.3 Summary

Wear tests were carried out on conventional MHT and experimental martensitic and carbide-free bainitic steels. Both conventional pearlitic, and experimental bainitic tyres were used. The wear rates for the different steels indicated that the hardness of both rollers is important, but that of the tyre roller probably more so. An experiment with two bainites of the same hardness but one carbide-free while the other was carbide-containing showed that the carbide-containing bainite was less wear resistant. This was ascribed to the lower toughness of the carbide-containing bainite which made it easier for cracking to occur and wear debris to be formed. The martensitic rail, which had a wear rate no better than that of conventional MHT rail, was shown to contain carbides.

The worn surfaces of the rollers showed clear evidence of material transfer. This implies an adhesive wear mechanism which involves material being transferred from one counterface to the other before finally breaking off to form a wear particle. The composition of individual flakes of the wear debris was also found to be a mixture of the parent materials and they appeared to be made up of many layers. The same wear mechanism appeared to be operating in steels of widely varying hardness and microstructure.

The worn surfaces of the steels showed an increase in hardness over the bulk. Pearlitic steels developed an extremely hard surface layer of white phase which may explain their good wear resistance. The wear resistant bainitic steel, by comparison, developed a relatively softer surface layer which will probably be tougher than the white phase layer and hence less prone to cracking and the generation of wear debris. However the difference between the hardness of the counterfaces is important, as well as the

absolute hardness, because experiments where the difference in hardness between the worn surfaces was small showed a low wear rate. The properties of the worn surfaces are likely to be of more use in modelling wear than those of the bulk.

4

Modelling of wear

This chapter contains work relating wear rates of experimental bainitic and pearlitic rail steels to material properties. British Steel Swinden Technology Centre provided wear rate, hardness and Charpy impact test fracture energy data for many experimental bainitic rail steels. These data were used to test likely wear equations. All the data are from wear tests carried out as described in Chapter 3.

4.1 Adhesion wear

According to Archard's theory of simple adhesion wear, the wear rate depends on the normal load and the hardness of the surfaces in contact.

$$Q = \frac{\kappa W}{H} \tag{4.1}$$

where Q is the wear rate, W is the normal load, H is the hardness of the surface being worn, and κ is the wear coefficient. This equation is derived in Chapter 2. There are several flaws in this theory. No account is taken of the hardness of the counterface; in fact, if wear occurs by straightforward adhesion the harder surface would not wear at all; the vast majority of the adhesive junctions would break at the weakest point, *i.e.* in the softer material. This is not observed in the laboratory wear tests described in Chapter 3. The hardness H refers to the hardness of the asperity tips in contact, which may differ from the bulk hardness as the asperity tips may be small enough for grain size not to affect their hardness. Work-hardening of the asperities must also be taken into account. The adhesion theory cannot explain the formation of wear debris as it merely considers the transfer of material from one surface to the other.

The measured wear rate of the experimental rails is plotted against the inverse rail and tyre hardnesses in Figure 4.1. The theory should also apply equally well to the tyres.

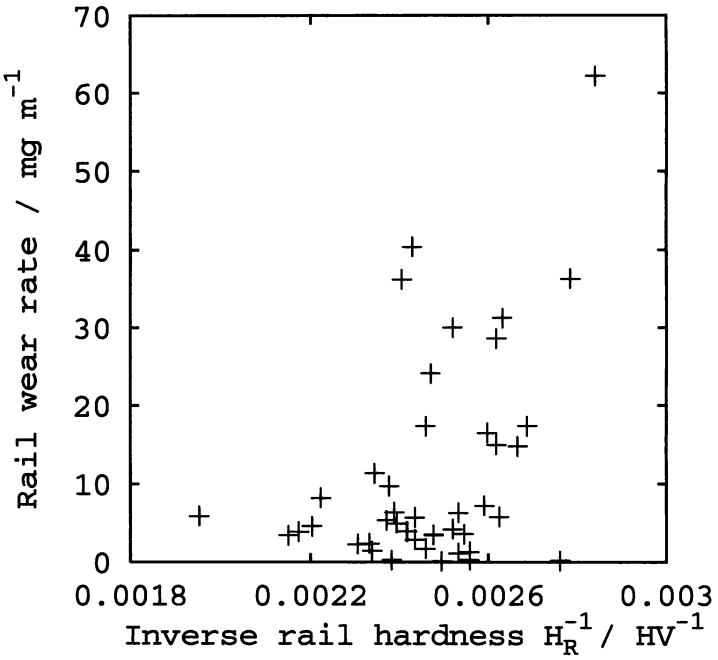

Figure 4.1 (a): Wear rate of rails *vs.* inverse rail hardness Given that the scatter in wear test results is quite large (British Steel scientists estimate it to be $\pm 3\,\mathrm{mg\,m^{-1}}$), there is a strong relationship here. Some additional scatter would also be expected because these results are for a variety of tyre steels. Work in Chapter 3 indicates that the tyre steel has a strong effect on the wear rate of the rail.

The graph for the rails (Figure 4.1 a) shows a reasonably good relationship between inverse hardness and wear rate. The correlation coefficient is 0.76. Given that tyres of several different hardnesses were used, and that wear testing usually produces results with a large scatter, this does not seem unreasonable. The graph for the tyres (Figure 4.1 b) is less satisfactory. The correlation coefficient is only 0.32. If the small group of very hard bainitic tyres (the isolated group of points on the left hand side of the graph) is neglected then the remaining group of tyres all have similar hardness, but are run against rails of widely varying hardness. If the hardness of both counterfaces is important then a lower correlation is expected for the tyres. Therefore the hardness of both rollers must be taken into account.

The simplest way to do this would be to plot the average hardness of the rollers

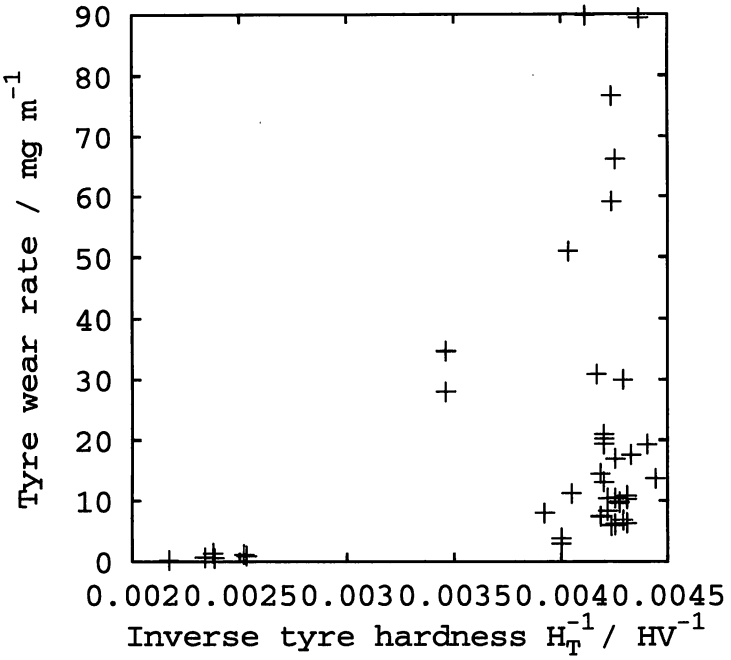

Figure 4.1 (b): Wear rate of tyres *vs.* inverse tyre hardness There is less of a relationship in this graph. The tyre data available fall into two categories: a few very hard experimental bainitic steels and many relatively soft standard pearlitic tyre steels. These are run against a wide variety of rails.

against the wear rate. This is shown in Figure 4.2. Rail and tyre wear rates are plotted on separate graphs to make the diagrams clear.

The correlation for the tyres in Figure 4.2 (b) has increased to 0.36 but that for the rails has decreased to 0.37. It seems that the the hardness of both counterfaces is important but that there must be a more complex relationship involved.

In adhesion wear, surfaces become damaged because junctions form between them and are then pulled apart. If the junction does not break exactly at the original plane of contact then one of the surfaces will lose material to the other. A simple estimate of the proportion of junctions which will break in one face, say the rail, is $H_T/(H_T + H_R)$ where H_R is the hardness of the rail and H_T is the hardness of the tyre.

The total area of contact (*i.e.* the area of junctions formed) will be inversely proportional to the hardnesses of the surface, as the softer the metal, the easier it is for the asperities to deform and increase the area of contact. So the total area of contact will be proportional to $1/H_R H_T$. Then the total amount of wear is proportional to both the amount of junctions formed, and the likelihood of the junctions' breaking in the surface

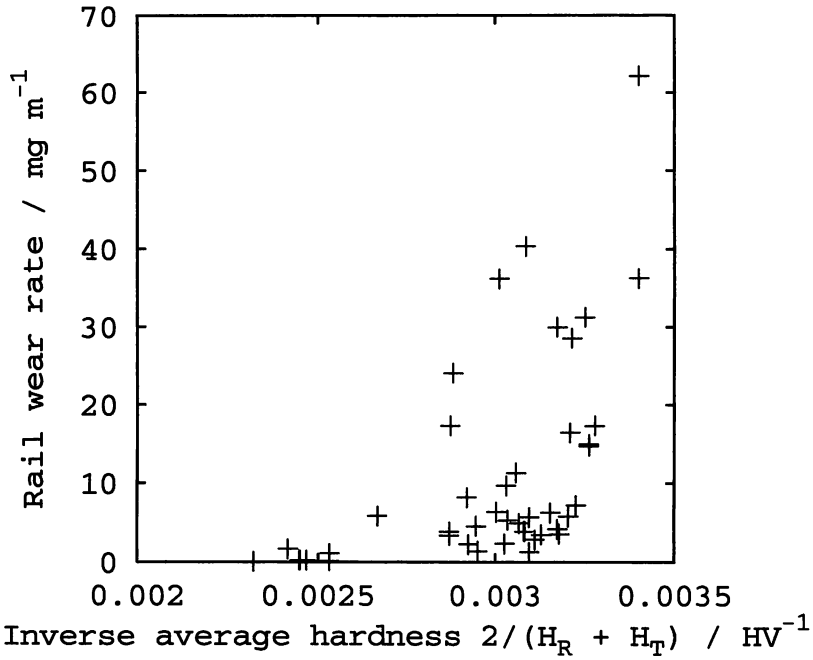

Figure 4.2 (a): Wear rate of rails *vs.* inverse average hardness

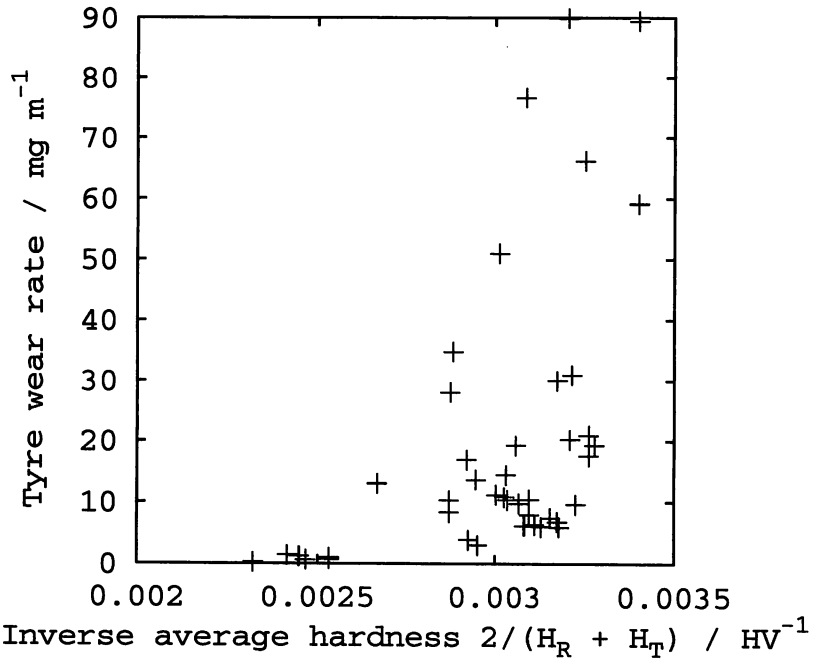

Figure 4.2 (b): Wear rate of tyres *vs.* inverse average hardness

of interest. For the rail this gives:

$$Q \propto \frac{1}{H_R(H_R + H_T)} \tag{4.2}$$

and for the tyre

$$Q \propto \frac{1}{H_T(H_R + H_T)} \tag{4.3}$$

These functions are plotted in Figure 4.3.

It can be seen from the graphs of wear rate *vs.* adhesion function that this model does not work either for the rail or the tyre. The correlation coefficients are 0.30 and 0.32 respectively. Other material properties may be significant as well as hardness, or we may be using an inappropriate value of hardness as investigated in the next section.

4.2 Surface hardnesses

In the previous models, bulk hardnesses were used. However the hardness at the surface of a roller during steady-state wear is very unlikely to be the same as that in the bulk due to work hardening and material transfer. Results presented in Chapter 3 show the surface hardness to be greatly increased for both bainitic and pearlitic steels. Since it is the properties of the surfaces in contact and not those of the bulk materials that will determine the wear rate, the previous analysis can be repeated using surface hardnesses for those samples where these have been measured. These plots are shown in Figure 4.4-Figure 4.6.

Unfortunately there are not really enough data to show whether using surface hardnesses is an improvement or not. The graphs for the tyres show an improvement as there is no longer a distinct split between the bainitic and pearlitic rail data (the samples for which peak hardnesses were measured did include both sorts of tyres). More surface hardnesses are required to provide a better comparison between the two sets of graphs; however this approach looks promising.

4.3 Toughness of steels

Another approach to modelling wear on rails is to consider the toughness of the steels as well as the hardness. British Steel have provided Charpy fracture energies for most of the steels considered above and these could be used as an empirical toughness parameter.

It has been found that the wear on rails is directly proportional to the amount of work done by the frictional force on the rail [McEwen and Harvey, 1985]. In Chapter 2 it was shown that the friction should depend on the hardness of the surfaces in contact (see

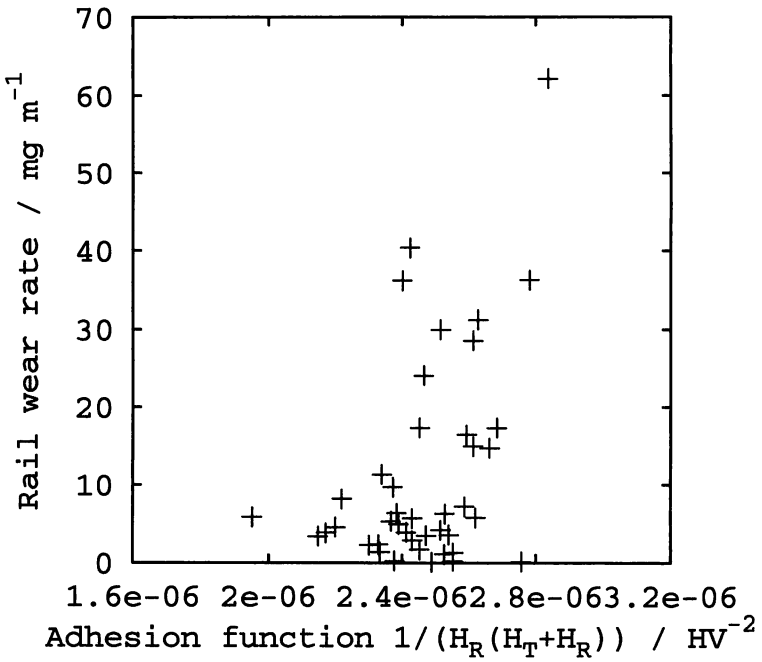

Figure 4.3 (a): Wear rate of rails *vs.* adhesion function

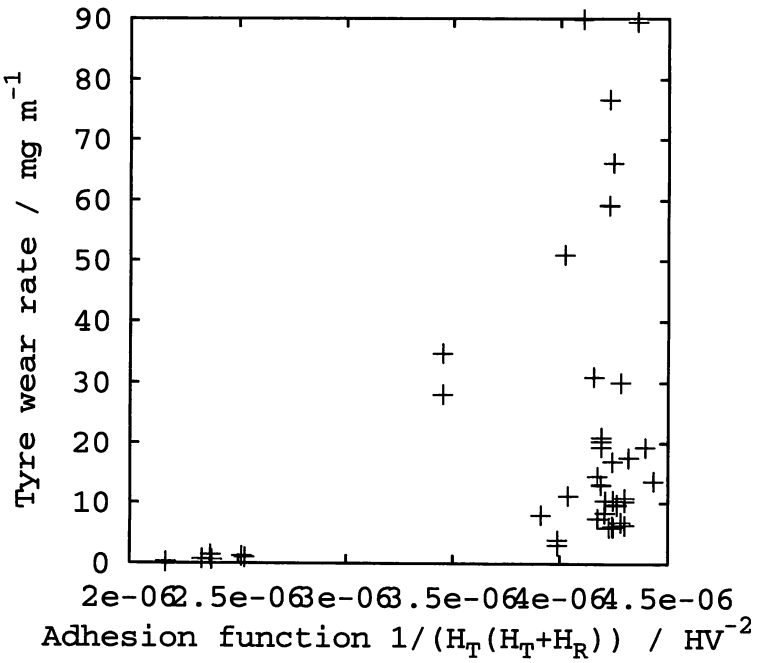

Figure 4.3 (b): Wear rate of tyres *vs.* adhesion function

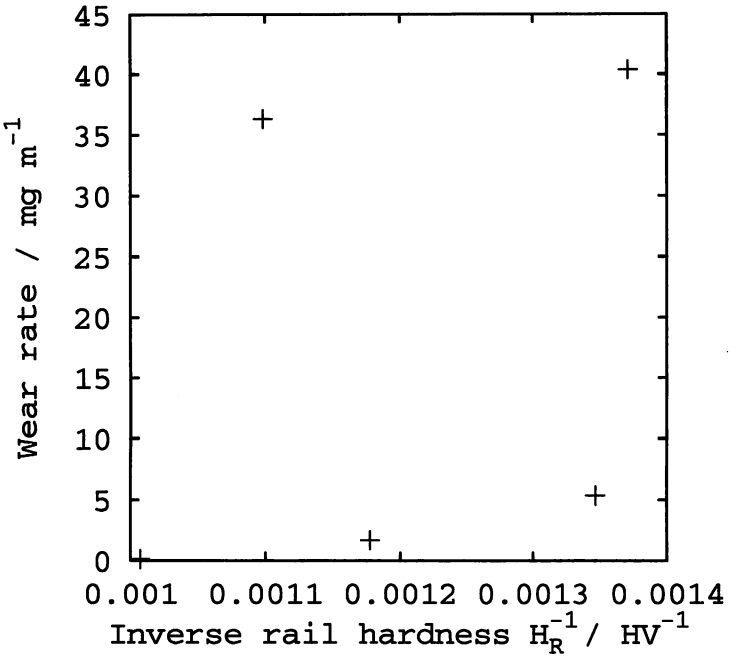

Figure 4.4 (a): Rail wear rate *vs.* inverse surface hardness

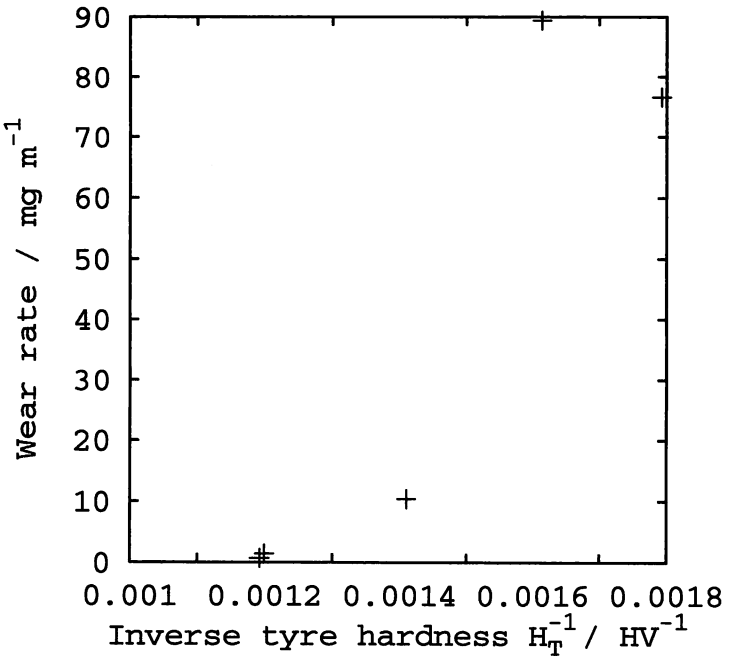

Figure 4.4 (b): Tyre wear rate *vs.* inverse surface hardness

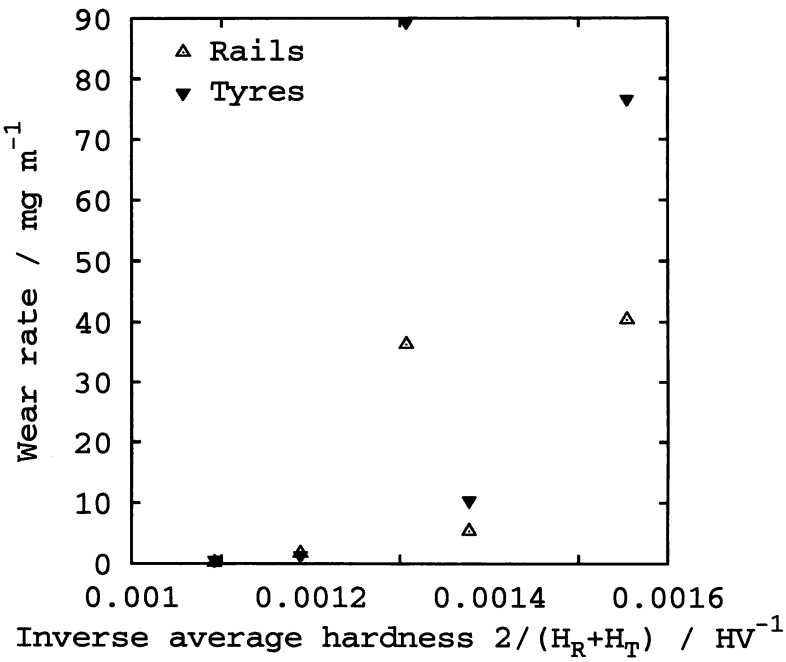

Figure 4.5: Wear rate *vs.* inverse average peak hardnesses

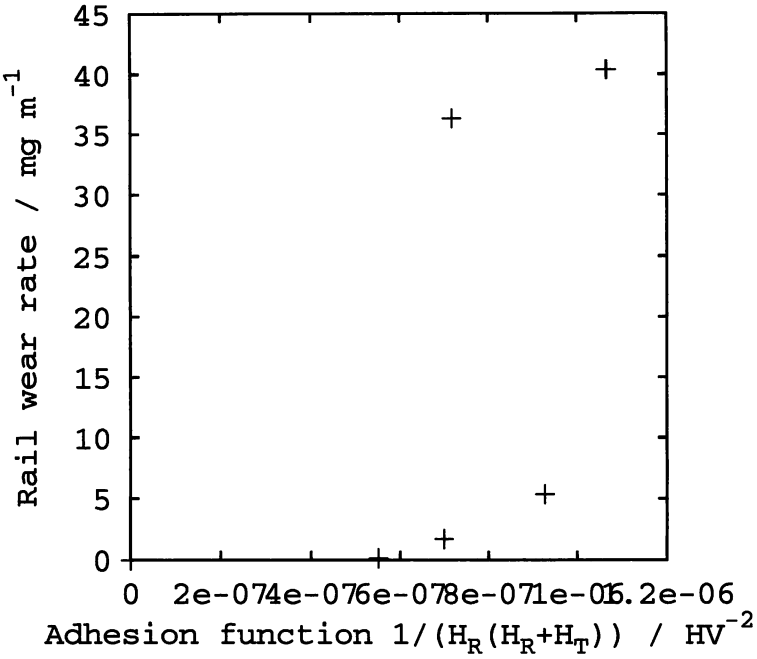

Figure 4.6 (a): Rail wear rate *vs.* adhesion function calculated from peak hardnesses

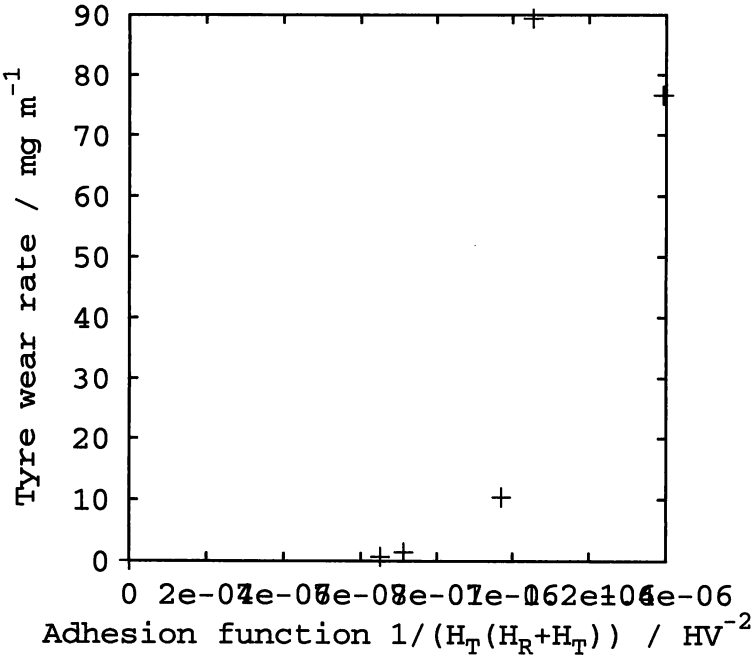

Figure 4.6 (b): Tyre wear rate *vs.* adhesion function calculated from peak hardnesses

equation 2.15). The creepage was the same in all tests, so the hardness would have been the main variable affecting the friction. Unfortunately it was not possible for British Steel to measure the friction force during the wear tests so it has to be assumed that it is proportional to $1/H$ as in Chapter 2, although there are many unreasonable assumptions in this model. Since the tyre is of similar hardness to the rail it seems sensible that its hardness will also affect the friction, so it can be assumed to be proportional to $1/H_R H_T$. The energy absorbed in breaking off a wear fragment will be proportional to some toughness parameter. The Charpy fracture energy is the only toughness parameter for which data were available. Dividing by this gives

$$Q \propto \frac{1}{H_R H_T C_V} \tag{4.4}$$

where C_V is the Charpy fracture energy. This function is plotted in Figure 4.7.

The graph shows that this model is actually worse than the ones based on hardness alone The correlation coefficient is only 0.20. A possible reason for this is that the toughness of the surface layer will be very different from that of the bulk as material is transferred from the counterface and has undergone large strains. The material at the surface is also under a large compressive stress; this will tend to make it harder for it to fracture. In addition, the Charpy test is an empirical test and the fracture energy is not a material parameter and so is not very suitable for modelling with.

4.4 Neural network modelling of wear

In addition to the modelling based on wear theory, neural network modelling was carried out on the data received from British Steel in an attempt to produce a useful empirical model.

4.4.1 Theory of neural network analysis

Neural network modelling is an empirical method similar to linear regression, but able to fit any shape of curve. The neural net model has a fixed set of input parameters, such as hardness and contact stress, which are multiplied by weights. Instead of summing these, as in linear regression, they are used as inputs to a hyperbolic tangent function [MacKay *et al.* 1996].

The network structure is illustrated in Figure 4.8. It consists of input nodes x_j, an output node y and a "hidden layer" of of nodes which take linear functions of the values of the input nodes and act on them with a hyperbolic tangent function:

$$h_i = \tanh\left(\sum_j w_{ij}^{(1)} x_j + \theta_i^{(1)}\right) \tag{4.5}$$

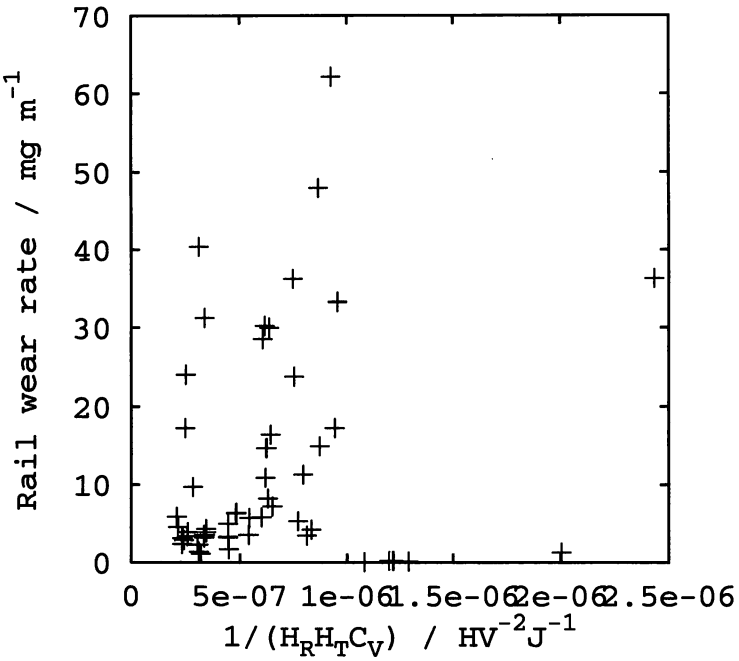

Figure 4.7: Rail wear rate *vs.* wear function which includes a toughness parameter

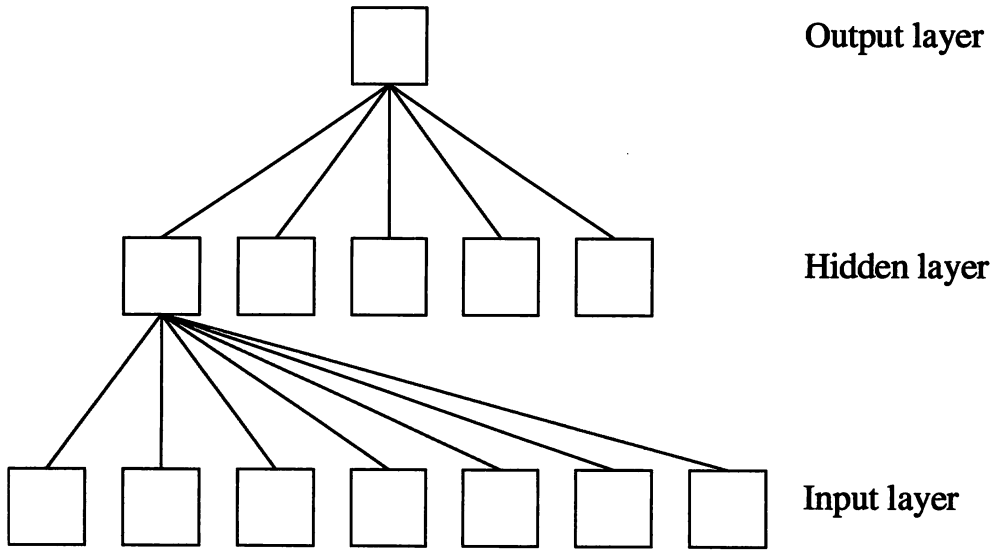

Figure 4.8: Structure of neural network. Not all connections are shown in order to improve clarity.

The output node then sums these results, multiplied by another set of weights, and adds another constant to produce the final output y:

$$y = \sum_i w_i^{(2)} h_i + \theta^{(2)} \tag{4.6}$$

Hyperbolic tangents are used because of their flexibility. Increasing the number of hidden nodes increases the non-linearity of the model as more hyperbolic tangents are added.

The model is produced by "training" on a database of experimental results. The weights are found by a process of minimising errors in the output. A quantity called the "test error" can be defined which is a measure of the ability of the model to generalize to unseen data. The ideal number of hidden units may be found by creating neural nets for a range of numbers and plotting a graph of test error *vs.* hidden units. The graph will reach a minimum beyond which greater complexity does not improve the model.

The main drawback of this technique is that the data may be over-fitted and may result in a very complex model which fits all the random noise in the data. If there are sufficient data this may be checked for by splitting the dataset into two and only training on one half of it. The second half can then be used to check the model is producing sensible results. If there are not enough data available then the complexity of the model can be limited by restricting the number of hidden units.

4.4.2 Method and results

The properties used as inputs to the model are shown in Table 4.1. Before creating the model, the data were normalised between the minimum and maximum values for each input, with the minimum value becoming -0.5 and the maximum 0.5. The model can only be used with data normalised in this way, and any predictions made with it have to be unnormalised before use.

Input	Minimum	Maximum	Mean	Standard Deviation
Rail hardness (HV)	310	512	404	34
Rail microstructure	0	1	0.9	0.2
Tyre hardness (HV)	225	461	261	60
Tyre microstructure	0	1	0.1	0.3
Charpy fracture energy (J)	5	45	21	11
Contact stress (MPa)	375	750	712	84

Table 4.1: Inputs for neural network model

A microstructural parameter was used to indicate whether each roller was pearlitic or bainitic. A pearlitic microstructure was given a value of zero and bainitic a value

of one. The output was the rail wear rate. Two different models were produced; one without Charpy fracture energy as an input and one with it.

There were not enough data to produce a reasonable model with only half the dataset, so all the data were used for training and there were no testing data. Only models with one to four hidden units were created in an attempt to avoid over-fitting the data.

The results from the best model without Charpy fracture energy, with one hidden unit, are shown in Figure 4.9. The model itself is specified in Table 4.2 by the weights and offsets as explained above.

Hidden layer weights	
Rail hardness	-1.5114×10^{0}
Rail microstructure	-3.1944×10^{0}
Tyre hardness	6.5597×10^{-5}
Tyre microstructure	-1.6858×10^{-5}
Contact stress	-1.1465×10^{0}
Offset	0.1547×10^{0}
Output layer weights	
Hidden unit 1	-7.3096×10^{-5}
Offset	0.4837×10^{0}

Table 4.2: Weights and offsets for neural net model for wear without Charpy fracture energy. The model has one hidden unit.

Most of the error bars touch the line but the uncertainty is so large that the model may not be of much practical use. This is usually a sign that the network has not been given sufficient data. It is possible to extract partial correlation coefficients for each input to see which were most important and these are plotted in Figure 4.10. The most significant variables are rail hardness and tyre microstructure. It should be remembered that the tyres fall into two groups: soft pearlitic steels and hard bainitic steels, and so tyre hardness is a very strong function of tyre microstructure, much more so than for the rails. Therefore there may not be anything special about microstructure, especially as it is not significant for the rails; the network may simply have picked it instead of hardness if the two are equivalent.

Results from the best model including Charpy fracture energy are shown in Figure 4.11. This model used four hidden units. The weights and offset are shown in Table 4.3. Again the model has large error bars. The partial correlation coefficients are shown in Figure 4.12. Charpy fracture energy is not a particularly significant variable.

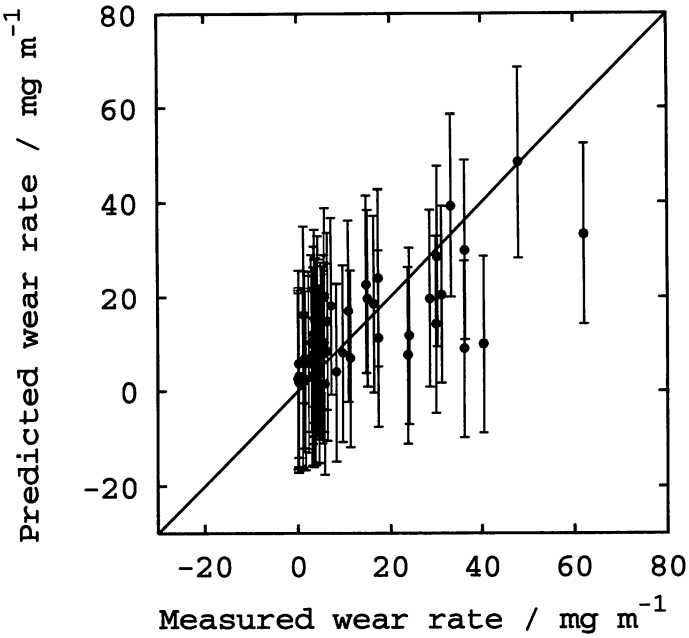

Figure 4.9: Neural network model for rail wear rate without Charpy fracture energy

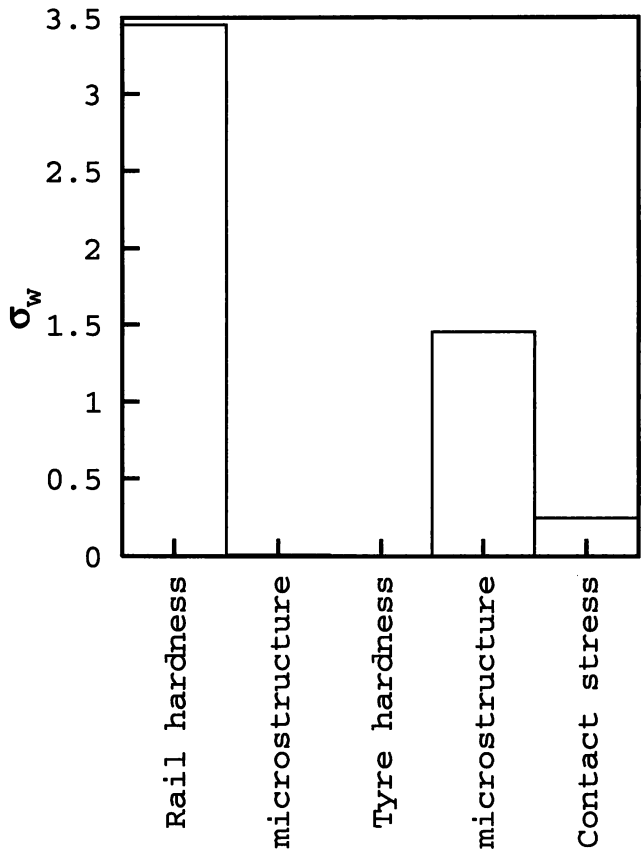

Figure 4.10: Partial correlation coefficients for neural net model for rail wear rate

This is probably because what actually afeects the wear rate is the toughness of the transferred and highly deformed surface layers, which are unlikely to to have the same toughness as the bulk.

	Hidden layer weights			
	1	2	3	4
Rail hardness	1.8181	0.8205	−1.1751	0.0622
Rail microstructure	4.1634	1.9022	−2.0800	−3.1413
Tyre hardness	0.0913	−0.0369	−0.0104	0.0206
Tyre microstructure	0.9270	0.0780	−0.2196	−0.0052
Charpy energy	0.1096	0.4170	−0.1010	−0.4705
Contact stress	0.1650	0.4539	0.2597	−0.0733
Offset	−2.1205	−0.5627	1.2219	1.1295
	Output layer weights			
Hidden unit 1	1.7897			
Hidden unit 2	2.2035			
Hidden unit 3	−2.9003			
Hidden unit 4	2.9475			
Offset	−1.3245			

Table 4.3: Weights and offsets for neural net model for wear with Charpy fracture energy. The model has four hidden units.

4.5 Summary

It is difficult to develop models for wear of rails because of the large scatter in wear testing data. The wear properties are likely to depend on the mechanical properties of the surfaces of the roller rather than the bulk, and wear models using bulk properties have been shown not to be effective. A small amount of data for surface hardnesses showed promising results but more should be gathered to test this model further.

An empirical approach using neural network modelling was not successful as there was not enough data for a reliable model to be generated.

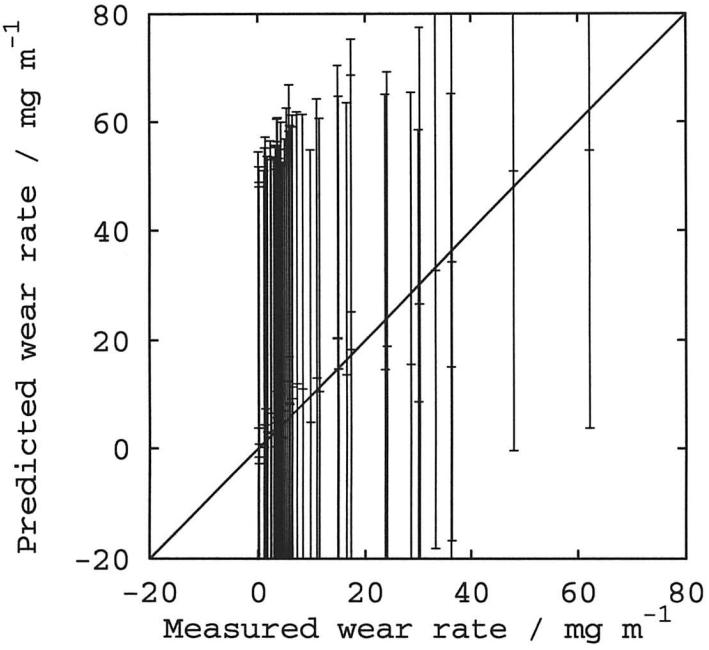

Figure 4.11: Neural network model for rail wear rate with Charpy fracture energy

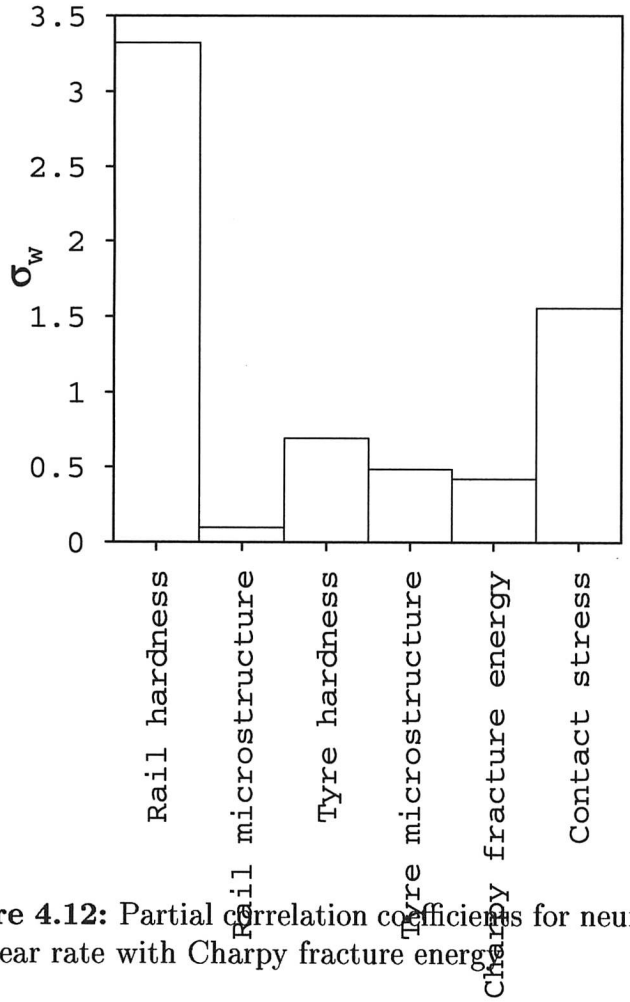

Figure 4.12: Partial correlation coefficients for neural net model for rail wear rate with Charpy fracture energy

5

Study of surfaces and wear debris from bainitic rails in track

This chapter describes the study of the surfaces and wear debris of experimental bainitic rails in track at British Steel's Scunthorpe Works and compares them with conventional rails at the same location.

5.1 Experimental

Experimental bainitic rails had been placed in track in two different curves; known as the torpedo route and the BOS perimeter. BOS stands for Basic Oxygen Steelmaking; the track was in this area of the site. On the torpedo route the trains have an axle load of 50 tonnes and the radius of curvature of the track is 140 m. This is a very high axle load and the trains move at a low speed; ten miles an hour. On the BOS perimeter the axle load is 25 tonnes and the radius of curvature is 110 m. Samples were always taken from the high rail of each curve. Four visits were made to the site to collect samples, at intervals of approximately six months. Two visits were made in the winter and two in the summer: December 1997, July 1998, February 1999 and June 1999.

Two different experimental bainitic compositions were in track on the torpedo route: the original boron-containing bainite, referred to as Bainite 1 in Chapter 3, and a boron-free composition. On the BOS perimeter there was a harder bainite (referred to as 440 HB bainite as this is its Brinell hardness) and another rail of the boron-free bainite. The 440 HB bainite was not in track on the first visit. The boron-free bainite on the

BOS perimeter was not in track on the first two visits. Samples were also taken from conventional mill-heat-treated pearlitic rails next to each bainitic rail, which had been in track a similar length of time to the bainitic rails.

It was not reasonable to cut samples from the rail so a technique was developed using cellulose acetate replicas of the rail surface. The rail was first cleaned with acetone, and then the surface was flooded with more acetone. A thin piece of cellulose acetate was gently lowered onto the wet surface. This was then left to dry completely (the time required varied from 30 minutes on a very cold day to less than five on a warm one) and teased off the rail with a fine pair of tweezers. Three thicknesses of acetate were tested: 180 μm, 125 μm, and 35 μm. The 35 μm acetate produced the best results although it was the most difficult to handle. Small pieces of cellulose acetate (less than 1 cm square) produced better results than large ones as they were less likely to distort or break when removed from the rail. It was vital to allow the acetate to dry completely or it became damaged on removing from the rail. The acetate was then mounted on an aluminium stub with carbon tape and conductive paint, gold coated for conductivity, and examined in a JEOL JSM 800 scanning electron microscope at a voltage of 3 kV to minimise specimen degradation due to the beam. Samples were taken from the running band and the gauge corner of each rail.

Wear debris was collected from along the length of each rail on the second and third visits; this was stuck onto carbon tape, gold coated, and examined in the JEOL JSM-820 SEM. Energy dispersive X-ray anaylsis for composition (EDX) was carried out on some samples of debris in a JEOL JSM-5800LV SEM.

Compositions, wear rates and amount of traffic seen for each rail were provided by British Steel for dates close to those of the first and second visits. For the fourth visit the wear rates were measured on the day of the visit. No data were available for the third visit.

5.2 Wear rates

Wear rates and amount of traffic seen, measured approximately at the time of each visit to the site, are shown in tables 5.1–5.3. British Steel scientists estimate the error in the wear rates to be of the order of 0.001 mm Mgt^{-1}. These units are mm of height lost per million gross tonnes of traffic which has passed over the rail. The weight of both the train itself and its load is counted. Compositions for the rails and their laboratory wear test results are shown in tables 5.4 and 5.5. It can be seen that, in the torpedo route

rails, the harder bainitic rail is only about as good as the conventional MHT rail. Wear rates for each rail *vs.* tonnage are plotted in Figure 5.1–Figure 5.2. The running bands of the rails in the torpedo route were not all yet broken in on the first visit to the site; this would correspond to tonnages over the rails at that point of up to 20 Mgt (million gross tonnes) on Figure 5.1 (a), with the exception of one of the MHT rails studied, MHT 1, which had seen 36 Mgt of traffic at this point and was probably broken in already. It is likely that running-band replicas taken during the first visit would show breaking-in behaviour, and those on the subsequent visits, steady-state wear.

The torpedo route running bands show a steady decrease in wear rate although there is some scatter. This is probably due to breaking-in of the surfaces. The bainitic rails on the whole behave like the MHT rails which is odd given the large differences found in the laboratory wear tests (Table 5.5).

It can be seen from Figure 5.1 that the torpedo route gauge corner wear rates have some scatter. The average wear rate does not decrease as the running band wear rate does. These locations will break in very much faster than the running bands because wear is more severe— the rails are the high rails of a curve. The wear rate of the bainitic rails seems to be decreasing as the total amount of traffic seen increases, although three measurements are not really enough to be sure. There is enough scatter in the MHT results that it seems plausible that the decreasing bainitic wear rates are just a coincidence and if results in the longer term were available the wear rates might be seen to be constant.

The rails in the BOS perimeter are not directly comparable with those in the torpedo route because of the lower axle load and tighter curvature. The latter explains the high gauge face wear seen on these rails. There is scatter in the data probably because of the small amount of traffic. Fewer results are available for these rails as they were put into track later. The bainitic rails are superior on the running bands, unlike in the higher axle load torpedo route, although more data are needed to confirm this. Studies have found that bainitic rails, unlike pearlitic rails, generally have a wear rate that varies in a non-linear way with load. Their wear resistance tends to become comparable with that of pearlitic steels at high contact pressures [Clayton *et al.* 1987, Devanathan and Clayton 1991] and they are not as good at lower pressures, so this result is surprising. However, 25 tonnes is not a particularly low axle load; this is typical for freight trains in Europe. The coaches of passenger trains exert a load of about 12 tonnes [Esveld 1989].

Location	Rail	Axle Load tonnes	Wear rate mm Mgt^{-1} Running Band	Gauge Corner	Total Traffic Mgt*
Torpedo	Boron-treated bainite	50	0.036	0.075	20.5
Route	MHT 1		0.016	0.079	36.8
	MHT 2		-	0.060	21.9
	Boron-free bainite		0.052	0.117	6.9
	MHT 3		0.095	0.055	6.9

* Million gross tonnes

Table 5.1: Track Wear Results (December 1997) The rails designated MHT 1 and 2 are conventional mill heat treated rails that are close in track to the boron-containing bainitic rail, and have seen roughly the same amount of traffic. MHT 3 is a conventional rail that was laid next to and at the same time as the boron-free bainitic rail.

Location	Rail	Axle Load tonnes	Wear rate mm Mgt^{-1} Running Band	Gauge Corner	Total Traffic Mgt*
Torpedo	Boron-treated bainite	50	0.026	0.059	29.9
Route	MHT 1		0.015	0.069	46.2
	MHT 2		0.005	0.077	30.0
	Boron-free bainite		0.026	0.085	16.3
	MHT 3		0.041	0.040	16.3
BOS	440 HB bainite	25	0.003	0.280	9.9
Perimeter	MHT 4		0.060	0.420	9.9

* Million gross tonnes

Table 5.2: Track Wear Results (July 1998) MHT 4 was laid next to and at the same time as the 440 HB bainite. The high wear rates for the BOS perimeter gauge corners are due to the smaller radius of curvature of the track

Location	Rail	Axle Load tonnes	Wear rate mm Mgt^{-1} Running Band	Gauge Corner	Total Traffic Mgt*
Torpedo Route	Boron-treated bainite	50	0.021	0.044	43.8
	MHT 1		0.012	0.058	60.1
	Boron-free bainite		0.024	0.066	30.2
	MHT 3		0.027	0.047	30.2
BOS Perimeter	440 HB bainite	25	0.025	0.320	13.0
	MHT 4		0.057	0.380	13.0
	Boron-free bainite		0.017	0.423	6.8
	MHT 5		0.123	0.494	6.8

* Million gross tonnes

Table 5.3: Track Wear Results (June 1999) MHT 5 was laid next to and at the same time as the boron-free bainite in the BOS perimeter. No data were provided for MHT 2 on this occasion.

Rail	Composition wt%							
	C	Si	Mn	P	S	Cr	Mo	B
Boron-treated bainite	0.21	1.97	1.98	0.013	0.015	0.48	0.47	0.0026
Boron-free bainite	0.27	1.86	1.98	0.014	0.015	0.50	0.59	-
440 HB bainite	0.23	1.94	1.98	0.013	0.014	1.91	0.45	-

Table 5.4: Compositions of experimental rails in track

Rail	Wear Rate mg m^{-1}	
	Rail	Tyre
Boron-treated bainite	5.33	10.37
Boron-free bainite	4.22	6.81
440 HB bainite	5.85	13.04
Typical MHT rail	36.29	89.40

Table 5.5: Laboratory wear rates for experimental steels The wear rates are measured in mg of weight lost per metre of slipping distance and are thus not directly comparable with the track wear rates.

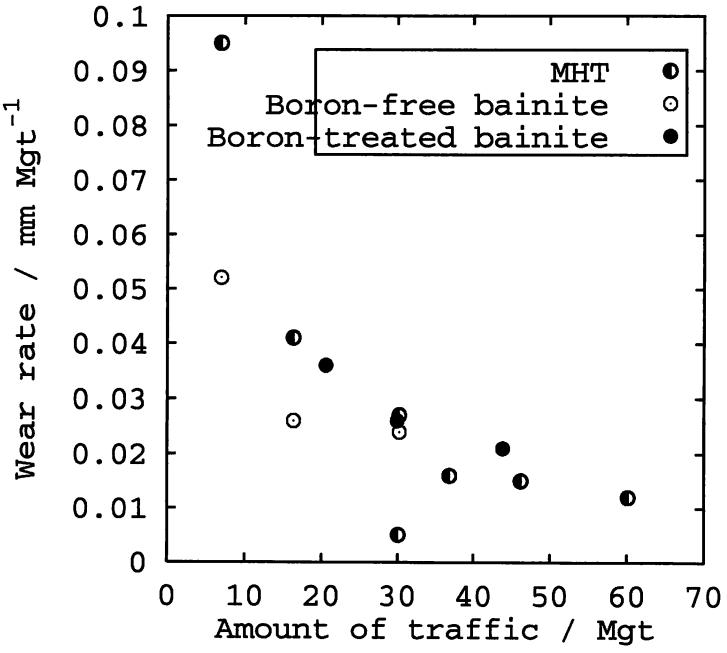

Figure 5.1(a): Wear rates *vs.* tonnages for rail running bands on the torpedo route

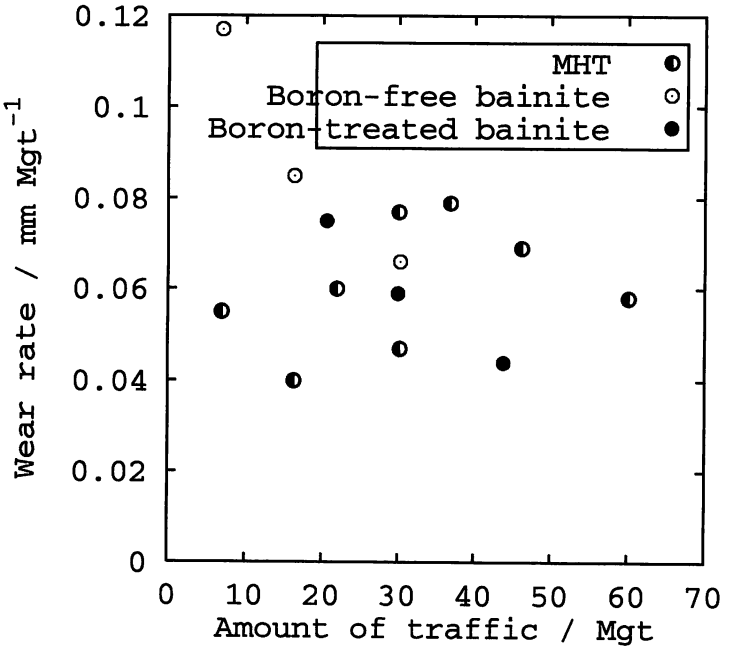

Figure 5.1(b): Wear rates *vs.* tonnages for gauge faces of rails in track on the torpedo route

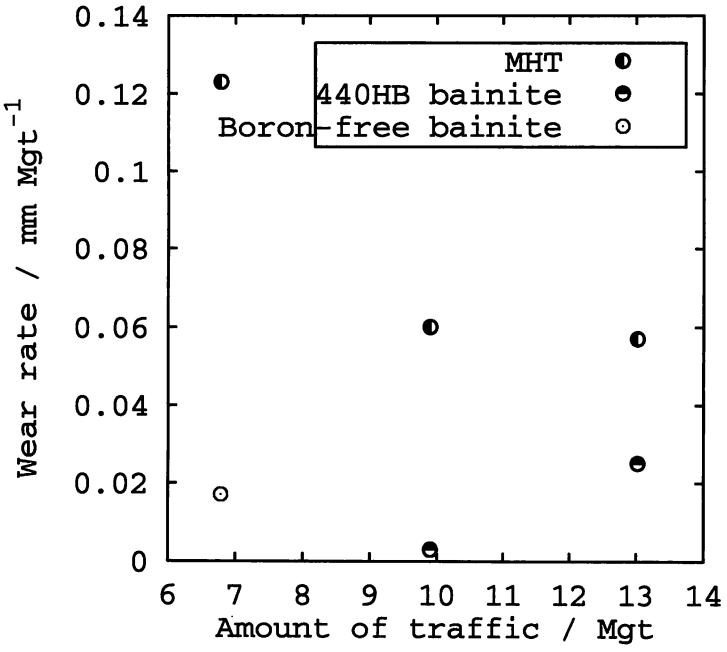

Figure 5.2(a): Wear rates *vs.* tonnages for rail running bands on the BOS perimeter

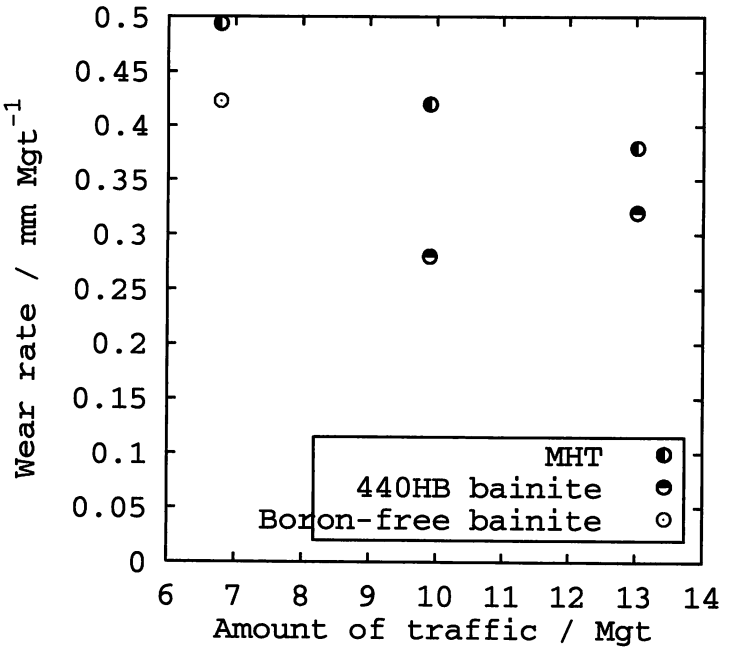

Figure 5.2(b): Wear rates *vs.* tonnages for gauge faces of rails in track on the BOS perimeter Note the change in y-axis scale from the previous graph.

The bainitic rails also do better on gauge corner wear, although here the wear rate is higher. The bainitic rails do not perform as well as might be expected from the laboratory wear test results.

5.3 Surface replicas

All micrographs referred to in this section are to be found at the end of the chapter.

SEM micrographs of the replicas taken in December 1997, the first visit to the track, are shown in Figure 5.3–5.5. The running-band replicas all contain areas similar to the "craters" seen in the laboratory specimens in Chapter 3. It should be remembered that the replica samples are negatives; what appears as a raised area on the image is really a sunken area on the rail surface and *vice versa.* The two bainitic rails, which had seen much less traffic than the MHT rail, have slightly smoother surfaces. These craters are probably produced by breaking off of parts of the transfer layer on the rail surface, as discussed in Chapter 3.

The gauge face replicas were different. They contained regular laps, with fairly featureless areas in between. The boron-containing bainitic sample was slightly less regular than the other two, with some rough areas and comparatively fewer laps. All the laps were oriented with their long direction parallel to the rail. The material appeared to have flowed down the gauge face under the action of the tyre flange.

The samples taken on the second visit in July 1998 were different (Figure 5.6-5.10). The running bands of the rails in the torpedo route all showed a pattern of parallel lines. These were in the form of ridges, and so would correspond to grooves on the actual rail. The boron-containing bainitic rail showed large featureless regions in addition to the grooves. These features appear to have been caused by abrasion by harder particles.

The gauge face samples were also distinctive, with many large laps and scars, showing severe damage. The surfaces were much rougher than those seen on the first visit. The boron-free bainite, and the MHT rail (MHT 3) which had been put in at the same time, were noticeably smoother than any of the other rails because these had seen less traffic.

The BOS perimeter samples, which had a lower axle load and had seen relatively little traffic, resembled the samples taken on the first visit. The running band of the bainitic rail contained the same type of crater-like feature seen previously. The gauge face was fairly smooth, with a smeared appearance and a few small laps.

Pictures of the replicas taken on the third visit to the site, in February 1999, are shown in Figure 5.11–5.18. In addition to the rails previously examined, replicas were

also taken from a boron-free bainitic rail and an equivalent MHT rail in the BOS perimeter track which had not been present on the previous visits.

The torpedo route samples all had craters on the running bands as observed the previous winter. The gauge faces almost all had laps orientated as before. The exception was the boron-containing bainite which had some craters; perhaps this steel is more resistant to the smearing action of the wheel flange. This makes it seem unlikely that the changes seen previously were the result of breaking-in behaviour despite the information that the rails were not fully broken-in on the first visit to the site in December 1997. There may be environmental effects that cause the changes between summer and winter; consequently a fourth visit was arranged to take place in June 1999.

The BOS perimeter samples varied in their appearance. The two rails that had been in track for the longest time, the 440 HB bainite and the adjacent MHT rail, had cratered running bands. The gauge corners were very uneven and disordered, with craters, holes, and scuffs. This is perhaps to be expected given that the curve is tight and hence causes severe wear on the gauge corner. The adhesion between the rail and tyre would be great, leading to the removal of large amounts of material. The two newer rails, the boron-free bainite and the corresponding MHT rail have flatter surfaces than the other two as they have seen less service.

The 440 HB bainitic rails had seen very little traffic when replicas were first taken from them and so the change in the appearance of the running bands may be due to breaking-in behaviour in these rails.

Replicas taken in June 1999 are shown in Figure 5.19–5.26. The torpedo route samples show the usual cratered running bands, with the exception of the MHT rail next to the boron-treated bainite which had some laps on the running band. All the gauge corners had laps. It was interesting to observe traces of grooves in the gauge corner of the boron-free bainitic rail, similar to those seen in July 1998.

On the BOS perimeter all the rails had cratered running bands. The gauge faces were severely worn with smears and laps. The experimental rails are not supposed to be lubricated but when the replicas were taken the boron-free bainitic rail was found to be very greasy, which implied it had been lubricated. If this is so, then the wear results may not be comparable with other rails as lubrication will greatly reduce wear and tends to promote rolling contact fatigue.

Diagrams showing surface appearance for all rails on the torpedo route as a function

of total traffic and wear rate are shown in Figure 5.27.

There is no correlation between total tonnage and surface appearance, but there is between date and appearance. This suggests that some external influence caused the change of wear apttern observed in July 1998 rather than breaking-in behaviour. The normal appearance of the rails is craters on the running abnd, caused by the detatchment of sections of the transfer layer, and laps on the gauge face caused by the flange of the wheel smearing the metal down the sidew of the rail. These laps will eventually break off and form wear debris.

5.4 Wear Debris

Wear debris was collected during the July 1998 and February 1999 visits. On the February visit it was hard to find debris to collect and so comparatively few particles were available to study. On examination in the SEM it was found that the debris fell into three categories. All debris collected along the torpedo route was in the form of shiny metallic flakes, up to 2 mm long and about 10 μm thick. These flakes were made up of many different layers of smaller flakes. They were very similar to those seem in laboratory wear testing, only larger. A picture of a typical example is shown in Figure 5.28.

Debris collected from the BOS perimeter in July 1998 consisted of very much smaller particles of the order of 5-100 μm length and thickness around 5 μm. Unlike the previous category, most of the particles seemed not to be made up of smaller units. An example is illustrated in Figure 5.29.

Debris collected from the BOS perimeter in February 1999 consisted of dull, sharp-edged particles of the order of 1 mm long and 0.1 mm thick. An example is shown in Figure 5.30. They were so unlike either of the other types of particles that their composition was investigated using EDX in a 5800 scanning electron microscope. The compositions of the particles varied. They were all mostly iron, but with up to 10 wt% calcium and silicon. Some contained small (less than 1 wt%) amounts of nickel and chromium. They also appeared to be much more corroded than the other two types of particle. The compositions clearly do not match either typical rail or tyre steel compositions, so these particles are probably not related to the rails at all but were blown from some other part of the steelworks onto the tracks.

5.5 Discussion

The torpedo route debris is similar in appearance to that collected in laboratory wear tests but much larger in scale. This is reasonable; the work of Zakharov *et al.*

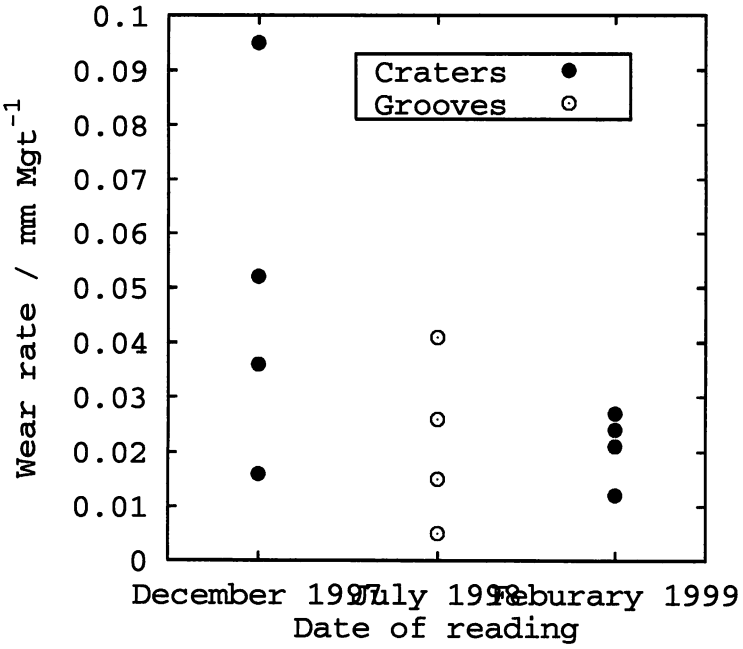

Figure 5.27 (a): Wear rates *vs.* total tonnage for all torpedo route running band measurements, showing surface appearance of each sample

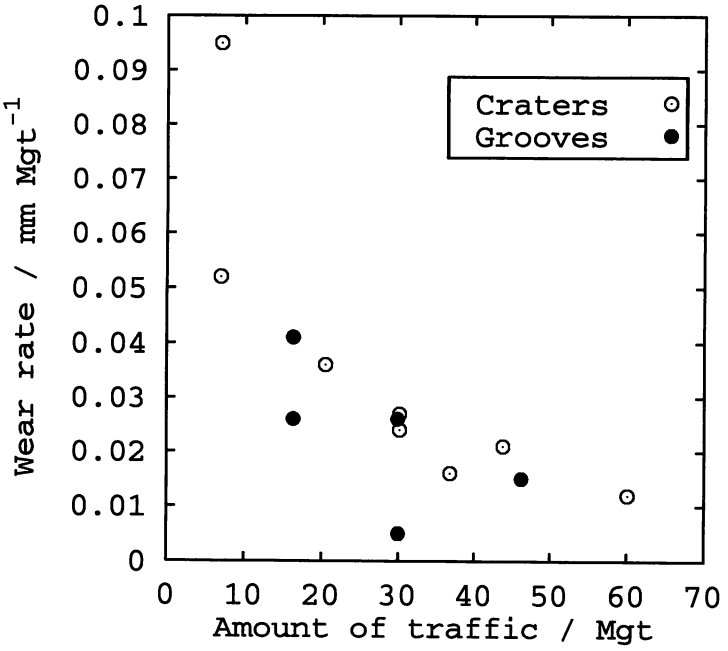

Figure 5.27 (b): Wear rates *vs.* date of measurement for all torpedo route running band measurements, showing surface appearance of each sample

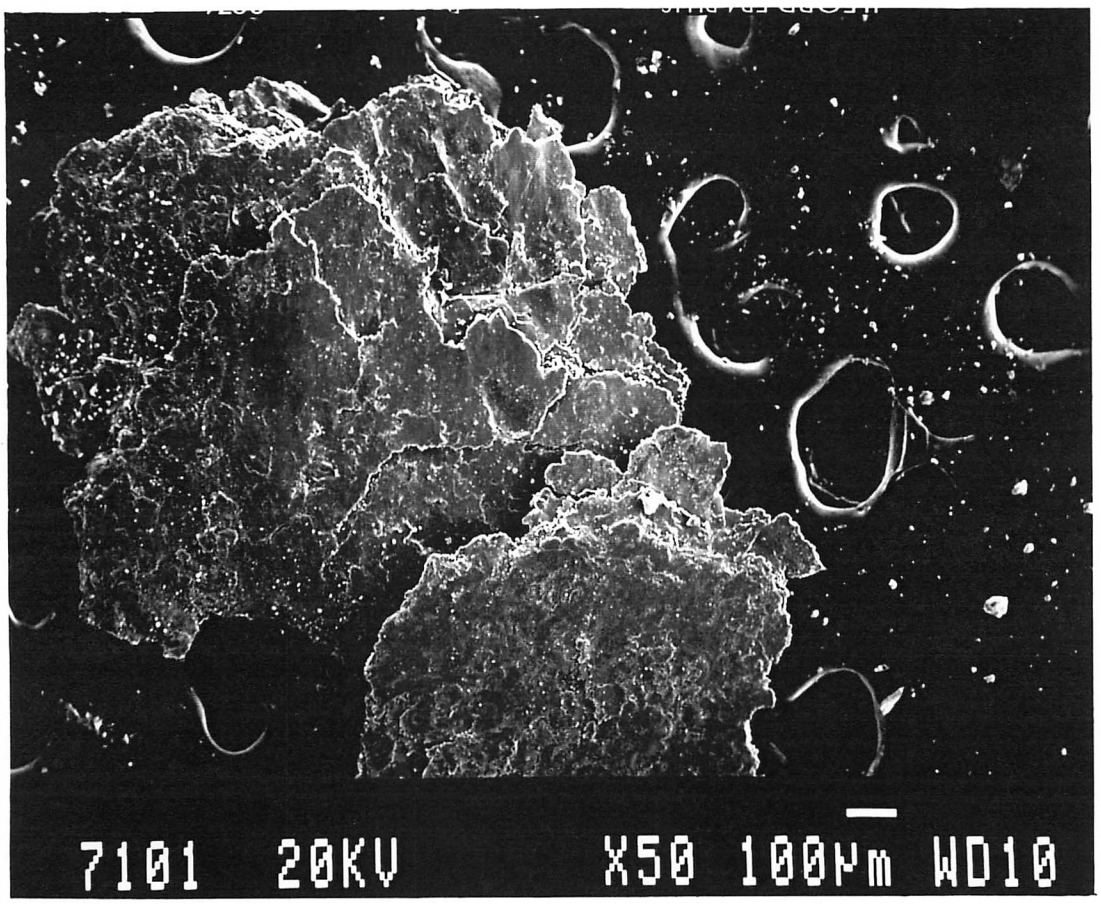

Figure 5.28: Wear debris collected from torpedo route The flakes are large and made up of many smaller particles. This particular example was collected from by the MHT rail immediately adjacent to the boron-free bainitic rail; however all wear debris collected along the torpedo route appeared the same

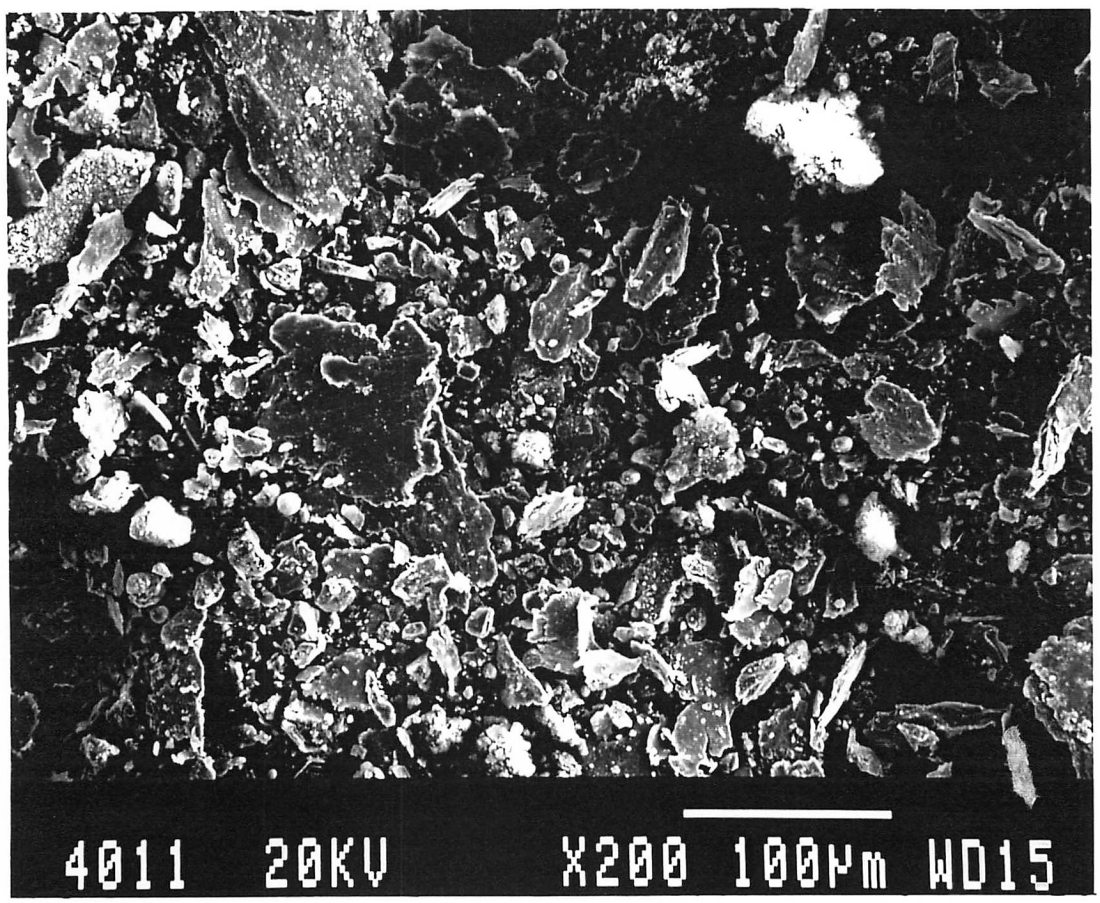

Figure 5.29: Wear debris collected from BOS perimeter July 1998 Note the change in scale from the previous picture as the particles are very much smaller. These were collected from by the 440 HB rail

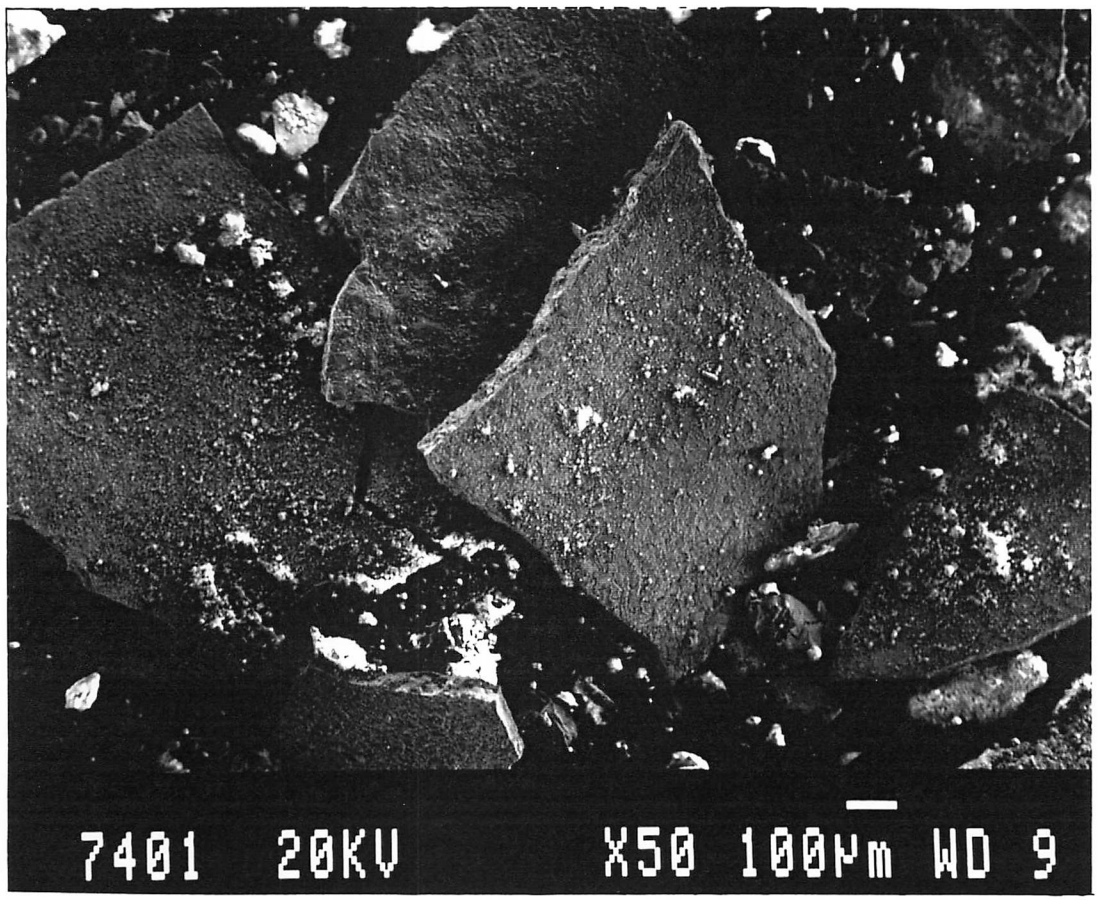

Figure 5.30: Wear debris collected from BOS perimeter February 1999 Note the change in scale from the previous picture as these particles are larger. These were collected from by the 440 HB rail

(1998) suggests that the size of the wear scars is proportional to the contact area, so the same may well apply to the wear debris. Smaller wear debris is therefore explained in the laboratory wear tests for the same mechanism.

The wear debris seen on the torpedo route is otherwise so similar to that found in laboratory wear tests that it seems reasonable to assume it was formed by the same mechanism. The results of laboratory tests should be therefore be applicable to interpreting the behaviour of steel in track; however, this does not seem to be so for bainitic rails. British Steel scientists report that wear rates for pearlitic steels in the laboratory do rank in the same order as those for track wear, but the bainitic steels studied here do not. However, the laboratory wear tests are greatly accelerated as creepages of 25% are used. There is also much more environmental variation on track than in the laboratory which may make a difference. The grooved wear pattern observed on all torpedo route rails in July 1998 has not been observed in the laboratory so a different wear mechanism, possibly abrasive wear, can occur on track.

The wear debris collected from the BOS perimeter is similar to that observed by Bolton and Clayton (1983) for what they defined as "Type III wear". However the actual wear surfaces do not appear much more damaged than on the torpedo route despite the fact that the gauge face wear is much higher due to the tightness of the curve.

Comparing the wear rates supplied by British Steel with the appearance of the wear surfaces reveals no obvious change of behaviour around July 1998, when the torpedo route surfaces were observed to contain grooves. This may be because the wear rates summarize the wear over a fairly long period of time and whatever caused the grooves was a relatively short-term effect. It therefore seems likely that some sort of variation in the environment of the rails on the torpedo route must have caused the grooves to form and was then subsequently reversed, causing the rails to recover their previous appearance. If this is true then the rails in track must see a much more varied set of conditions than in the laboratory wear tests, hence the differences in the behaviour of the bainitic steel between them.

The running bands of the rails examined in this study contain large craters and appear to correspond to "Type III wear", also called "catastrophic wear" [Zarkhov *et al.* (1998)]. This is not usually reported on rail running bands, only on gauge faces. The grooves which were observed in July 1998 have not been reported elsewhere. This could

possibly be due to higher axle loads in the test track but it is hard to be sure as the studies comparing laboratory wear regimes with those seen on track do not report the axle loads. However the 50 tonne axle load experienced by the rails in the torpedo route is exceptionally high compared with that on most tracks. This corresponds to a contact pressure of around 750 MPa, which is what was used in the laboratory wear tests.

The gauge corners, on the other hand, show a variety of types of wear. The regular laps seen on the torpedo route are similar to "Type II wear" as seen by Bolton and Clayton (1983), and Danks and Clayton (1987). Bolton and Clayton saw this type of wear at the gauge corners of the side-worn rails they studied. Zarkhov *et al.* (1998) also saw wear like this on the gauge corners of the rails they studied, although they have called it "mild wear". This does not appear to be the same as the "mild wear" described by Danks and Clayton (1987). The torpedo route rails showed a different wear pattern on the gauge corner in July 1998 which was more like "Type III wear". There are two possibilities to explain this anomaly: either the July 1998 gauge corner replicas were mistakenly taken lower down on the rail than all the rest (the studies mentioned above found "Type III wear" lower down on the gauge face) or that something in the environment of the rails had changed. Given that the running bands too showed a different wear pattern to that observed on other visits, the latter seems most likely.

5.6 Summary

A replica technique has been used to study the worn surfaces of conventional MHT and experimental bainitic rails in track in two curves over a period of a year and a half. Wear debris was also collected from the rails and wear rates measured.

The wear surfaces on the rail running bands generally displayed craters which are thought to correspond to "Type III" or "catastrophic" wear as it is sometimes known. This does not seem to have been reported on running bands previously. One of the curves on one visit to the site displayed a very different wear pattern on the rail running bands which appeared to be caused by abrasive wear. This wear pattern was subsequently replaced by more craters although traces of it were found in one of the rails a year later. No obvious change in measured wear rate could be connected with the appearance of the unusual patterns.

The wear rate on the running bands on the 50-tonne axle load torpedo route appears to drop from an initial high breaking-in value to a lower steady-state value. The bainitic rails perform no better than conventional MHT rails despite having shown much lower

wear rates in rolling-sliding laboratory tests. The wear rate on the running bands on the 25-tonne axle load BOS perimeter is lower than that on the torpedo route and here the bainitic steels seem to perform slightly better, but more data is required to confirm this. The BOS perimeter rails have seen so much less traffic than the torpedo route rails that they might not yet be properly broken in and so the situation may change in the future.

The gauge corners are worn a lot more than the running bands and so they break in much more quickly. They normally display cold laps where the metal has been pushed down and folded over by the action of the wheel flange. The wear rate is much higher, as would be expected, particularly on the tighter curve in the BOS perimeter. The appearance of the surfaces seems to correspond to "Type II wear" or in some cases "Type III wear" as reported by other researchers. There appears to be some reduction of wear rate with traffic seen for the bainitic rails on the torpedo route but more data needs to be collected to be sure.

The wear debris found along the torpedo route is similar to that found in laboratory wear tests but on a much larger scale which is to be expected. The debris found on the BOS perimeter was much smaller in scale and did not appear to have been formed in the same way. Some of the particles collected from this location were shown not to have come from the rails at all. The difference in size and shape between the particles that are believed to be genuine wear debris may be a function of the differing axle loads on the two curves.

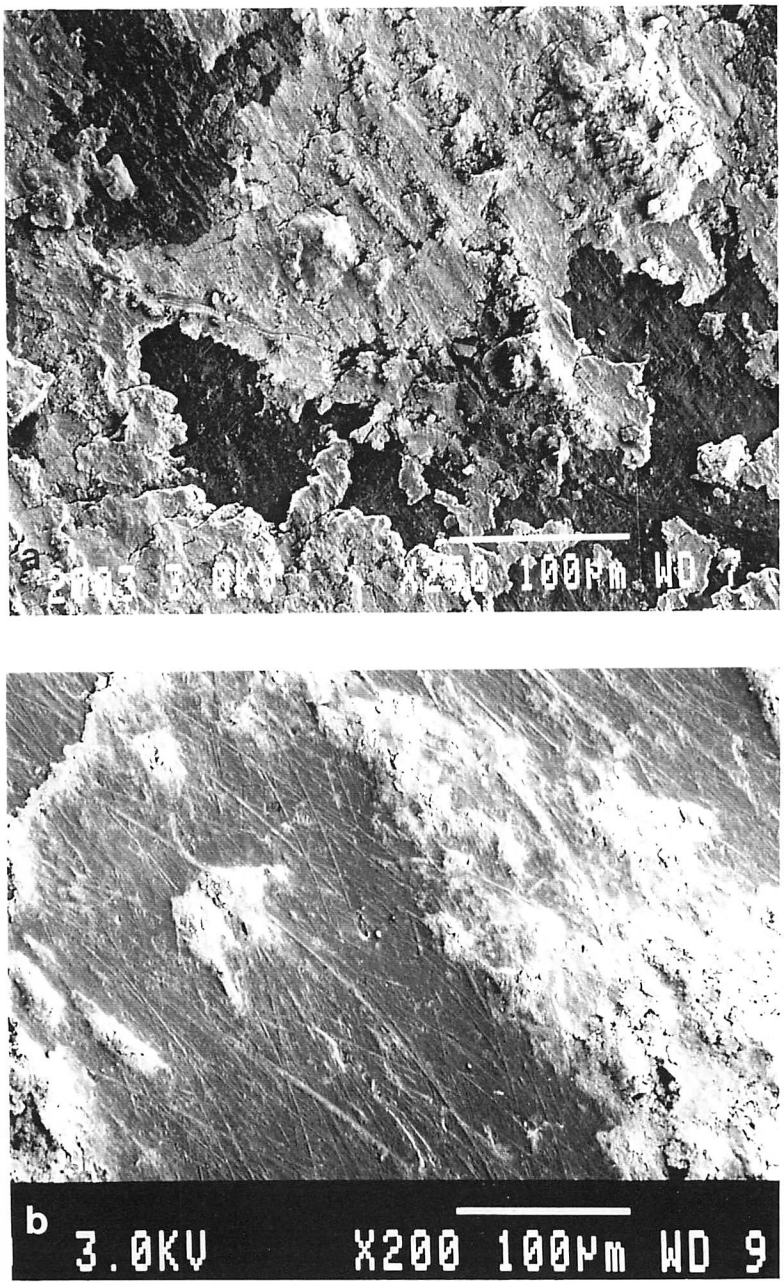

Figure 5.3: Boron containing bainitic rail replicas Torpedo route December 1997
a) Running band with crater-like features
b) Gauge corner with lap visible in top left-hand corner

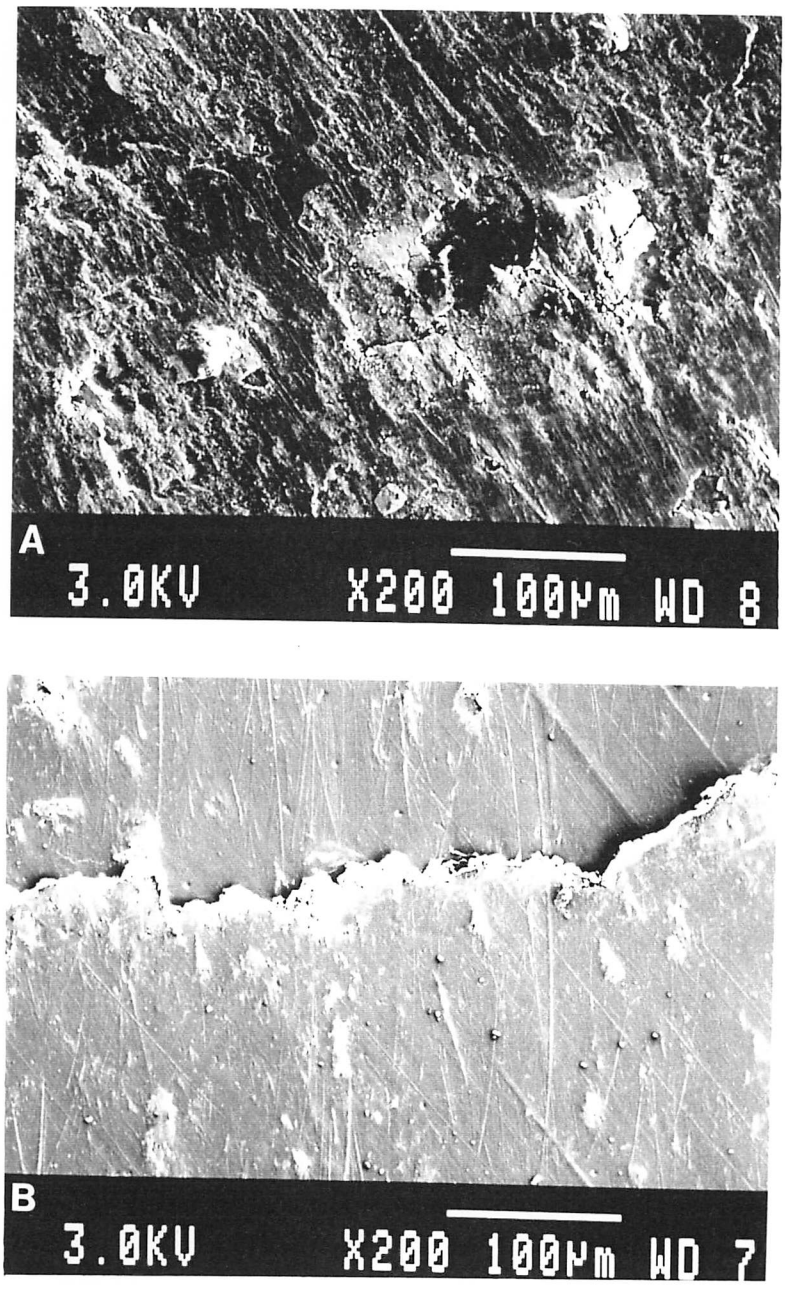

Figure 5.4: Boron free bainitic rail replicas Torpedo route December 1997
a) Running band with crater-like features
b) Gauge corner with laps

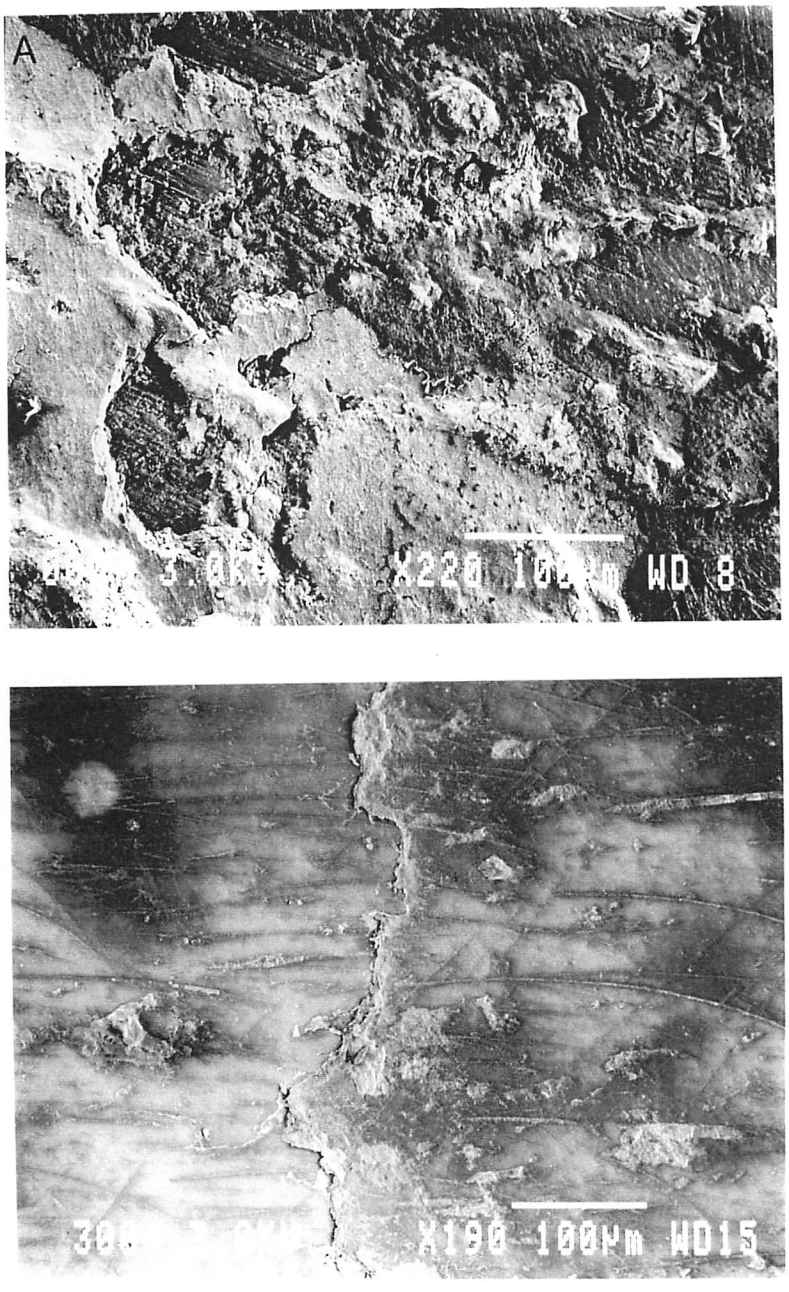

Figure 5.5: MHT rail replicas Torpedo route December 1997
a) Running band with crater-like features
b) Gauge corner with very shallow laps

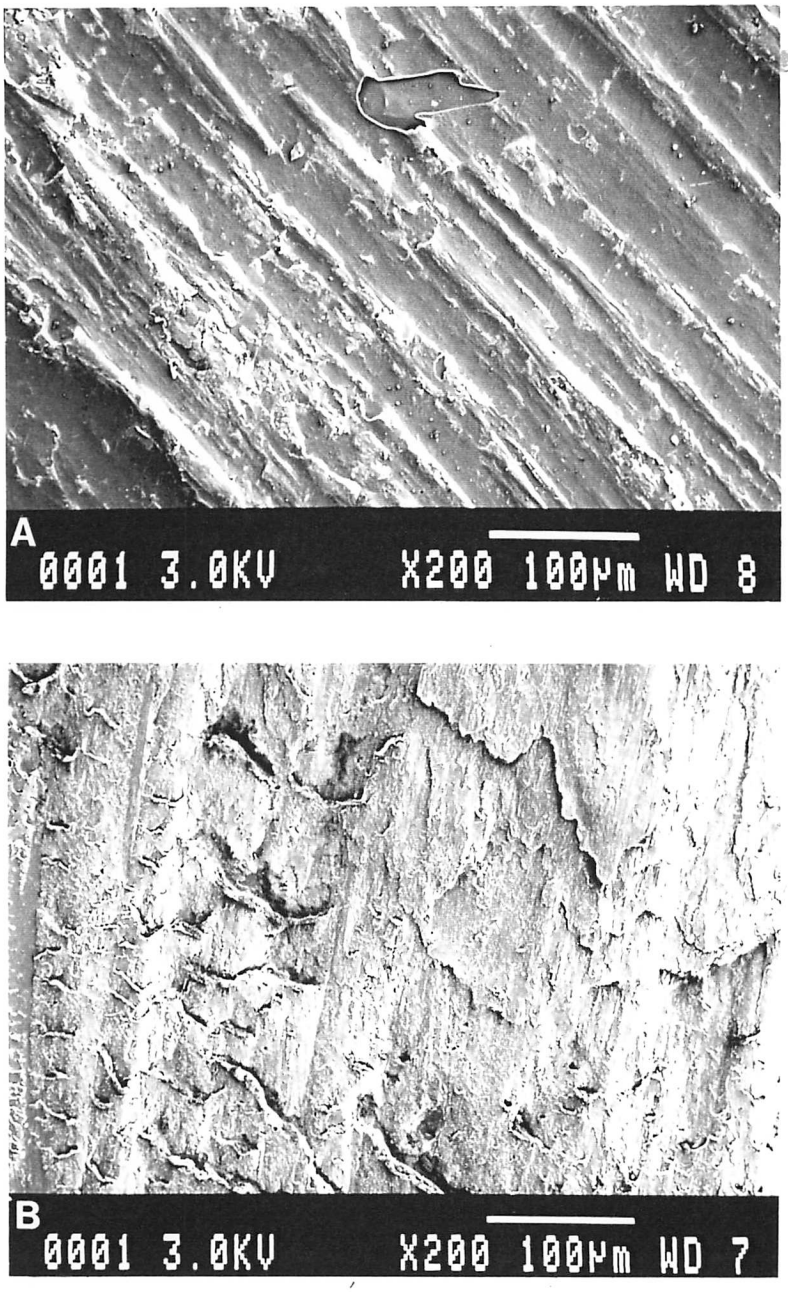

Figure 5.6: Boron containing bainitic rail replicas Torpedo route July 1998
a) Running band with distinctive grooves (also had some featureless regions)
b) Gauge corner with severely worn irregular surface

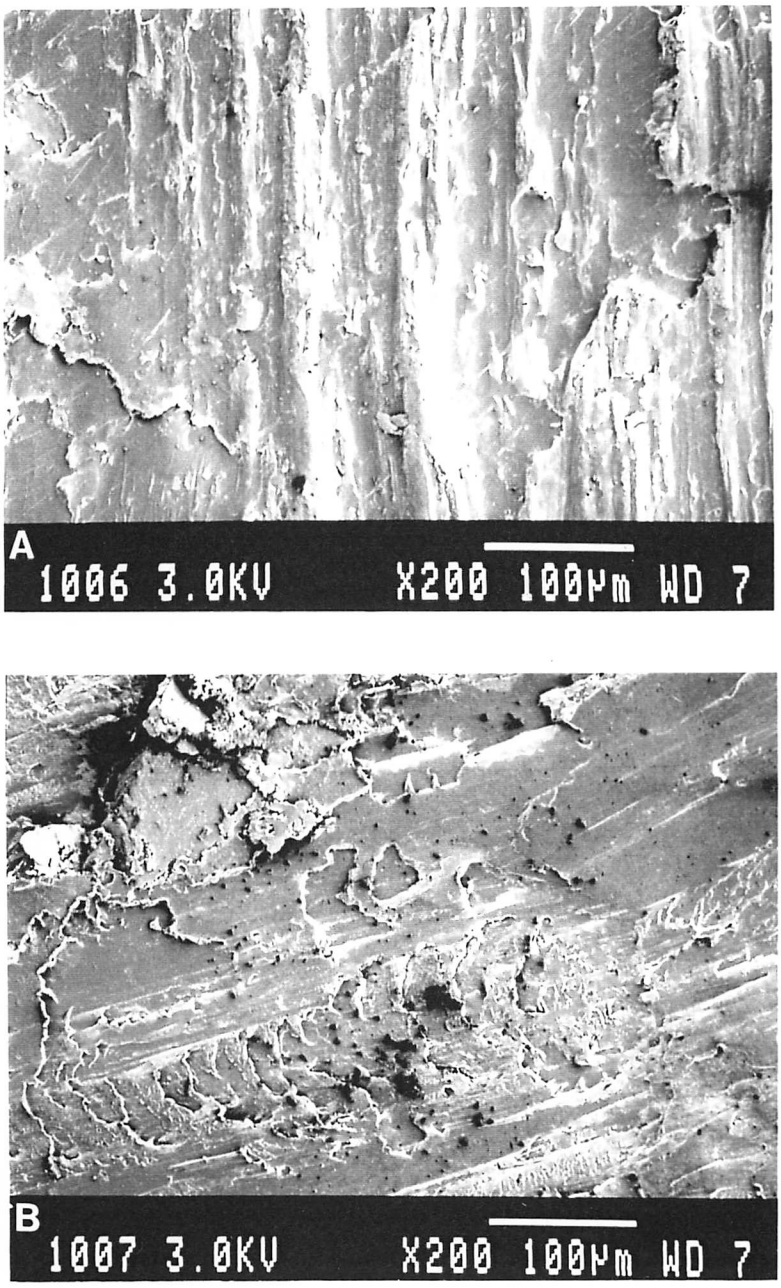

Figure 5.7: MHT adjacent to boron containing bainitic rail replicas
Torpedo route July 1998
a) Running band with grooves
b) Gauge corner with laps and scars

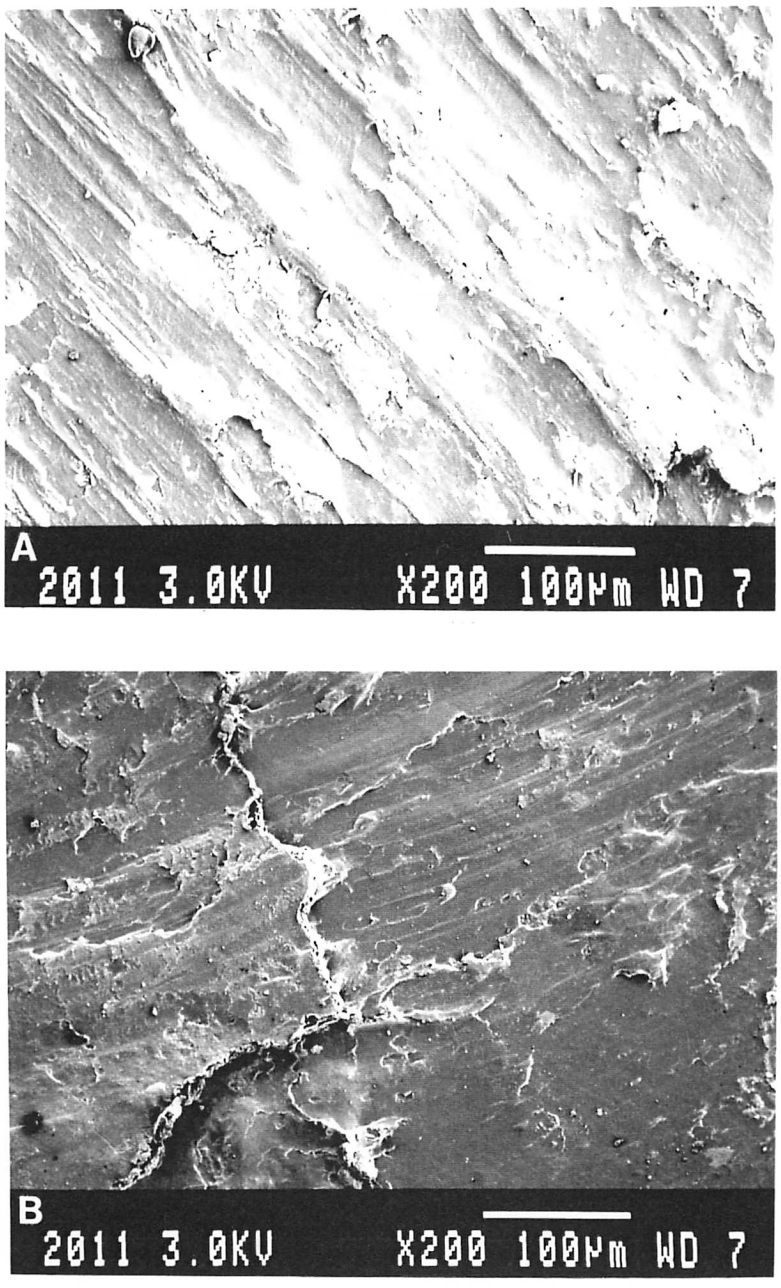

Figure 5.8: Boron free bainitic rail replicas Torpedo route July 1998
a) Running band with signs of grooves
b) Gauge corner

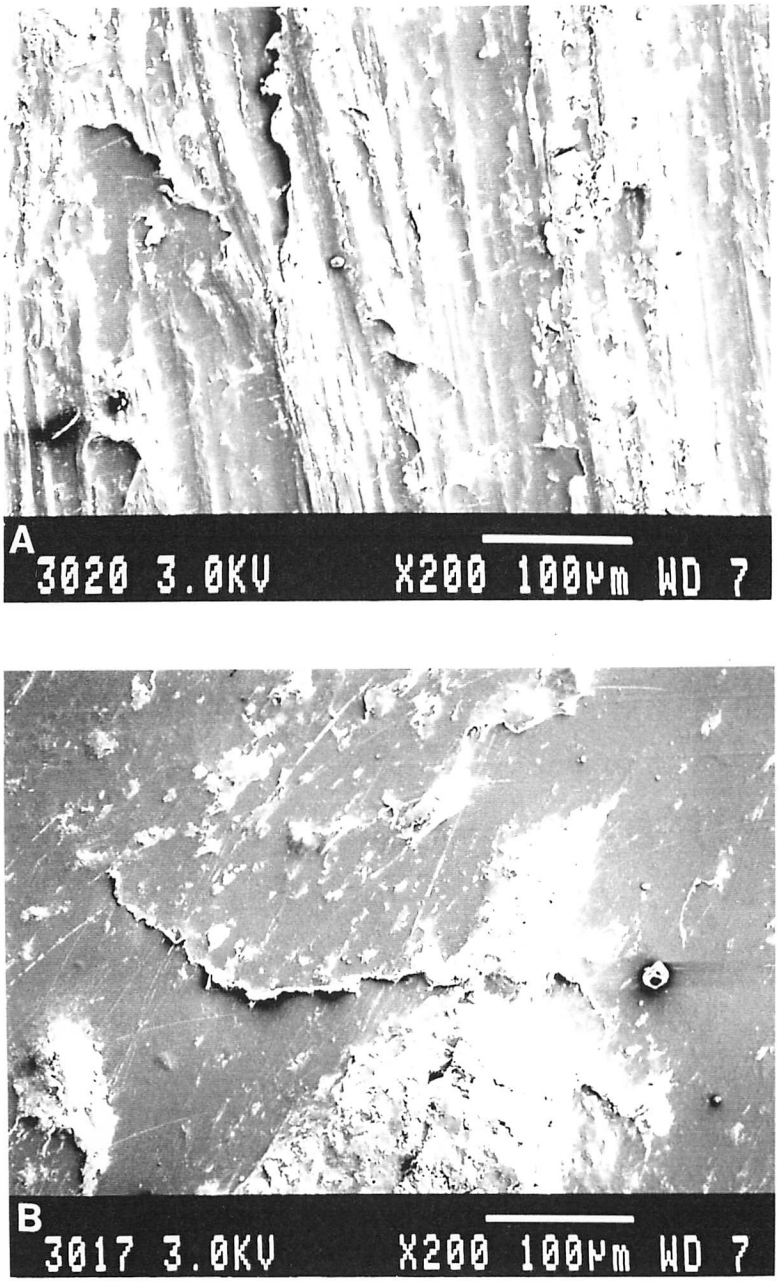

Figure 5.9: MHT adjacent to boron free bainitic rail replicas Torpedo route July 1998
a) Running band with grooves
b) Gauge corner with signs of laps

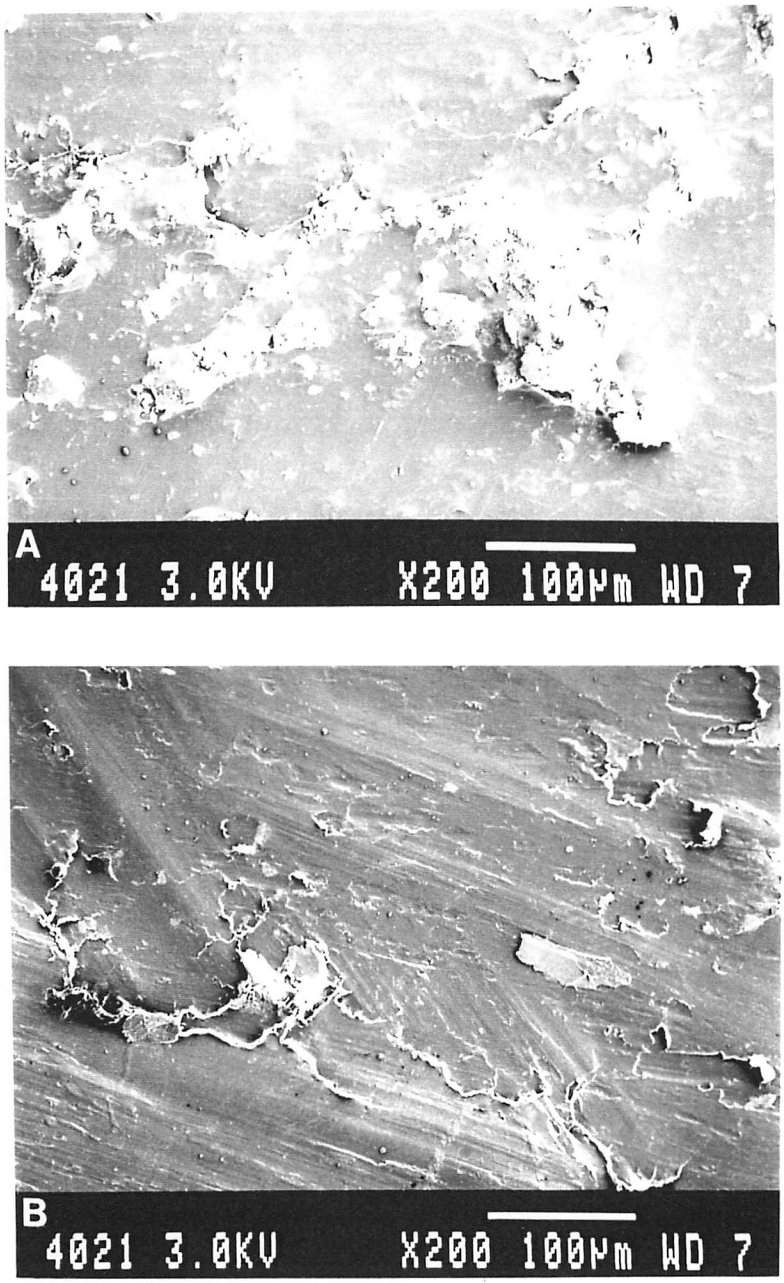

Figure 5.10: 440 HB bainitic rail replicas BOS perimeter July 1998
a) Running band with craters
b) Gauge corner with "smeared" appearance

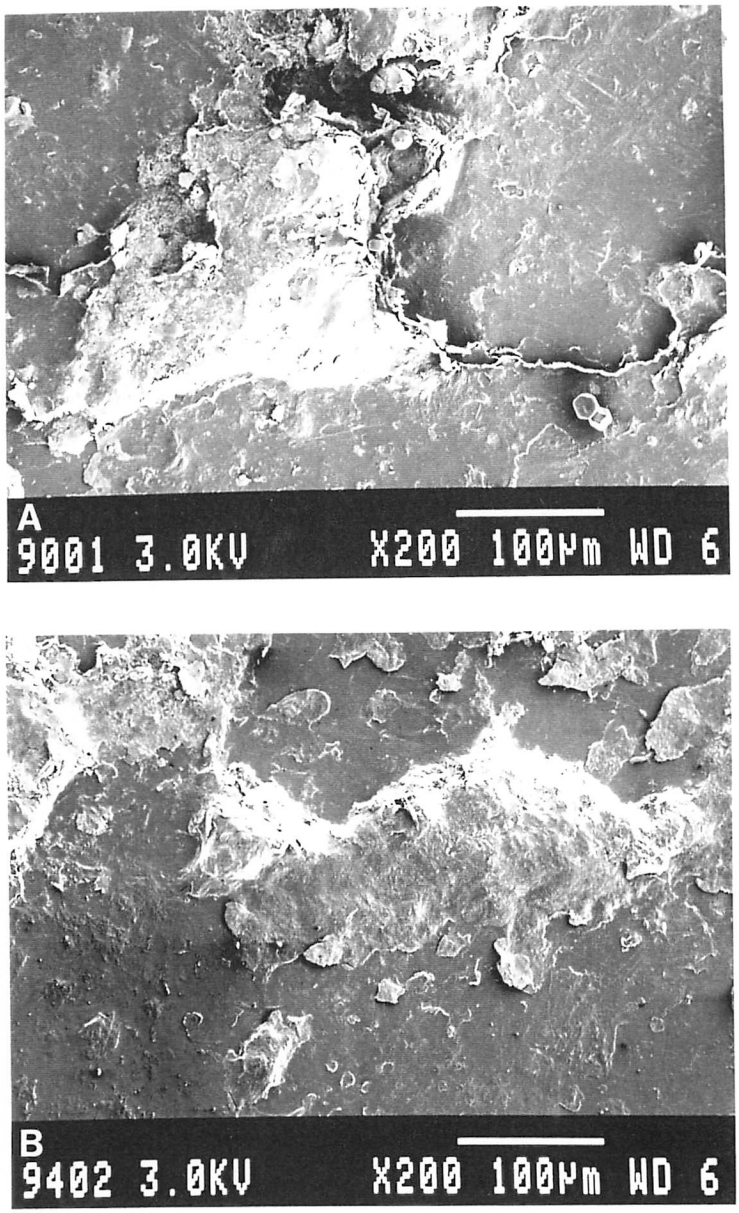

Figure 5.11: Boron containing bainitic rail replicas Torpedo route February 1999
a) Running band with craters
b) Gauge corner with craters

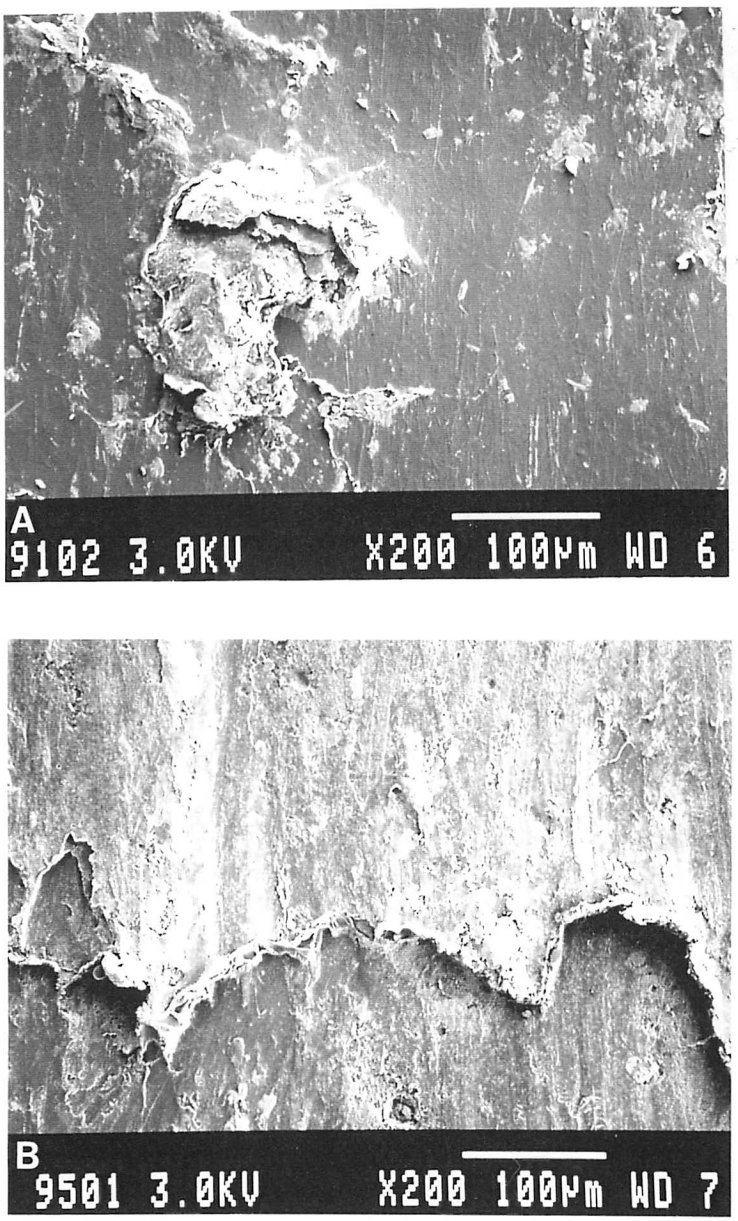

Figure 5.12: MHT adjacent to boron containing bainitic rail replicas
Torpedo route February 1999
a) Running band with craters
b) Gauge corner with laps

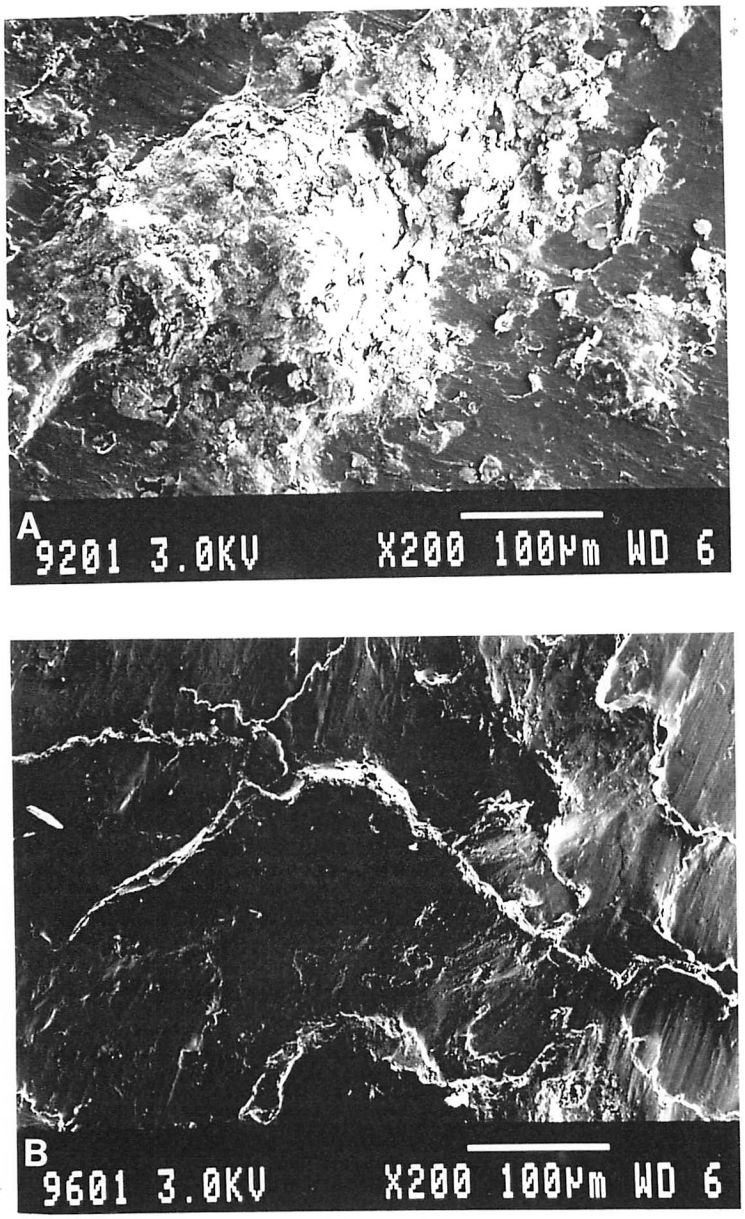

Figure 5.13: Boron free bainitic rail replicas Torpedo route February 1999
a) Running band with craters
b) Gauge corner with laps

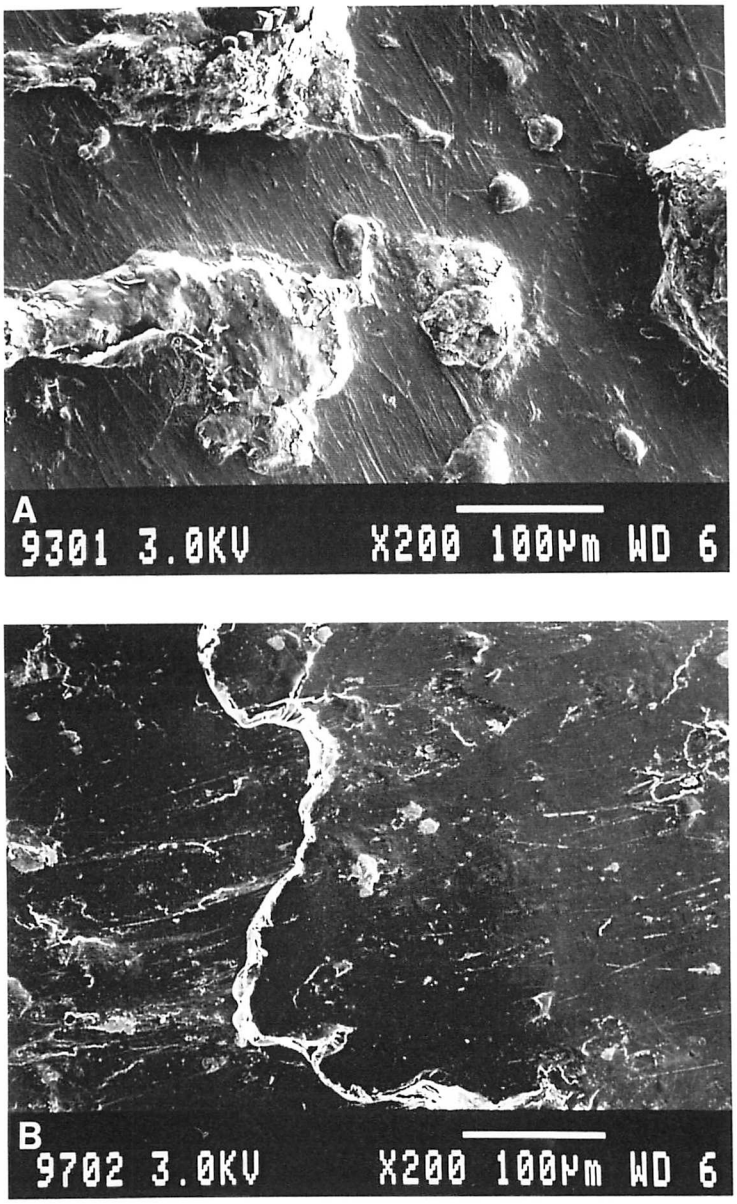

Figure 5.14: MHT adjacent to boron free bainitic rail replicas Torpedo route February 1999
a) Running band with small craters
b) Gauge corner with laps

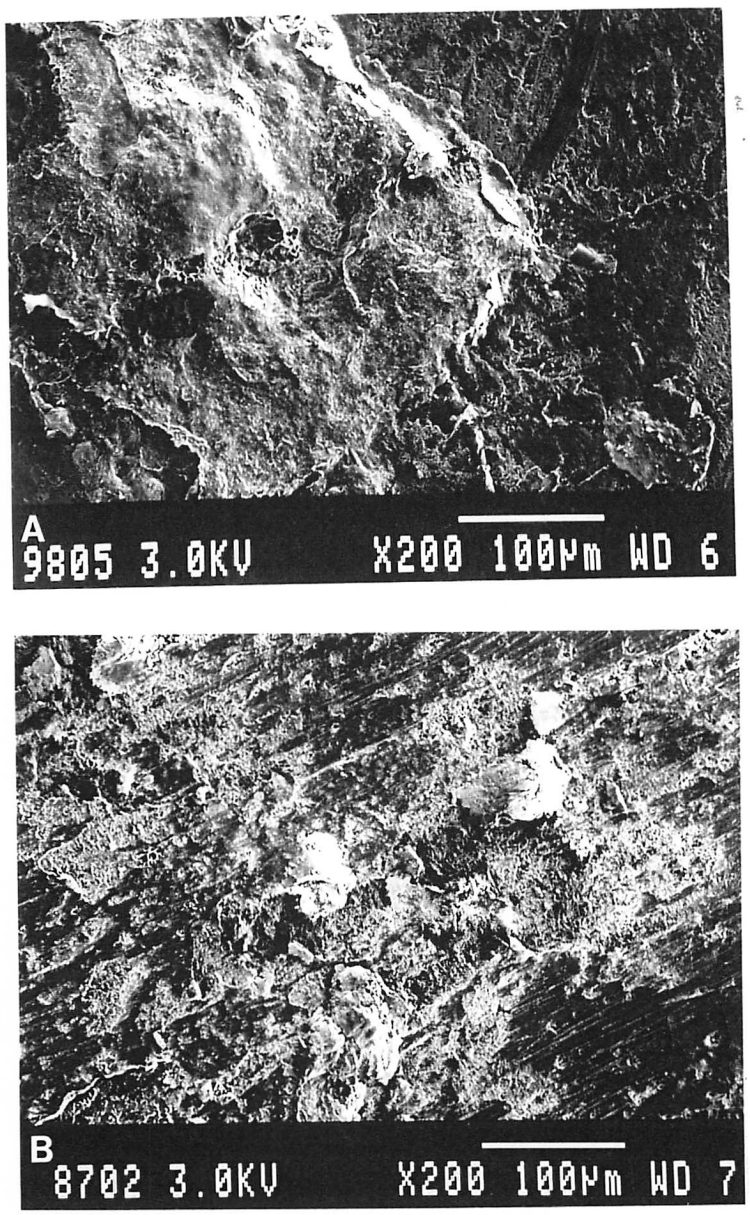

Figure 5.15: 440 HB bainitic rail replicas BOS perimeter February 1999
a) Running band with craters
b) Gauge corner with small craters and holes

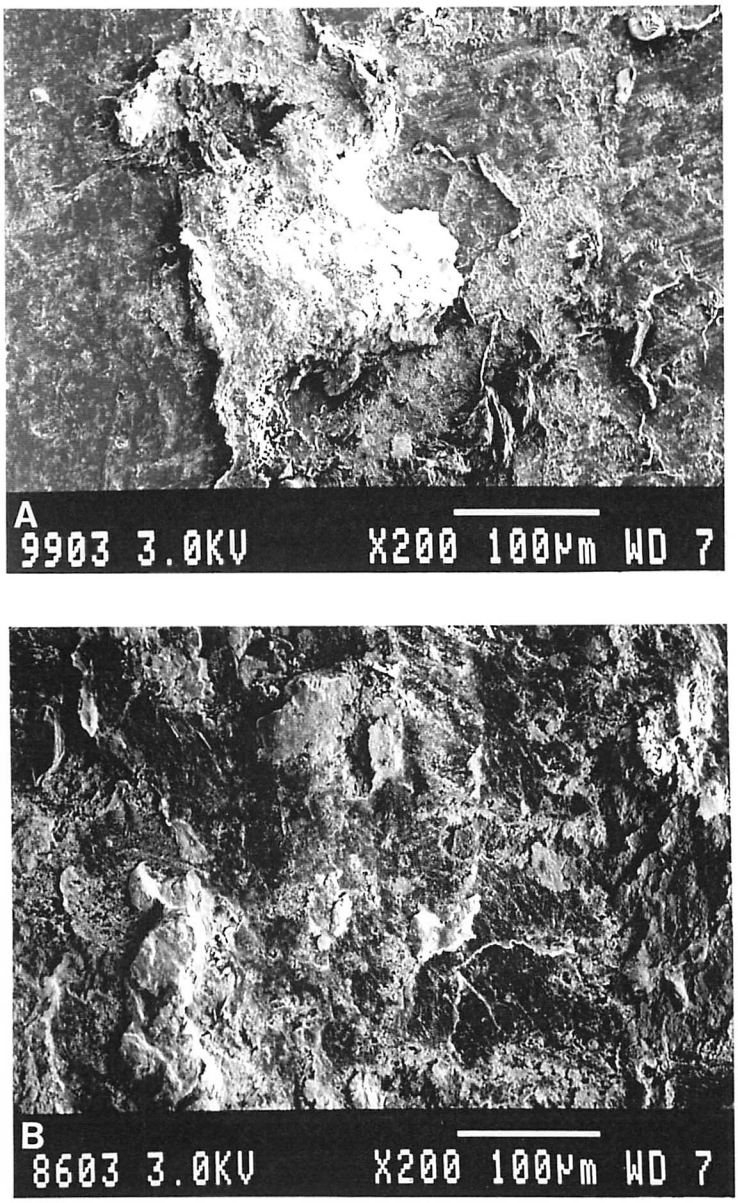

Figure 5.16: MHT adjacent to 440 HB bainitic rail replicas BOS perimeter February 1999
a) Running band with craters
b) Gauge corner with small craters and holes

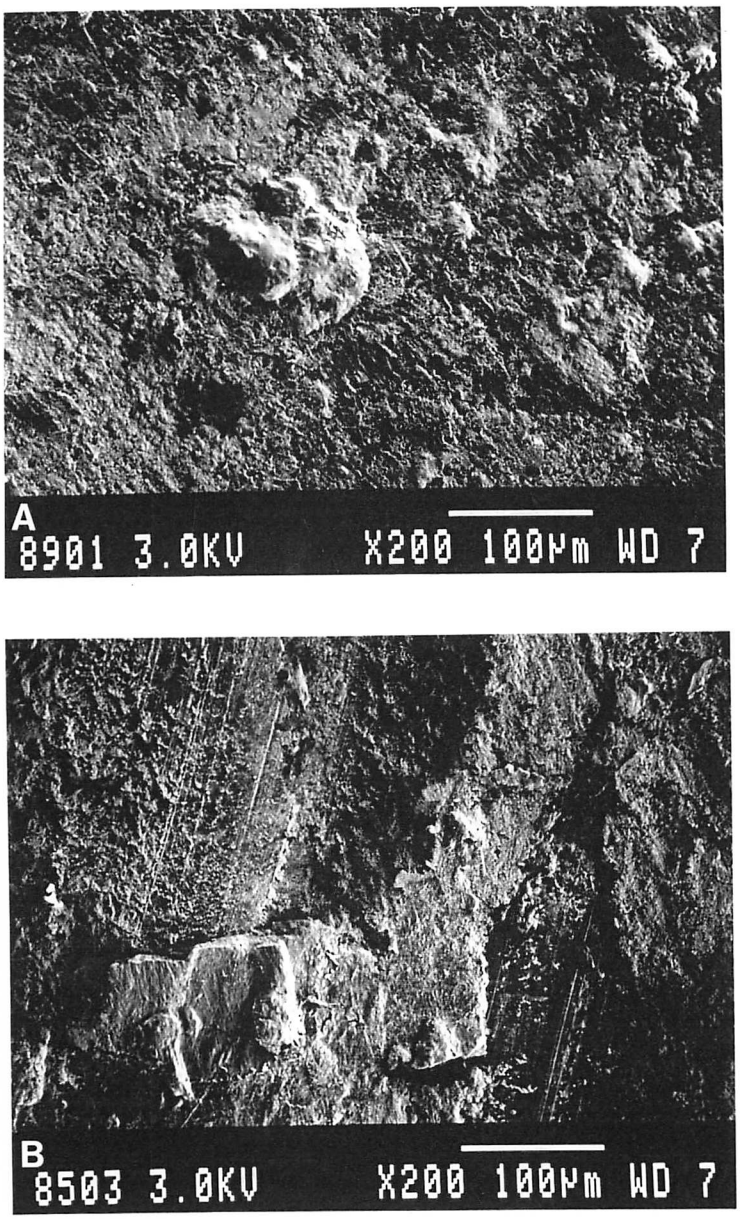

Figure 5.17: Boron free bainitic rail replicas BOS perimeter February 1999
a) Running band with small craters
b) Gauge corner with craters and scores

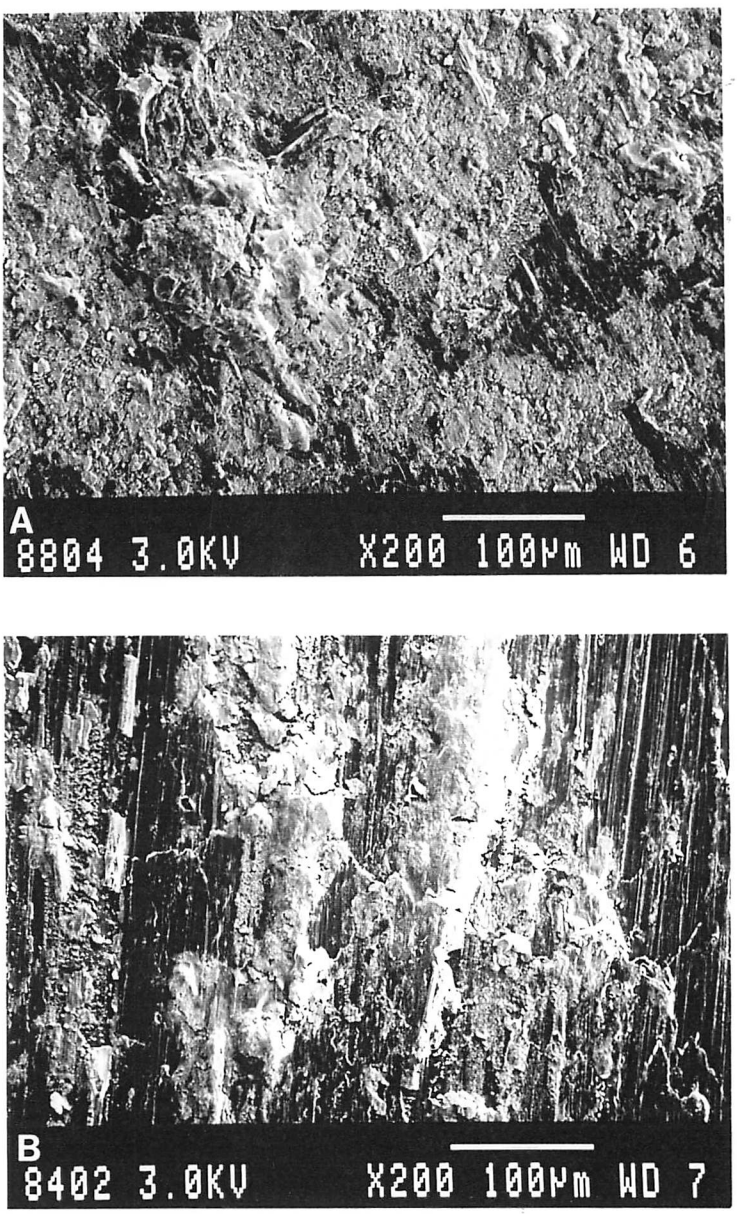

Figure 5.18: MHT adjacent to boron free bainitic rail replicas BOS perimeter February 1999
a) Running band with craters
b) Gauge corner with craters and scuffs

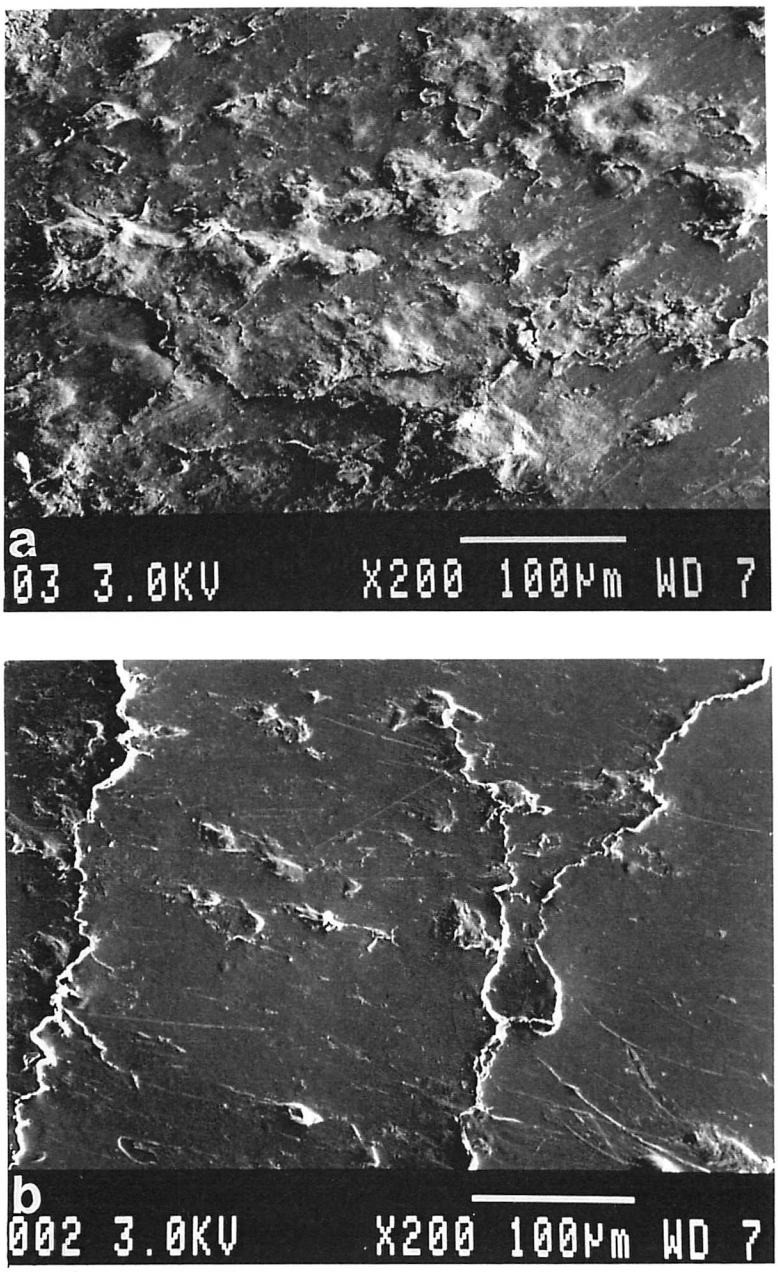

Figure 5.19: Boron containing bainitic rail replicas Torpedo route June 1999
a) Running band with small craters
b) Gauge corner with laps

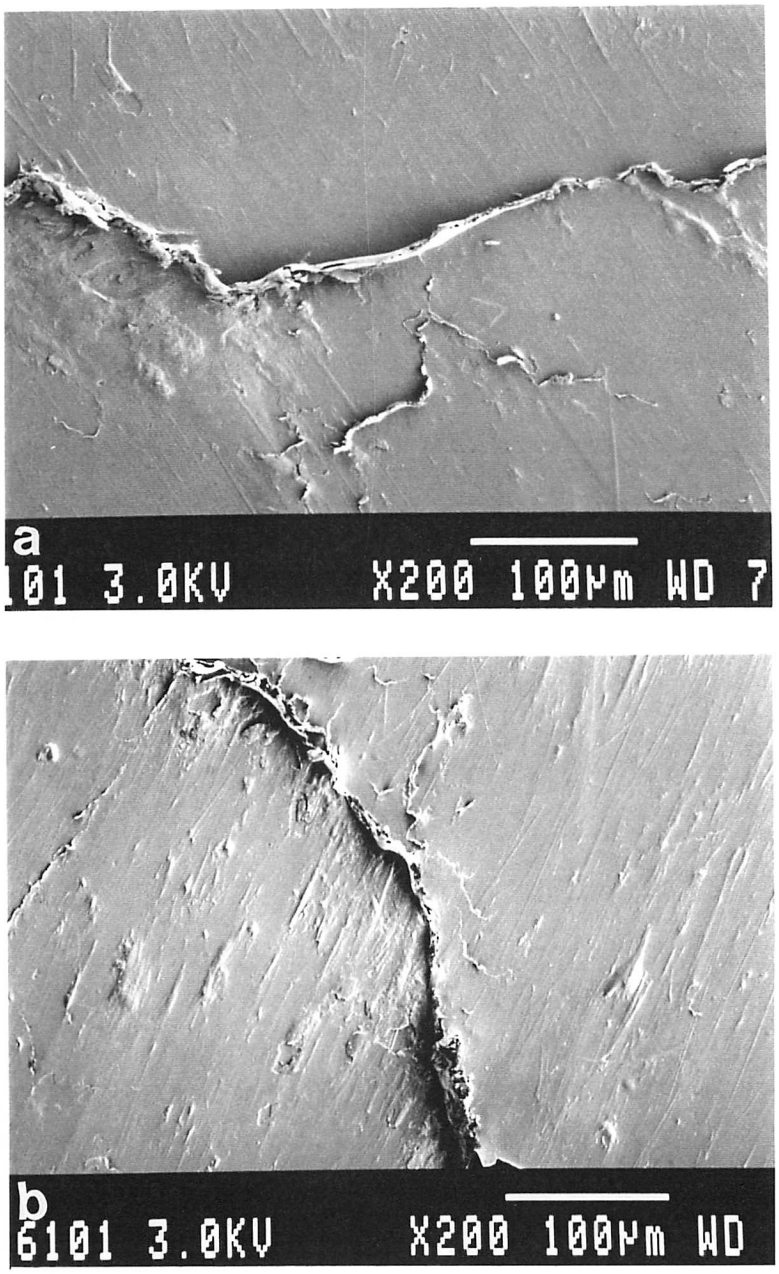

Figure 5.20: MHT adjacent to boron containing bainitic rail replicas
Torpedo route June 1999
a) Running band with laps
b) Gauge corner with laps

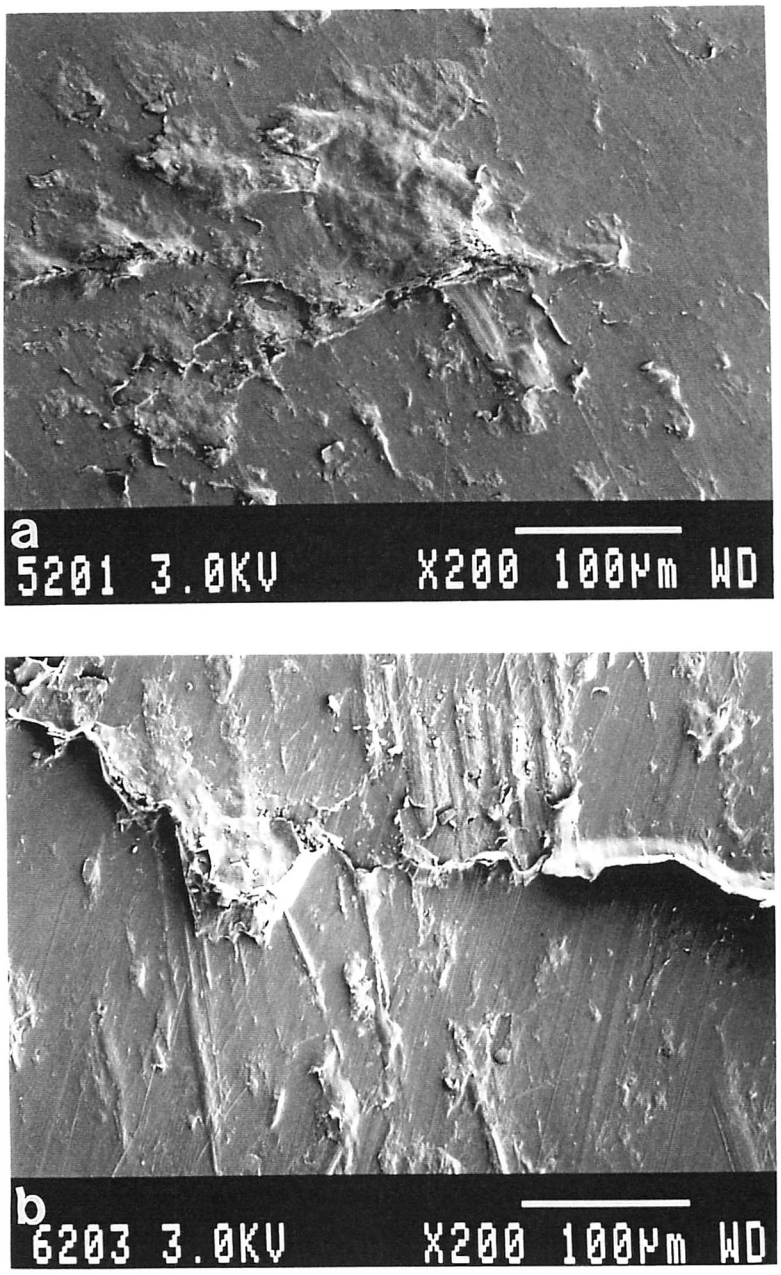

Figure 5.21: Boron free bainitic rail replicas Torpedo route June 1999
a) Running band with craters
b) Gauge corner with laps and traces of grooves

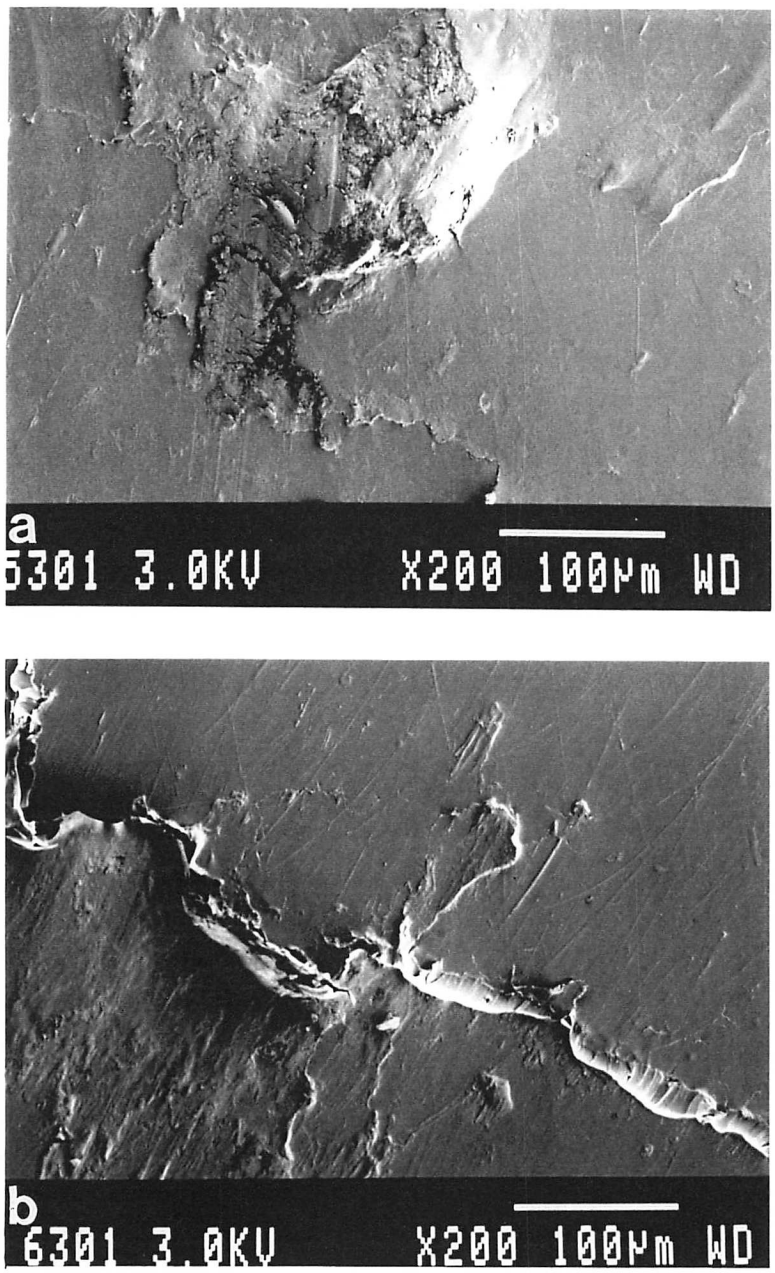

Figure 5.22: MHT adjacent to boron free bainitic rail replicas Torpedo route June 1999
a) Running band with craters
b) Gauge corner with laps

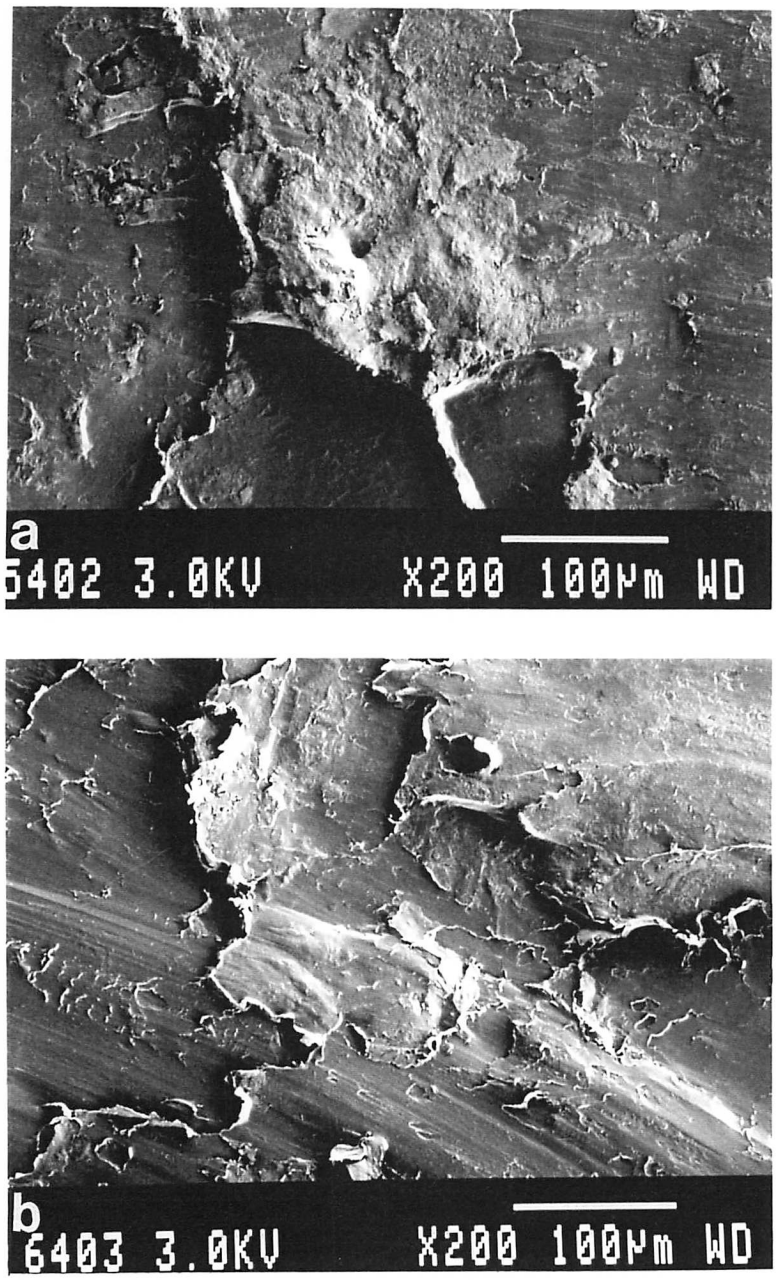

Figure 5.23: 440 HB bainitic rail replicas BOS perimeter June 1999
a) Running band with craters
b) Gauge corner with smeared laps

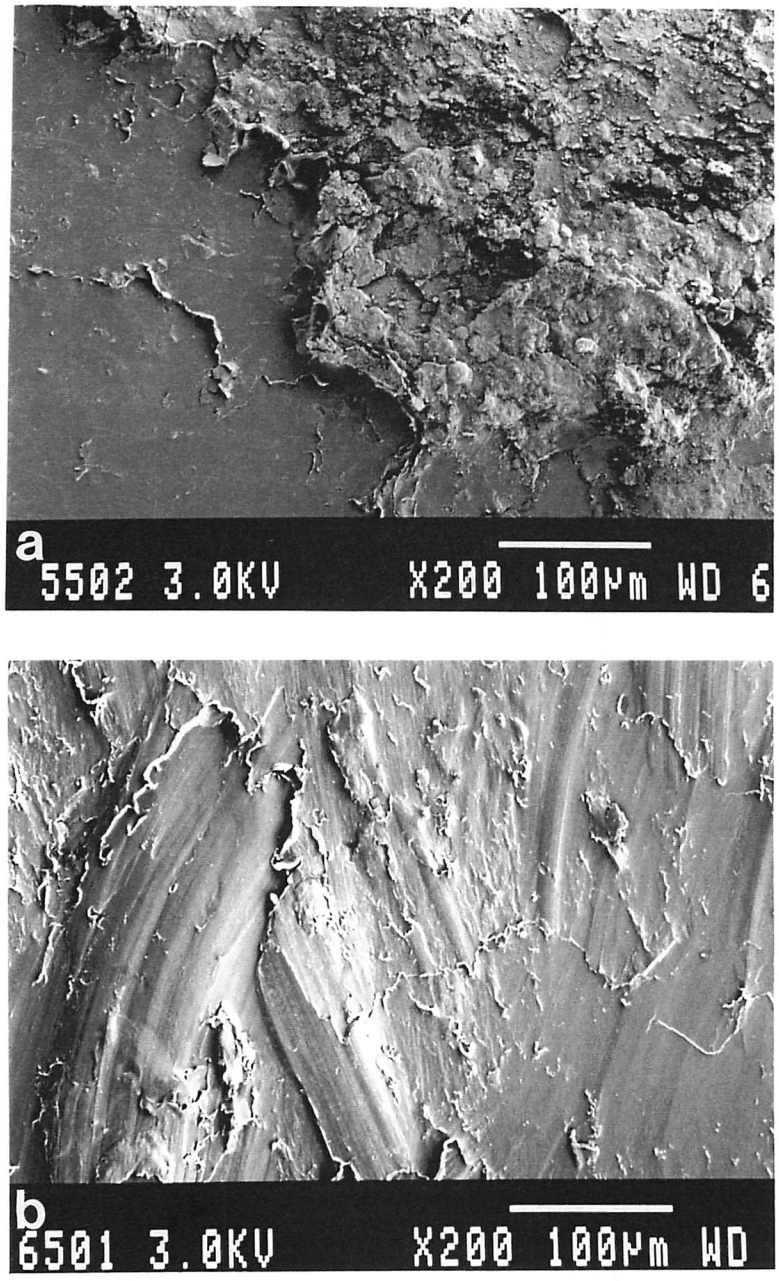

Figure 5.24: MHT adjacent to 440 HB bainitic rail replicas BOS perimeter June 1999
a) Running band with craters
b) Gauge corner with smears

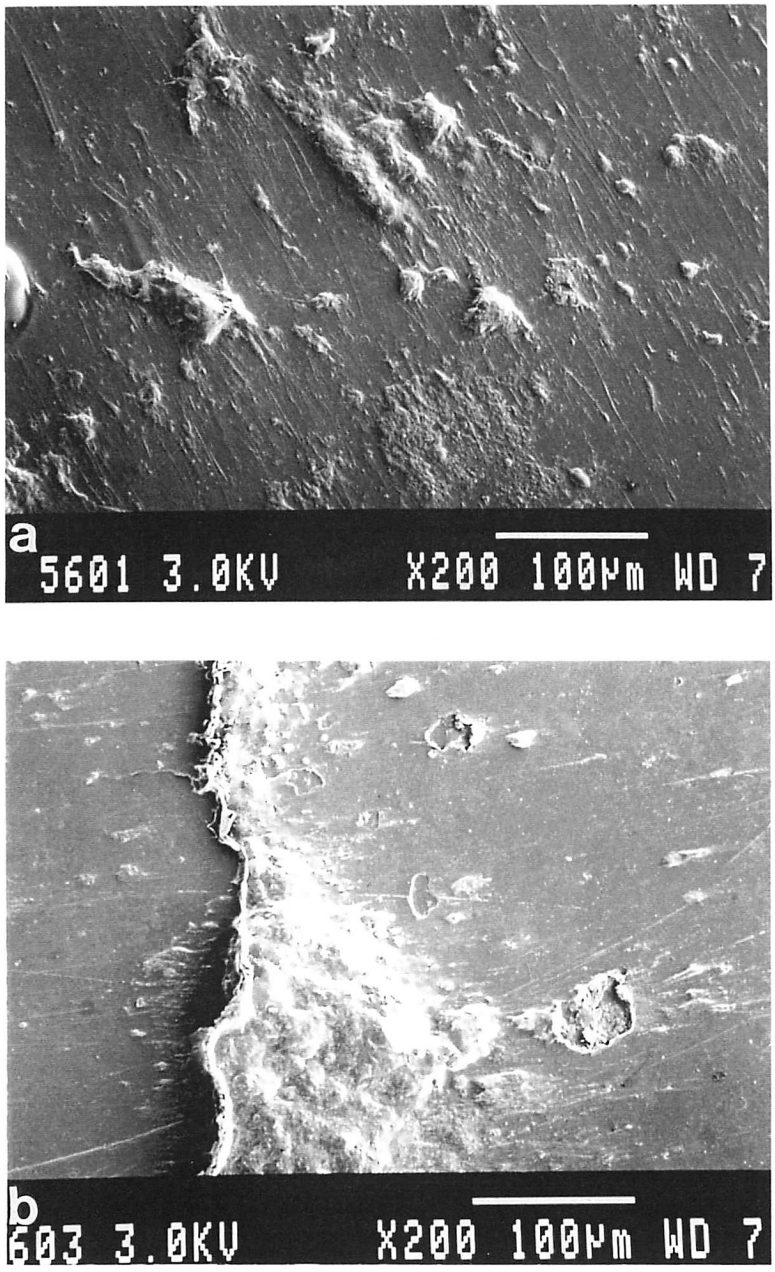

Figure 5.25: Boron free bainitic rail replicas BOS perimeter June 1999
a) Running band with small craters
b) Gauge corner with laps

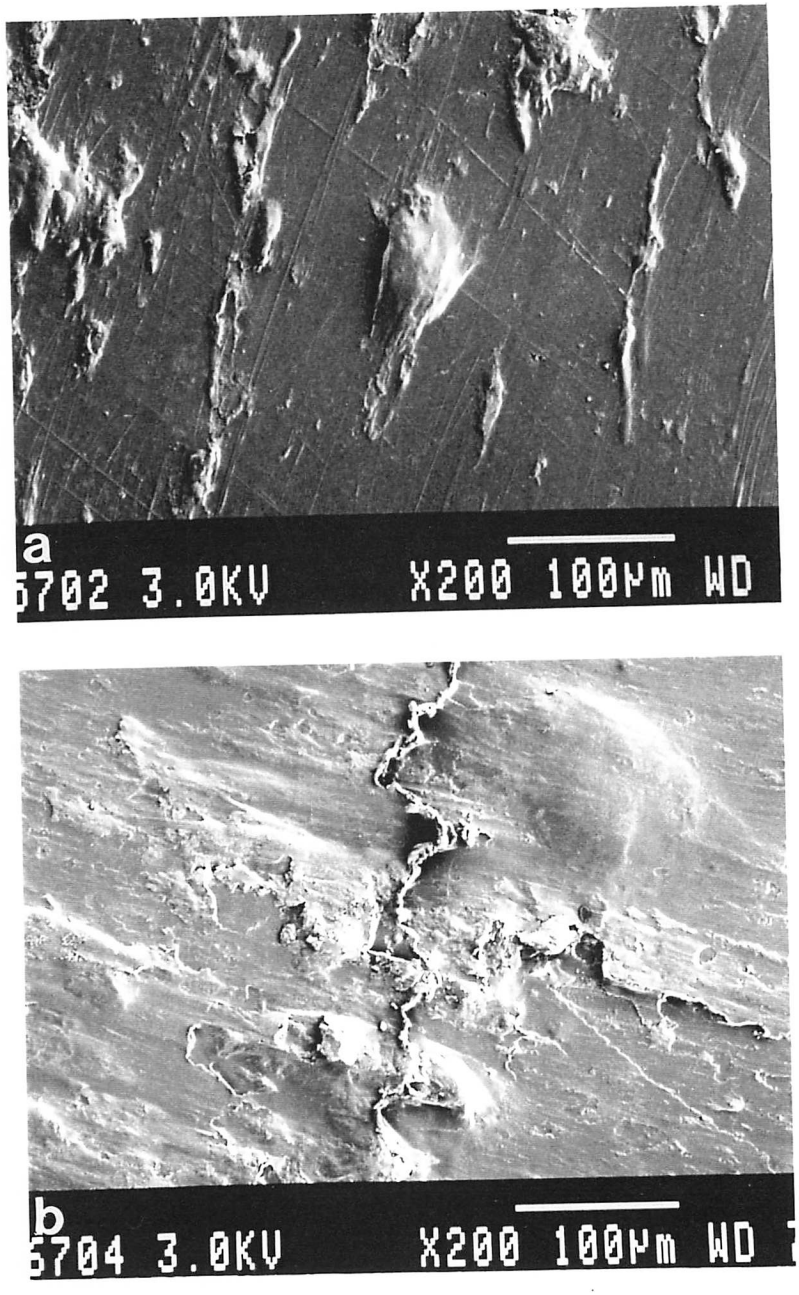

Figure 5.26: MHT adjacent to boron free bainitic rail replicas BOS perimeter June 1999
a) Running band with small craters
b) Gauge corner with laps

6

Modelling of hardness variations and segregation

It is useful to be able to estimate the properties of new experimental alloys before actually making them so as to allow the choice of the most promising compositions. Ideally a physical model would be developed to make these predictions. However in some cases the problem is too complex to be solved with current methods, and hence empirical models can be useful for solving immediate alloy design problems while work continues on developing physical models.

This chapter contains work on empirical models for predicting some mechanical properties of carbide-free bainitic rail steels from a knowledge of the composition. Linear regression and neural network modelling have been used to develop models for hardness, 0.2% proof stress, and tensile strength. Neural network modelling is a generalised method of regression which has the advantage that it can cope with relationships of almost arbitrary complexity.

In addition to the above, an attempt is made to predict the degree of chemical segregation in carbide-free baintic rail steels. Segregation has been identified as a problem in these alloys. Regions of untempered martensite form in the areas which are high in alloying elements and this leads to a reduction in the toughness. The greater toughness of bainite compared with conventional pearlitic rail steels is one of the reasons for using bainite, so the segregation may be a serious problem. The degree of segregation in five experimental steels was quantified by means of microhardness measurements. A model was then developed to predict the hardness variations in segregated carbide-free bainite,

and the results of this compared with the experimental results. The model used the theromdymanic modelling package MTDATA to predict compositions for the alloy-rich and poor areas of the steel, and these were then put into the empirical model for hardness to provide an estimate of the hardness distribution.

6.1 Neural network modelling of mechanical properties

6.1.1 Method and results

The basic theory of neural network analysis was presented in Chapter 4. A database was made containing all of the experimental carbide-free bainitic alloys provided by British Steel and their mechanical properties. All the samples from which properties had been measured had been hot-rolled to 30 mm plate and allowed to air-cool, then tested, so it was not necessary to allow for variables such as heat-treatment parameters in the model. The cooling rate at the centre of a 30 mm plate is very similar to the cooling rate at the centre of a rail, about $0.11\,\mathrm{K\,s^{-1}}$. There were enough data to model 0.2 % proof stress, tensile strength and Vickers hardness. The inputs and outputs to the model are shown in Table 6.1.

	Minimum	Maximum	Mean	Standard deviation
Inputs				
C wt%	0.1	0.46	0.23	0.06
Si wt%	0.99	2.16	1.85	0.25
Mn wt%	1.06	2.26	1.93	0.30
Cr wt%	0.00	2.09	1.03	0.73
Mo wt%	0.00	0.74	0.23	0.21
Ni wt%	0.00	2.07	0.10	0.40
B wt%	0.00	0.003	0.001	0.001
Outputs				
0.2 % proof stress (MPa)	498	1142	760	133
Tensile strength (MPa)	806	1609	1247	174
Vickers hardness (HV)	267	599	396	59

Table 6.1: Inputs and outputs for neural network model

Linear regression analysis was also carried out on the data. The relationships found are shown in Table 6.2—6.4.

Neural net models were created for 0.2 % proof stress, tensile strength and hardness, at first varying in complexity from one to eight hidden units. As there were enough data the dataset was split into two and the model was trained only on one half. The remaining

Input	Coefficent / MPa	Standard error / MPa
wt% C	838	196
wt% Si	42	49
wt% Mn	144	42
wt% Cr	140	18
wt% Mo	162	53
wt% Ni	67	27
wt% B	2584	8747
Constant	29	72
Correlation coefficient $r = 0.840$		

Table 6.2: Linear regression coefficients for 0.2 % proof stress

Input	Coefficent / MPa	Standard error / MPa
wt% C	457	354
wt% Si	48	72
wt% Mn	154	56
wt% Cr	191	32
wt% Mo	384	85
wt% Ni	67	40
wt% B	11820	13198
Constant	479	90
Correlation coefficient $r = 0.883$		

Table 6.3: Linear regression coefficients for tensile strength

Input	Coefficent / HV	Standard error / HV
wt% C	558	73
wt% Si	30	18
wt% Mn	78	16
wt% Cr	67	7
wt% Mo	83	20
wt% Ni	24	10
wt% B	824	3304
Constant	-30	27
Correlation coefficient $r = 0.902$		

Table 6.4: Linear regression coefficients for Vickers hardness

data were used to test that the model had not over-fitted the original data. Graphs of test error *vs.* number of hidden units for each model are plotted in Figure 6.1—6.2.

There are five points for each number of hidden units because the models have to be seeded with a random number to begin the calculation. Five different starting numbers

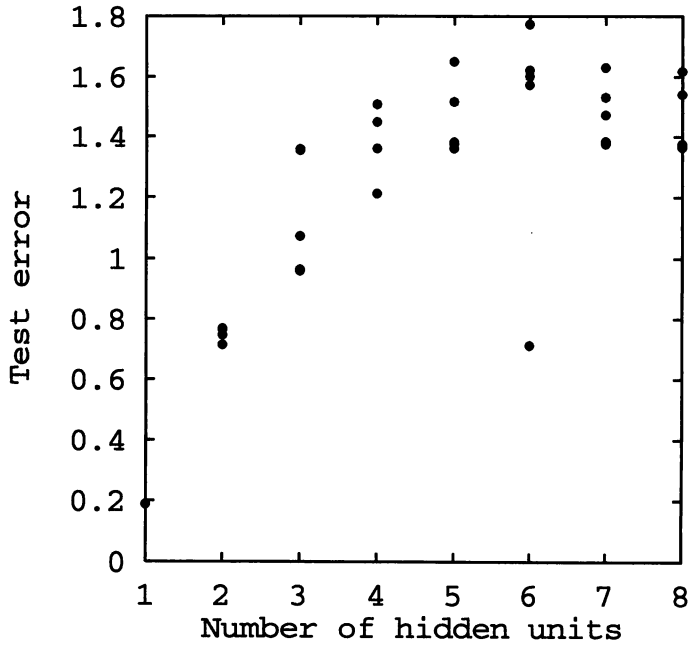

Figure 6.1: Test error *vs.* number of hidden units for all proof stress models created using the original dataset

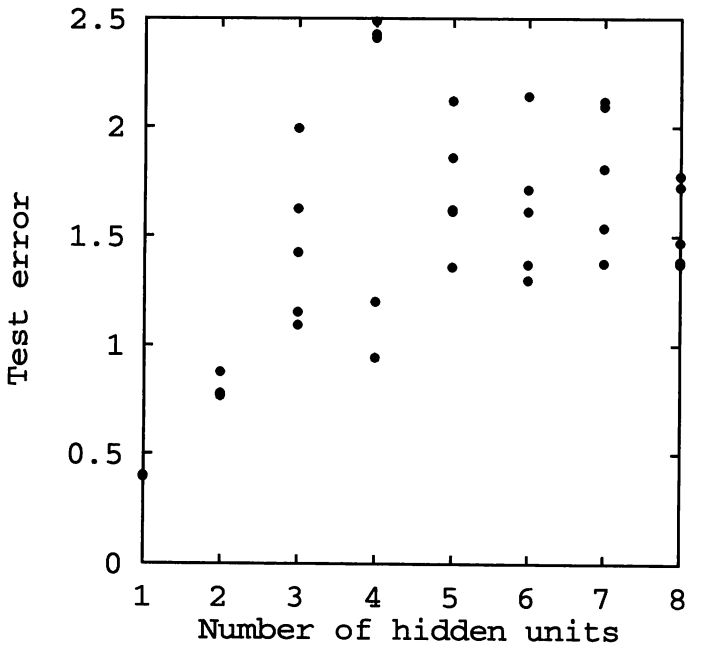

Figure 6.2: Test error *vs.* number of hidden units for all tensile strength models created using the original dataset

were used for each number of hidden units. These graphs are expected to level off or have a minimum at the ideal number of hidden units for the model.

The models with the lowest test error produced are shown in Figure 6.3—6.4. Predicted values are plotted *vs.* measured, for both training and testing data. The scatter in both graphs for each property should be about the same if the model has not over-fitted the training data. For a good model, the total scatter should be small. It can be seen that there is a lot of scatter in both models. The error bars are $\pm 1\sigma$. They represent a combination of the level of noise in the input data and the reliability of the model.

The test error is plotted against number of hidden units for the different hardness models in Figure 6.5. Models with up to sixteen hidden units are included in the graph because it was not clear if it had levelled off after eight, so more models were created to check this. The graph levels off at two or three hidden units. The best model had two hidden units, although it can be seen from the plots of testing and training data in Figure 6.6 that there are a few extreme compositions that the model does not cope with well. It is thought that some of the steels provided by British Steel did not have an essentially bainitic microstructure and therefore do not behave in the same way as the rest. The weights and offsets for this model are specified in Table 6.5.

Hidden layer weights		
	1	2
wt % C	1.3911	1.0552
wt % Si	−1.8270	-2.6602
wt % Mn	0.0102	−0.0917
wt % Cr	−0.0092	-0.3518
wt % Mo	0.5752	-0.0610
wt % Ni	0.0997	-0.0702
wt % B	0.0608	-0.1457
Offset	0.1762	0.1562
Output layer weights		
Hidden unit 1	−1.4788	
Hidden unit 2	4.5170	
Offset	−3.1201	

Table 6.5: Weights and offsets for neural net model for hardness. The model has two hidden units.

The models for proof stress and tensile strength were not good enough to be used for predictions. Sometimes an improvement can be made by combining several of the best models produced into a committee model. This was attempted for the proof stress

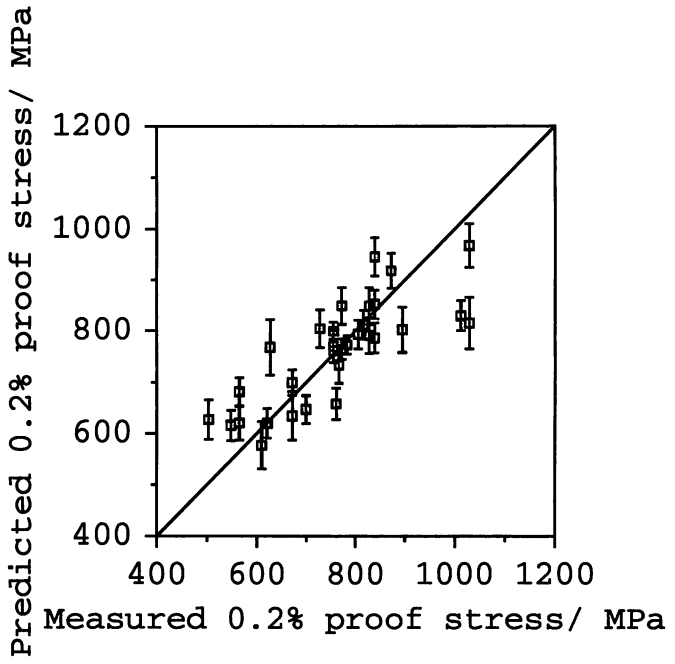

Figure 6.3 (a): Predicted *vs.* measured proof stress for training data from neural network model. This model had one hidden unit.

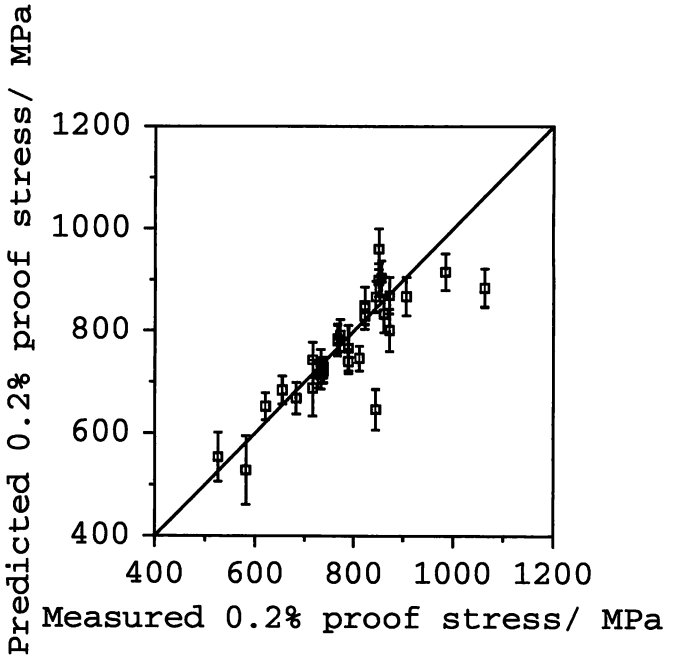

Figure 6.3 (b): Predicted *vs.* measured proof stress for testing data from neural network model. This model had one hidden unit.

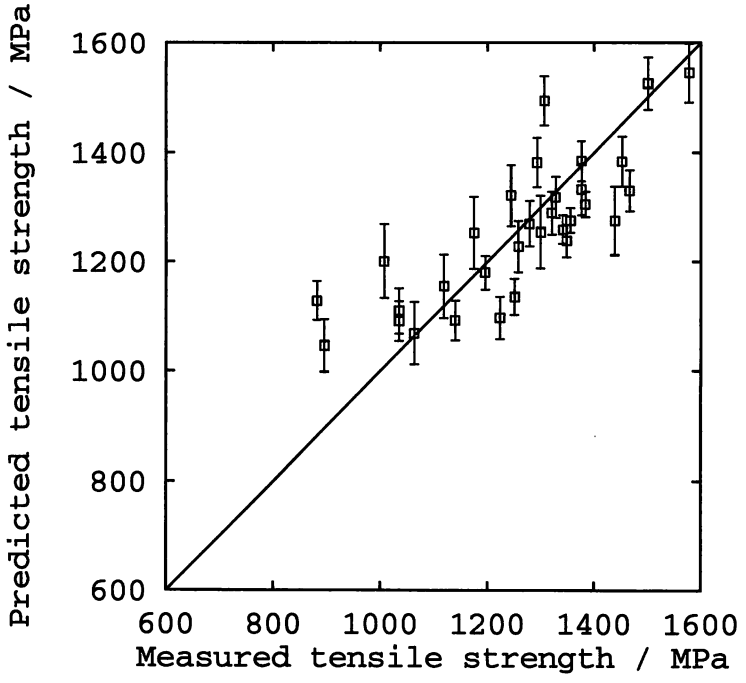

Figure 6.4 (a): Predicted *vs.* measured tensile strength for training data from neural network model. This model had one hidden unit.

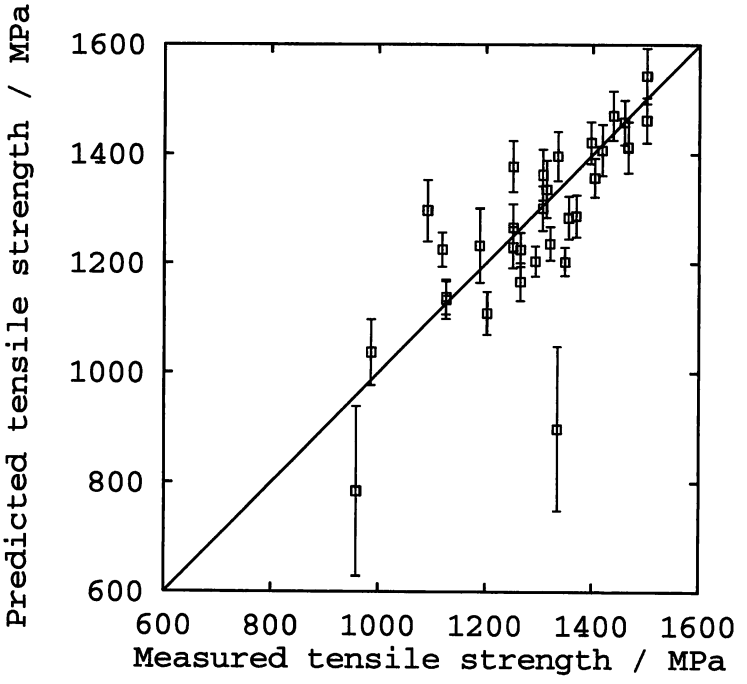

Figure 6.4 (b): Predicted *vs.* measured tensile strength for testing data from neural network model. This model had one hidden unit.

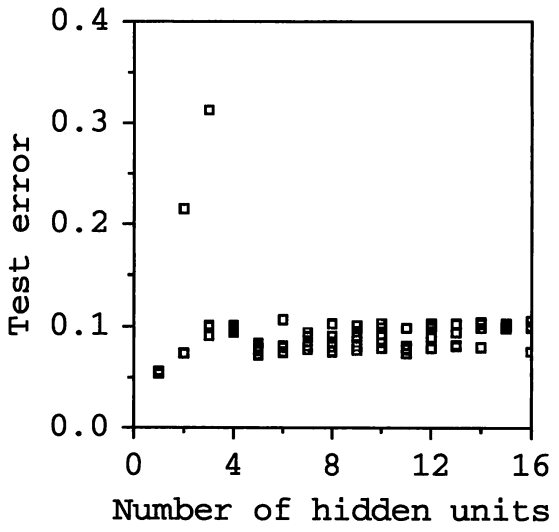

Figure 6.5: Test error *vs.* number of hidden units for hardness models

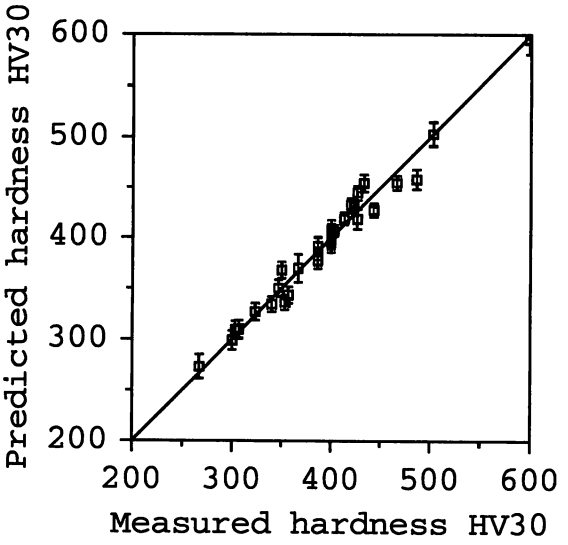

Figure 6.6 (a): Predicted *vs.* measured hardness for training data from neural network model. This model had two hidden units.

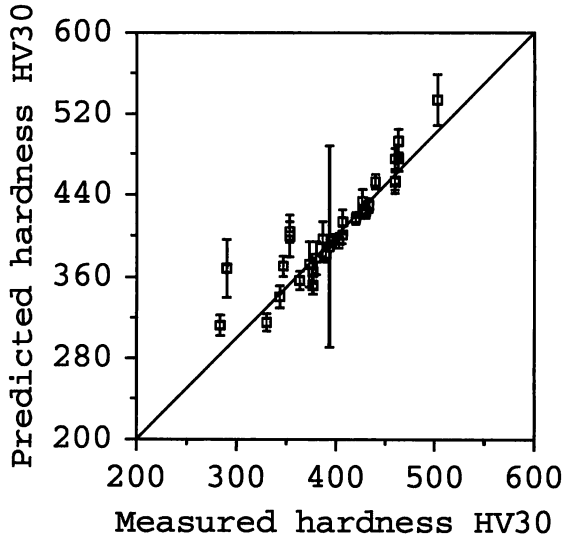

Figure 6.6 (b): Predicted *vs.* measured hardness for testing data from neural network model. This model had two hidden units.

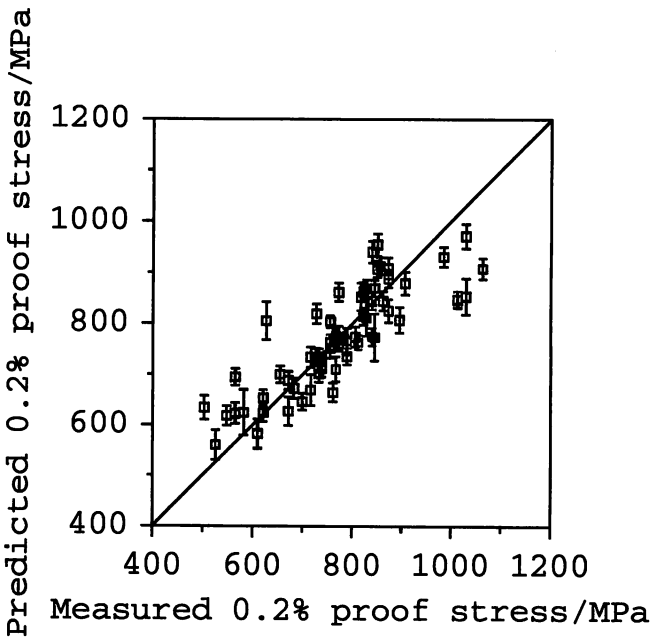

Figure 6.7: Predicted *vs.* measured proof stress for training data from neural network committee model

models. Combinations of up to the best six models were tested. The committee with the lowest test error contained two models. A plot of predicted *vs.* experimental data for this committee is shown in Figure 6.7. This model is still not good enough to be used for making predictions.

The ten best tensile strength models were also combined into various committee models, but it was found that this did not produce any improvements.

To try to make better models for proof stress and tensile strength the original database was extended to include all measurements made of each property for each composition, whereas previously it had only contained the average for each composition. It was thought that this would help because it is very hard to measure the proof stress accurately in carbide-free bainite as the microstructure contains a large amount of retained austenite. This transforms under strain to martensite, causing the stress-strain curve to be very smooth and making it hard to define a discrete yield strength.

Some statistics for the extended dataset is shown in Table 6.6.

	Minimum	Maximum	Mean	Standard deviation
Inputs				
C wt%	0.1	0.46	0.24	0.06
Si wt%	0.99	2.16	1.82	0.25
Mn wt%	1.06	2.26	1.91	0.31
Cr wt%	0.00	2.09	0.98	0.71
Mo wt%	0.00	0.74	0.23	0.20
Ni wt%	0.00	2.07	0.11	0.41
B wt%	0.00	0.003	0.001	0.001
Outputs				
0.2 % proof stress (MPa)	498	1142	760	133
Tensile strength (MPa)	806	1609	1247	174

Table 6.6: Inputs and outputs for neural network model on extended dataset

Neural network models containing one to sixteen hidden units were created from the extended dataset. These proved to be much better than previous attempts. The best model found for proof stress had nine hidden units, and for tensile strength seven hidden units. Plots of test error *vs.* number of hidden units, and testing and training data are shown in Figure 6.8—6.11. It can be seen that there are still a few extreme compositions that the model cannot cope with. The weights that speicfy these models are shown in Table 6.7—6.8.

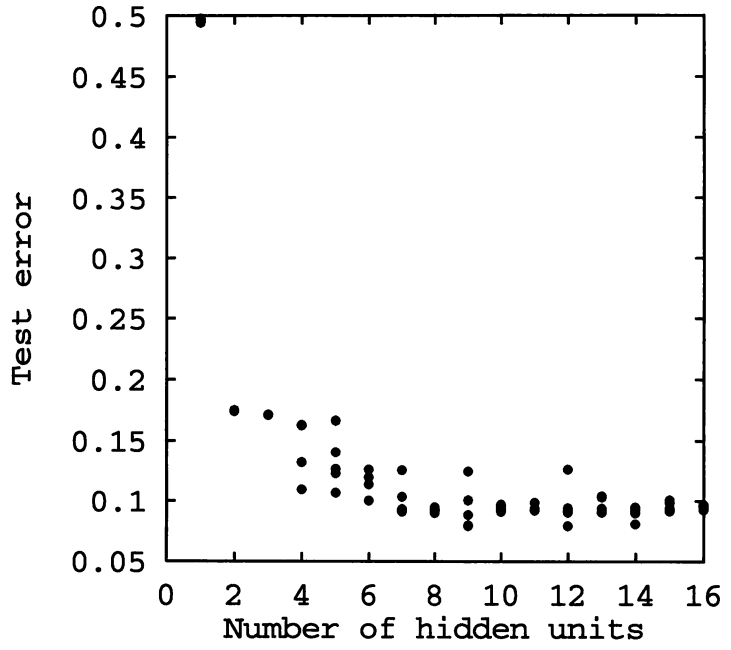

Figure 6.8: Test error *vs.* number of hidden units for proof stress model on extended database. The graph levels off at about nine hidden units

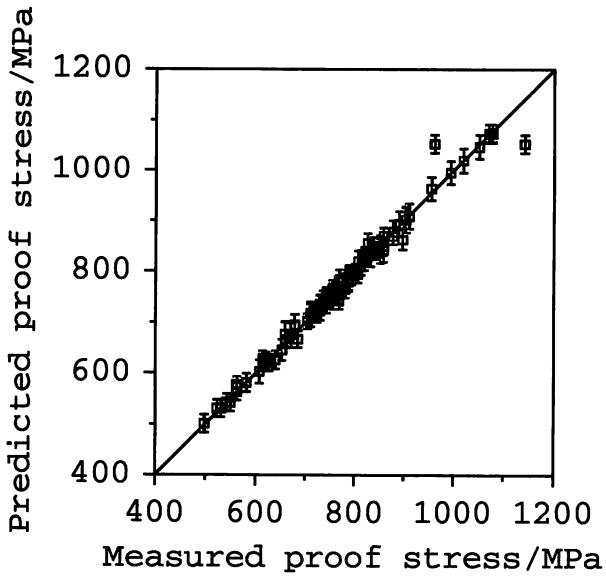

Figure 6.9 (a): Predicted *vs.* measured proof stress for training data from neural network model on expanded dataset. This model had nine hidden units.

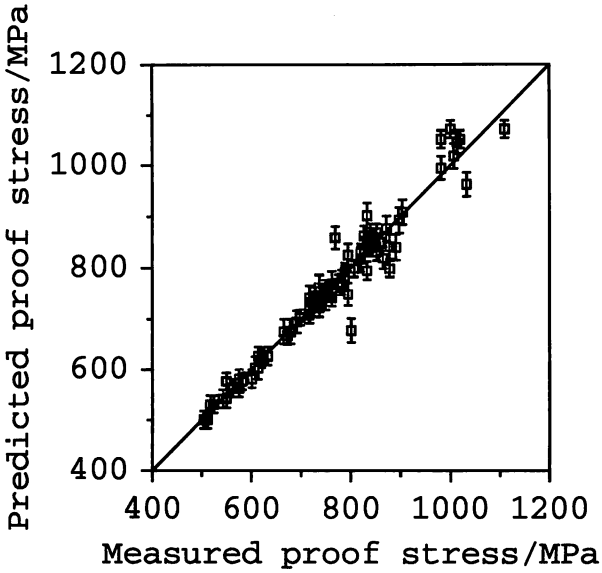

Figure 6.9 (b): Predicted *vs.* measured proof stress for testing data from neural network model on expanded dataset. This model had nine hidden units.

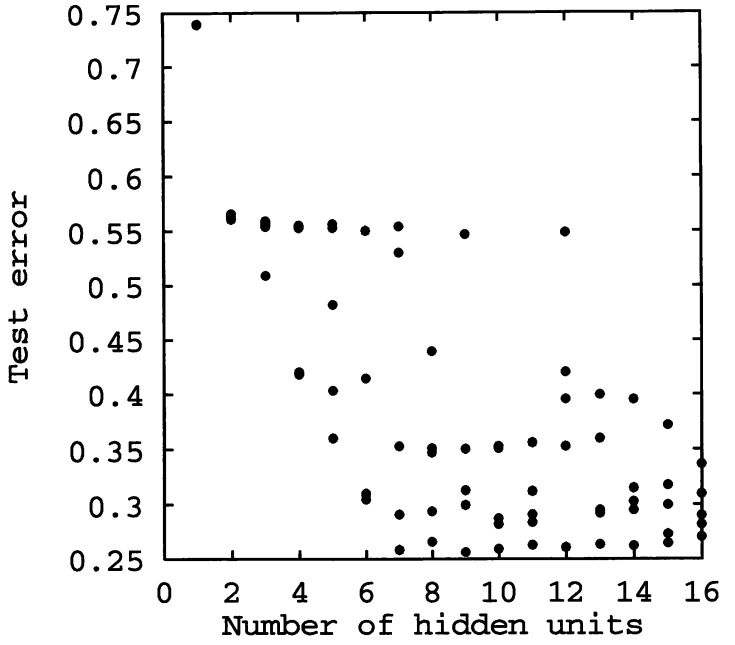

Figure 6.10: Test error *vs.* number of hidden units for tensile strength model on extended database. The graph levels off at about seven hidden units

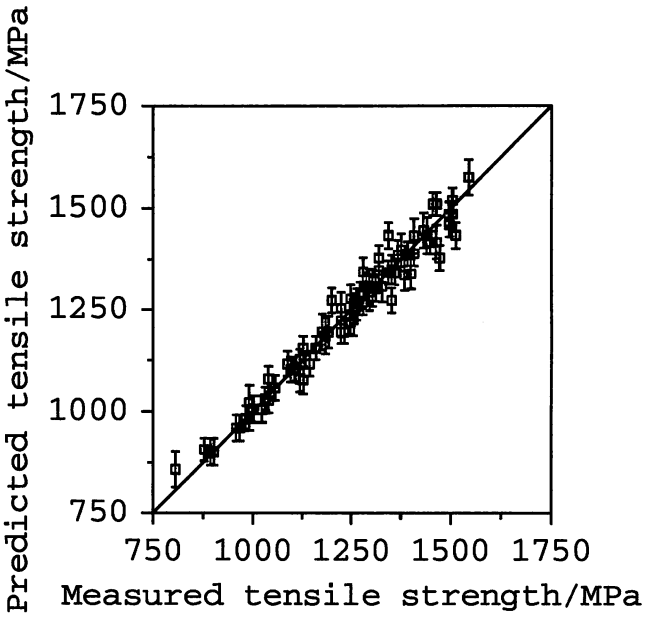

Figure 6.11 (a): Predicted *vs.* measured tensile strength for training data from neural network model on expanded dataset. This model had seven hidden units.

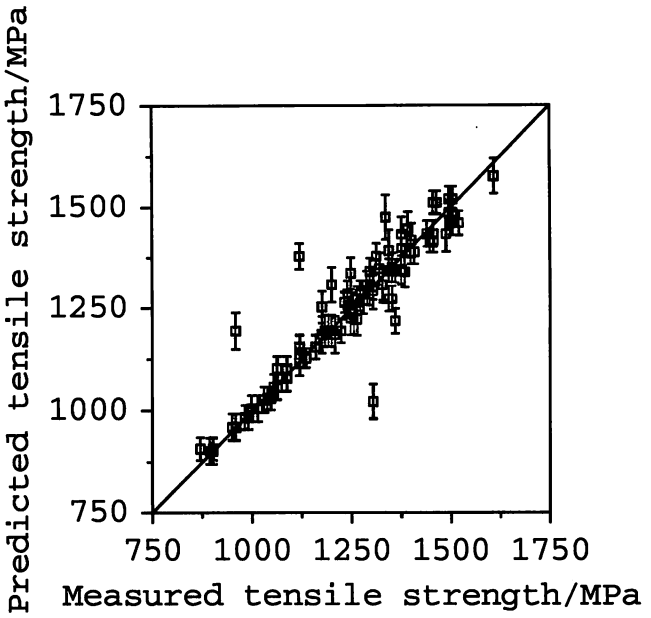

Figure 6.11 (b): Predicted *vs.* measured tensile strength for training data from neural network model on expanded dataset. This model had seven hidden units.

	Hidden layer weights								
	1	2	3	4	5	6	7	8	9
wt % C	−0.0266	0.0143	0.1262	0.0487	−0.1106	−0.3878	−0.1123	−0.0345	0.0417
wt % Si	1.3514	2.8814	−1.2004	0.8579	−2.5949	−2.3585	2.0353	−2.1514	−3.0268
wt % Mn	0.2643	0.2909	0.0803	0.0785	−0.1001	−0.2894	−0.1609	−0.7523	0.0320
wt % Cr	1.1430	−0.8991	−0.1591	−0.8039	−0.4636	0.7404	−0.6153	−0.5544	−0.0522
wt % Mo	−0.3542	0.2707	−1.7581	0.7627	1.4075	0.5013	−0.2652	−0.3315	−1.1556
wt % Ni	−0.3691	−0.2114	0.0756	−0.6447	0.0599	−0.2751	0.1522	−0.1529	−0.2564
wt % B	−0.1174	0.1683	0.0623	−0.0606	0.0186	−0.0046	−0.0480	−0.0033	−0.0040
Offset	−0.0482	−0.0542	0.0203	−0.2429	−0.1146	0.1695	−0.1562	0.3045	−0.1344
Output layer weights									
Hidden unit 1	−0.6995								
Hidden unit 2	4.7366								
Hidden unit 3	4.2819								
Hidden unit 4	−4.3958								
Hidden unit 5	−4.7070								
Hidden unit 6	3.1518								
Hidden unit 7	−5.2154								
Hidden unit 8	−2.4384								
Hidden unit 9	4.1625								
Offset	2.8317								

Table 6.7: Weights and offsets for neural net model for proof stress on the extended database. The model has nine hidden units.

	Hidden layer weights						
	1	2	3	4	5	6	7
wt % C	−0.0671	−0.0389	0.1182	0.0437	−0.3989	−0.2509	−0.1105
wt % Si	−5.0237	−3.7824	2.9270	−4.3499	−2.6711	3.3695	3.2112
wt % Mn	−0.0777	0.0042	−0.0481	−0.0435	−0.0423	0.0026	−0.1047
wt % Cr	0.7162	0.0605	0.6255	0.2524	0.5456	0.7815	0.0790
wt % Mo	−0.7512	−1.4619	−0.3559	0.5649	−0.3285	−1.4223	0.6508
wt % Ni	−0.3432	0.2137	0.5014	−0.2008	−0.9352	0.3514	−0.6590
wt % B	0.0292	−0.0620	−0.0700	−0.0146	−0.0539	0.0281	−0.0661
Offset	0.1703	0.1505	0.2601	−0.0638	−0.2167	0.1893	0.0189
Output layer weights							
Hidden unit 1	−0.3973						
Hidden unit 2	9.0733						
Hidden unit 3	−11.3665						
Hidden unit 4	10.6094						
Hidden unit 5	−12.9074						
Hidden unit 6	7.3233						
Hidden unit 7	−8.5251						
Offset	−10.7332						

Table 6.8: Weights and offsets for the neural net model for tensile strength on the expanded database. The model has seven hidden units.

The trends in hardness produced by varying different alloying additions were examined by taking an average composition and varying each element in turn between its minimum and maximum value, then making hardness predictions using the model for each composition produced. The compositions used for predictions are summarized in Table 6.9. These results are plotted in Figure 6.12.

	Composition wt%						
	C	Si	Mn	Cr	Mo	Ni	B
Average	0.26	1.95	1.95	0.49	0.46	0.02	0.000
Minimum	0.10	0.99	1.06	0.00	0.00	0.00	0.000
Maximum	0.46	2.16	2.26	2.09	0.74	2.07	0.003

Table 6.9: Compositions used for investigating trends in hardness. Each element in turn was varied between its minimum and maximum values given in the table, while the rest were held at the "average" value. The hardness of each compsoition so produced was predicted by the neural network model.

The hardness model has also been used to predict hardnesses of possible experimental alloys for British Steel, and was shown to be correct within the 95 % confidence limits when the alloys were made and tested. These results are shown in Table 6.10.

Composition (all wt%)							Predicted	Error	Measured
C	Si	Mn	Cr	Mo	Ni	B	HV	HV	HV
0.30	1.79	2.06	1.01	0.25	-	-	489	56	446
0.32	1.71	2.04	1.07	0.49	-	-	567	96	481

Table 6.10: Hardness predictions made for British Steel for potential new bainitic steels compared with measured hardness for the same alloys

6.1.2 Discussion

The linear regression analysis for proof stress and tensile strength has very large errors in the coefficients. This implies that the relationship is not well modelled by a linear function. The case is slightly better for hardness, but still not very good. The neural net models would be expected to be better because they can model non-linear behaviour.

The neural net models for proof stress and tensile strength needed more hidden units than the model for hardness. This is perhaps not surprising as the linear regression analysis modelled hardness better than the other two properties, so hardness is a more

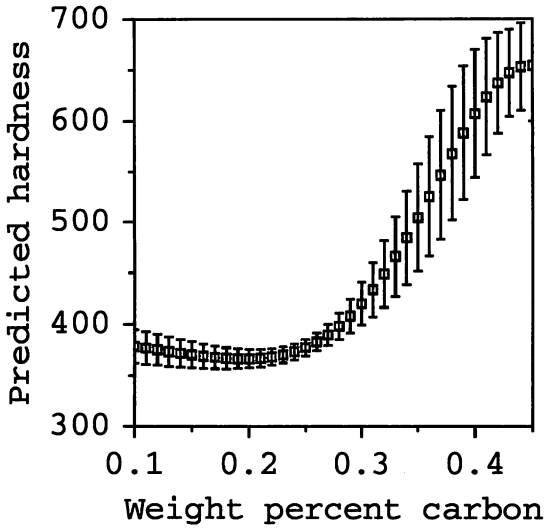

Figure 6.12 (a): Hardness predictions *vs.* carbon content

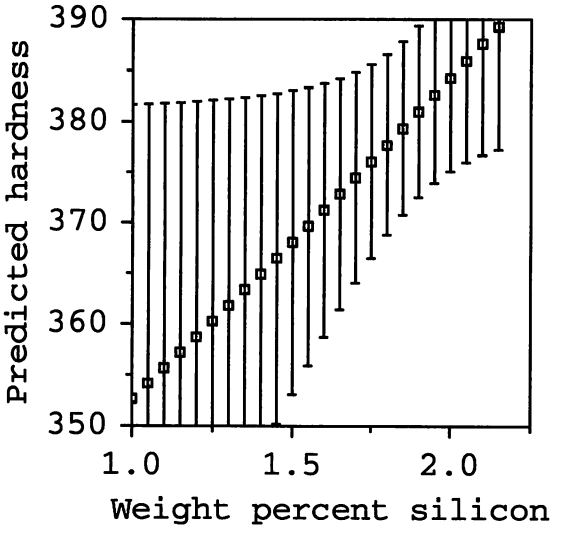

Figure 6.12 (b): Hardness predictions *vs.* silicon content

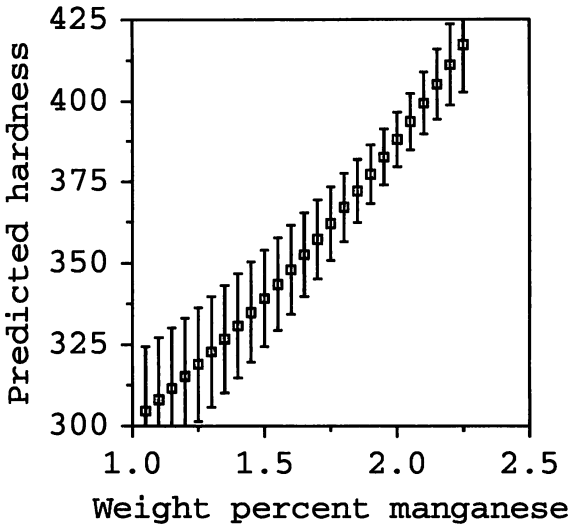

Figure 6.12 (c): Hardness predictions *vs.* manganese content

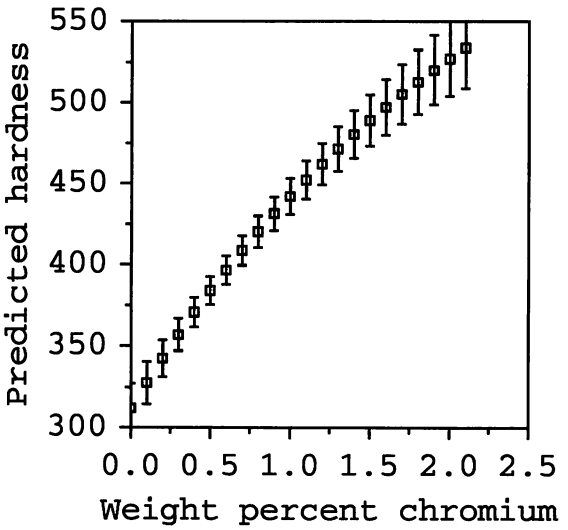

Figure 6.12 (d): Hardness predictions *vs.* chromium content

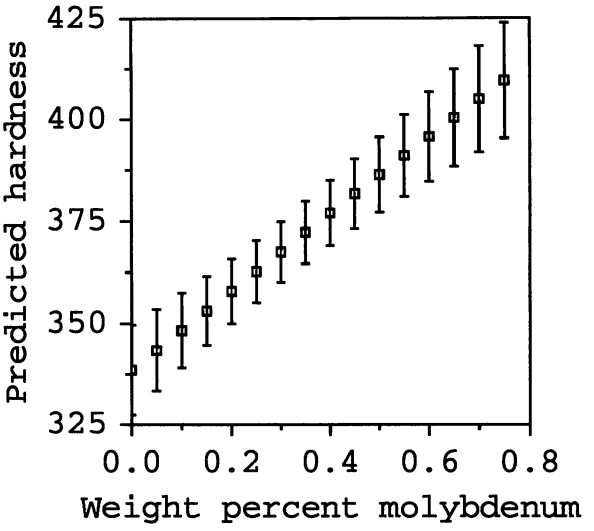

Figure 6.12 (e): Hardness predictions *vs.* molybdenum content

linear function of composition. All the graphs show some points which do not touch the line. These may be due to extreme compositions which the model cannot cope with; it is thought that a few of the steels in the database may not have been completely bainitic which would have altered their behaviour.

The graphs of hardness variation with each alloying element show sensible trends. The effect of carbon, Figure 6.12 (a), is very non-linear, but this can be explained in terms of the effect it has on the microstructure. The large increase in strength above 0.25 wt% carbon is caused by the formation of increasing amounts of martensite. Below this the microstructure is expected to be mostly bainitic. As the carbon content decreases and the proportion of bainitic ferrite increases with respect to the retained austenite, there will be a slight increase in strength and this is what is seen in the graph.

The trend for silicon, Figure 6.12 (b), is unclear because of the large error bars. This is not unexpected as the role of silicon in this microstructure is to suppress carbide formation rather than to solid-solution harden. There is little variation in silicon content in the input data because all the steels contain a large amount of silicon to suppress carbide formation. This makes it harder to deduce the effect of silicon has.

The graphs for manganese and chromium, Figure 6.12 (c) and (d), show a strong linear relationship between hardness and alloy content. Manganese is often used as a solid solution strengthener.

The effect of molybdenum, Figure 6.12 (e), is to increase the hardness almost linearly. Molybdenum is included in this steel for temper embrittlement resistance.

6.2 Modelling of segregation

Chemical segregation has been identified as a problem in British Steel's experimental bainitic rail steels. Regions of the steel which are high in alloying elements transform to martensite rather than bainite on cooling the steel, leading to a reduction in toughness. It would be desirable to be able to predict the likely degree of segregation in a potential new alloy before manufacture.

An attempt was made to quantify the degree of segregation in samples of five experimental bainitic rail steels by means of microhardness measurements. It is possible, using thermodynamics, to calculate the equilibrium condition of an alloy at any temperature during cooling. Although the alloy in actuality is not at equilibrium (or it would not be segregated) it is possible to estimate the composition of the alloy-rich and poor areas by looking at the compositions of the solid and liquid regions during cooling. Knowing

these compositions, the neural network model for hardness discussed earlier can be used to predict the hardness of the different regions. This model for predicting hardness variations was compared with the results from the five experimental steels and then used to predict which elements enhanced segregation and hence should be used with care in the design of subsequent tough bainitic microstructures.

6.2.1 Experimental methods and modelling

Five experimental bainitic rail steel were examined, provided by Swinden Technology Centre, in the form of broken Charpy samples. The steels had been cast in 50 kg laboratory vacuum melts, rolled to 30 mm plate, and machined into standard Charpy samples. The compositions are given in Table 6.11. No information was provided on the part of the plate from which each sample was machined.

Steel	C	Si	Mn	Cr	Mo
28C	0.25	1.83	2.16	1.03	0.25
29C	0.30	1.79	2.06	1.01	0.25
30C	0.27	1.74	2.11	1.09	0.50
32C	0.26	1.92	1.94	2.00	0.25
34C	0.26	1.87	1.89	2.00	0.50

Table 6.11: Compositions of experimental steels in weight percent

Heat treatment was carried out on part of each original Charpy specimen to try to compensate for variations in cooling rate the samples may have undergone. Cylinders 12 mm long and 8 mm in diameter were machined from one half of the specimen and heat treated in a Thermecmastor Z thermomechanical tester. The samples were heated to 1000 °C with an RF coil for five minutes to ensure complete reaustenisation, then cooled rapidly to 50 °C above the bainite start temperature, B_s. Between this point and the martensite start temperature, M_s, they were cooled at 0.1 $°Cs^{-1}$. From M_s they were rapidly cooled to room temperature. Nitrogen gas was used to cool the samples and the temperature was measured using a platinum/platinum-rhodium thermocouple welded to the side of the specimen, giving an accuracy of $\pm$ 3 °C. The B_s and M_s temperatures were calculated using a program `mucg46` [MAP_STEEL_MUCG46] for each composition. Dilatation and temperature-time curves were recorded for each treatment. A typical graph is shown in Figure 6.13.

Pieces of the the original samples were prepared for optical metallography by cutting off one end of the Charpy specimen, mounting it with the square face uppermost, pol-

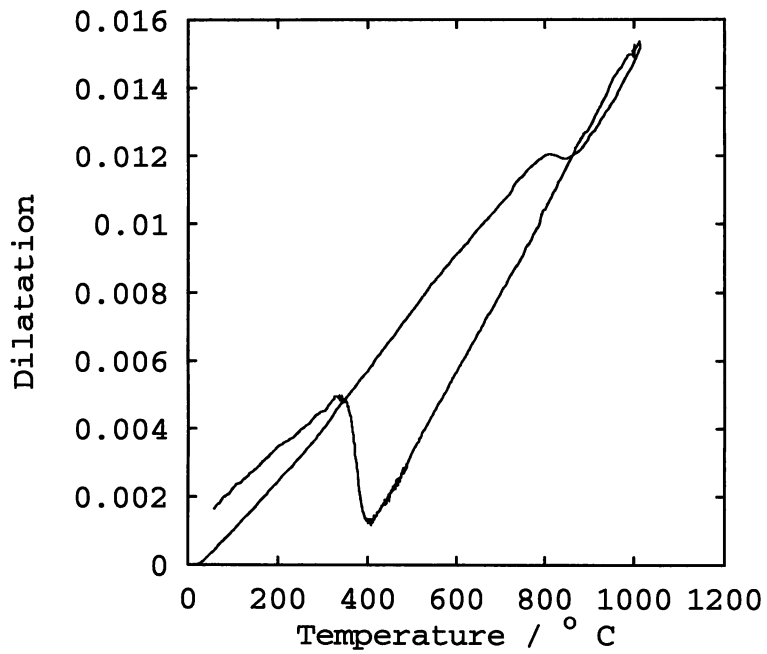

Figure 6.13: Typical temperature/dilation-time curve for heat treatment (steel 32C). The cycle starts at room temperature and zero dilatation. The sample is heated quickly up to 1000 °C and transforms, as seen by the inflexion in the curve. It is held at 1000 °C to ensure complete transformation, and then cooled rapidly to the bainite start temperature. The bainitic transformation is seen by the increase in strain starting at about 400 °C.

ishing to 1 μm finish and etching in 2 % nital. The microstructures were photographed. Cylindrical heat treated samples were sectioned parallel to the axis of the cylinder and polished in the same way. They were not etched as this makes it harder to measure microhardness indents.

Microhardness tests were carried out on the samples using a Mitutoyo Vickers microhardness tester. The etched, original, samples were tested with a load of 50 g. A short traverse was carried out on one sample at intervals of 50 μm but this did not show any clear hardness difference between the light and dark regions on the sample. Consequently a hardness distribution for each sample was found by taking a traverse across the whole sample at intervals of 0.5 mm, generating about 20 readings, and finding the mean and standard deviation of the results. A load of 100 g was chosen for the heat treated samples to minimise errors, and 60 readings taken in a straight traverse at 0.2 mm intervals along the length of each section.

An attempt was made to predict the extremes of composition which would be produced during solidification in the samples by using a program for the calculation of phase diagrams [MTDATA]. In a system of the appropriate composition the temperature was stepped until a temperature was found at which 80 % of the metal was solid and 20 % liquid. The phases allowed in the system were initially liquid, austenite, and δ-ferrite. The calculations did not always converge at the temperature of interest and so various mixtures of phases were tried until it did. The other phases which were eventually included were graphite and cementite. The compositions of the solid and liquid in weight percent were found, at the temperatures of interest, and the hardness of the solid composition predicted using the neural net model for macrohardness which was developed on similar experimental bainitic rail steels. The maximum hardness of the martensite that forms in an alloy with this liquid composition was assumed to be 800 HV [Bhadeshia and Edmonds, 1983]. The value of 20 % for the amount of highly-alloyed martensitic bands was chosen because it seemed reasonable.

The predicted range of hardness for each composition was plotted against the measured range, and also against the standard deviation, to test the model for both original and heat-treated samples.

The model was then used to investigate the effect on segregation of different solutes. The compositions used to make predictions were variations on a base alloy composition shown in Table 6.12. The amount of each element was changed in turn while holding

the others constant in order to separate the effects of each variable. The elements were varied between limits based on the range of the data used to construct the hardness prediction part of the model. These are also shown in Table 6.12. The model was run on each composition in turn and graphs of predicted hardness range *vs.* composition plotted.

Element	C	Si	Mn	Cr	Mo	Ni	B
Base alloy content	0.26	1.95	1.95	0.49	0.46	0	0
Range	0.20–0.45	1.5–2.2	1.0–2.0	0.0–2.0	0.0-0.8	-	-

Table 6.12: Base composition and ranges used for predictions This composition was chosen because it is a typical carbide-free bainite. The silicon range was chosen to begin as high as 1.5 wt % because around 2 wt % Si is required to make these steels carbide-free.

6.2.2 Results

The etched microstructures showed considerable variation in segregation as shown in Figure 6.14 and Figure 6.15. It is not possible to compare the banding in different steels with confidence as it is not known which parts of the plate the samples originated from. Segregation will have varied throughout the original cast and there will also be an effect of cooling rate on the hardness developed, hence the need to heat treat all the samples so they have cooled at the same rate.

The predicted solute-enriched and solute-depleted compositions for each steel are shown in Table 6.13.

Steel	Composition	C	Si	Mn	Cr	Mo
28C	High	0.59	2.56	2.90	1.38	0.36
	Low	0.17	1.65	1.98	0.94	0.22
29C	High	0.70	2.50	2.77	1.36	0.37
	Low	0.20	1.62	1.89	0.93	0.22
30C	High	0.63	2.44	2.82	1.45	0.72
	Low	0.18	1.56	1.93	1.00	0.44
32C	High	0.84	2.41	2.88	2.31	0.34
	Low	0.11	1.80	1.70	1.92	0.23
34C	High	0.73	2.49	2.68	2.46	0.68
	Low	0.15	1.72	1.70	1.89	0.46

Table 6.13: Predicted maximum and minimum compositions of segregated steels in weight percent

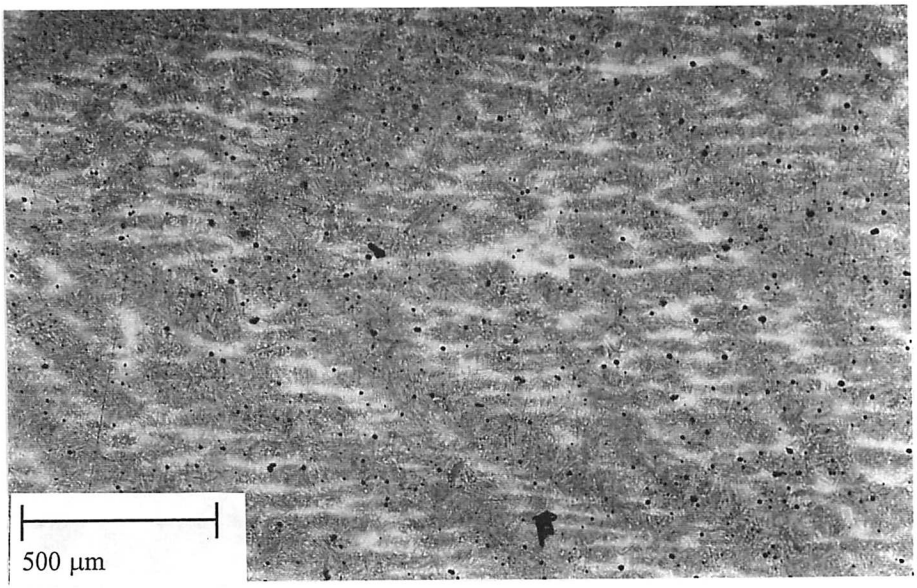

Figure 6.14: Segregation in steel 30C

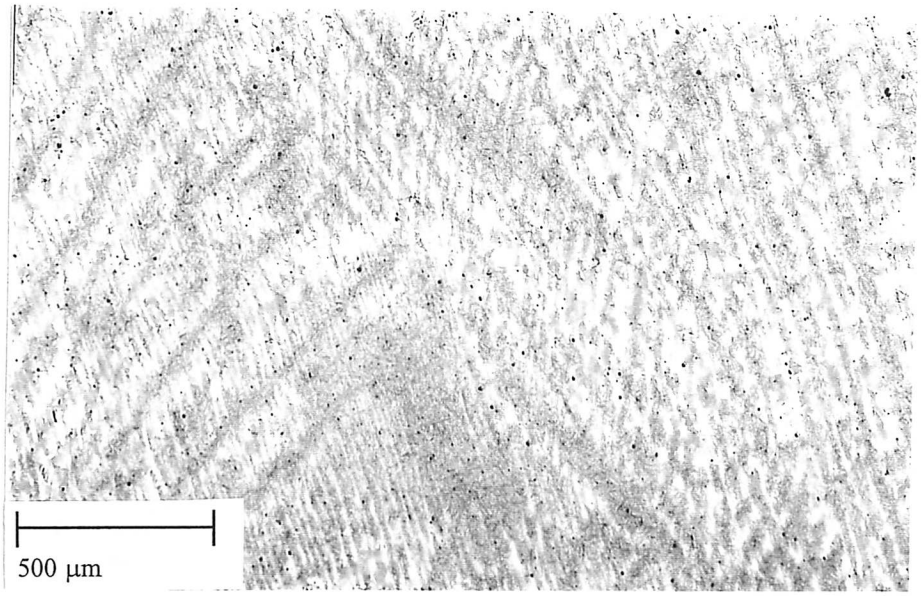

Figure 6.15: Segregation in steel 34C

The graphs of predicted against calculated hardness range for the original samples are shown in Figure 6.16 and Figure 6.17. The error bars on the y-axis are the errors given by the neural net model for the predicted hardness of the solute-depleted composition. The error bars on the x-axis in Figure 6.17 are the combined errors in the highest and lowest hardnesses, estimated from the accuracy to which the hardness indentation could be measured. The predicted hardness range appears to have a similar trend to the measured standard deviation. However, this does not agree with the measured range where the trend is in the opposite direction.

The equivalent graphs are shown for the heat treated samples in Figure 6.18 and Figure 6.19. It can be seen that there is a linear relationship between predicted and measured hardness ranges and standard deviations but the absolute values of hardness range do not match.

Graphs of hardness range *vs.*composition for varying amounts of carbon, silicon, manganese, chromium, and molybdenum are shown in Figure 6.20. There is no significant trend in any of these except for the chromium and carbon results. In chromium the hardness range decreases as the chromium content increases, and in carbon the hardness range goes through a peak and then falls.

6.2.3 Discussion

The non-heat-treated samples do not behave as predicted by the model. The predictions of the model seem fairly sensible and so it seemed likely that the problem was with the experiments. It was thought that the samples may have come from different parts of the original plate and so been subjected to different cooling rates. The hardness ranges from the heat treated samples, all cooled at the same rate through the transformation, did have a linear relationship with the predictions which strengthens this argument. However the greater number of data from the heat-treated samples may have played a role in improving the results. A higher load was also used to reduce errors in measuring the hardness indents. This would have the effect of narrowing the measured hardness range as one indent would cover a wider area of the microstructure and be less likely to fall entirely within one very hard or soft area.

Although the heat treated samples show that the trends predicted by the model are correct, there is still the problem that the hardness ranges predicted by the model are approximately twice those measured. The use of a large indenter may have caused a narrowing of the measured hardness distribution as described above. Unfortunately this

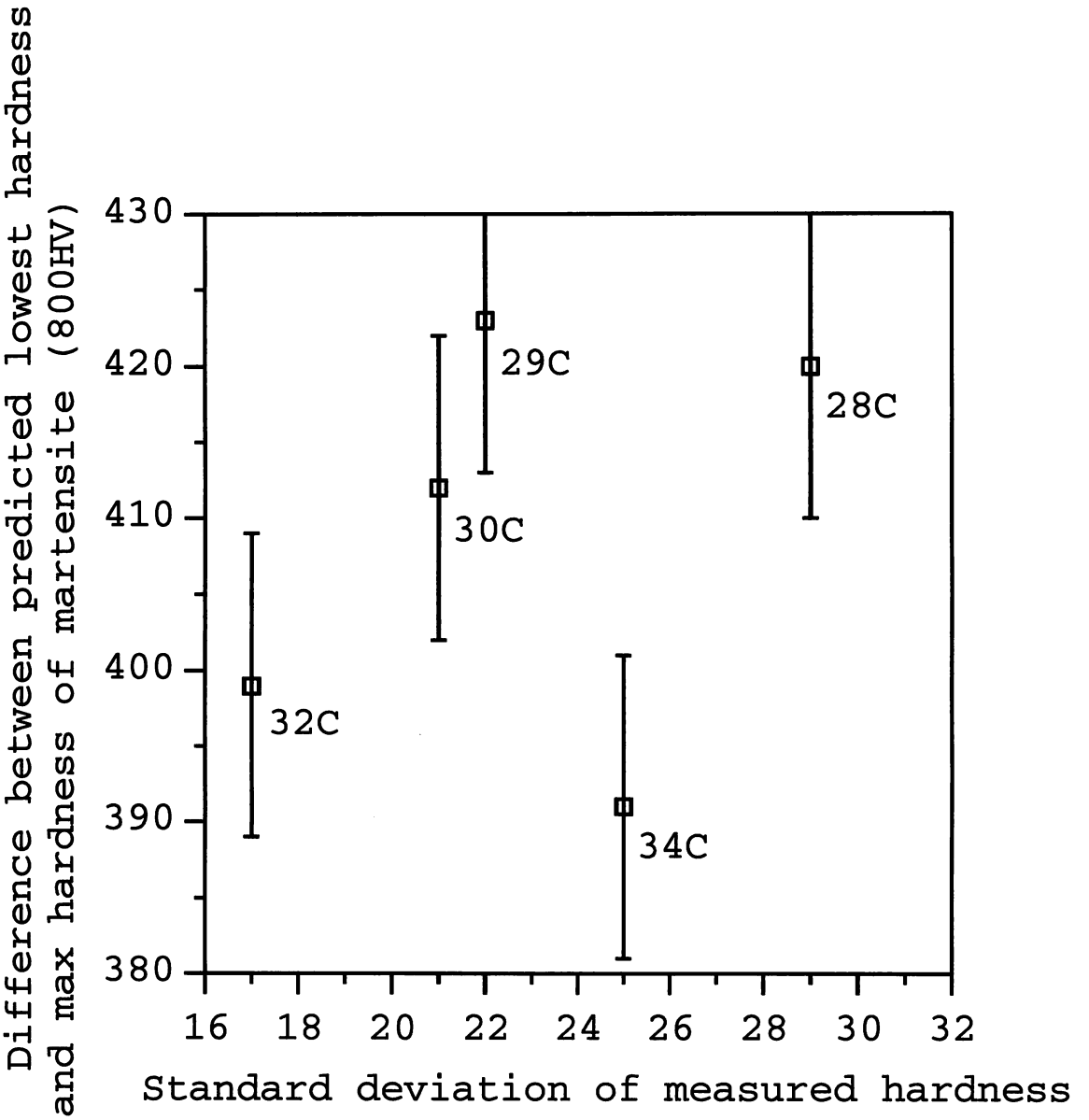

Figure 6.16: Graph of predicted hardness range *vs.* measured hardness range for samples before heat treatment

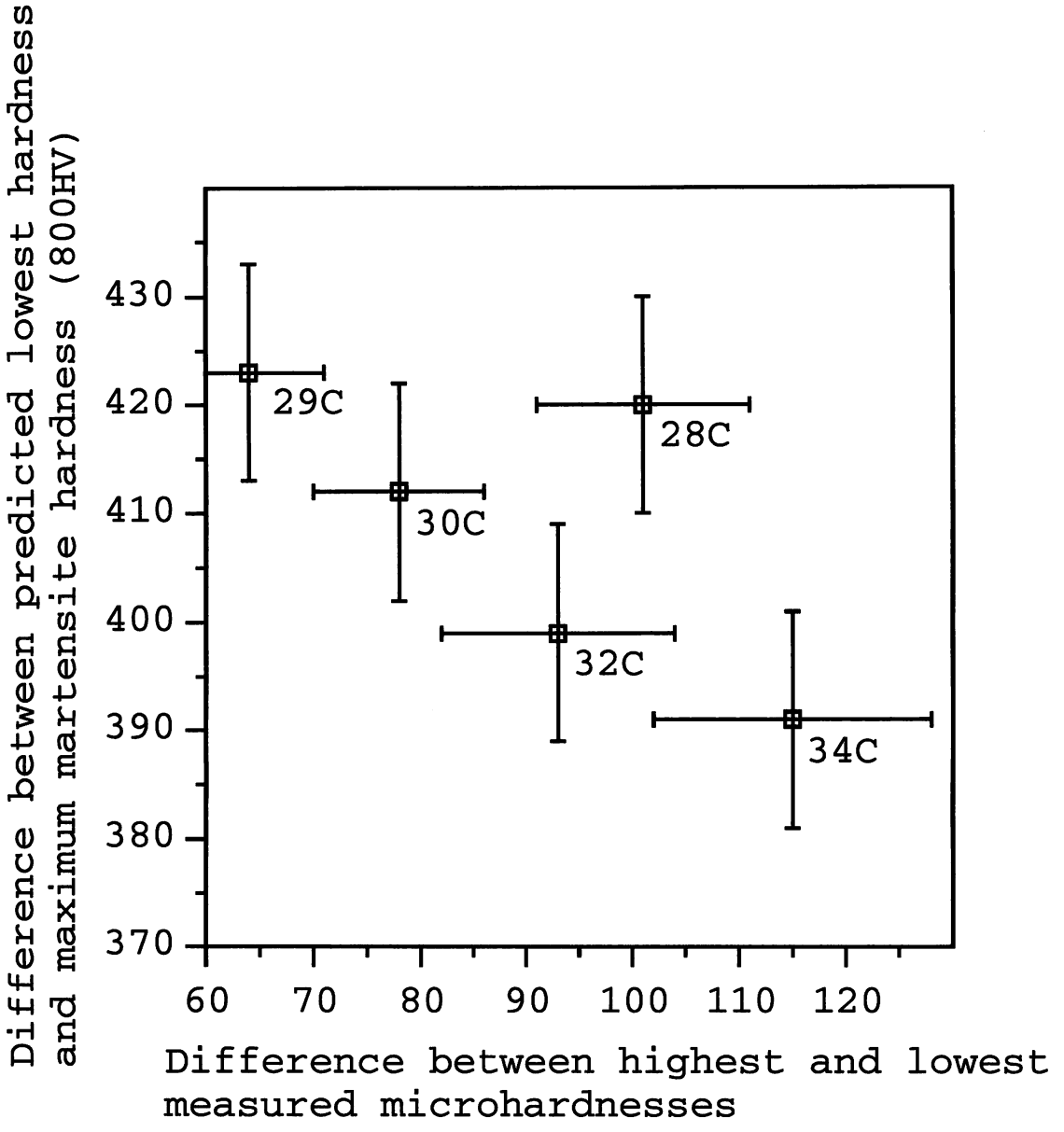

Figure 6.17: Graph of predicted hardness range *vs.* measured hardness standard deviation for samples before heat treatment

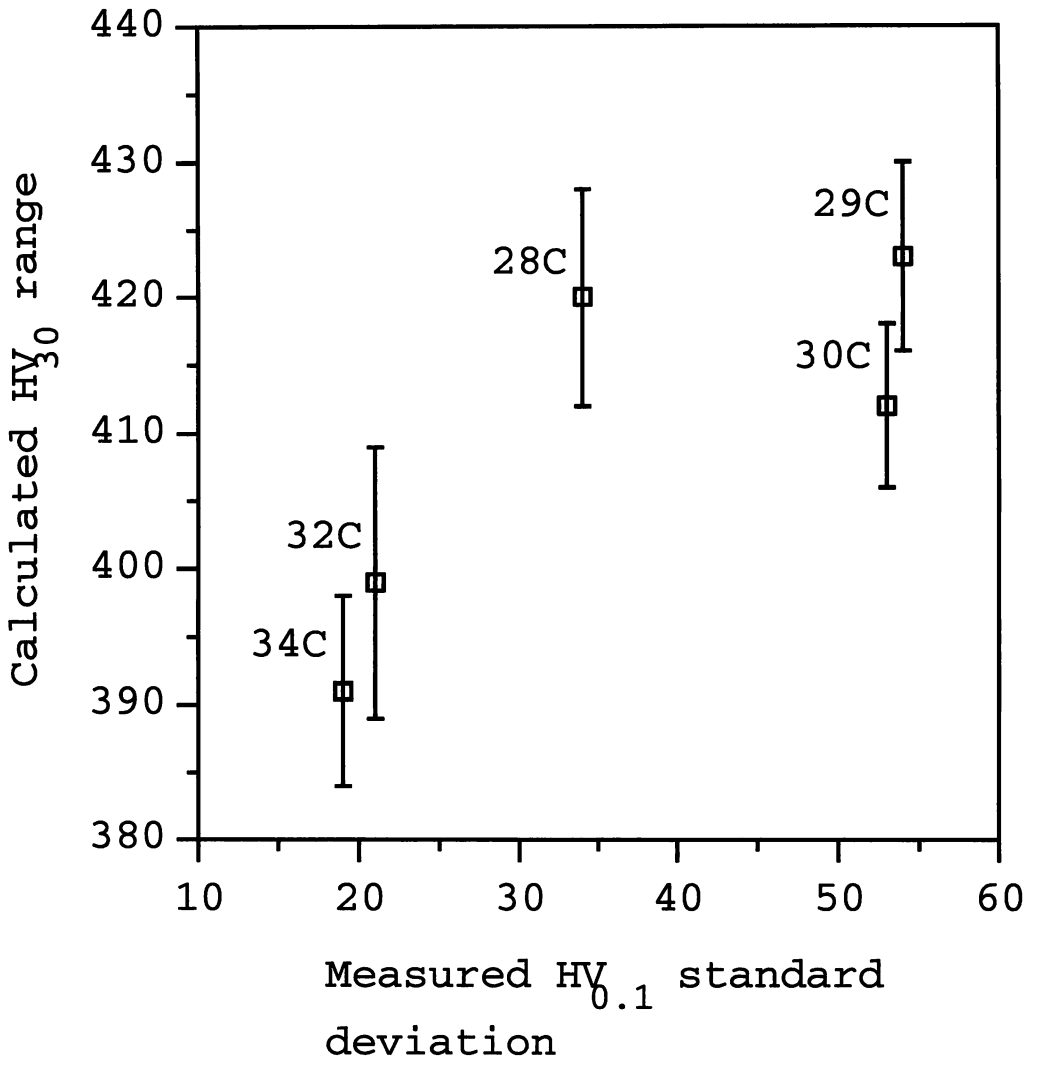

Figure 6.18: Graph of predicted hardness range *vs.* measured hardness range for samples after heat treatment. The y-axis values are macrohardness predictions. The model the predictions were made with was based on data measured with a load of 30 kg. The x-axis values are measured microhardnesses; the load used was 100 g.

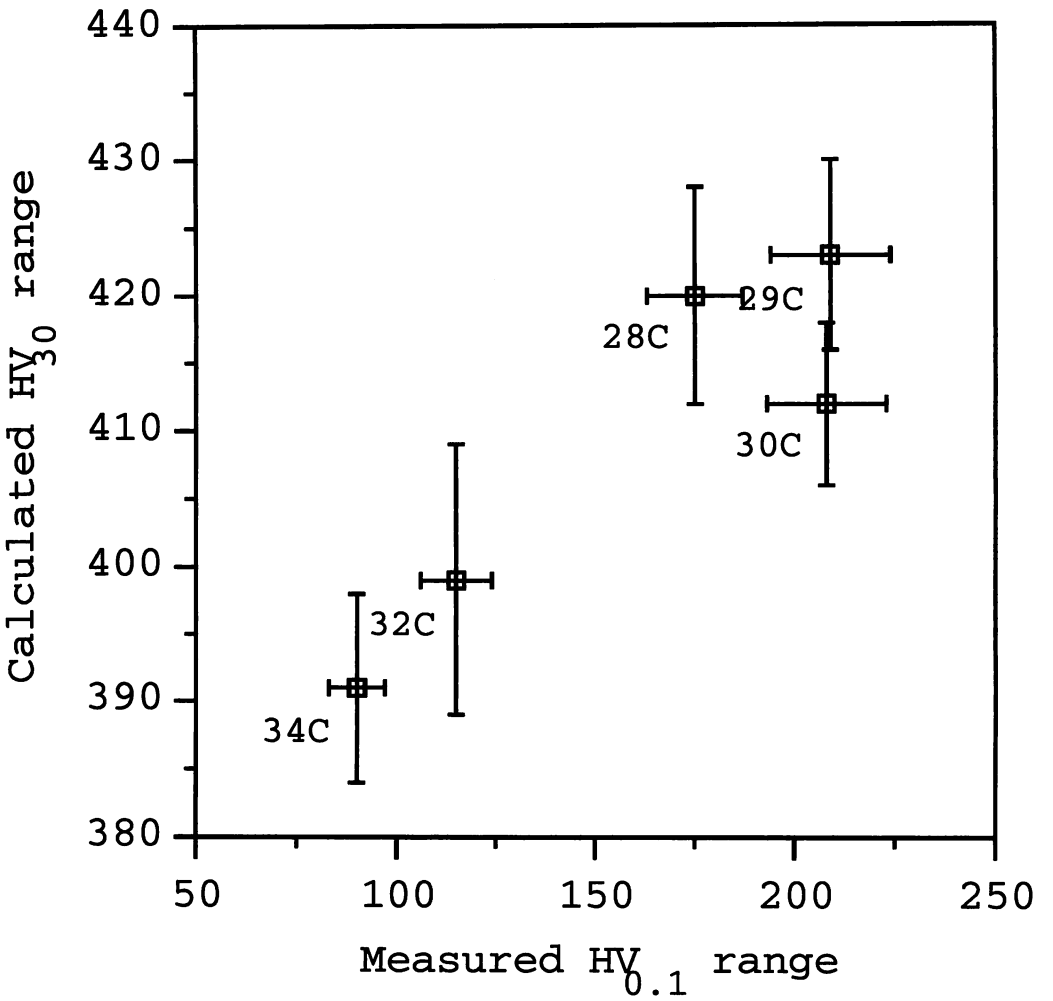

Figure 6.19: Graph of predicted hardness range *vs.* measured hardness range for samples after heat treatment. The y-axis values are macrohardness predictions. The model the predictions were made with was based on data measured with a load of 30 kg. The x-axis values are measured microhardnesses; the load used was 100 g.

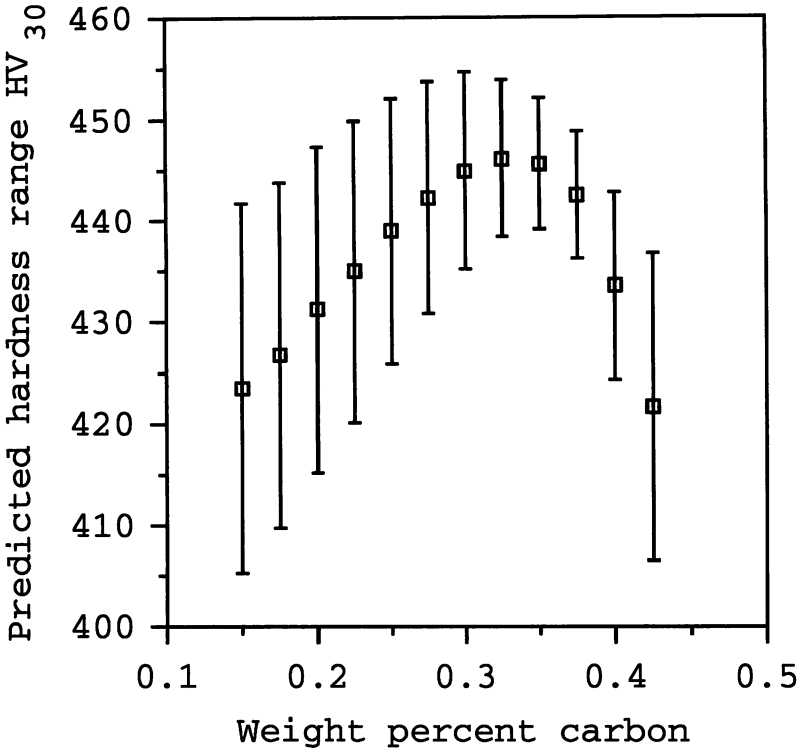

Figure 6.20 (a): Graphs of predicted hardness range *vs.* carbon content

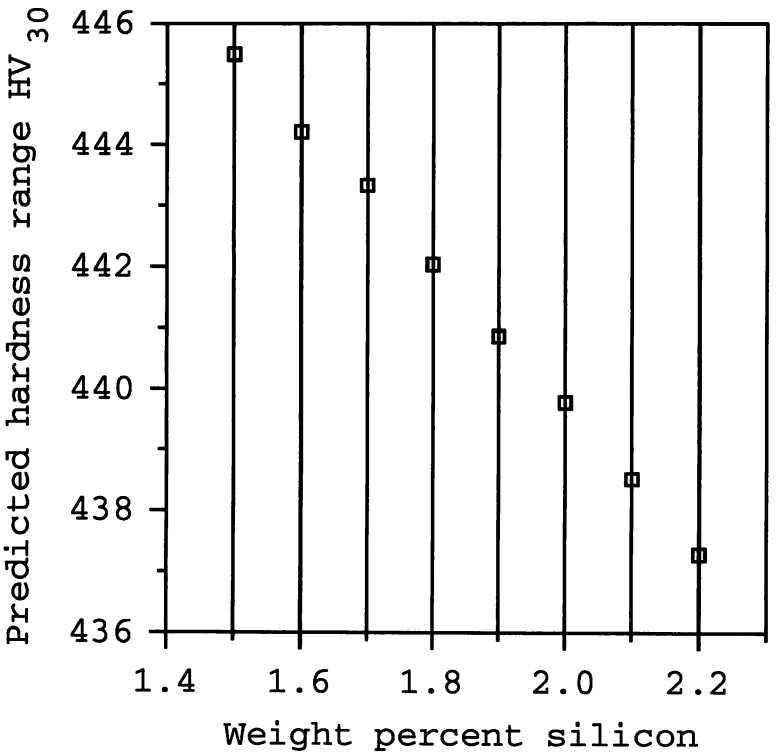

Figure 6.20 (b): Graphs of predicted hardness range *vs.* silicon content

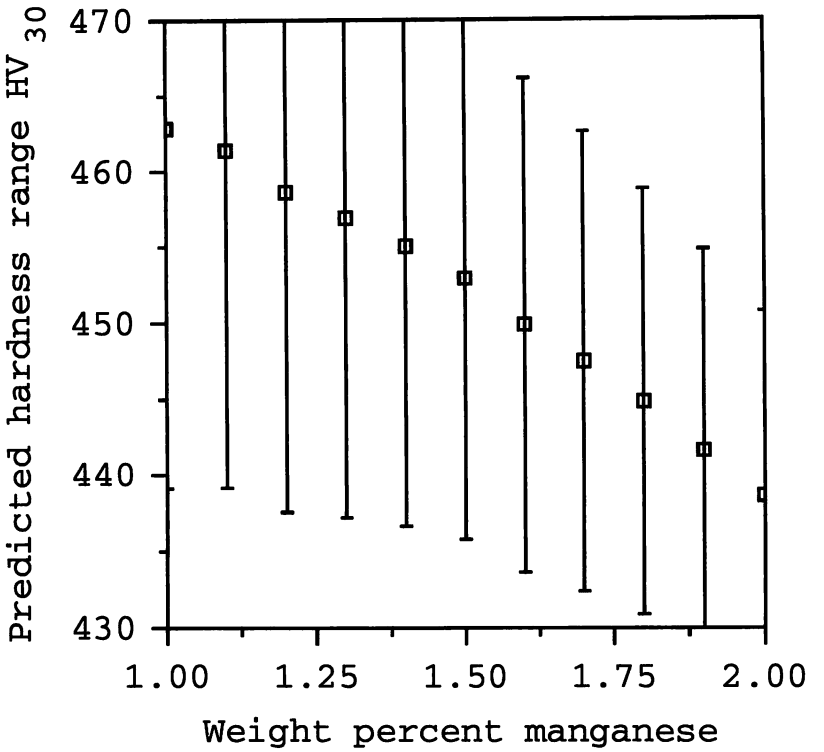

Figure 6.20 (c): Predicted hardness range *vs.* manganese content

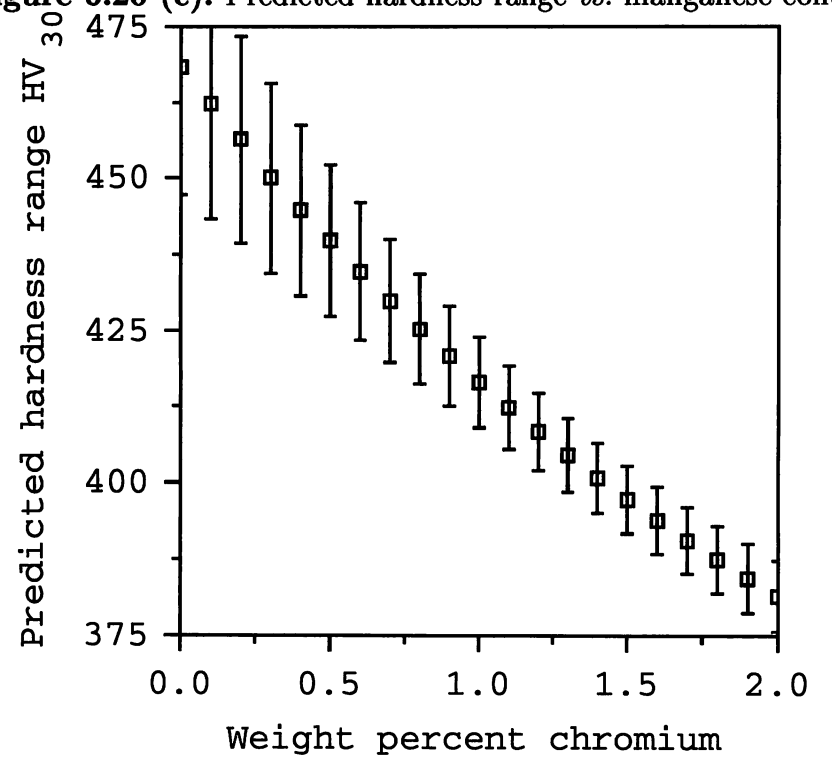

Figure 6.20 (d): Predicted hardness range *vs.* chromium content

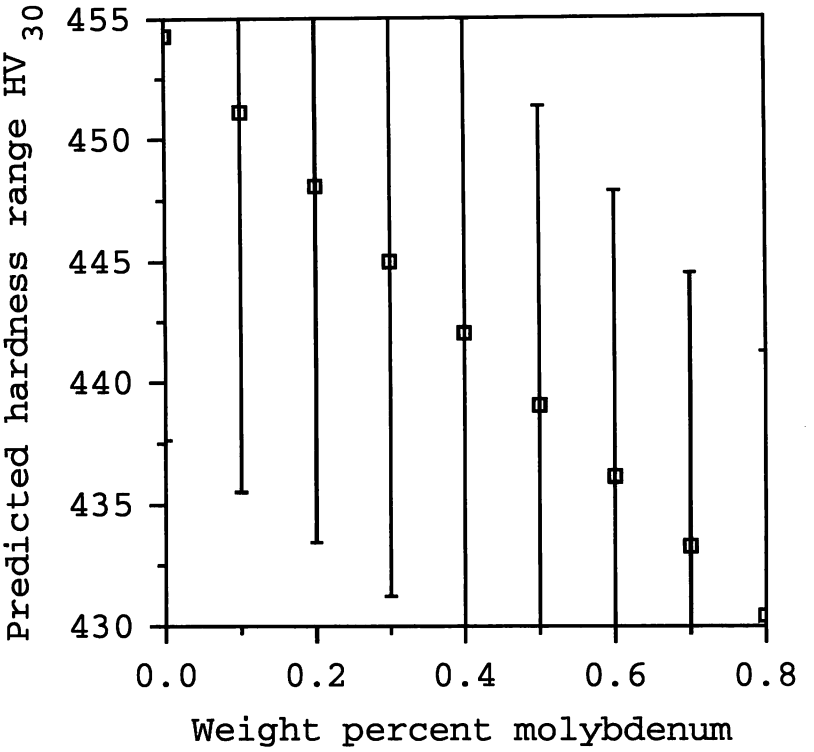

Figure 6.20 (e): Predicted hardness range *vs.* molybdenum content

is difficult to avoid since a smaller load is associated with greater errors. A load of 50 g was found to be the practical minimum. 100 g was chosen for the heat treated steels because it was easier to work with and the errors were lower. Microhardness values tend to be much larger than macrohardness values although the ranking order would be the same. This is due to the differences between micro and macro plasticity, which are not taken into account in the basic theory of hardness testing.

Finally, the assumptions in the model may not be accurate. If the fraction of solid and liquid at which the compositions are calculated is changed, the predicted hardnesses will change. Also although the theoretical maximum hardness may be 800 HV, this was not measured in any of the samples.

The results for varying compositions predicted by the model show that only carbon and chromium would have a significant effect on the hardness range. In general it is expected that the hardness range will decrease with increasing alloying additions. This is because a certain amount of the sample becomes martensite of the maximum possible hardness (800 HV) and the hardness of the remaining material, which will transform to a mixture of bainite, austenite, and martensite, depends on the composition and would be expected to increase with greater alloying additions. This decreases the total hardness range, and this behaviour is predicted by the model for chromium.

The behaviour of carbon is slightly more complex as the hardness range goes through a peak and then drops. The non-linear variation of hardness with carbon content as predicted by the neural network hardness model explains this behaviour.

6.3 Summary

Neural network models have been developed to predict the 0.2 % proof stress, tensile strength, and hardness of carbide-free bainitic steels. These models are better than linear regression models calculated using the same data. The hardness model predicts sensible trends with varying alloy content although there are a few compositions in the original dataset which the model cannot predict reliable values for. This may be due to extreme compositions that contain phases such as allotriomorphic ferrite.

The hardness model has been used in conjunction with MTDATA to predict hardness variations in segregated carbide-free bainitic steels. The trends predicted by the model have been verified by experiment but the absolute values are incorrect. This may be due to the difference between micro and macro hardness measurements. This new model was used to predict the effect on hardness variations of altering the composition of the steels.

Chromium and carbon were found to be the only two elements which had a significant effect on segregation.

7

Tensile properties of bainitic rails

The tensile properties of the bainitic rails in the straightened and unstraightened condition were investigated to understand the effect of the straightening process on the microstructure. Straightening of rails is carried out after rolling and cooling. The rails develop a bend during cooling as the head of the rail cools more slowly than the foot. This has to be removed by passing them through a set of rollers in the horizontal and vertical planes, which strain the rail plastically and straighten it [Sperring 1982, Esveld 1986].

Samples of the rail steels were also tested after tempering and liquid nitrogen heat treatments. The effect of these treatments on the retained austenite content was investigated using X-ray diffraction, and the microstructural changes related to the tensile properties.

7.1 Material and experimental methods

Samples of bainitic rail steel were provided by Swinden Technology Centre in both the straightened and unstraightened conditions. Straightening is carried out after hot rolling and cooling the rails. The rails are put through a series of rollers in the vertical and horizontal planes to control rail straightness and flatness. This involves plastic deformation, so any unstable retained austenite in the bainitic steel may well transform during this process, altering the properties of the steel. Samples of an experimental martensitic rail were also provided for comparison. All the steel was provided in the

form of "NTR19" tensile specimens which have a diameter of 7.98 mm and a gauge length of 40 mm. The compositions of the steels are given in Table 7.1. The samples were taken from the gauge corners of rails, as illustrated in Figure 7.1.

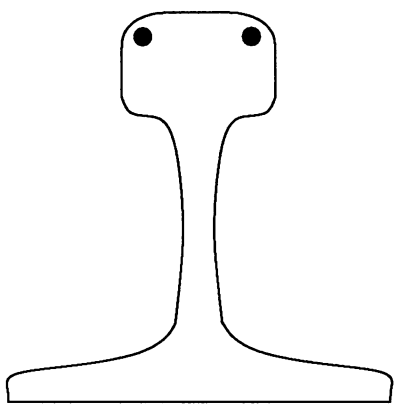

Figure 7.1: Origin of tensile samples taken from rail

	Composition wt%							
	C	Si	Mn	P	S	Cr	Mo	B
Bainite	0.21	1.97	1.98	0.013	0.015	0.48	0.47	0.0026
Pearlite	0.57	0.19	0.64	0.021	0.011	0.26	0.06	-
Martensite	0.18	0.39	1.33	0.010	0.013	0.33	0.33	0.0023

Table 7.1: Compositions of experimental steels

Some of the bainitic samples were heat-treated to investigate the effect this would have. The so-called "bainitic" rails actually have a mixed microstructure consisting mainly of plates of bainitic ferrite separated by films of high-carbon retained austenite. The larger regions of austenite, tend to be less stable than the films. There may also be some untempered martensite since not all the austenite left after bainitic tranformation is retained. Low-temperature heat-treatments may be used to temper the martensite

with consequent changes in the tensile properties. Some of the blocky austenite may be induced to transform to martensite by cooling in liquid nitrogen.

A number of tensile samples of straightened and unstraightened bainite were prepared; some were tempered for one hour at 250°C and 350°C and some were held in liquid nitrogen for 24 hours.

The samples were tested in a Mayes-ESH 100 kN tensile machine. The cross-head speed was set to $2\,\mathrm{mm\,min^{-1}}$, giving a strain rate of approximately $8.3 \times 10^{-4}\,\mathrm{s^{-1}}$. Extension, load, and cross-head displacement were recorded on a computer during the test. The data were analysed to determine the 0.2% proof stress, ultimate tensile strength, total elongation, and a work-hardening coefficient. The latter was measured by fitting the plastic region of the true stress/true strain curve to

$$\sigma = B\epsilon^n \tag{7.1}$$

where σ is true stress, ϵ is true strain, K is a constant and n is the work-hardening coefficient. Data up to 3% strain were recorded reliably using an extensometer and it is these which are used to determine n.

Fractography was carried out on the fracture surfaces using a CamScan S2 and a JEOL 820 scanning electron microscope. The hardnesses of both tensile tested and untested samples were measured on a Vickers machine with a 20 kg load. The samples were sectioned perpendicular to the lonmg axis and polished down a 1 μm finish before hardness testing. For the samples which had been tensile tested, the measurements were made in the un-necked region of the sample.

The retained austenite content of the samples before tensile testing was measured using X-ray diffraction on a vertical diffractometer. The sample surfaces were ground to a 1 μm finish before testing. One sample was etched with 2% nital and tested a second time to see if this made any difference to the results. Two other samples were also tested: one cut from the uniform elongation region of the tested plain straightened bainitic sample, and a piece of unstraightened rail tempered at 600 °C for one hour to get a completely annealed microstructure. The samples were scanned from 45 to 125 ° 2θ to get three non-overlapping peaks for each phase. The peaks used in the calculation were 200α, 211α, 310α, 200γ, 220γ, and 311γ.

7.2 Results

The proof stress, UTS, elongation, and work-hardening coefficients for all samples are shown in Table 7.2. Engineering stress-strain curves are shown in Figure 7.2.

Sample (bainitic unless indicated)		0.2% Proof stress MPa	UTS MPa	Elongation	Work-hardening coefficient
Plain	unstraightened	852	1377	26	0.17
	straightened	977	1362	27	0.18
Liquid nitrogen	unstraightened	883	1394	22	0.17
	straightened	957	1362	25	0.18
250°c/1 hr	unstraightened	870	1350	26	0.15
	straightened	1086	1352	25	0.11
350°c/1 hr	unstraightened	990	1255	23	0.07
	straightened	1116	1322	22	0.07
Martensitic	-	1222	1378	14	0.07

Table 7.2: Tensile testing results. Note work-hardening coefficients are calculated from the plastic portion of the stress-strain curve between strains of 0.2% and 3%

Sample (untested unless indicated)		Retained austenite content %
Plain	unstraightened	16 ± 1
	straightened	15 ± 1
Liquid nitrogen	unstraightened	9 ± 1
	straightened	14 ± 1
250 °C/1 hr	unstraightened	18 ± 2
	straightened	14 ± 2
350 °C/1 hr	unstraightened	14 ± 1
	straightened	11 ± 2
600 °C/1 hr	unstraightened	none found
Uniform elongation region of tested plain sample		none found

Table 7.3: Retained austenite contents

The retained austenite contents measured for the samples are shown in Table 7.3.

Straightening the rail clearly increases the proof stress but has little effect on the UTS. Straightening has little effect on the retained austenite content, the only significant reduction caused by cooling in liquid nitrogen. This result is unexpected because liquid nitrogen and straightening should reduce retained austenite content. The retained austenite measurements were repeated twice but with the same results so the anomaly cannot be explained.

Since the retained austenite content does not decrease, the rise in proof stress due to straightening must be attributed to gerneal work-hardening. The strain involved in

a)

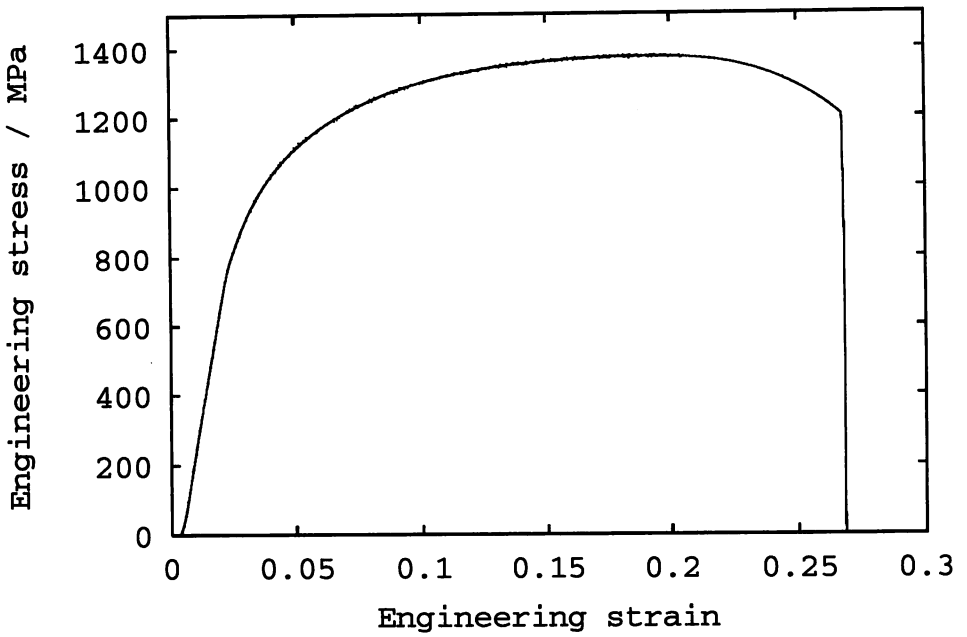

b)

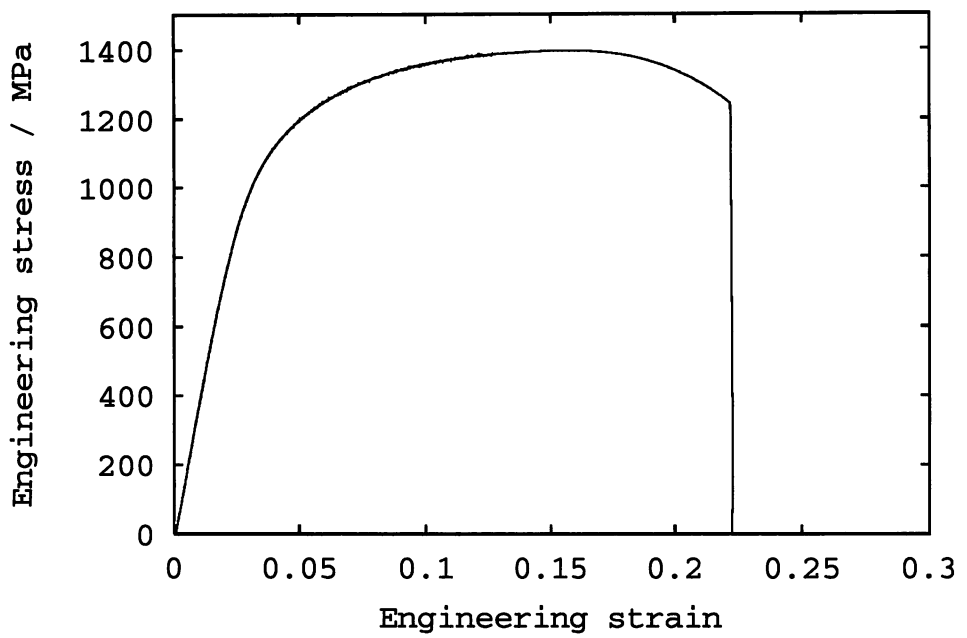

Figure 7.2 a)–b): Engineering stress-strain curves for unstraightened bainite a) No heat treatment
b) Cooled in liquid nitrogen for 24 hours

the straightening process is about 1% so it can be concluded that the retained austenite is not affected by such small strains. The inability to detect retained austenite in the uniform elongation sample, which had been strained to about 20%, shows that it does eventually decompose.

c)

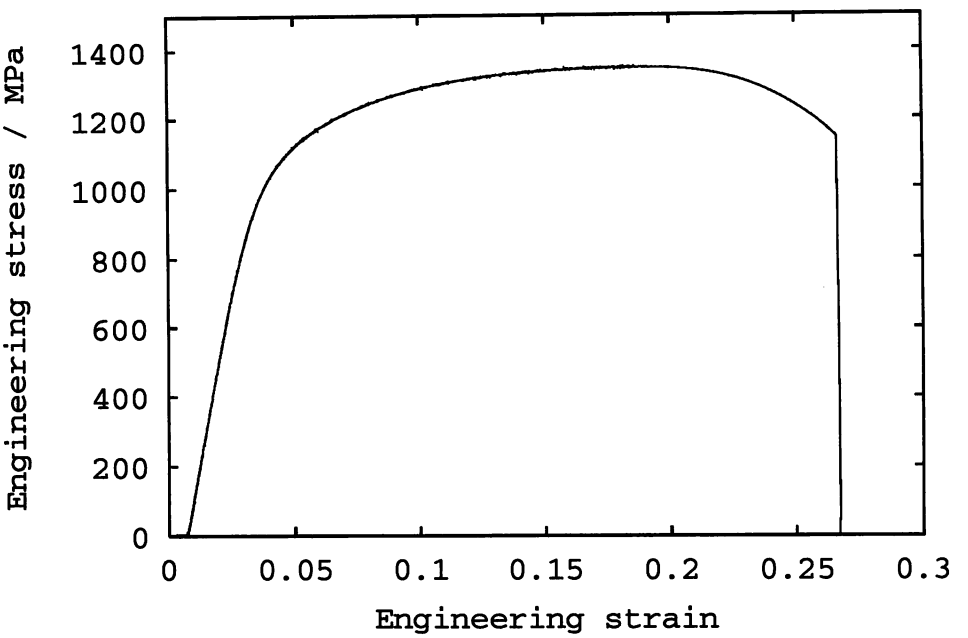

d)

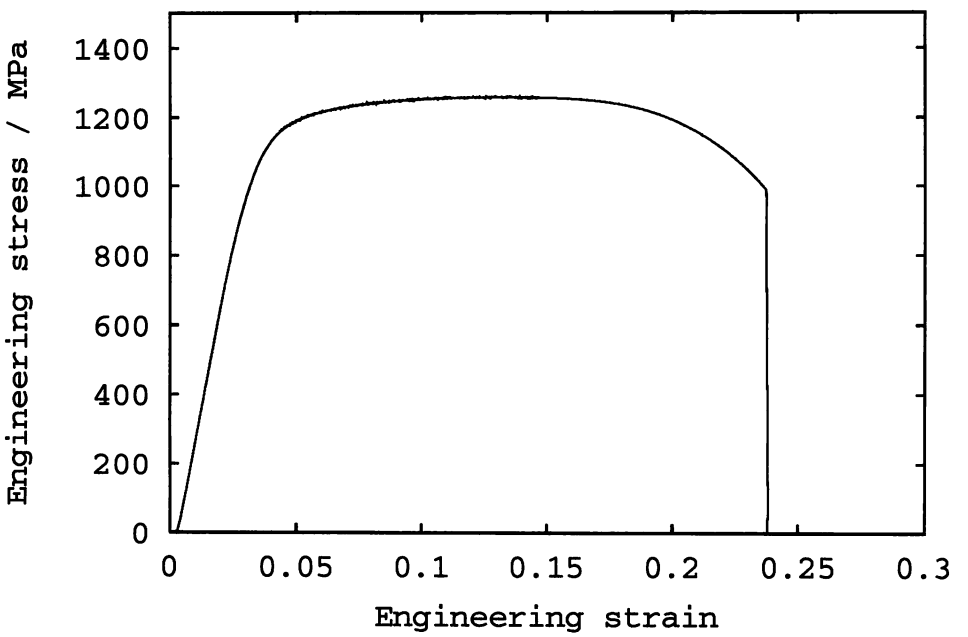

Figure 7.2 c)–d): Engineering stress-strain curves for unstraightened bainite c) Tempered at 250 °C for one hour
d) Tempered at 350 °C for one hour

As expected, the straightening process does not alter the UTS because the straightening strain is small compared with that at which necking begins.

Cooling in liquid nitrogen does not have much effect on the retained austenite in this microstructure. Previous studies on similar steels [Bhadeshia 1979, Rao *et al.* 1976]

e)

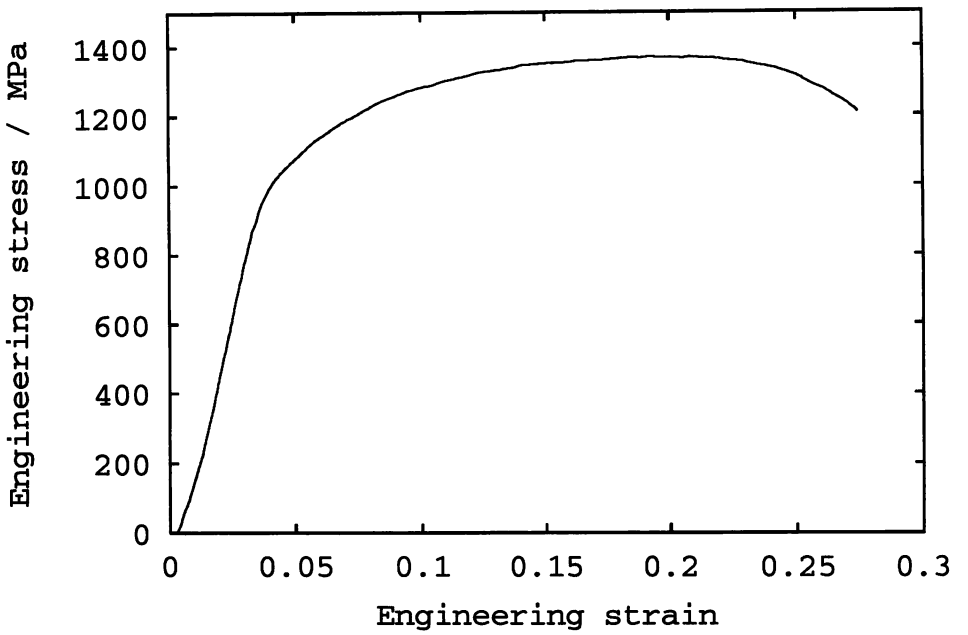

f)

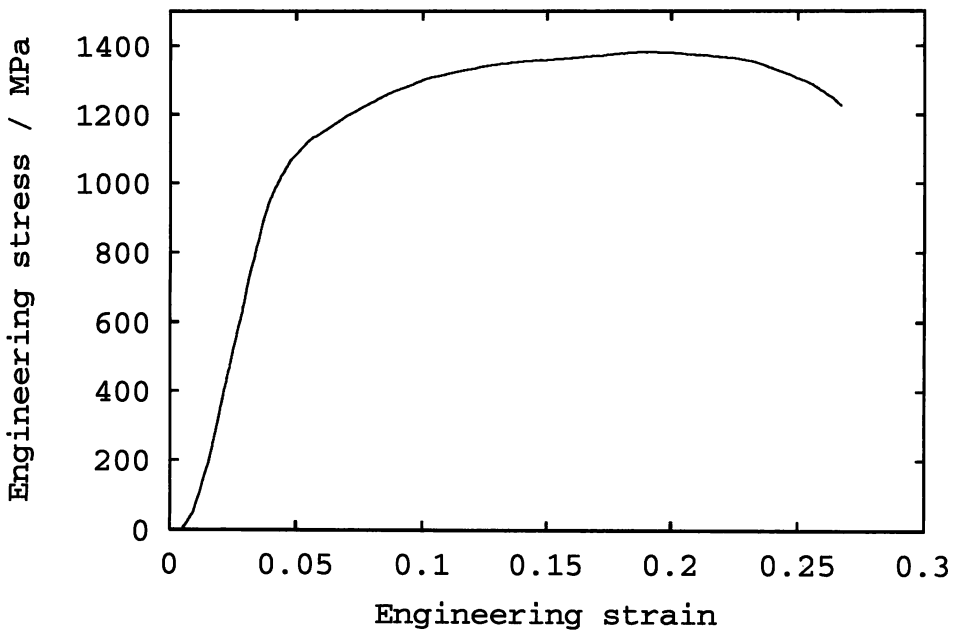

Figure 7.2 e)–f): Engineering stress-strain curves for straightened bainite e) No heat treatment
f) Cooled in liquid nitrogen for 24 hours

have also shown this.

Tempering the steel at 250 and 350 °C for one hour raises the proof stress but lowers the UTS, the greater effect being for 350 °C. Tempering should cause carbide precipitation in the martensitic regions with associated softening and a decrease in the

g)

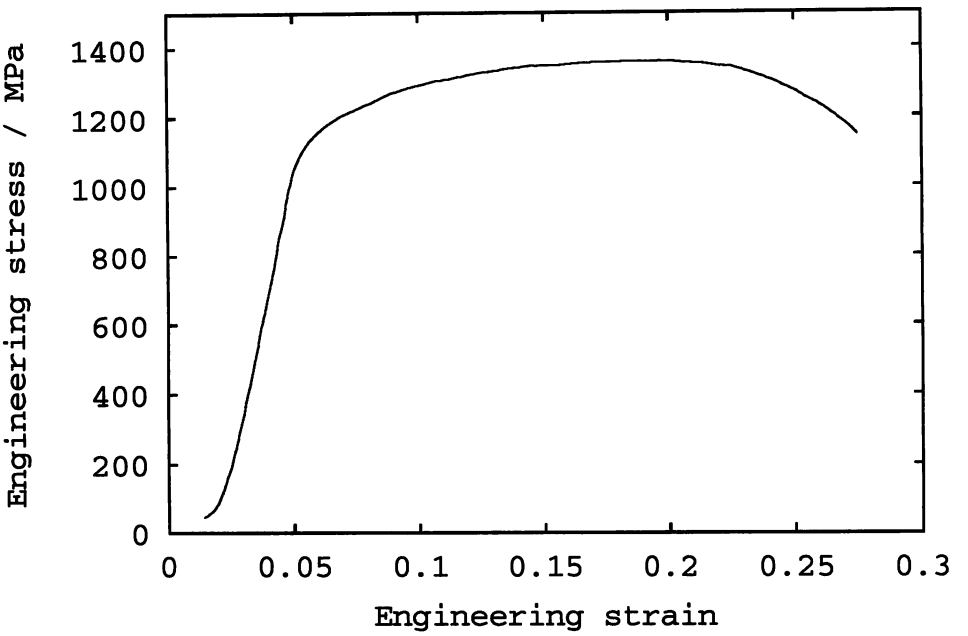

h)

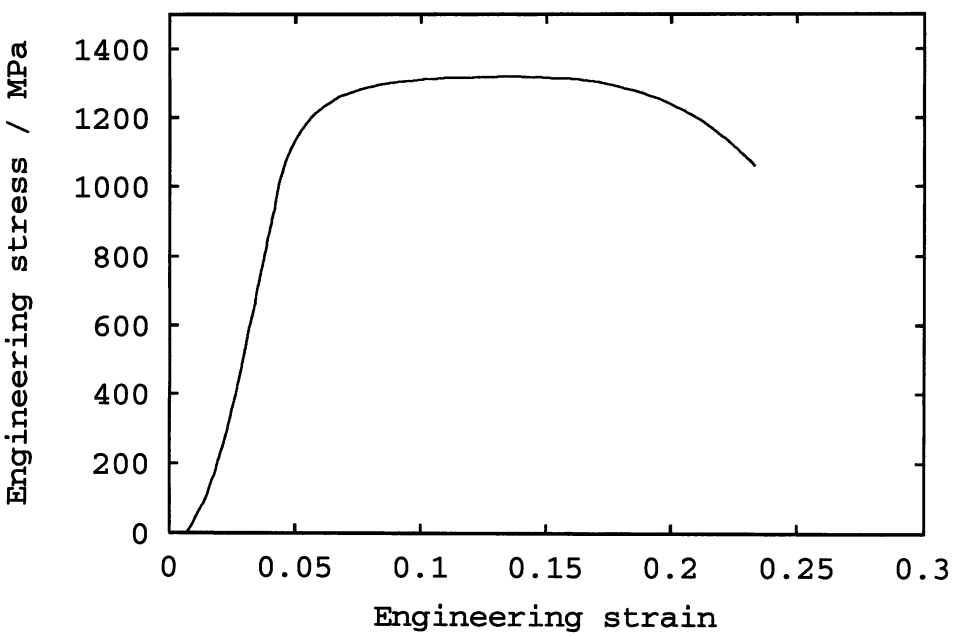

Figure 7.2 g)–h): Engineering stress-strain curves for straightened bainite g) Tempered at 250 °C for one hour
h) Tempered at 350 °C for one hour

UTS. The proof stress increases because the microstructure becomes more uniform so that yielding is not focused in the softer regions. The tempering has no effect on the retained austenite content, which is expected. The 600 °C heat treatment caused all of the retained austenite in the microstructure to transform as shown by the fact that none

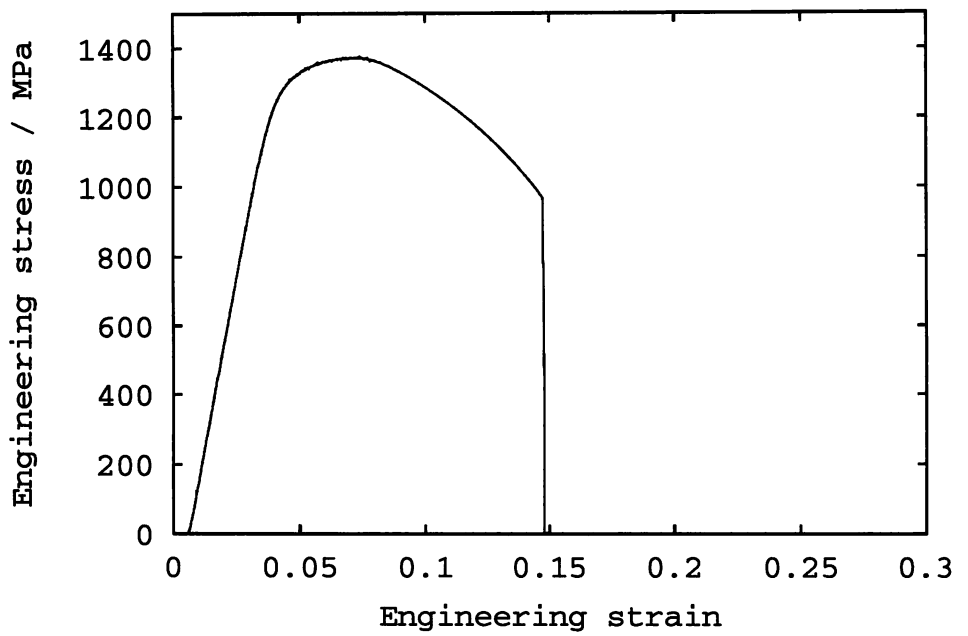

Figure 7.2: Engineering stress-strain curve for martensitic rail

was detected in the X-ray diffraction experiments (Table 7.3).

The work-hardening coefficients are similar for the straightened and unstraightened rail and cooling in liquid notrigen did not acheieve any change. The work-hardening coefficients decreased following tempering. Tempering causes the proof stress to rise so there is less hardening before the UTS is reached.

A "standard" pearlitic mill heat-treated sample tested by British Steel Swinden Technology Centre in compression was found to have a work-hardening coefficient of 0.15, comparable with that measured for bainitic steels. Good wear resistance is frequently associated with a high work-hardening coefficient but this does not seem to be the case here; the bainitic steel has a wear rate several times lower than the standard rail steel.

Sample		Hardness HV_{20} Before testing	After testing
Plain	unstraightened	408	484
	straightened	429	471
Liquid Nitrogen	unstraightened	422	478
	straightened	424	460
250°C/1 hr	unstraightened	409	458
	straightened	428	468
350°C/1 hr	unstraightened	417	449
	straightened	428	448

Table 7.4: Hardness of tensile specimens before and after tensile testing

The hardnesses of the bainitic rails are shown in Table 7.4.

It can be seen that the hardnesses before testing of the unstraightened rails are lower than those of the straightened rails, as expected, whereas the hardnesses after testing are much closer together when all the samples have undergone a large plastic strain. The tempered samples all have lower hardnesses than the equivalent untempered samples. This shows that the hardness test is a measure of strength at a fairly high strain, otherwise the hardnesses would be expected to increase in line with the proof stress.

All of the samples showed ductile fracture surfaces. Examples of the straightened rails are shown in Figure 7.3, and of the unstraightened rails in Figure 7.4.

7.3 Summary

Tensile tests have been carried out on straightened and unstraightened bainitic rail steels, and on an experimental martensitic rail steel.

Tempering at low temperatures is shown to reduce the work-hardening coefficent, raise the proof stress, and lower the UTS. These effects agree with what we know about the microstructure of this steel. The retained austenite in the bainitic microstructure is very stable and does not transform when cooled in liquid nitrogen, or under the influence of small plastic strains.

The bainitic steel does not have a particularly high work-hardening coefficient. This rules out any theory that the excellent wear resistance is associated with greater work-hardening.

The martensitic steel has a much higher proof stress and UTS but a low work-

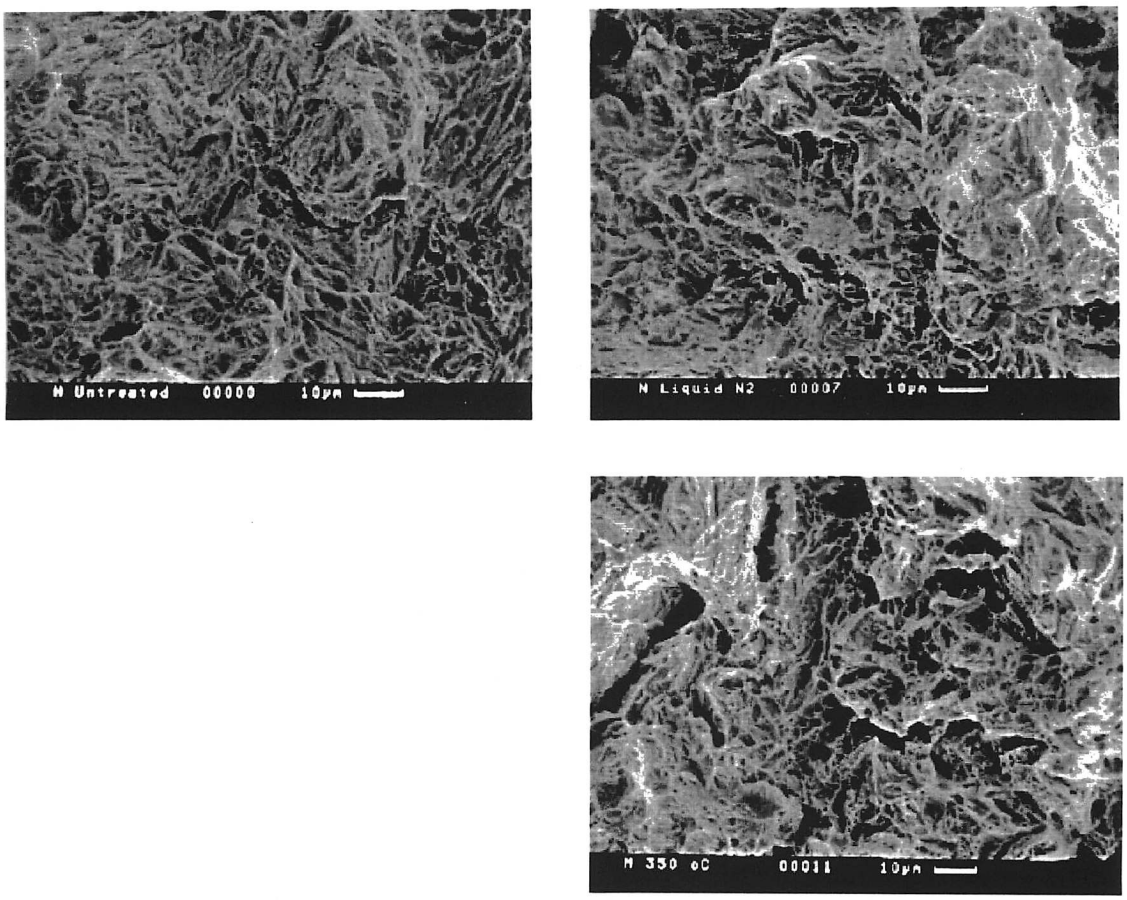

Figure 7.3: Fracture surfaces of straightened rail The scale bars are 10 μm. No picture is available for the sample treated at 250 °C because the sample surface was badly damaged in an accident with the tensile testing machine.

hardening coefficient.

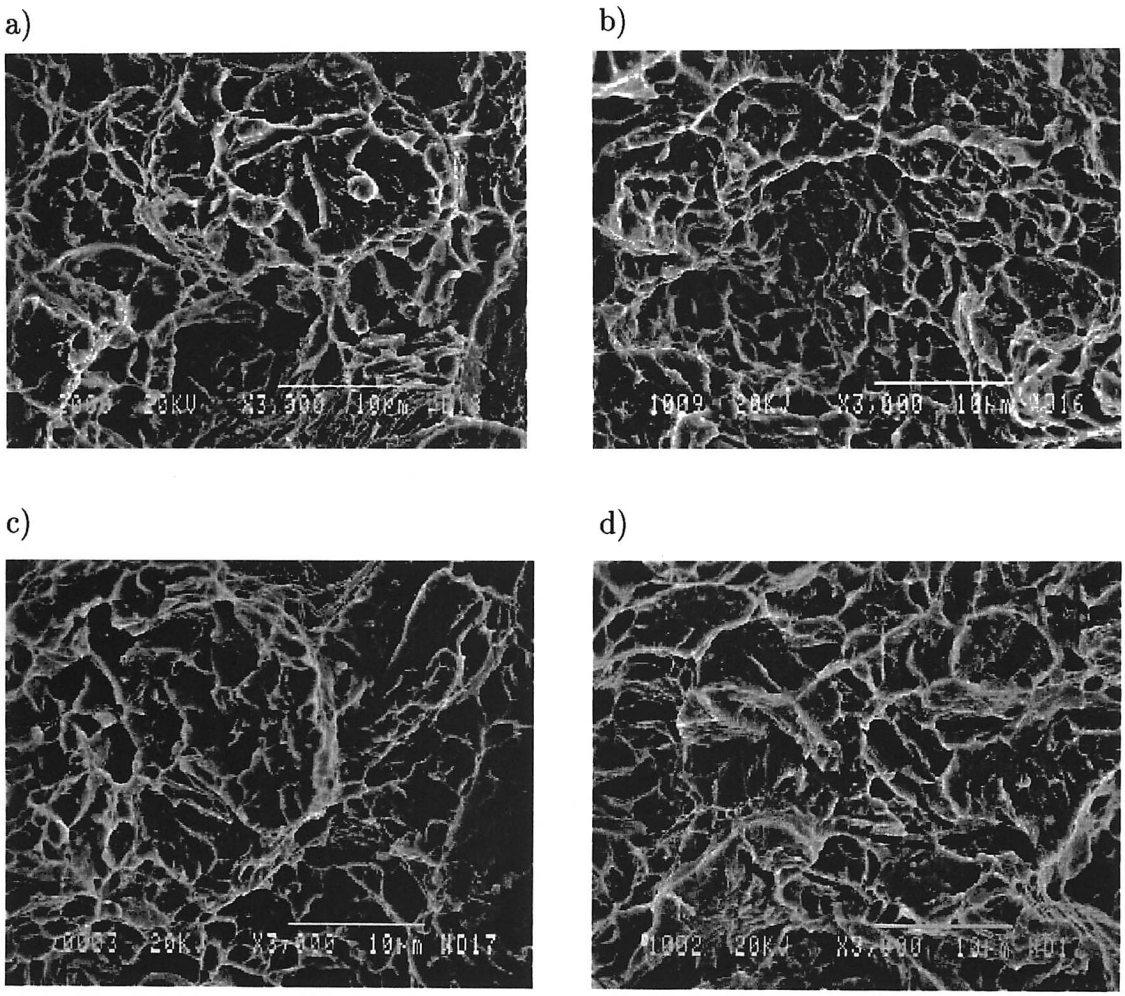

Figure 7.4: Fracture surfaces of unstraightened bainitic rail a) plain rail
b) liquid nitrogen for 24
c) 250 °C for 1 hour
d) 350 °C for 1 hour
The scale bars are 10 μm

9

References

Beynon, J.H., Garnham, J.E. and Sawley, K.J. (1996): Rolling contact fatigue of three pearlitic rail steels, *Wear*, **191**, 94–111

Bhadeshia, H.K.D.H (1979): *Ph.D. Thesis*, University of Cambridge

Bhadeshia, H.K.D.H. (1992): Bainite in steels, *The Institute of Materials*, London, UK

Bhadeshia, H.K.D.H (1996): Hyperbolic tangents and alloys of iron, *Materials World*, November 1996, 643–645

Bhadeshia, H.K.D.H., and Edmonds, D.V. (1983): Bainite in silicon steels: new composition property approach Part 1, *Metal Science* **17**, 411–419

Bhattacharyya, S. (1980): Wear and friction in steel, aluminium and magnesium alloys Part 1, *Wear*, **61**, 133–141

Bold, P.E., Brown, M.W. and Allen, R.J. (1991): Shear mode crack growth and rolling contact fatigue, *Wear*, **144**, 301–311

Bolton, P.J. and Clayton, P. (1984): Rolling-sliding wear damage in rail and tyre steels, *Wear*, **93**, 145–165

Boutorabi, S.M.A., Young, J.M., Kondic, V. and Salhei, M. (1993): The tribological behaviour of austempered spheroidal graphite aluminium cast iron, *Wear*, **165**, 19–24

Bower A.F., and Johnson, K.L. (1991): Plastic flow and shakedown of the rail surface in repeated rail-wheel contact, *Wear*, **144**, 1–18

British Steel Track Products (1992): The Track Handbook, *BSTP publications*, Workington

Callender, R. (1983): Bainitic steels for railway applications, *Ph.D. Thesis*, University of Sheffield

Cannon, D.F. and Pradier, H. (1996): Rail rolling contact fatigue: Research by the ERRI, *Wear*, **191**, 1–13

Chang, L. (1995): Bainite transformation and novel bainitic rail steels, *Ph.D. Thesis*, Univ. of Cambridge

Chipperfield, C.G., Skinner, D.H. and Marich, S. (1981): Influence of inclusions on the fatigue of rail steels, *IISI Meeting*, March 1981

Clayton, P. (1980): The relationships between wear behaviour and basic material properties for pearlitic steels, *Wear*, **60**, 75–93

Clayton, P. (1996): Tribological aspects of wheel-rail contact: a review of recent experimental research, *Wear*, **191**, 170–183

Clayton, P. and Danks, D. (1987): Comparison of the wear process for eutectoid rail steels: field and laboratory tests, *Wear*, **120**, 233–250

Clayton, P. and Danks, D. (1990): Effect of interlamellar spacing on the wear resistance of euctectoid steels under rolling-sliding conditions, *Wear*, **135**, 369–389

Clayton, P. and Devanathan, R. (1992): Rolling/sliding wear of a chromium molybdenum rail steel in pearlitic and bainitic conditions, *Wear*, **156**, 121–131

Clayton, P. and Hill, D.N. (1987): Rolling contact fatigue of a rail steel, *Wear*, **117**, 319–334

Clayton, P. and Jin, N. (1996): Unlubricated sliding and rolling/sliding wear behaviour of continuously cooled low/medium carbon bainitic steels, *Wear*, **200** 74–82

Clayton, P., Sawley, K.J., Bolton, P.J. and Pell, G.M. (1987): Wear behaviour of bainitic steels, *Conference on Wear of Materials*, Houston, Texas

Devanathan, R. and Clayton, P. (1991): Rolling-sliding wear behaviour of three bainitic steels, *Wear*, **151**, 255–267

Dikshit, V. and Clayton, P. (1992): A simple material model for water lubricated rolling contact fatigue in eutectoid steels, *Lubrication Engineering*, **48**, 606–614

Dikshit, V., Clayton, P. and Christensen, D. (1991): Investigation of rolling contact fatigue in a head hardened rail, *Wear*, **144**, 89–102

Esveld, C. (1989): Modern Railway Track, *MRT Productions*, W. Germany

Fegredo, D.M., Kalousek, J. and Shehata, M.T. (1993): The effect of progressive minor spheroidisation on the dry-wear rates of a standard carbon and a Cr-Mo alloy rail steel, *Wear*, **161**, 29–40

Garnham, J.E. (1989): Crack initiation in rolling contact fatigue; report for year 1, *One year contract report*, University of Leicester

Garnham, J.E. and Beynon, J.H. (1992): Dry rolling-sliding wear behaviour of bainitic and pearlitic steels, *Wear*, **157**, 81–109

Ghonem, H., Kalousek, J. and Stone, D. (1982): On the fracture and wear characteristics of chromium-molybedenum bainitic steel, *Specialty steels and hard materials*, Pergamon Press, Oxford, 259–265

Heller, W. and Schweitzer, R. (1982): Hardness, microstructure and wear behaviour of rail steels, *Proceedings of the 2nd International Heavy Haul Railways Conference*, Colorado Springs, Colorado

Hellier, A.K. Corderoy, D.J.H. and McGirr, M.B. (1985): A study of subsurface rail wheel contact stresses with application to modelling rail fatigue, *Rail International*

Hutchings, I.M. (1992): Tribology, *Edward Arnold*, London

Ichinose, H., Takehara, J., Iwasaki, N. and Ueda, M. (1978): Investigation on contact fatigue and wear resistance in rail steels, *Heavy Haul Railways Conference*, Perth, Australia

Ishida, M. and Abe, N. (1996): Experimental study on rolling contact fatigue from the aspect of residual stress, *Wear*, **191**, 65–71

Jerath, V. (1992): Rail research and development, *Paper 4.7.1, 4th RIA Track Sector course*

Jerath, V. (1996): Rolling contact fatigue of rails, British Steel internal note

Jin, N. and Clayton, P. (1997): Effect of microstructure on rolling/sliding wear of low carbon bainitic steels, *Wear*, **202**, 202–207

Johnson, K.L. (1985): Contact Mechanics, Cambridge University Press, Cambridge, UK

Johnson, K.L. (1989): Rolling contact fatigue failure of rails: The mechanics aspect, ERRI report

Kalousek, J., Fegredo, D.M. and Laufer, E.E. (1985a): The wear resistance and worn metallography of pearlite, bainite and tempered martensite rail steel microstructures of high hardness, *Wear*, **105**, 199–222

Kalousek, J., Ghonem, H and Steele, R. (1985b): Wear and lubrication effect on subsurface failure of several steels, *Proceedings of the 11th Leeds-Lyon Symposium*, Leeds

Laufer, E.E. Ghonem, H. Kalousek, J. and Stone, D.H. (1982): Aspects of plastic deformation and fatigue damage in pearlitic rail steel, *The 2nd International Heavy Haul Railways Conference*, Colorado Springs, Colarado USA

Lowenheim, F. (1974): Modern Electroplating, New York

Luo, Q., Xie, J. and Song, Y. (1995): Effects of microstructures on the abrasive wear behaviour of spheroidal graphite cast iron, *Wear*, **184**, 1–10

MAP_STEEL_MUCG46: `http://www.msm.cam.ac.uk/map/steel/programs/mucg46-b.html`

MTDATA: Metallurgical thermochemical data (1995) Mational Physical Laboratory, Teddington, Middlesex, UK

MacKay, D.J.C., Gavard, L., Bhadeshia, H.K.D.H. and Suzuki, S. (1996): Bayesian neural network model for austenite formation in steels, *Materials Science and Technology*, **12**, 453–463

McEwen, I.J., and Harvey, R.F. (1985): Full-scale wheel-on-rail wear testing: Comparisons with service wear and a developing theoretical predictive method, *Lubrication Engineering*, **41**, 80–88

Masumoto, H., Sugino, K. and Hayashida, H. (1978): Development of wear resistant and anti-shelling high strength rails in Japan, *Heavy Haul Railways Conference*, Perth, Australia

Masumoto, H., Sugino, K., Nishida, S., Hattori, N. and Terada, T. (1982): Production and properties of a rail of high serviceability, *61st Transportation Research Board Annual Meeting*, January 1982, Washington D.C.

Marich, S., Cottam, J.W. and Curcio, P. (1978): Laboratory investigation of transverse

defects in rails, *Heavy Haul Railways Conference*, Perth, Australia

Moore, D.F. (1975): Principles and applications of Tribology, Pergamon Press Ltd, UK

Moore, M.J. (1979): Energy dissipation in abrasive wear, *Proceedings of the International Conference on Wear of Materials* 636–638

Muster, H., Schmedders, H., Wick, K. and Pradier, H. (1996): Rail rolling contact fatigue: The performance of naturally hard and head-hardened rails in track, *Wear*, **191**, 54–64

Mutton, P.J. and Watson, J.D. (1978): Some effects of microstructure on the abrasion resistance of metals, *Wear*, **48**, 385–398

ORE (Office for Research and Experiments of the International Union of Railways) (1990): Review of rolling contact fatgue in rails, ORE, Utrecht, Netherlands

Perez-Unzueta, A. (1992): Wear resistance of pearlitic rail steels, *Ph.D. Thesis*, Univ. of Leicester

Rao, V.N., Miller, R.W, and Thomas, G. (1976): Heat treatment, microstructure and mechanical properties of experimental high strength Fe-4Cr-0.4C steels, *Proc. Int. Conf. Heat Treatment*, the Metals Society, London

Saka, N. (1978): Effect of microstructure on friction and wear of materials, *Proceedings of the international conference on the fundamentals of tribology*, Cambrideg, Massachusetts, USA

Samuels, L. (1967): Metallographic polishing by mechanical methods, *Sir Isa ac Pitman and Sons Ltd*, UK

Shipway, P.H., Wood, S.J. and Dent, A.H. (1997): The hardness and sliding wear behaviour of a bainitic steel, *Wear*, **203-204**, 196–205

Singh, U.P. and Singh, R. (1993): Wear investigation of wheel and rail steels under conditions of sliding and rolling-sliding contact with particular regard to microstructural parameters, *Wear*, **170**, 93–99

Sperring, D.G. (1986): Rail wear and associated problems, *Paper C3, 2nd RIA Track Sector course*

Srinivasan, M. (1977): Rail in the track structure, *Rail International*, January 1977

Steele, R.K. (1990): Performance requirements of railroad steel, *Mechanical working and steel processing proceedings*

Steele, R.K., Rungta, R. and Rice, R.C. (1987): Metallurgical cleanliness improves rail fatigue life, *Railway Gazette International*, March 1987

Stone, D.H. (1982): The increasing demands on the serviceability of rail steels, *Canadian Metallurgical Quarterly*, **21**, 17–24

Su, X. and Clayton, P. (1996): Surface-initiated rolling contact fatigue of pearlitic and low carbon bainitic steels, *Wear*, **197**, 137–144

Sugino, K., Kageyama, H., Kuroki, T., Urashima, C. and Kikuchi, A. (1996): Metallurgical investigation of transverse defects in worn rails in service, *Wear*, **191**, 141–148

Suh, N.P. (1973): The delamination theory of wear, *Wear*, **25**, 111–124

Suh, N.P. (1977): An overview of the delamination theory of wear, *Wear*, **44**, 1-16

Timoshenko, S. and Goodier, J. (1984): Theory of Elasticity (3rd edition) *McGraw-Hill Book Co.*, London

Tyfour, W.R., Beynon, J.H. and Kapoor, A. (1996): Deterioration of rolling contact fatigue life of pearlitic rail steel due to dry-wet rolling sliding line contact, *Wear*, **197**, 255–265

Wang, Y. and Lei, T. (1996): Wear behaviour of steel 1080 with different microstructures during dry sliding, *Wear*, **194**, 44–53

Wang, Y., Pan, L. and Lei, T. (1991): Sliding wear behaviour of pearlitic structures in eutectoid steel, *Wear*, **143**, 57–69

Wong, S.L., Bold, P.E., Brown, M.W. and Allen, R.J. (1996): A branch criterion for shallow-angled rolling contact fatigue cracks in rails, *Wear*, **191**, 45–53

Xu, L. and Kennon, N.F. (1991): A study of the abrasive wear of carbon steels, *Wear*, **148**, 101–112

Zakharov, S., Komarovsky, I. and Zharov, I. (1998): Wheel flange/rail head wear simulation, *Wear*, **215**, 18–24

Zhou, W. and Zhou, Q. (1993): Lubricated sliding and rolling wear of austempered ductile iron, *Wear*, **162-164**, 696–702

Zum Ghar, K. (1987): Microstructure and wear of materials, *Elsevier*, Amsterdam